Université de Montréal

Complexes NCN de Ni(II) et Ni(III) : Synthèse, caractérisation et rôle dans le mécanisme de couplage C-O, C-N et C-halogènes

par Jean-Philippe Cloutier

Département de chimie
Faculté des arts et des sciences

Thèse présentée
en vue de l'obtention du grade de Philosophiæ Doctor (Ph.D.)
en Chimie

Septembre 2018

Résumé

La présente thèse décrit la synthèse, caractérisation et réactivité des complexes pinceurs de type NCN du Ni^{II} et Ni^{III}. Elle comporte trois parties. La première traite de la synthèse d'une nouvelle famille de complexes de Ni^{II} basé sur le ligand 1,3-bis(pyrazole),5-R-C_6H_3 (R= H, OMe). La synthèse du ligand est effectuée par couplage d'Ullman entre le pyrazole et le 1,3-diiodobenzène ou le 1,3-dibromo,5-méthoxybenzène. La réaction à reflux des ligands avec le précurseur de nickel $\{[NiBr_2(iPrCN)]\}_n$ en présence de triéthylamine mène à la formation des complexes pinces $(NCN^{pz})Ni^{II}Br$ et (MeO-$NCN^{pz})Ni^{II}Br$ par activation du lien C-H (pz = pyrazole). Le complexe de Ni^{II} de type alcoolate $(NCN^{pz})Ni(BHT)$ (BHT = 2,6-*t*-Bu_2-4-Me-OC_6H_2) est isolé à partir de la réaction du complexe $(NCN^{pz})Ni^{II}Br$ avec NaBHT. Les tentatives d'oxydation des complexes isolés n'ont pu mener à la caractérisation d'authentiques complexes de Ni^{III}. La réaction des complexes bromo avec H_2O_2 mène à la formation de Br-$NC(OH)N^{pz}$ et $NC(OH)N^{pz}$ à partir du complexe $(NCN^{pz})Ni^{II}Br$ et MeO-$NC(OH)N^{pz}$ à partir du complexe (MeO-$NCN^{pz})Ni^{II}Br$. La réaction aérobique du complexe $(NCN^{pz})Ni^{II}Br$ avec différents alcools et amines mène aux produits de fonctionnalisation du ligand $NC(OR)N^{pz}$ et $NC(NR_2)N^{pz}$.

Le deuxième thème montre la fonctionnalisation du lien C_{ispo}-Ni^{III} du complexe $(NCN)Ni^{III}Br_2$. La réaction de $(NCN)Ni^{III}Br_2$ avec H_2O, divers alcools, amines et acides forts mène à la formation de lien C-O, C-N et C-halogènes. Une étude cinétique montre que la réaction est d'ordre 1 en Ni^{III} excluant la possibilité d'une réaction de disproportionation entre 2 Ni^{III} menant à un complexe de Ni^{IV}. La mesure d'un effet cinétique isotopique inverse de 0.47 de la réaction avec $MeOH/CD_3OD$ indique un transfert de proton provenant d'un pré-équilibre ayant lieu avant l'étape déterminante. L'observation de rendements inférieurs à 50% pour la fonctionnalisation s'explique par une réaction de comproportionation entre le Ni^{I} issu de l'élimination réductrice avec le Ni^{III} de départ. Ces observations permettent la proposition d'un mécanisme pour la formation de lien C-O, C-N et C-halogènes à partir du complexe $(NCN)Ni^{III}Br_2$.

La troisième partie traite de la synthèse de nouveaux complexes de Ni^{III} cationiques et dicationique à partir du complexe $(NCN)Ni^{III}Br_2$. En présence d'$AgSbF_6$ et d'acétonitrile, le complexe $(NCN)Ni^{III}Br_2$ réagit pour former le complexe dicationique $[(NCN)Ni^{III}(MeCN)_3]^{2+}$ avec un rendement de 83%. La réaction entre $(NCN)Ni^{III}Br_2$ et $[(NCN)Ni^{III}(MeCN)_3]^{2+}$ mène à la formation du complexe cationique $[(NCN)Ni^{III}(Br)(MeCN)]^{+}$ avec un rendement de 84%. Ces complexes sont caractérisés par diffraction des

rayons-X et résonance paramagnétique de l'électron. La réaction de ces complexes avec MeOH mènent à la formation du produit fonctionnalisé NC(OMe)N et d'un complexe de nickel divalent cationique suggérant une comproportionation entre $[(NCN)Ni^{III}(Br)(MeCN)]^{+}$ ou $[(NCN)Ni^{III}(MeCN)_3]^{2+}$ avec le Ni^{I} généré par la formation du lien C-O. La réaction avec $MeNH_2$ mène à la formation du produit fonctionnalisé NC(NHMe)N avec des rendements typiques de 30%. Ces rendements s'expliquent par l'oxydation de la méthylamine par les Ni^{III} cationiques et dicationiques. Une étude DFT exhaustive met en lumière le mécanisme de réaction pour la formation de lien C-O et C-N. La première étape est la coordination du substrat au centre métallique trivalent. Ensuite la déprotonnation du MeOH est assurée par un des bras azotés de la pince alors que celle de $MeNH_2$ provient de la sphère externe. L'élimination réductrice est l'étape limitante pour la formation de lien C-O et C-N. La valeur de l'effet cinétique isotopique de 0.62 est aussi rationalisée par des calculs vibrationnels issus de la DFT.

Mots-clés : Complexes pinces, Ni^{II}, Ni^{III}, Ni^{IV}, complexes pinces NCN, NCN, fonctionnalisation, couplage C-O, couplage C-N, couplage C-halogènes, Élimination Réductrice, disproportionation, comproportionation, activation C-H, DFT

Abstract

This thesis describes the synthesis, characterization and reactivity of NCN type Ni^{II} and Ni^{III} pincer complexes. The thesis is divided in three parts. The first discusses the synthesis of a new family of Ni^{II} complexes based on the 1,3-bis(pyrazole),5-R-C_6H_3 ligand (R = H, OMe). Ligand synthesis is executed by Ullman coupling between pyrazole and 1,3-diiodobenzene or 1,3-dibromo,5-methoxy-benzene. Refluxing ligands with nickel precursor $\{[NiBr_2(iPrCN)]\}_n$ in the presence of triethylamine leads to the formation of pincer complexes $(NCN^{pz})Ni^{II}Br$ and $(MeO\text{-}NCN^{pz})Ni^{II}Br$ by C-H activation (pz = pyrazole). The alkoxide-type Ni^{II} complex $(NCN^{pz})Ni(BHT)$ (BHT = 2,6-t-Bu_2-4-Me-OC_6H_2) is isolated from the reaction between $(NCN^{pz})Ni^{II}Br$ and NaBHT. Oxidation attempts did not lead to the characterization of an authentic Ni^{III} species. Reacting bromo complexes with H_2O_2 leads to the formation of $Br\text{-}NC(OH)N^{pz}$ and $NC(OH)N^{pz}$ when starting from $(NCN^{pz})Ni^{II}Br$ and $MeO\text{-}NC(OH)N^{pz}$ when starting from $(MeO\text{-}NCN^{pz})Ni^{II}Br$. The aerobic reaction of $(NCN^{pz})Ni^{II}Br$ with different alcohols and amines leads to the functionalization products of the ligand $NC(OR)N^{pz}$ and $NC(NR_2)N^{pz}$.

The second theme is the functionalization of the $C_{ispo}\text{-}Ni^{III}$ bond in $(NCN)Ni^{III}Br_2$. The reaction of $(NCN)Ni^{III}Br_2$ with H_2O, various alcohols, amines and strong acids leads to the formation of C-O, C-N and C-halogen bonds. A kinetic study shows that Ni^{III} displays first order behavior excluding the possibility of a disproportionation reaction between 2 Ni^{III} which would lead to a Ni^{IV} species. Measurement of an inverse kinetic isotopic effect of 0.47 for the reaction with $MeOH/CD_3OD$ indicates a proton transfer arising from one or several pre-equilibria occuring before the rate determining step. The observation of yields of less than 50% for the functionalization reaction indicates a comproportionation reaction between the Ni^{I} resulting from the reductive elimination and the starting Ni^{III}. These observations allow proposition of a mechanism for C-O, C-N and C-halogen bond formation from the $(NCN)Ni^{III}Br_2$ complex.

The third part reports the synthesis of new cationic and dicationic Ni^{III} complexes starting from $(NCN)Ni^{III}Br_2$. In the presence of $AgSbF_6$ and acetonitrile, $(NCN)Ni^{III}Br_2$ reacts to give dicationic complex $[(NCN)Ni^{III}(MeCN)_3]^{2+}$ in 83% yield. The reaction between $(NCN)Ni^{III}Br_2$ and $[(NCN)Ni^{III}(MeCN)_3]^{2+}$ leads to the formation of the cationic $[(NCN)Ni^{III}(Br)(MeCN)]^{+}$ with a yield of 84%. These complexes are characterized by X-ray diffraction and electron paramagnetic resonance. Reacting these complexes with MeOH leads to the formation of the functionalized product NC(OMe)N and a cationic

divalent nickel complex suggesting a comproportionation between $[(NCN)Ni^{III}(Br)(MeCN)]^{+}$ or $[(NCN)Ni^{III}(MeCN)_3]^{2+}$ with the Ni^{I} generated by the formation of the C-O bond. Reacting $[(NCN)Ni^{III}(Br)(MeCN)]^{+}$ or $[(NCN)Ni^{III}(MeCN)_3]^{2+}$ with MeNH2 leads to the formation of the functionalized product NC(NHMe)N with typical yields of 30%. These low yields are explained by the ability of the ionized Ni^{III} complexes to oxidize $MeNH_2$. A comprehensive DFT study highlights the reaction mechanism steps for C-O and C-N bond formation. The first step is the coordination of the substrate with the trivalent metal center. Then deprotonation of MeOH is provided by the pincer's amine moiety while deprotonation of $MeNH_2$ arises from an outer sphere process. Reductive elimination was found to be the limiting step for C-O and C-N bond formation. The value of the isotopic kinetic effect of 0.62 is also rationalized by a DFT vibrational analysis.

Keywords: Pincer complexes, Ni^{II}, Ni^{III}, Ni^{IV}, high-valent, NCN, NCN pincer complexes, functionalization, C-O coupling, C-N coupling, C-halogen coupling, reductive elimination, comproportionation, disproportionation, C-H activation, DFT

Table des matières

Liste des tableaux

Liste des Figures

Liste des schémas

Liste des abréviations

br	Broad (NMR spectroscopy)
COD	1,5-Cyclooctadiene
DCM	Dichloromethane
DPPE	1,2-Bis(diphenylphosphino)ethane
d	doublet (NMR spectroscopy)
dd	doublet of doublet (NMR spectroscopy)
i-Pr	Groupement isopropyl
m	multiplet (NMR spectroscopy)
MeCN	Acetonitrile
MeOH	Methanol
$[NBu_4][PF_6]$	Tetrabutylammonium Hexafluorophosphate
NMR	Nuclear Magnetic Resonance
NCN	1,3-bis(amino)benzène
$POC_{sp^2}OP$	1,3-bis(phosphinito)benzène

$POC_{sp}^{3}OP$	1,3-bis(phosphinito)propane
POCN	1-(phosphinito)-3-aminobenzène
RPE	Résonance Paramagnétique Électronique
t	triplet (NMR spectroscopy)
THF	Tertrahydrofurane
t-Bu	Groupement tert-Butyl
t.p.	Température Ambiante/pièce
δ	Déplacement Chimique

Remerciements

Je tiens avant tout à remercier mon directeur de recherche **Davit Zargarian** de m'avoir accueilli dans son groupe de recherche. Après une excursion un peu ratée dans le domaine de la physique, j'avais le sentiment de ne pas avoir ma place en science. J'ai rapidement changé d'idée en suivant le cours de chimie organométallique enseigné par le professeur Zargarian. Je lui suis extrêment reconnaissant pour la confiance qu'il m'a accordée durant mes années de maîtrise et doctorat, pour sa patience et ses qualités de pédagogue.

Je veux aussi remercier les anciens **Richou Declercq**, **Fabien Lindeperg** et **Boris Vabre** pour une atmosphère de travail idéale lors de mon arrivée dans le groupe. **Michel Simard** et **Francine Gariépy** pour l'aide en crystallographie, **Elena Nadezhina** pour les services d'analyse élémentaire et le service RMN de l'UdeM. **Radu Iftimie** pour m'avoir aidé dans mes premiers pas en DFT, **Christine Lepetit** du LCC à Toulouse et **Daniel Ess** de BYU en Utah pour m'avoir aider à aller plus loin en chimie computationnelle. Merci aussi à **Yves Canac** pour de très bonne discussion sur la chimie lors de mon stage à Toulouse et pour avoir, avec **Lionel Rechignat**, mesuré nos spectres en RPE.

Merci à mes amis Nadia et Martin pour les soupers. Alexandre, Téssier, Bianca, Émilie et Lorena pour les soirées de jeux de société. Merci à ma mère Francine pour son support moral et financier. Je remercie aussi mon ami et collègue **Loïc Mangin** pour les discussions non seulement sur la chimie mais aussi celles à propos de tout et rien. Merci à **Laurianne**, ma copine, qui a fait de ma dernière année de doctorat une des plus belle de ma vie.

Chapitre 1: Introduction

Les catalyseurs sont des espèces chimiques pouvant réduire grandement l'énergie à fournir pour effectuer une transformation chimique. Dans un contexte de développement durable il est important de mettre sur pied des systèmes catalytiques efficaces, basés sur des métaux peu toxiques et peu couteux. Il est important de connaître les mécanismes par lesquels les catalyseurs transforment une molécule A en molécule B car il devient plus facile d'optimiser sa réactivité. La formation de liens carbone-hétéroatome par les complexes de Ni^{III}/Ni^{IV} a connu un essor important ces dernières années. Ces états d'oxydation sont souvent proposés comme intermédiaires dans les mécanismes mais rarement isolés. Les travaux présentés dans cette thèse viennent mettre en évidence le rôle joué par ces états d'oxydation dans les mécanismes réactionnels. La première partie du chapitre 1 montre différents mécanismes de couplage au nickel pour lesquels l'intervention d'intermédiaire haut-valent est soupçonnée. La deuxième partie donne des exemples de complexes de Ni^{III} et Ni^{IV} bien définis actifs dans la fromation de lien C-C, C-O, C-N et C-halogène.

1.1 Propositions impliquant Ni^{III}

Le nickel est un métal de transition faisant partie du groupe 10 possédant la configuration électronique atomique $[Ar]3d^8 4s^2$. On lui connait les états d'oxydation 0, +I, +II, +III et +IV, l'état d'oxydation +II étant le plus répandu. En chimie de coordination comme en chimie organométallique, les états d'oxydation +III et +IV sont plutôt rares. En chimie de synthèse, les métaux comme le nickel et le palladium sont connus pour leur rôle dans la formation de lien carbone-hétératomes.[1] Les travaux pionniers de R. J. P. Corriu et Makoto Kumada ont démontré que certains complexes de Ni^{II} pouvaient promouvoir la formation de liens C-C.[2,3] En effet, la réaction stœchiométrique entre un réactif de Grignard et un halogénure d'aryle catalysée par un halogénure de Ni^{II} mène à la formation d'un lien carbone-carbone entre les deux groupements hydrocarbyle (Schéma 1.1).

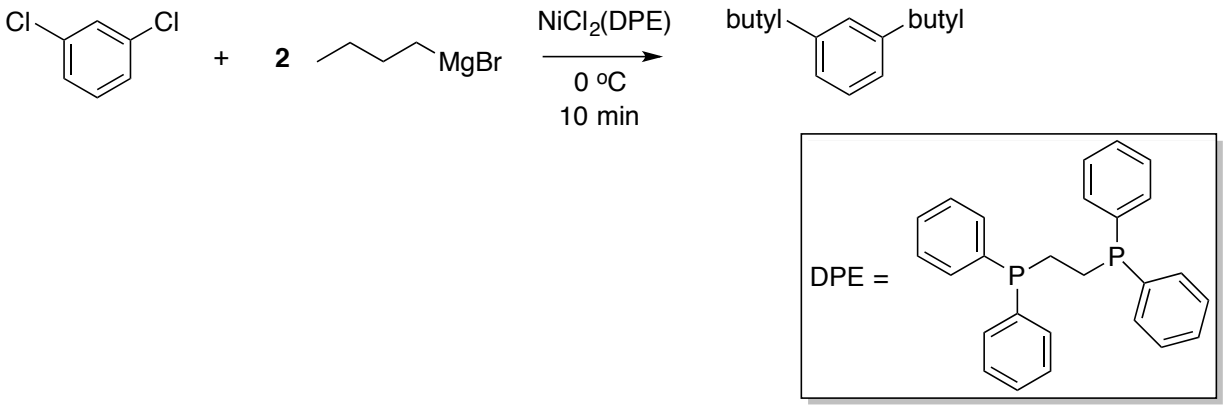

Schéma 1.1. Formation de lien C-C catalysée par un complexe de Ni^{II} (couplage de Kumada-Corriu)

Les travaux de Richard Heck, Ei-ichi Negishi et Akira Suzuki ont par la suite popularisé l'usage du palladium comme catalyseur dans le couplage C-C. Par exemple la réaction de Heck promeut le couplage d'un halogénure d'aryle avec un alcène à l'aide d'une base et d'un catalyseur de Pd^0. [4] Le couplage de Negishi effectue la formation de lien C-C entre un halogénure d'aryle et un composé organozincique le tout encore une fois catalysé par un complexe de Pd^0. [5] Finalement couplage de Suzuki est une méthode de formation de lien C-C très semblable au couplage de Negishi faisant intervenir, respectivement, un acide boronique à la place d'un organozincique comme agent de transmétallation. [6]

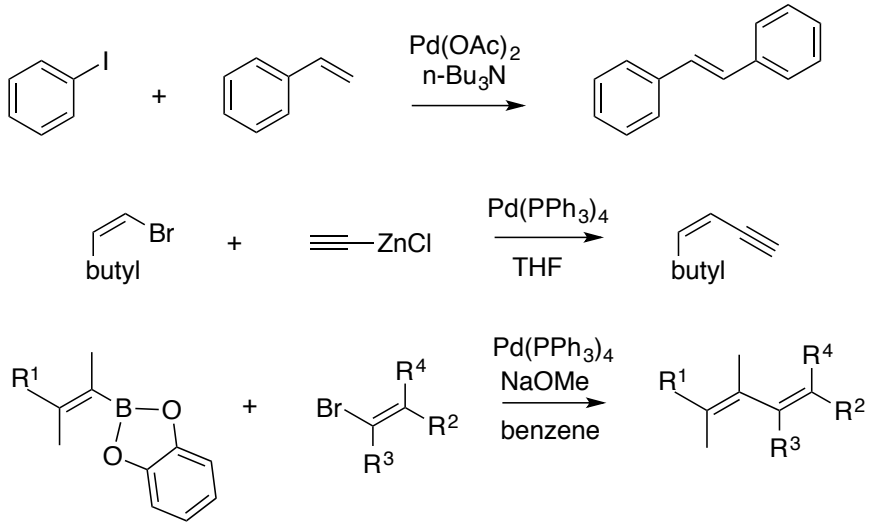

Schéma 1.2. Couplages croisés de Heck, Negishi et Suzuki

Les mécanismes des couplages de Kumada, Suzuki et Negishi sont très semblables et ne diffèrent souvent que par l'agent de transmétallation utilisé. Ils peuvent être résumés par le cycle catalytique illustré

au schéma 1.3. La première étape consiste en l'addition oxydante du composé Ar-X sur le complexe de Pd^0 générant ainsi un complexe de Pd^{II} contenant un lien métal-carbone (il est à noter qu'un précatalyseur dans lequel le métal se trouve à l'état d'oxydation +II est parfois utilisé, ce précatalyseur est réduit à l'état 0 *in situ*). Par la suite, l'halogène présent sur le complexe est remplacé par un agent de transmétallation, ici un acide boronique, afin d'installer sur le centre métallique le groupement R' à être couplé. Afin que l'élimination réductrice puisse avoir lieu, le complexe doit s'isomériser afin que les deux ligands à être couplés soient en position *cis* l'un par rapport à l'autre. La dernière étape consiste en l'élimination réductrice des fragments R et R' afin de former le produit désiré et régénérer le catalyseur.[7] Le mécanisme présenté ci-dessus est basé sur un cycle Pd^0/Pd^{II} et est celui généralement accepté quoique l'on retrouve aussi des cycles impliquant un duo Pd^{II}/Pd^{IV}.[8]

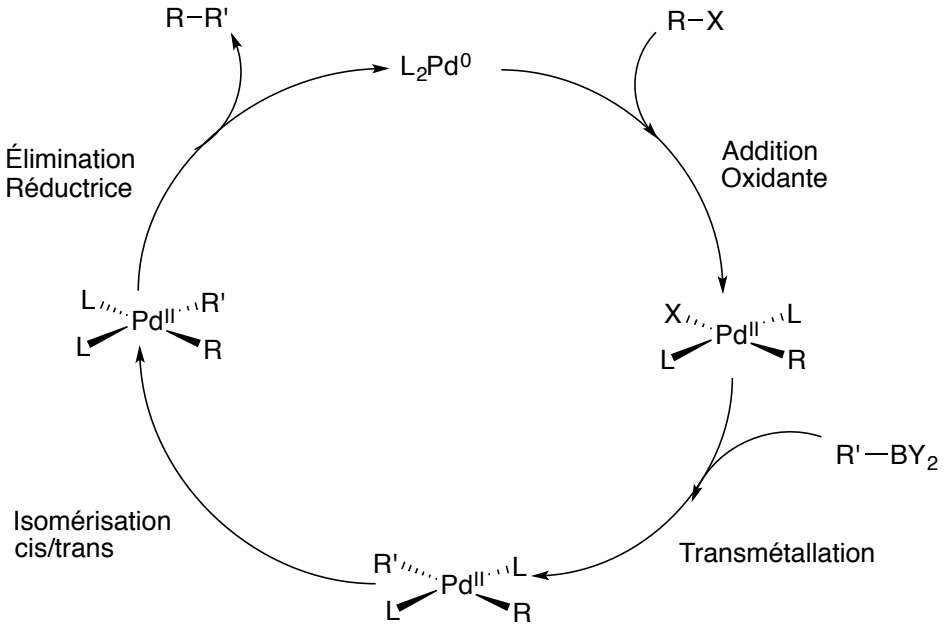

Schéma 1.3. Cycle catalytique d'un couplage de Suzuki

Le palladium étant un métal de transition dispendieux, il est souhaitable de pouvoir faire ces transformations en utilisant des catalyseurs à base de nickel. Cependant, les mécanismes de couplage croisé utilisant le nickel comme catalyseur sont beaucoup plus ambigus. Les métaux de transition de la première rangée sont en effet sujets aux réactions de transfert d'électron célibataire (single electron transfer, SET).[9] Le couplage au nickel peut donc se faire selon un cycle Ni^0/Ni^{II} mais beaucoup de travaux tendent à démontrer l'implication d'espèces de nickel à haute-valence tel Ni^{III} et même Ni^{IV}.[10] Par exemple les travaux pionniers de Kochi montrent l'implication d'espèces de Ni^I et Ni^{III} dans le couplage menant à la formation de biaryles.[11] Le Schéma 1.4 montre d'abord l'addition oxydante d'un halogénure d'aryle sur

un complexe de nickel monovalent formant ainsi un complexe de Ni^{III} (éq. 1). L'équation 2 décrit le transfert d'un groupement aryle radicalaire sur un complexe de nickel divalent, générant un complexe de nickel trivalent portant maintenant les deux groupements. Dans la dernière étape, le lien C-C est formé par élimination réductrice régénérant du même coup le complexe de Ni^{I}. Afin d'initier le cycle catalytique, les auteurs proposent le transfert d'un électron du Ni^{II} à l'halogénure d'aryle générant ainsi un complexe de Ni^{III} cationique et un aryle radicalaire portant une charge négative.

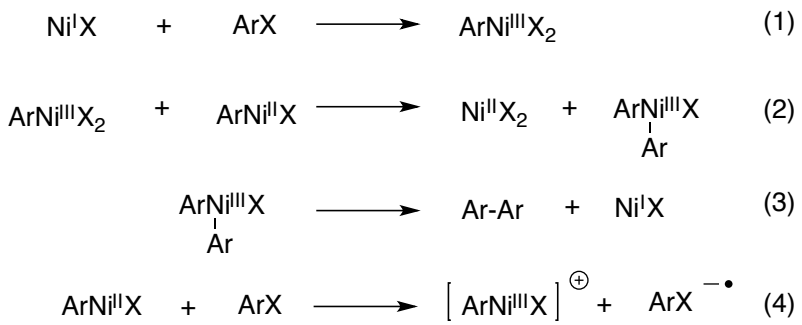

Schéma 1.4. Cycle Ni^{I}/Ni^{III} proposé par Kochi et al.

Vicic et al. ont aussi proposé l'implication d'espèces trivalentes du nickel dans le couplage carbone-carbone.[12] Leur mécanisme propose d'abord une réaction radicalaire entre un halogénure d'alkyle et un complexe de Ni^{II} dans lequel un électron est délocalisé sur le ligand. Cette réaction génère un intermédiaire de Ni^{III} qui subit une élimination réductrice afin de former le produit de couplage. Le mécanisme proposé passe par un intermédiaire de Ni^{III} qui n'est cependant pas isolé et caractérisé.

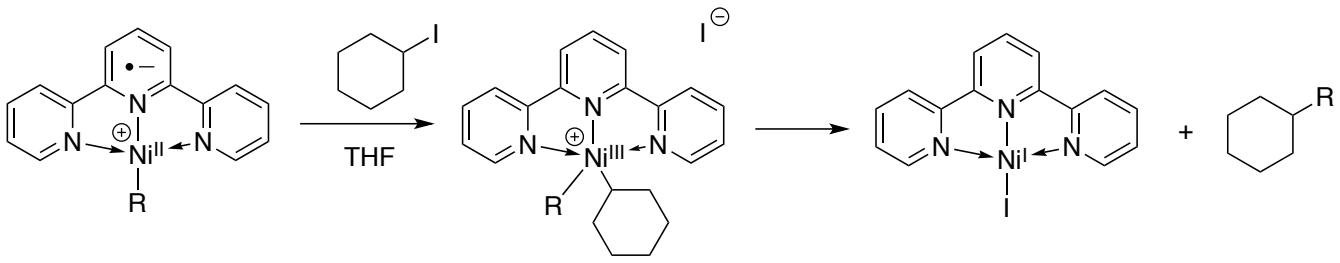

Schéma 1.5. Formation d'un lien C-C à partir d'un Ni^{II} porté par un ligand radicalaire anionique.

Les travaux de Hillhouse ont montré que des complexes de Ni^{II} de type alcoolate et amidure peuvent former des liens C-N et C-O lorsqu'ils sont oxydés en Ni^{III} (Schéma 1.6).[13] La deuxième réaction est d'importance car elle indique que l'addition oxydante est facilitée par un centre métallique de basse valence (Ni^{0}) et que cette réaction n'est pas réversible puisque le complexe de Ni^{II} formé est stable. Il est

cependant possible de reformer l'aziridine de façon irréversible en oxydant le Ni^{II} nouvellement formé, l'élimination réductrice est donc favorisée cinétiquement et thermodynamiquement par le Ni^{III}. Ceci indique aussi que le Ni^{I} généré par cette étape est incapable de faire l'addition oxydante de l'aziridine.

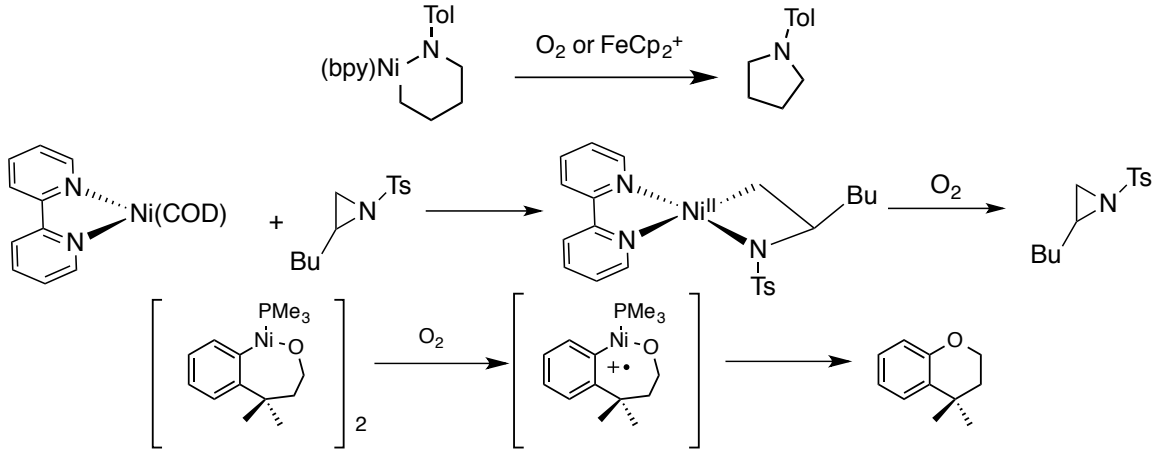

Schéma 1.6. Formation de liens C-O et C-N induite par l'oxydation d'un Ni^{II} en Ni^{III}

Plus récemment, dans un rare exemple de couplage C-O promut par le nickel, MacMillan propose un Ni^{III} comme espèce active dans leur système photocatalytique couplant des halogénures d'aryle à des alcools.[14]

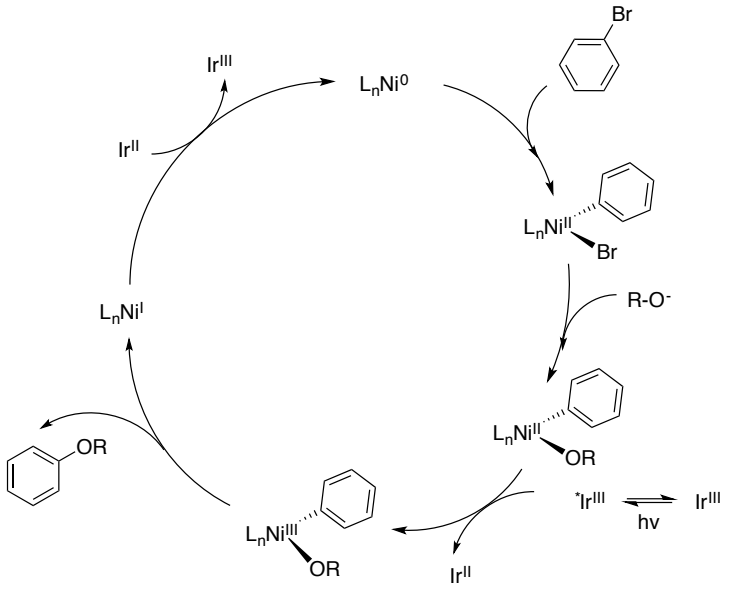

Schéma 1.7. Cycle photocatalytique proposé pour la formation de lien C-O catalysé par le nickel

Le schéma 1.7 décrit le mécanisme de formation du lien C-O. D'abord un complexe de Ni^{0} promeut l'addition oxydante de l'halogénure d'aryle afin de former un Ni^{II}. Il y a ensuite substitution du ligand par

un groupement alcoolate. La formation d'un complexe de Ni^{II} de type alcoolate rend le centre métallique plus riche en densité électronique et permet son oxydation par un photocatalyseur d'iridium. En effet, ce photocatalyseur d'Ir^{III} à l'état excité est un puissant oxydant et arrache un électron au Ni^{II} formant ainsi un complexe de Ni^{III} et un complexe d'Ir^{II}. Le Ni^{III} nouvellement formé subit une élimination réductrice pour former le composé désiré et un complexe de Ni^{I}. Ce dernier est réduit en Ni^{0} par le complexe d'Ir^{II} formé à l'étape précédente.

Le groupe de Sanford a pu démontrer qu'il est possible de former des liens C-Br lorsqu'un complexe de Ni^{II} contenant un lien Ni-C est oxydé par du brome.[15] Dans ces travaux, le complexe de Ni^{II} obtenu par addition oxydante d'un lien C-Br sur un précurseur de Ni^{0}. Sanford fait remarquer la réaction inverse, l'élimination réductrice, n'est pas observée à partir des complexes de Ni^{II}. Cependant, lorsqu'exposé à l'oxydant approprié, on génère le produit de couplage. Elle propose trois possibilités mécanistiques. D'abord, une attaque directe du carbone formant le lien C-Ni sur Br_2 laissant l'état d'oxydation du nickel inchangé. Ensuite, l'oxydation du centre métallique en Ni^{III} suivi de l'élimination réductrice. Finalement, l'article propose une oxydation en complexe de Ni^{IV} suivi de la formation du lien C-Br de la même façon qu'à la proposition précédente. Sur la base des travaux de Kochi discutés précédemment et de quelques expériences convaincantes, les auteurs privilégient la deuxième voie. Puisque chaque système est différent, ces questions restent importantes et seront centrales à cette thèse.

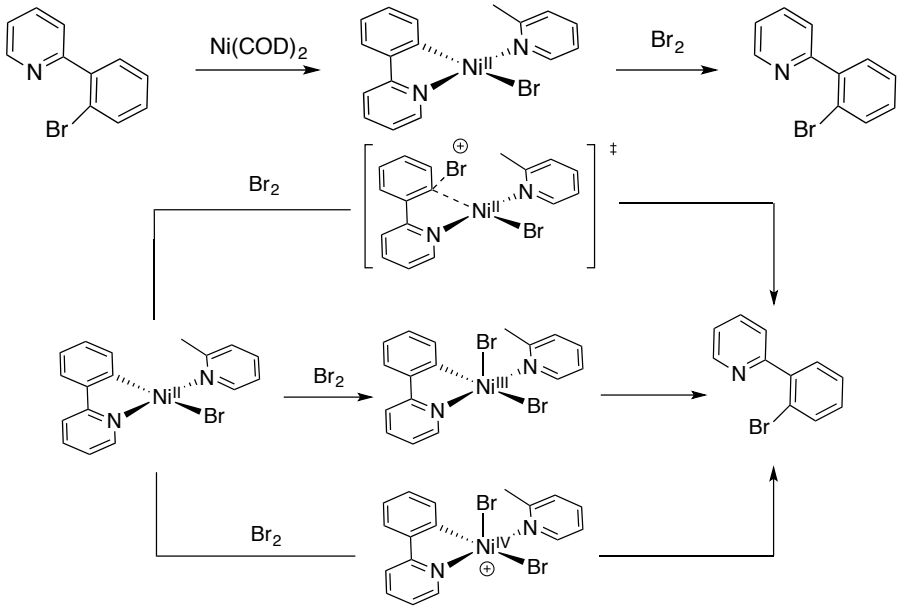

Schéma 1.8. Couplage C-Br à partir d'un complexe organométallique de Ni^{II} ainsi que 3 propositions mécanistiques menant à la formation du lien C-Br.

1.2 Propositions impliquant Ni^{IV}

Chatani propose quant à lui la formation d'un complexe de Ni^{IV} pour expliquer la réaction indiquée au schéma 1.9. [16]

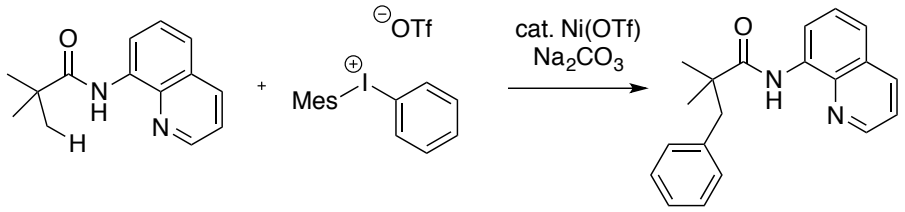

Schéma 1.9. Couplage C_{sp2}-C_{sp3} à l'aide d'un composé d'iode hyper-valent catalysé par le nickel

Le couplage commence par la déprotonation du ligand par la base et sa chélation au catalyseur de nickel. La complexation au nickel rend le proton situé sur le groupement méthyle plus acide, probalement à cause d'un possible interaction entre le centre métallique et le carbone sp^3 portant ce même proton. Ce proton peut maintenant être arraché par une base pour former un lien C-Ni. Ce lien métal-carbone favorise l'oxydation du centre métallique en Ni^{IV} et ce dernier subit l'élimination réductrice formant le produit de couplage désiré.

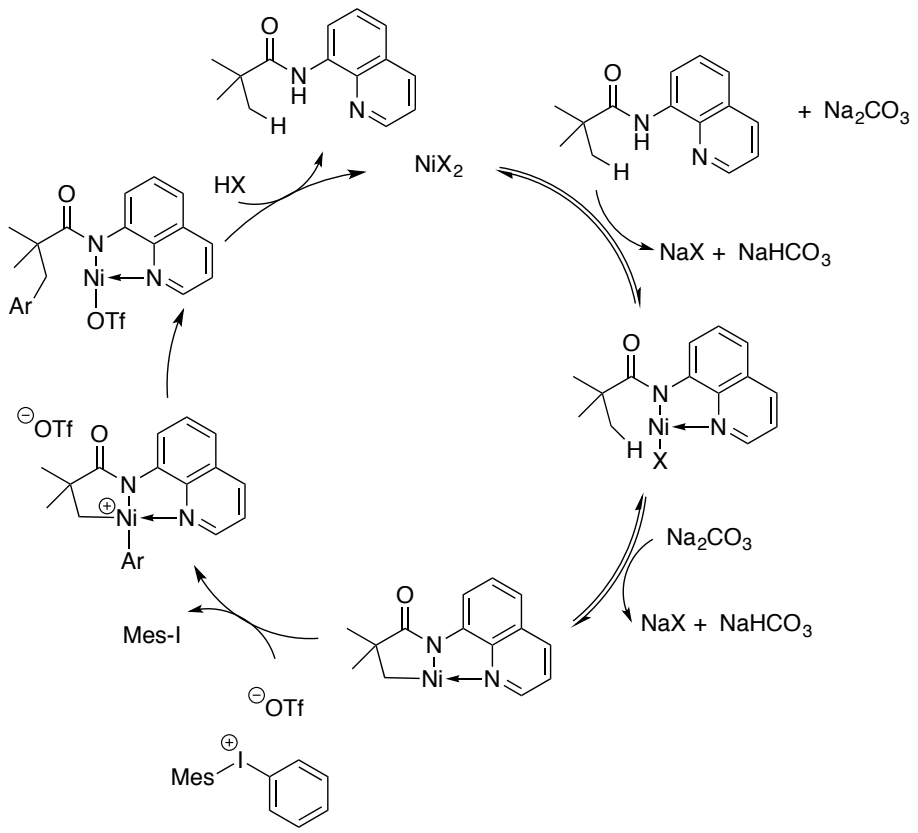

Schéma 1.10. Cycle catalytique proposé pour le couplage C_{sp2}-C_{sp3} catalysé par le nickel

Nous avons d'abord discuté d'exemples de couplage C-C et C-hétéroatomes dans lesquels le mécanisme proposé implique un Ni^{III} ou Ni^{IV}. De façon générale, l'élimination réductrice de liens C-O, C-N et C-halogène est difficile à partir du Ni^{II}. Comme nous avons vu, une stratégie possible est l'oxydation du centre métallique rendant l'élimination réductrice thermodynamiquement favorable et diminuant la barrière cinétique. D'un point de vue mécanistique, les états d'oxydation III et IV sont souvent proposés mais il existe très peu de complexes de nickel possédant ces états. Ces complexes sont en effet très réactifs et les mécanismes proposés ci-haut démontrent bien que ces intermédiaires font preuve d'une fragilité cinétique et thermodynamique. Nous allons maintenant présenter quelques complexes authentiques de Ni^{III}/Ni^{IV} et discuter de leur géométrie, configuration électronique et réactivité face au couplage C-C, C-O, C-N et C-halogène. Bien qu'ils soient difficiles à isoler et à caractériser, la littérature comporte tout de même plusieurs exemples notables dont il faut discuter.

1.3 Complexes de Ni^{III} isolés et formation de lien C-C et C-hétéroatomes

La nature paramagnétique des complexes de nickel(III) les a longtemps rendus élusifs puisqu'ils sont souvent invisibles en résonance magnétique nucléaire. En effet, les complexes de Ni^{III} possèdent une configuration électronique d^7 et la mesure de leur susceptibilité magnétique n'indique que la présence d'un électron non-apparié sans toutefois pouvoir indiquer où cet électron est localisé. L'arrivée de la résonance paramagnétique électronique a permis de distinguer entre un électron délocalisé sur le ligand et un véritable complexe de Ni^{III}. Un signal isotrope et une valeur du facteur g de l'électron proche de celle de l'électron libre (g = 2,0032) indique la présence d'un électron localisé sur le ligand et donc d'un centre métallique Ni^{II} stabilisant un ligand radicalaire. Par contre un signal anisotropique et une valeur de « g » différente de celle de l'électron libre permettent de décrire le caractère de l'orbitale dans laquelle se trouve l'électron célibataire, une orbitale « d » dans le cas des complexes de Ni^{III}.[17] Le premier complexe de Ni^{III} à être ainsi caractérisé est l'anion $[NiS_4C_4(CN)_4]^-$ (figure 1.1) dans lequel le centre métallique adopte une géométrie carrée-plane et pour lequel les signaux obtenus en RPE indique la présence d'un électron célibataire dans les orbitales « d » associées au centre métallique.[18] Comme autre complexe d'intérêt on note le composé neutre $NiBr_3(P(Me_2)(Ph))_2$. Ce complexe adopte une structure bipyramide-trigonale pour laquelle on peut observer une élongation de la distance entre le centre métallique et un des ligands bromure causée par l'effet Jahn-Teller puisque le complexe possède un électron non-apparié dans une de ses orbitales « d ».[19]

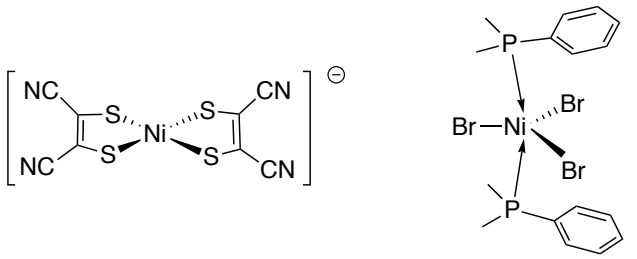

Figure 1.1. Complexe anionique $[NiS_4C_4(CN)_4]^-$ (gauche) et complexe neutre $NiBr_3((P(Me)_2(Ph))_2$ (droite**)**

Le premier complexe de Ni^{III} portant un lien Ni-C a été isolé par van Koten il y a près de 40 ans.[20] Le centre métallique trivalent est supporté par un ligand de type pinceur. Les complexes pinceurs sont basés sur un squelette tridenté illustré à la figure 1.2.

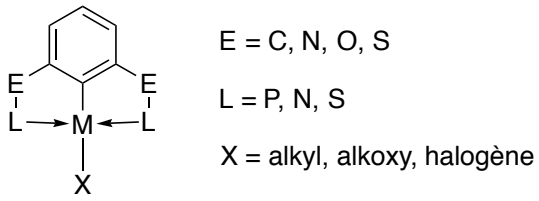

Figure 1.2. Forme générale d'un complexe pinceur

Ce type de géométrie offre plusieurs avantages. D'abord elle offre un environnement électronique modulable à plusieurs positions (E, L et X sur la figure) et une stabilité conférée par la pince tridentée. On nomme généralement un ligand pinceur en indiquant les atomes le reliant au centre métallique (dans le schéma L-C-L). Le schéma 1.11 décrit la synthèse du complexe NCN plan carré Ni^{II} et de son homologue Ni^{III}.

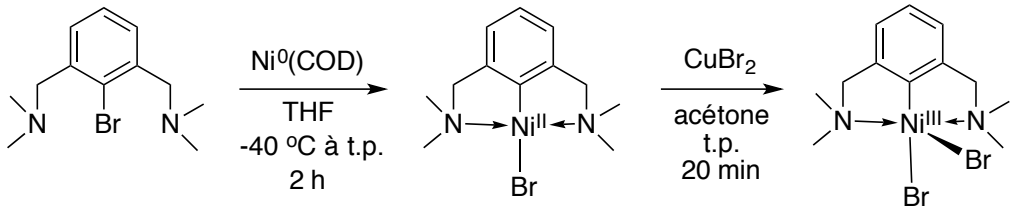

Schéma 1.11. Synthèses d'un complexe pinceur de Ni^{II} et de Ni^{III}

La première étape consiste en la synthèse d'un complexe de Ni^{II} par addition oxydante d'un lien C-Br à un complexe de Ni^0. Cette synthèse génère une certaine quantité de $(NCN)Ni^{III}Br_2$ et le mécanisme proposé par van Koten et al. pour en expliquer la présence rappelle celui proposé par Kochi pour le couplage C-C mentionné plus haut.[21] Les équations (1)-(3) montrent comment, à l'aide d'une série de SET, on arrive à générer le complexe de Ni^{II} désiré. Les équations (4) et (5) montrent l'addition oxydante du lien C-Br à un nickel monovalent cationique pour générer un Ni^{III} cationique, ce dernier réagissant rapidement avec l'ion bromure généré par la réaction (2) pour former $(NCN)Ni^{III}Br_2$. Les auteurs s'appuient aussi sur le fait que l'installation d'un groupement électro-donneur sur le cycle aromatique du ligand diminue les rendements considérablement.

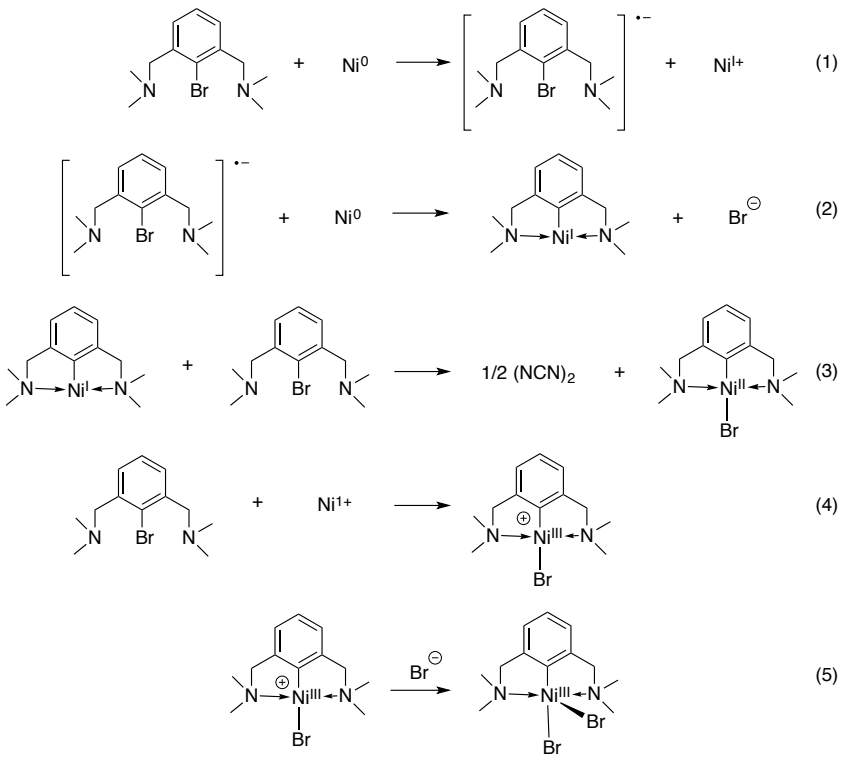

Schéma 1.12. Mécanisme proposé rationalisant la présence de Ni^{III} dans la synthèse du complexe $(NCN)Ni^{II}Br$

La stabilisation d'un complexe trivalent du nickel s'explique en partie par la densité électronique conférée au Ni^{II} par la plateforme NCN. D'abord, les azotes ainsi que le groupement aryle sont de très bons donneurs σ. Aussi, ce ligand empêche la rétro-donation des orbitales « d » du métal vers les bras azotés puisque ceux-ci ne possèdent pas d'orbitale de symétrie π accessibles. Cet accroissement de la densité électronique au centre métallique rend donc son oxydation plus facile. La voltampérométrie cyclique permet d'ailleurs de quantifier cette richesse électronique en mesurant l'énergie requise pour oxyder le métal. Le potentiel à fournir afin d'enlever un électron au complexe tel qu'indiqué dans le Schéma 1.12 est de 0.24 V par rapport au couple Ag/AgCl dans l'acétone. Il est donc possible d'oxyder le complexe chimiquement en utilisant un réactif dont le potentiel redox sera supérieur à 0.24 V dans l'acétone comme $CuBr_2$.[22]

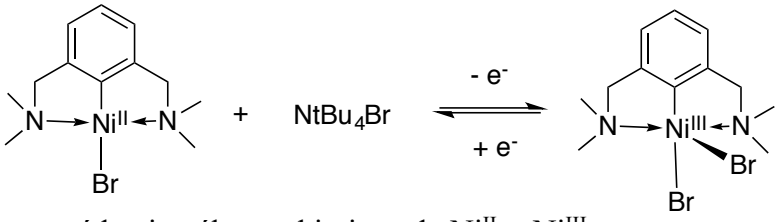

Schéma 1.13. Oxydation et réduction électrochimique du Ni^{II} et Ni^{III}

Le complexe (NCN)$Ni^{III}Br_2$ est de géométrie pyramide à base carrée et de configuration électronique bas-spin d^7. Les mesures en RPE indiquent la présence d'un électron non-apparié dans une orbitale majoritairement localisée sur le centre métallique et perpendiculaire au plan carré puisque le spectre ne montre pas de couplage hyperfin avec les isotopes ^{14}N des bras du pinceur. Des mesures cristallographiques confirment cette hypothèse et place l'électron célibataire dans l'orbitale d_z^2 du nickel.[17]

van Koten et al. ont aussi pu démontrer l'activité du complexe (NCN)$Ni^{II}Br$ comme catalyseur dans la formation de lien carbone-carbone par l'entremise d'une réaction appelée addition de Kharasch. La réaction implique le clivage d'un lien C-X dans CX_3Y (X = halogène, y = H, halogène, groupement éléctroattracteur) et l'addition des fragments résultant sur un alcène.

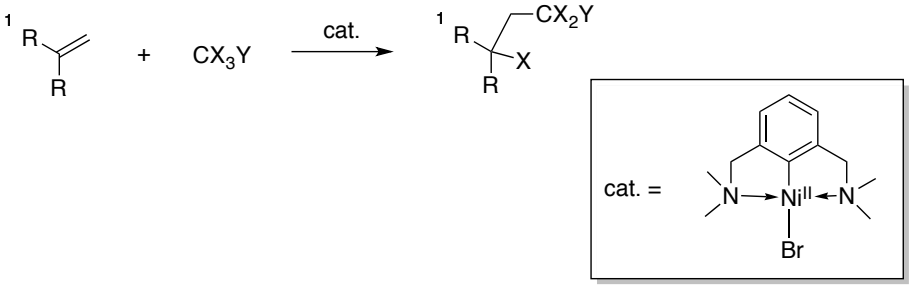

Schéma 1.14. Addition de Kharasch catalysée par le Ni^{II}.

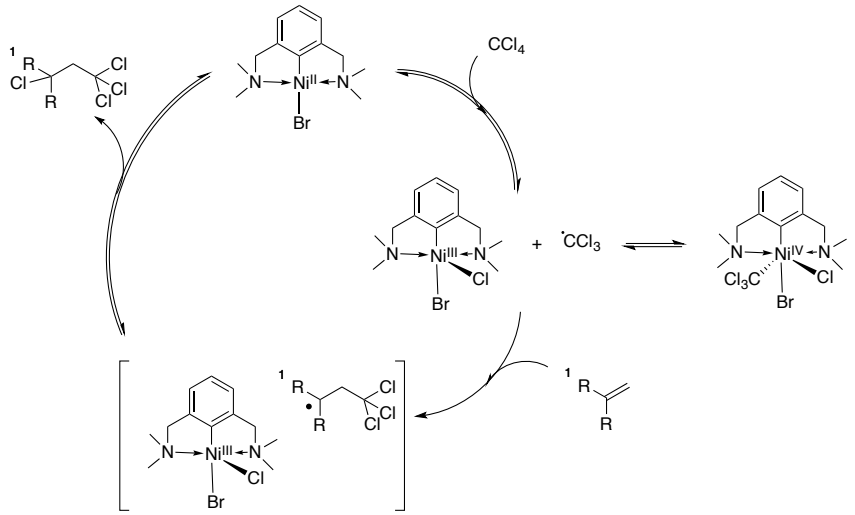

Schéma 1.15. Mécanisme proposé pour l'addition de Kharasch catalysée par le Ni^{II}.

La première étape de ce cycle consiste en l'activation du CCl_4 et le transfert d'un Cl radicalaire vers un centre métallique formant ainsi un complexe de Ni^{III} et un fragment radicalaire CCl_3. Ces derniers sont en équilibre avec un complexe de Ni^{IV}. Vient ensuite la réaction de couplage entre l'alcène et le fragment CCl_3 radicalaire, cette réaction est l'étape limitante. Finalement, le transfert d'un Cl forme le produit désiré et régénère le catalyseur.[23]

Notre groupe a aussi démontré la capacité du squelette pinceur à stabiliser des complexes de nickel trivalents. Deux complexes de Ni^{III} basé sur des ligands de type $POC_{sp}{}^3OP$, $PC_{sp}{}^3P$ et $POC_{sp}{}^2N$ ont pu être isolés et caractérisés.[24]

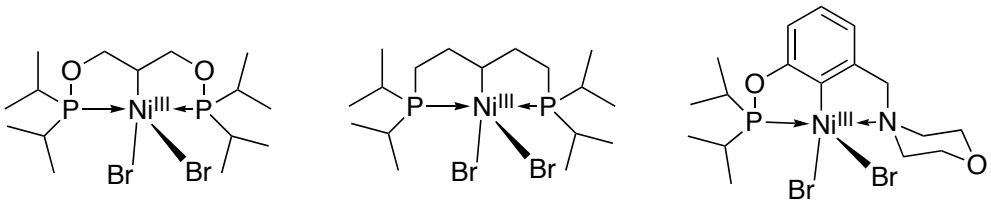

Figure 1.3. Complexes de Ni^{III} $POC_{sp}{}^3OP$, $PC_{sp}{}^3P$ et $POC_{sp}{}^2N$

En examinant les cyclovoltampérogrammes des complexes ci-dessus on remarque que l'oxydation du complexe $PC_{sp}{}^3P$ est la plus facile suivi du complexe $POC_{sp}{}^3OP$ et finalement du $POC_{sp}{}^2N$. Pourtant les complexes $POC_{sp}{}^3OP$ et $PC_{sp}{}^3P$ décomposent en solution à température pièce alors que le complexe de type $POC_{sp}{}^2N$ est stable dans ces conditions. Ce n'est donc pas parce que la synthèse d'un complexe de Ni^{III} est favorable thermodynamiquement qu'il sera stable cinétiquement.

Un étonnant complexe de Ni^{III} tricoordiné a été synthétisé par Tilley et son groupe. Ce complexe est obtenu de la réaction entre un complexe de Ni^{I} et de l'iodure de méthyle (CH_3I), constituant ainsi un exemple rare d'addition oxydante à partir d'un nickel monovalent bien défini.

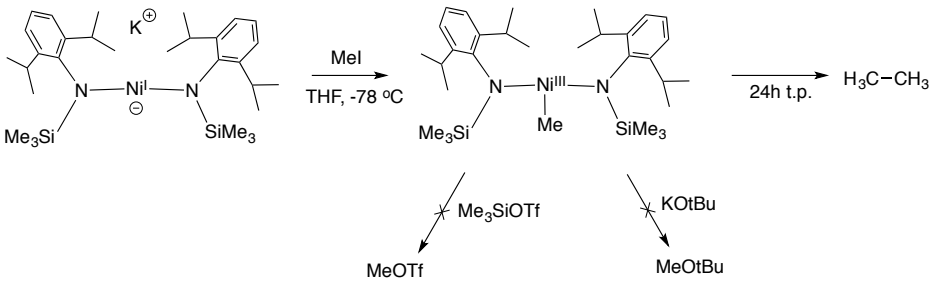

Schéma 1.16. Synthèse d'un complexe de Ni^{III} à partir de l'addition oxydante de MeI sur un Ni^{I} et sa décomposition en éthane.

Le complexe obtenu est de configuration électronique bas-spin d^7 et de géométrie en « T ». Il n'est pas stable en solution à température ambiante et génère de l'éthane en décomposant. Toutes tentatives de couplage entre le ligand méthyle et des électrophiles pour former des liens C-O sont sans succès. Il est aussi inerte face à des solutions d'halogénure comme Cl^-, Br^- et I^- indiquant que l'addition oxydante est irréversible.[25]

La formation d'éthane a aussi été étudiée par Mirica et son groupe. Ses études démontrent qu'un complexe de type $Ni^{II}(Me)_2$ forme de l'éthane de façon lente avec un rendement très faible.[26]

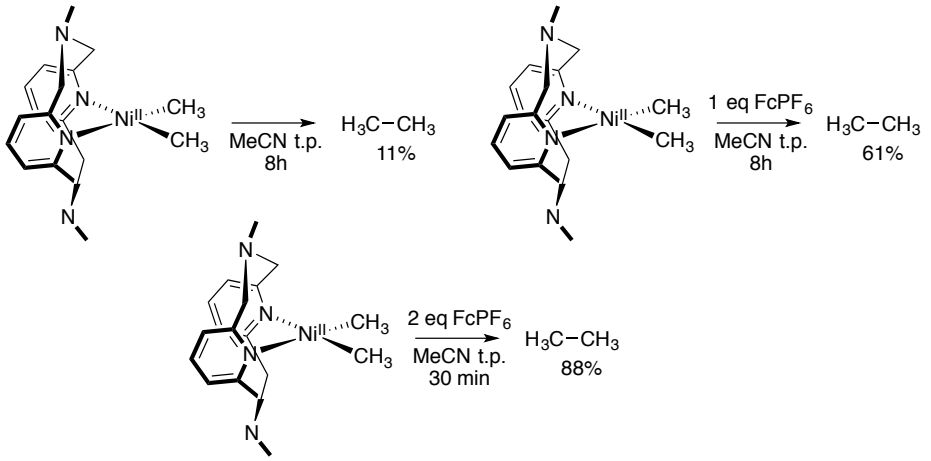

Schéma 1.17. Formation d'éthane à partir d'un complexe de Ni^{II} avec et sans oxydant externe

La cyclovaltampérométrie du complexe de Ni^{II} révèle montre un potentiel d'oxydation autour de -1.5 V par rapport au couple ferrocène/ferrocénium (Fe^{II}/Fe^{III}) signifiant qu'il est possible d'oxyder chimiquement le complexe à l'aide du ferrocénium ($FcPF_6$). En traitant le complexe de Ni^{II} avec 1 équivalent de $FcPF_6$ il est donc possible d'obtenir de l'éthane avec un rendement amélioré de 61% pour un temps de réaction similaire. Cependant, l'addition de 2 équivalents d'oxydant génère de l'éthane en seulement 30 minutes. Ceci soulève la possibilité qu'un intermédiaire de Ni^{IV} soit responsable de l'élimination réductrice. Afin de tester cette hypothèse, les auteurs ont pu isoler le complexe de Ni^{III} cationique et tester la formation d'éthane à partir de celui (schéma 1.18).

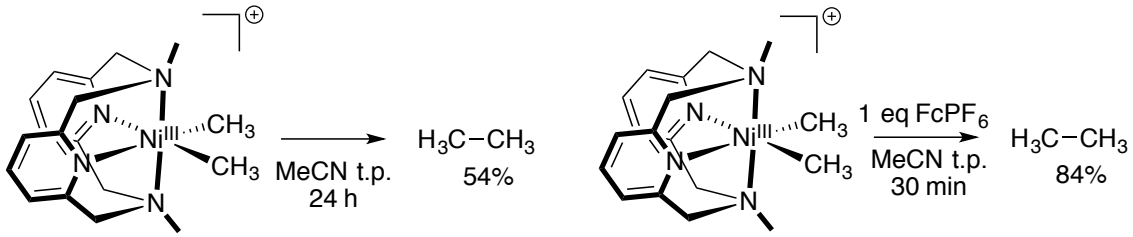

Schéma 1.18. Formation d'éthane à partir d'un complexe de Ni^{III} avec et sans oxydant externe

Le complexe de Ni^{III} cationique obtenu génère de l'éthane sans oxydant externe (54%, 24 h) et 84 % en 24 h avec oxydation. Une expérience faisant réagir une quantité équimolaire de $Ni^{II}(CH_3)_2$ et son isotopologue $Ni^{II}(CD_3)_2$ mène à la formation de CH_3CH_3, CH_3CD_3 et CD_3CD_3 dans des proportions de 1 :1 :1. Ces observations combinées mènent les auteurs aux 2 propositions mécanistiques illustrées au schéma 1.19. Le rendement de 54% obtenu lorsque l'on effectue la réaction à partir d'un complexe de Ni^{III} et un mélange d'éthane deutérée et non deutérée suggère le transfert lent d'un groupement méthyl radical pour former un complexe de Ni^{IV} dans lequel un des bras est décoordiné. Lorsque l'on utilise 2 équivalents (Schéma 1.19 bas) la réaction est rapide et le rendement supérieur à 50% (88%). De plus les expériences isotopiques montrent majoritairement CH_3CH_3 et CD_3CD_3 et très peu de CH_3CD_3 indiquant l'absence de transfert de méthyl radicalaire. Ces expériences ouvrent la possibilité qu'un complexe de Ni^{III} bien défini puisse disproportionner en Ni^{II} et Ni^{IV} et que le couplage provienne de ce dernier.

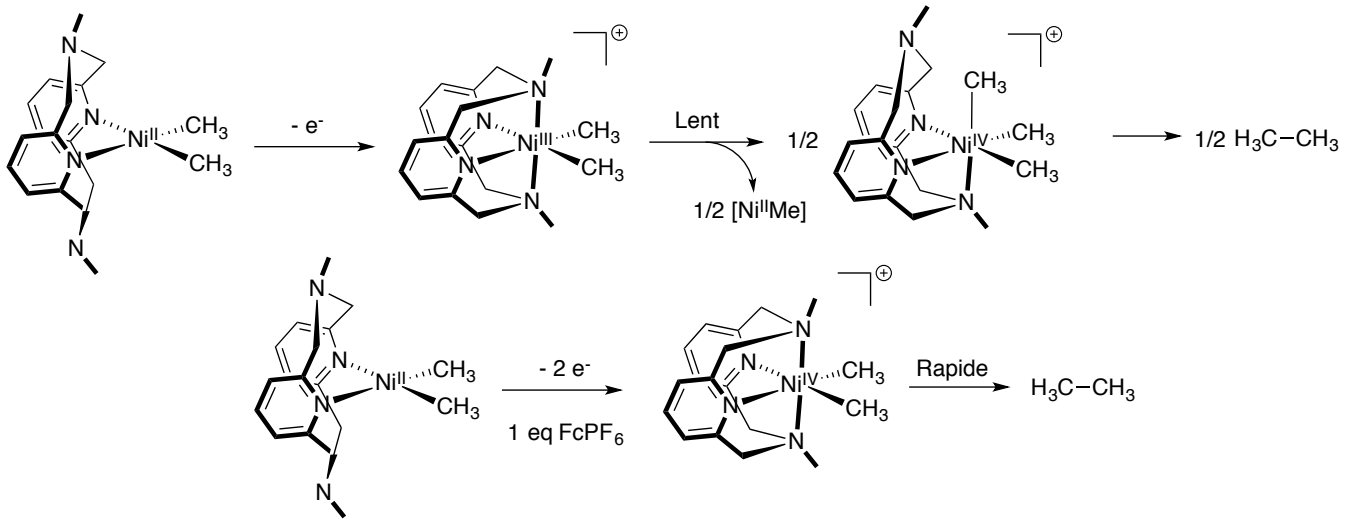

Schéma 1.19. Mécanisme de formation d'éthane à partir de l'oxydation d'un Ni^{II} à 1 et 2 électrons.

Un autre exemple de couplage C-C à partir d'un complexe de Ni^{III} isolé et complètement caractérisé provient du groupe Sanford. [27] Ce travail montre qu'un complexe de Ni^{III} est capable de promouvoir des couplages plus difficiles comme le couplage entre un groupement trifluorométhyle et un groupement aryle. Le schéma 1.20 montre la synthèse d'un complexe de nickel divalent contenant un groupement trifluorométhyle et un groupement aryl en Ni^{III} à l'aide d'$AgBF_4$ et sa décomposition en trifluorométhylbenzène.

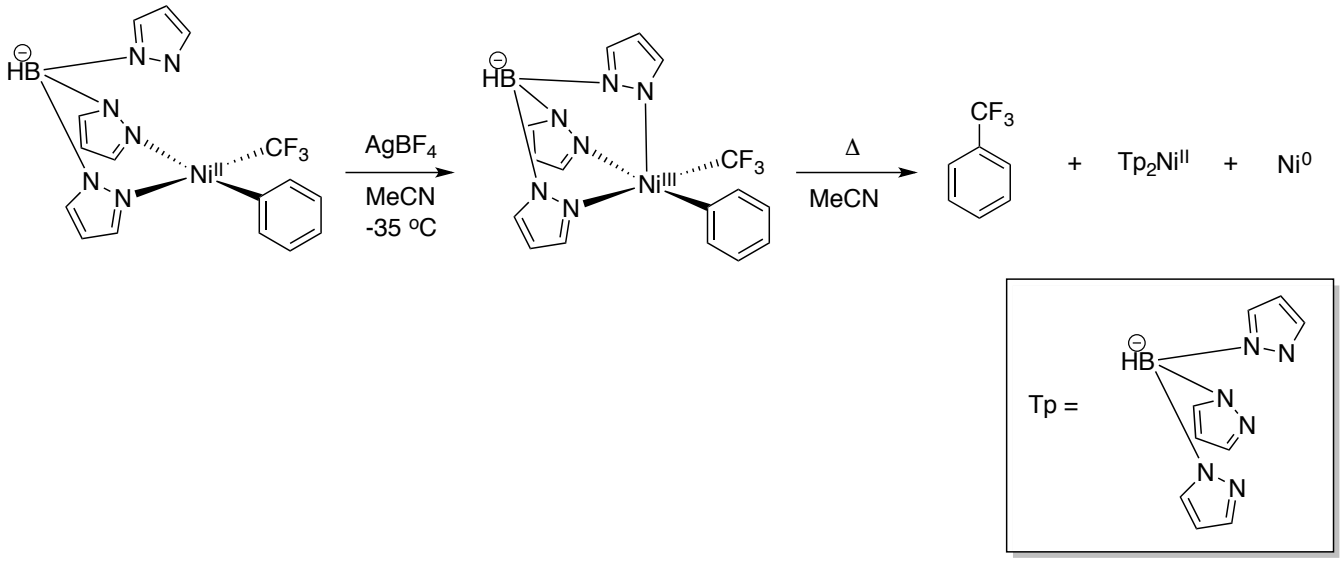

Schéma 1.20. Synthèse d'un complexe de Ni^{III} et formation d'un lien C-C à partir de ce dernier

Le rendement en trifluorométhylbenzène est de 47% à température ambiante et 59% à 80 °C. L'article entrevoie 3 possibilités mécanistiques pour expliquer la formation du produit.

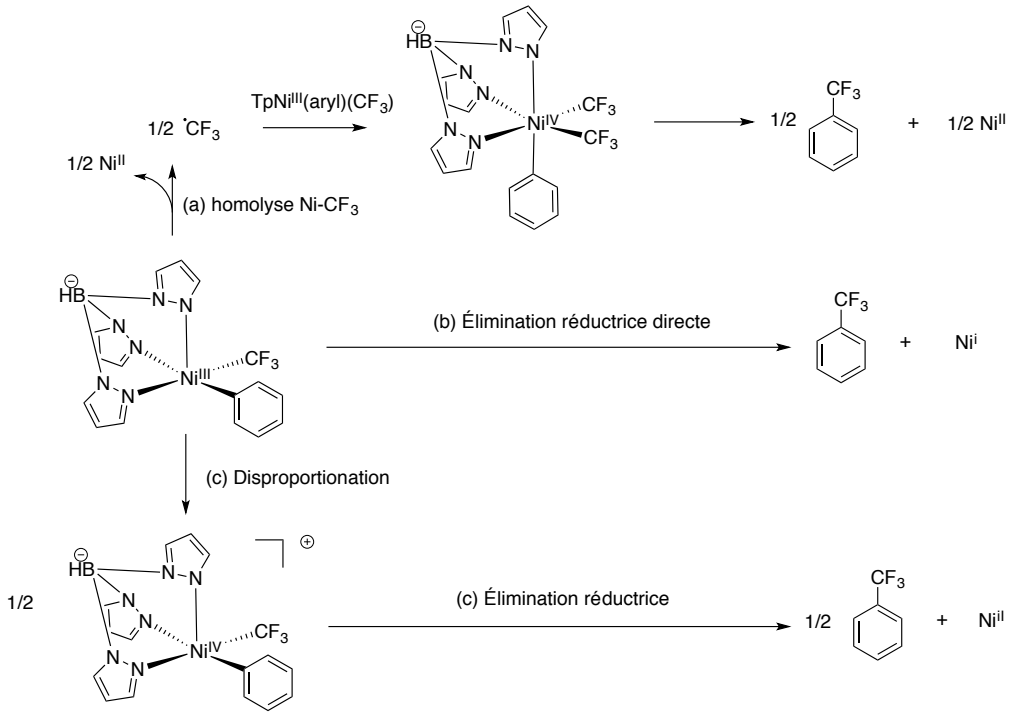

Schéma 1.21. Possibilités mécanistiques pour la formation de trifluorométhylbenzène

D'abord, de façon similaire à Mirica pour la formation d'éthane, la première voie (a) propose le clivage homolytique du lien Ni^{III}-CF_3 générant ainsi un demi équivalent de Ni^{II}(aryl) et un demi équivalent de CF_3 radicalaire. Ce dernier réagit avec le composé de départ restant pour générer un complexe de Ni^{IV} qui subit une élimination réductrice formant le produit désiré et du Ni^{II} avec un rendement maximal de 50%. La voie (b) propose l'élimination réductrice directement du complexe de Ni^{III} de départ. Ceci génère un rendement maximum de 100% ainsi que du Ni^{I} comme sous-produit. Finalement la voie (c) propose une réaction de disproportionation bimoléculaire de deux Ni^{III} en Ni^{II} et Ni^{IV}. Le complexe de Ni^{IV} génère ensuite le produit attendu par élimination réductrice. Une expérience faisant intervenir un piège à radicaux (TEMPO) montre que le chauffage du complexe de départ ne génère pas de CF_3 radicalaire en solution et que la présence du piège ne diminue pas le rendement. La voie (c) est aussi examinée en déterminant le potentiel redox du complexe trivalent de départ. La CV montre un potentiel d'oxydation de 0.35 V par rapport au ferrocène, indiquant que l'état d'oxydation IV est atteignable en utilisant par exemple $NOBF_4$ (0.84 V par rapport au ferrocène). L'oxydation chimique du complexe de départ mène bien à la formation du trifluorométhylbenzène avec un rendement de 50%. Cependant le mélange réactionnel de la réaction

original (Schéma 1.20) ne contient pas d'oxydants externes, la seule façon de générer le Ni^{IV} est par réaction de disproportionation illustrée ci-dessous.

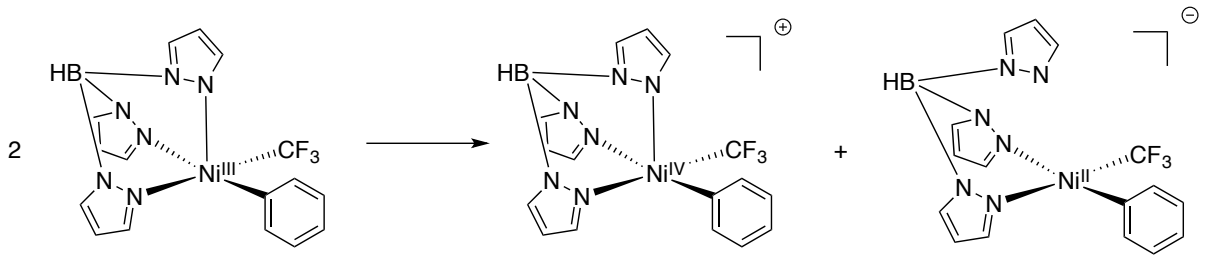

Schéma 1.22. Disproportionation de Ni^{III} en Ni^{II} et Ni^{IV}

Un suivi cinétique indique cependant que l'ordre réactionnel du Ni^{III} est de 1. Il est donc peu probable que cette voie soit celle qui prévaut. La voie (b) indique que le rendement maximal est de 100% ce qui ne semble pas être le cas expérimentalement avec un rendement observé de 59%. Les auteurs expliquent ce détail en indiquant avec justesse que le Ni^{I} engendré par l'élimination réductrice peut produire des réactions secondaires faisant diminuer le rendement. La réaction effectuée en présence d'oxydant plus doux (incapable de générer du Ni^{IV}) fait d'ailleurs augmenter le rendement de façon considérable en réagissant avec le Ni^{I} produit et en empêchant les réactions secondaires. Contrairement à l'étude précédente dans laquelle on proposait un intermédiaire de Ni^{IV} pour expliquer la formation d'un lien C-C, l'article privilégie un Ni^{III}.

Plus tôt dans cette introduction, un système photocatalytique pouvant former des liens C-O a été présenté. Le mécanisme proposé pour ce couplage fait intervenir un complexe de Ni^{III} sans toutefois l'isoler. D'autres travaux permettent cependant de démontrer que cet état d'oxydation est bel est bien capable d'engendrer ce genre la formation de lien C-O. Mirica et al. ont démontré qu'il est possible de former des liens C-O à partir d'un Ni^{III} semblable à celui décrit pour la formation d'éthane vu plus haut.[28] Les auteurs préparent à cet effet deux complexes de Ni^{III}, un cationique et l'autre dicationique, dans lesquels un des ligands pyridine est remplacé par un groupement aryle, remplaçant ainsi un lien N-Ni par un lien anionique C-Ni. Le schéma suivant décrit les deux synthèses.

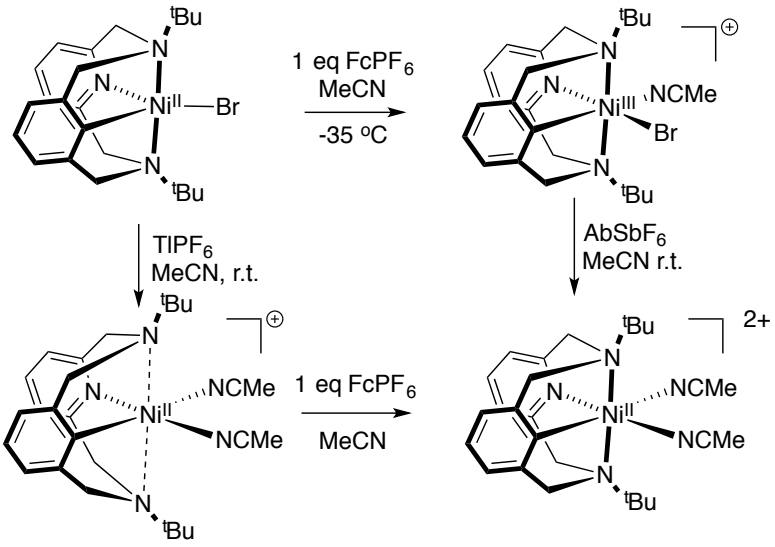

Schéma 1.23. Synthèse de complexes cationique et dicationique de Ni^{III}

Le complexe de Ni^{II} de départ peut facilement être oxydé par ferrocénium. Cette réaction génère un Ni^{III} cationique de géométrie octaédrique. La RPE du complexe confirme la présence d'un électron non-apparié dans l'orbitale d_z^2 puisqu'il est possible d'observer un couplage hyperfin avec les atomes d'azotes dans la direction g_z. Il est aussi possible d'obtenir un complexe de Ni^{III} dicationique par deux voies synthétiques différentes. La première consiste d'abord en l'abstraction d'un ligand bromure par un complexe de thallium. Ceci génère un Ni^{II} cationique pour lequel les auteurs attribuent une géométrie carrée plane dans laquelle le centre métallique présente une faible interaction avec les bras azotés. Cette affirmation est appuyée par la nature diamagnétique du complexe, un complexe octaédrique serait normalement paramagnétique avec une valeur de S = 1 et un état fondamental triplet. L'oxydation de ce complexe produit un complexe de Ni^{III} dans lequel le centre métallique possède une charge formelle de +2. Le complexe présente une géométrie octaédrique et la RPE confirme qu'il s'agit d'un complexe ne possédant qu'un seul électron non-apparié dans la direction g_z (direction des bras azotés) et donc un état fondamental doublet (S = ½). Afin de tester la formation de lien C-O, le complexe de Ni^{III} dicationique est traité avec 4 équivalents de NaOMe afin d'obtenir un complexe de Ni^{III} dans lequel le ligand méthanolate est en position cis par rapport au carbone lié au nickel. Cette position est optimale pour engendrer l'élimination réductrice qui fonctionnalisera le ligand et formera le lien C-O attendu.

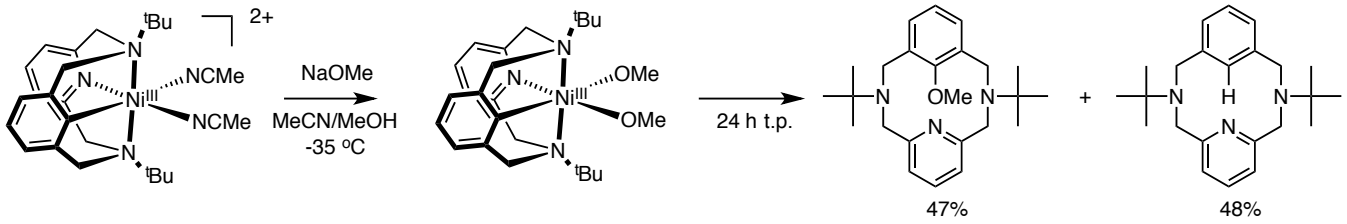

Schéma 1.24. Synthèse de complexes Ni^{III} de type alkoxy et formation d'un lien C-O

Le complexe alkoxy de Ni^{III} a pu être caractérisé par diffraction des rayons-X et RPE. Il est cependant instable en solution à température et décompose en produits indiqués dans le schéma 1.24. La présence de ligand non fonctionnalisé s'explique par une réaction d'élimination β-hydrure provenant du ligand méthoxy générant aussi formaldéhyde. Les auteurs remarquent aussi que l'usage d'un excès de NaOMe et/ou l'ajout d'un oxydant externe augmentent les rendements, diminuent le temps de réaction et limite la réaction secondaire d'élimination β-hydrure. Ils arrivent à la proposition mécanistique suivante.

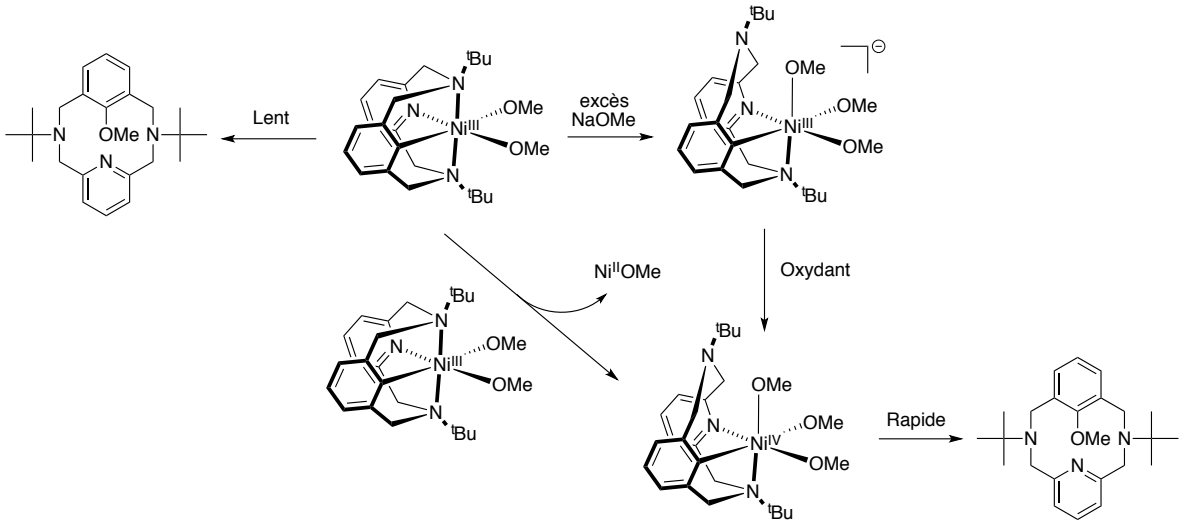

Schéma 1.25. Mécanisme de formation d'un lien C-O à partir d'un Ni^{III} alkoxy

En l'absence d'oxydant externe, le complexe de Ni^{III} alkoxy peut soit générer le produit fonctionnalisé de façon lente ou subir une réaction de disproportionation lente générant un Ni^{II} et un Ni^{IV}. L'ajout d'un excès combiné à un oxydant externe génère un complexe de Ni^{IV} favorisant l'élimination réductrice C-O et la formation rapide du produit.

Comme mentionné précédemment, l'addition oxydante de lien C-halogène sur des précurseurs de Ni^{0} est chose commune. La réaction inverse est cependant rarement observée et il faut oxyder le Ni^{II} en

Ni^{III} pour voir se former un lien C-halogène. Mirica offre ici un exemple de complexe de Ni^{III} authentique pouvant promouvoir la formation de lien C-Br.[29]

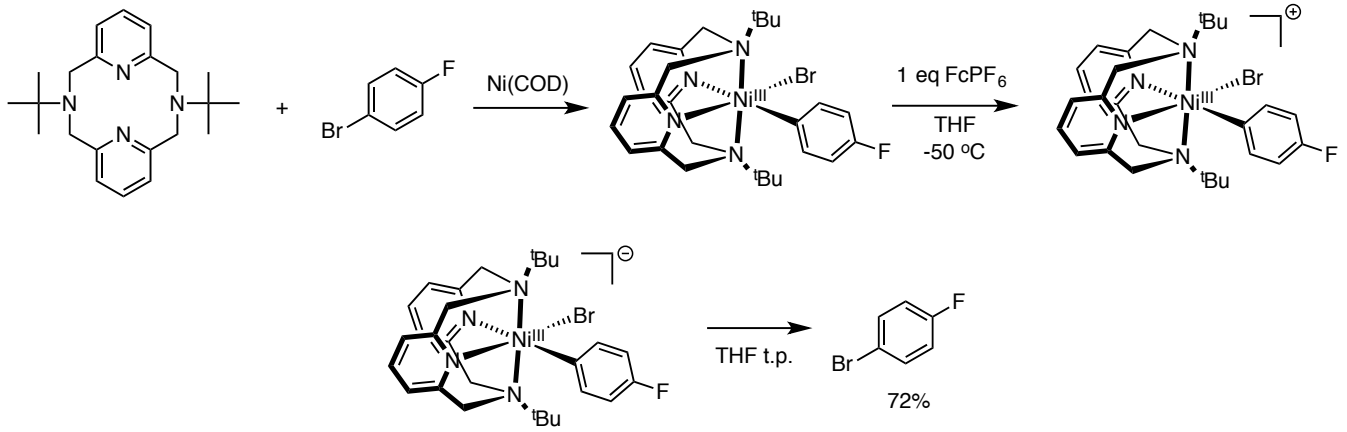

Schéma 1.26. (haut) Formation d'un Ni^{II} à partir de l'addition oxydante d'un lien C-Br et oxydation en Ni^{III}. (bas) Formation du lien C-Br par élimination réductrice

La synthèse du complexe de Ni^{II} se fait par l'addition oxydante du 1,4-bromofluorobenzène sur un précurseur de Ni^0. Le complexe ainsi obtenu est de configuration électronique d^8 paramagnétique de géométrie octaédrique. L'oxydation de ce dernier génère un complexe de Ni^{III} cationique d^7 avec son électron non-apparié localisé principalement dans une orbitale à caractère d. Lorsque laissé en solution à température pièce, il décompose en générant 1,4-bromofluorobenzène. Le complexe est aussi capable de catalyser la réaction de Kumada lorsque traité avec un réactif de Grignard et un iodure d'aryle. Cette dernière observation vient appuyer l'idée que le mécanisme de Kumada passe par l'intermédiaire d'un Ni^{III}.

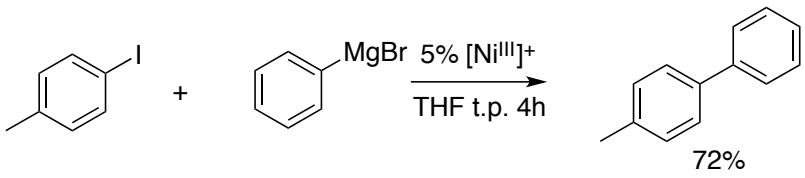

Schéma 1.26 Réaction de Kumada catalysée par un Ni^{III} cationique.

1.4 Complexes de Ni^{IV} isolés et formation de lien C-C et C-hétéroatomes

Les exemples de complexes de Ni^{IV} contenant un lien Ni-C sont très rares malgré qu'ils soient souvent proposés comme intermédiaire dans les réactions de couplage C C. Récemment, 2 exemples de Ni^{IV} ont été isolés par le groupe de Mélanie Sanford. Ces travaux mettent en lumière la capacité qu'ont ces complexes à former des liens C-C, C-O, C-S et C-N. [30] Le premier exemple est un Ni^{IV} cationique synthétisé à partir de l'oxydation à 2 électrons d'un précurseur de Ni^{II} par une source de CF_3^+. Le complexe obtenu est un octaèdre diamagnétique possédant la configuration électronique d^6 et il est singulet à l'état fondamental.

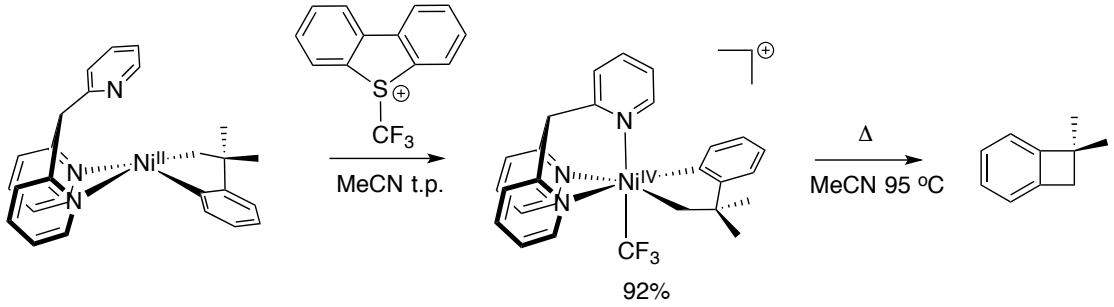

Schéma 1.27 Synthèse d'un complexe de Ni^{IV} cationique par une oxydation à 2 électrons

Lorsque chauffé à 95 °C pendant 7 heures, le ligand subit une élimination réductrice pour former le benzocyclobutane. Cette réactivité constitue un rare exemple de formation de lien C_{sp}^2-C_{sp}^3. Le complexe est aussi capable de générer des liens C-O lorsque traité avec un nucléophile comme acétate (schéma 1.28).

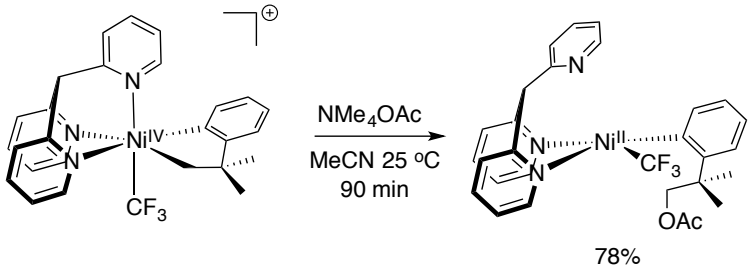

Schéma 1.28 Formation d'un lien C-O à partir de d'une attaque nucléophilique sur un carbone sp^3

Les tentatives de couplage avec de meilleurs nucléophiles comme $^{-}$OPh et $^{-}$SPh mènent à des mélanges réactionnels compliqués. Les auteurs proposent que la charge positive du complexe de Ni^{IV} cationique rend le centre métallique très électrophile causant ainsi des réactions secondaires indésirables et proposent la synthèse d'un complexe de Ni^{IV} neutre pour pallier à cet effet (schéma 1.19).

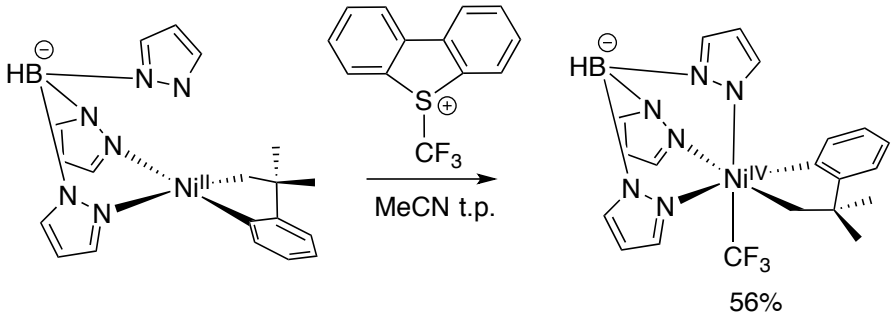

Schéma 1.29. Synthèse d'un complexe de Ni^{IV} neutre par une oxydation à 2 électrons

Le complexe ainsi obtenu est diamagnétique, de configuration électronique d^6 et singulet à l'état fondamental. Sa réactivité face à différents nucléophiles est illustrée au schéma suivant.

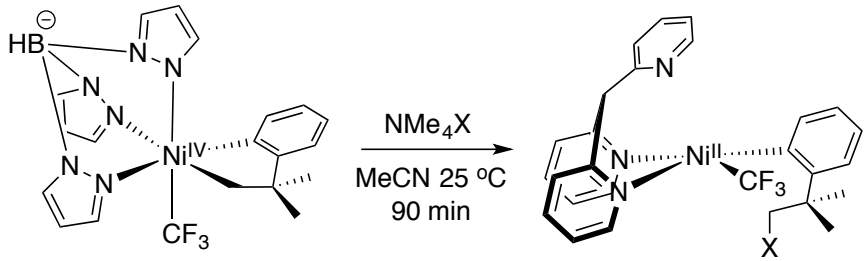

X = OPh (78%), SPh (94%), (Me)N(O_2SMe) (90%)

Schéma 1.30. Formation de liens C-O, C-S et C-N à partir de d'une attaque nucléophilique sur un carbone sp^3

Le nouveau complexe obtenu est capable de former de liens C-O, C-S et C-N avec de très bons rendements. Des expériences mécanistiques indiquent un processus de type S_N2, c'est-à-dire une attaque nucléophile directement sur le carbone sp^3. En effet, des expériences cinétiques montrent un ordre de 1 en complexe de Ni^{IV} et 1 pour le nucléophile tel qu'attendu pour un processus bimoléculaire. Un graphique de type Swain-Scott montre une relation linéaire entre la vitesse de réaction et la nucléophilie du substrat, c'est-à-dire qu'un meilleur nucléophile réagit plus rapidement.

Le dernier exemple provient de l'équipe de Nicolas Mézailles qui sont parvenu à isoler un complexe de Ni^{IV} par l'oxydation d'un Ni^{II} avec du difluorure de Xénon, une source de F_2.[31]

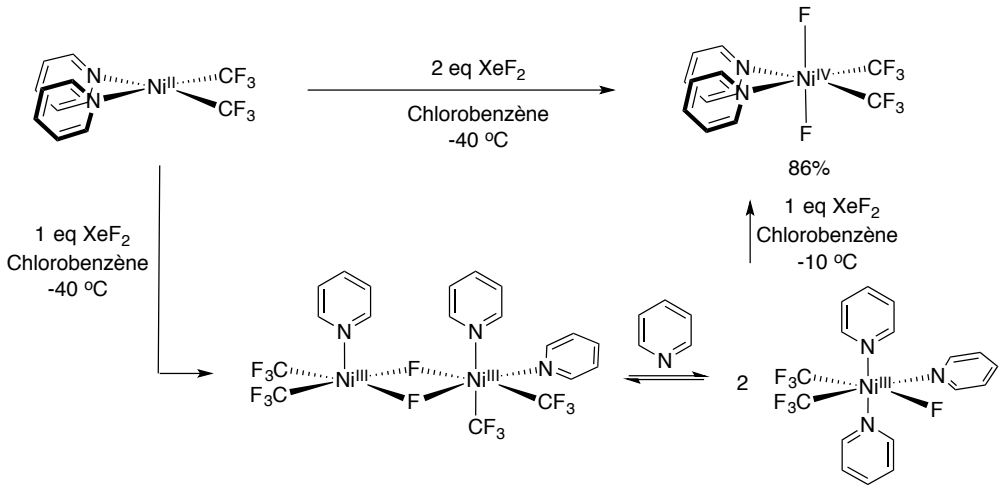

Schéma 1.31. Formation d'un complexe de Ni^{IV} (haut) directement à partir d'un complexe de Ni^{II} (bas) par l'entremise d'un complexe de Ni^{III}

L'apparition et la disparition subséquente d'une couleur rouge-violet lorsque le complexe de départ est traité avec 1 équivalent de XeF_2 laisse croire à la présence transitoire d'une espèce Ni^{III}. Les auteurs ont en effet pu isoler un tel complexe (schéma 1.31 bas). Ce dimère est un Ni^{III} de géométrie bipyramide à base carrée et un centre octaédrique. Des mesures en RPE montre que le complexe est paramagnétique donc les deux électrons non-appariés sont à l'état triplet. Leurs travaux démontrent qu'en traitant le complexe de Ni^{IV} avec 1,2-dichlorobenzène permet l'activation d'un des liens C-H et l'installation d'un groupement trifluorométhyle avec d'excellents rendements.

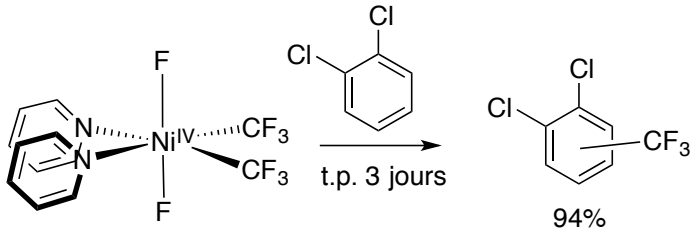

Schéma 1.32. Trifluorométhylation d'un lien C-H

Un suivi cinétique de la réaction illustrée au schéma 1.32 montre que la formation du produit trifluorométhylé suit deux régimes.

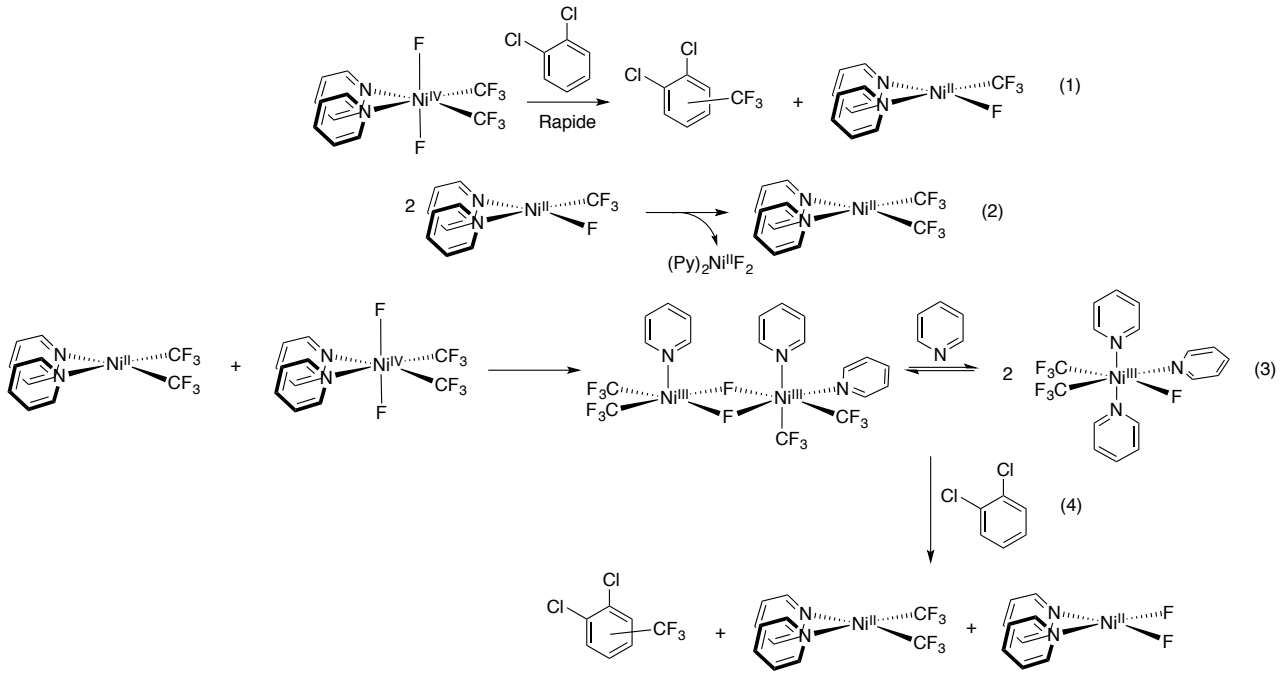

Schéma 1.33 Formation d'un complexe de Ni^{IV} (haut) directement à partir d'un complexe de Ni^{II} (bas) par l'entremise d'un complexe de Ni^{III}

D'abord il y a formation rapide du produit désiré directement à partir du Ni^{IV} jusqu'à l'atteinte d'un plateau équivalent à un rendement d'environ 60%. L'étape (1) génère aussi un complexe de $Ni^{II}(F)(CF_3)$ qui peut subir une rédistribution de ligands pour générer un $Ni^{II}(F)_2$ et un $Ni^{II}(CF_3)_2$. La réaction qui suit consiste en la comproportionation d'un Ni^{II} et d'un Ni^{IV} pour générer le dimère de Ni^{III} discuté précédemment. Ce dernier réagit de façon lente avec le substrat organique pour former le produit désiré et un demi équivalent de chaque complexe de Ni^{II} illustré. Les auteurs ont aussi constaté que le complexe de Ni^{IV} de départ décompose en 2 jours générant de la pyridine trifluorométhylée. Cette étude illustre bien qu'il n'est pas suffisant d'avoir un précurseur de Ni^{II} avec un centre métallique riche en densité électronique et facile à oxyder. Il est possible d'imaginer que l'échange des deux groupements trifluorométhyles par des méthyles ferait diminuer le potentiel d'oxydation du complexe. Il est aussi important de limiter les voies de décomposition cinétique. Ici, l'élimination réductrice F-CF_3 n'est pas favorisée cinétiquement et la formation de pyridine-CF_3 est lente.

En résumé, les complexes de nickel à haute-valence sont souvent proposés dans les mécanismes de réaction de couplage C-C, C-O et C-N. Leur tendance naturelle face à l'élimination réductrice et leur propension aux réactions de type SET font en sorte qu'ils sont souvent difficiles à isoler. L'utilisation de

ligands azotés, bons donneurs σ, peut stabiliser ce type de complexe. Bien-sûr l'oxydation du précurseur de Ni^{II} doit être favorable thermodynamiquement et la cyclovoltampérométrie est un outil efficace qui permet la sélection judicieuse de l'oxydant à utiliser. Les complexes de Ni^{III} et Ni^{IV} sont particulièrement susceptibles aux réactions d'élimination réductrice et aux processus redox à un électron. Le mécanisme de formation de liens C-hétéroatomes à partir de ces complexes soulève, de façon générale, les questions suivantes. D'abord quel est l'état d'oxydation du nickel responsable de la formation du lien puisqu'il existe des exemples avec Ni^{II}, Ni^{III} et Ni^{IV}. Ensuite, a-t-on affaire à une élimination réductrice telle que proposée par Mirica ou bien à un processus ayant lieu dans la seconde sphère de coordination du métal comme le démontre les travaux sur le Ni^{IV} de Mélanie Sanford? Finalement quel est le sort du fragment métallique résultant de l'élimination réductrice, est-il impliqué dans des réactions subséquentes comme dans les études sur le couplage C-C de Sanford et al. et les travaux sur le Ni^{IV} menés par Mézailles et son groupe?

1.5 Objectifs de la thèse

Cette thèse propose dans un premier lieu la synthèse d'une nouvelle famille de complexes de type pinceur basée sur un ligand pyrazole par activation C-H. Ces nouveaux complexes sont complètement caractérisé par spectroscopie RMN, diffraction des rayons-X et UV-visible. Ils sont ensuite traités avec différents oxydants afin de tenter d'isoler de nouveaux complexes haut-valent bien définis.

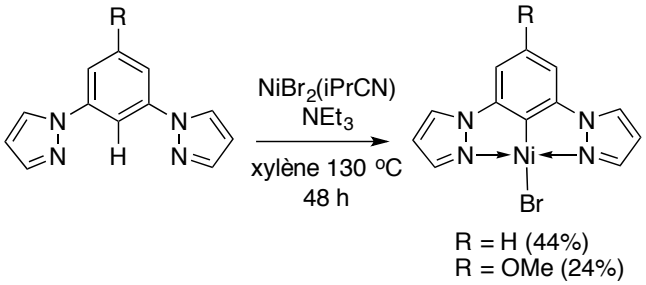

Schéma 1.34. Synthèse de complexes pinceurs par activation de lien C-H

Les tentatives d'oxydation n'ont pu permettre l'isolation d'un authentique complexe de Ni^{III} cependant les complexes démontrent la capacité de former de liens C-O et C-N lorsqu'ils sont traités avec certains alcools et amines en condition aérobique donc oxydante.

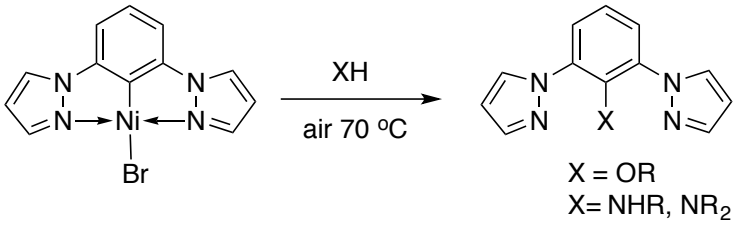

Schéma 1.35. Formation de liens C-O et C-N à partir du complexe de Ni^{II} à l'air

La réaction illustrée au schéma 1.35 demande la présence d'oxygène afin de fonctionner indiquant la possible participation d'un intermédiaire de Ni^{III} dans le mécanisme. Une étude mécanistique détaillée de cette réaction est difficile puisque les tentatives d'isoler un Ni^{III} à partir de ce complexe furent sans succès. Il faut donc se tourner vers le ligand NCN mis sur pied par van Koten puisque celui-ci stabilise les complexes de nickel trivalent. Il offre donc la possibilité d'étudier le mécanisme de fonctionnalisation du ligand directement à partir d'un complexe de Ni^{III}.

Le chapitre 3 est donc consacré à l'étude de la formation de lien C-O, C-N et C-halogène à partir du complexe $(NCN)Ni^{III}Br_2$. À l'image du complexe de Ni^{II} présenté au chapitre 2, le complexe de Ni^{III} réagit avec les alcools et les amines pour former d'abord un complexe de type alkoxy ou amidure pour ensuite subir une élimination réductrice avec le ligand et former le lien désiré. Contrairement aux réactions partant de Ni^{II}, les réactions de fonctionnalisation à partir de Ni^{III} peuvent être effectués sous azote puisque l'oxydation n'est pas nécessaire. Le chapitre propose un mécanisme basé sur plusieurs expériences pertinentes.

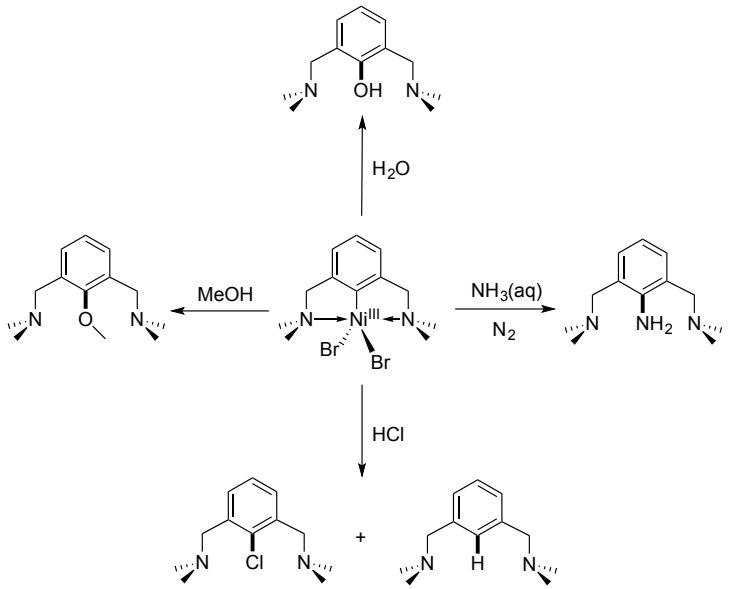

Schéma 1.36. Formation de liens C-O, C-N et C-Cl à partir du complexe de Ni^{III}

Tel que proposé au chapitre 2, la réaction de fonctionnalisation du ligand à partir du pinceur de Ni^{II} en condition aérobique requiert l'oxydation de celui-ci par O_2. Cette oxydation doit former en principe un Ni^{III} cationique tel qu'illustré au schéma 1.37. Afin de tester cette hypothèse, le chapitre 4 propose la synthèse, caractérisation et réactivité de nouveaux complexes NCN de Ni^{III} cationiques et dicationiques.

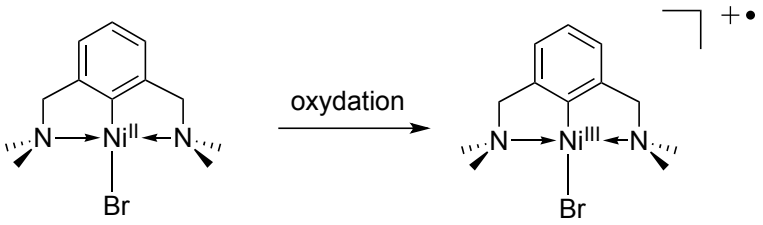

Schéma 1.37. Oxydation du Ni^{II} en Ni^{III} cationique

Ce volet de la thèse montre la synthèse de complexes analogues et leur réactivité face au méthanol et à la méthylamine. On y fait plusieurs observations expérimentales qui sont appuyées par des calculs D.F.T. Les calculs confirment certaines hypothèses mécanistiques émises auparavant et mettent en lumière de nouveaux aspects importants au sujet de la réactivité observée.

1.6 Références

[1] (a) Rosen, B. M.; Quasdorf, K. W.; Wilson, D. A.; Zhang, N.; Resmerita, A.-M.; Garg, N. K.; Percec, V. *Chem. Rev.* **2011**, *111* (3), 1346–1416. (b) Ruiz-Castillo, P.; Buchwald, S. L. *Chem. Rev.* **2016**, *116* (19), 12564–12649.

[2] Corriu, R. J. P.; Masse, J. P. *J. Chem. Soc., Chem. Commun.* **1972**, *0* (3), 144a-144a.

[3] Tamao, K.; Sumitani, K.; Kumada, M. *J. Am. Chem. Soc.* **1972**, *94* (12), 4374–4376.

[4] Heck, R. F. *J. Am. Chem. Soc.* **1969**, *91* (24), 6707–6714.

[5] King, A. O.; Okukado, N.; Negishi, E. *J. Chem. Soc., Chem. Commun.* **1977**, *0* (19), 683–684.

[6] Miyaura, N.; Yamada, K.; Suzuki, A. *Tetrahedron Letters* **1979**, *20* (36), 3437–3440.

[7] Knappke, C. E. I.; Wangelin, A. J. von. *Chem. Soc. Rev.* **2011**, *40* (10), 4948–4962.

[8] Sehnal, P.; Taylor, R. J. K.; Fairlamb, I. J. S. *Chem. Rev.* **2010**, *110* (2), 824–889.

[9] Smith, K. M. *Organometallics* **2005**, *24* (5), 778–784.

[10] Hu, X. *Chem. Sci.* **2011**, *2* (10), 1867–1886.

[11] Tsou, T. T.; Kochi, J. K. *J. Am. Chem. Soc.* **1979**, *101* (25), 7547–7560.

[12] Jones, G. D.; Martin, J. L.; McFarland, C.; Allen, O. R.; Hall, R. E.; Haley, A. D.; Brandon, R. J.; Konovalova, T.; Desrochers, P. J.; Pulay, P.; et al. *J. Am. Chem. Soc.* **2006**, *128* (40), 13175–13183.

[13] (a) Koo, K.; Hillhouse, G. L. *Organometallics* **1995**, *14* (9), 4421–4423. (b) Han, R.; Hillhouse, G. L. *J. Am. Chem. Soc.* **1997**, *119* (34), 8135–8136. (c) Lin, B. L.; Clough, C. R.; Hillhouse, G. L. *J. Am. Chem. Soc.* **2002**, *124* (12), 2890–2891.

[14] Terrett, J. A.; Cuthbertson, J. D.; Shurtleff, V. W.; MacMillan, D. W. *Nature* **2015**, *524* (7565), 330–334.

[15] Higgs, A. T.; Zinn, P. J.; Simmons, S. J.; Sanford, M. S. *Organometallics* **2009**, *28* (21), 6142–6144.

[16] Iyanaga, M.; Aihara, Y.; Chatani, N. *J Org Chem* **2014**, *79* (24), 11933–11939.

[17] Haines, R. I.; McAuley, A. *Coordination Chemistry Reviews* **1981**, *39* (1–2), 77–119.

[18] Maki, A. H.; Edelstein, N.; Davison, A.; Holm, R. H. *J. Am. Chem. Soc.* **1964**, *86* (21), 4580–4587.

[19] Meek, D. W.; Alyea, E. C.; Stalick, J. K.; Ibers, J. A. *J. Am. Chem. Soc.* **1969**, *91* (17), 4920–4921.

[20] Grove, D. M.; Van Koten, G.; Zoet, R.; Murrall, N. W.; Welch, A. J. *J. Am. Chem. Soc.* **1983**, *105* (5), 1379–1380.

[21] van de Kuil, L. A.; Luitjes, H.; Grove, D. M.; Zwikker, J. W.; van der Linden, J. G. M.; Roelofsen, A. M.; Jenneskens, L. W.; Drenth, W.; van Koten, G. *Organometallics* **1994**, *13* (2), 468–477.

[22] Grove, D. M.; Van Koten, G.; Mul, P.; Zoet, R.; Van der Linden, J. G. M.; Legters, J.; Schmitz, J. E. J.; Murrall, N. W.; Welch, A. J. *Inorg. Chem.* **1988**, *27* (14), 2466–2473.

[23] van de Kuil, L. A.; Grove, D. M.; Gossage, R. A.; Zwikker, J. W.; Jenneskens, L. W.; Drenth, W.; van Koten, G. *Organometallics* **1997**, *16* (23), 4985–4994.

[24] (a) Castonguay, A.; Beauchamp, A. L.; Zargarian, D. *Organometallics* **2008**, *27* (21), 5723–5732. (b) Pandarus, V.; Zargarian, D. *Chem. Commun.* **2007**, 9 , 978–980. (c) Spasyuk, D. M.; Zargarian, D.; van der Est, A. *Organometallics* **2009**, *28* (22), 6531–6540.

[25] Lipschutz, M. I.; Yang, X.; Chatterjee, R.; Tilley, T. D. *J. Am. Chem. Soc.* **2013**, *135* (41), 15298–15301.

[26] Schultz, J. W.; Fuchigami, K.; Zheng, B.; Rath, N. P.; Mirica, L. M. *J. Am. Chem. Soc.* **2016**, *138* (39), 12928–12934.

[27] Bour, J. R.; Camasso, N. M.; Meucci, E. A.; Kampf, J. W.; Canty, A. J.; Sanford, M. S. *J. Am. Chem. Soc.* **2016**, *138* (49), 16105–16111.

[28] Zhou, W.; Schultz, J. W.; Rath, N. P.; Mirica, L. M. *J. Am. Chem. Soc.* **2015**, *137* (24), 7604–7607.

[29] Zheng, B.; Tang, F.; Luo, J.; Schultz, J. W.; Rath, N. P.; Mirica, L. M. *J. Am. Chem. Soc.* **2014**, *136* (17), 6499–6504.

[30] Camasso, N. M.; Sanford, M. S. Design, Synthesis, and Carbon-Heteroatom Coupling Reactions of Organometallic Nickel(IV) Complexes. *Science* **2015**, *347* (6227), 1218–1220.

[31] D'Accriscio, F.; Borja, P.; Saffon-Merceron, N.; Fustier-Boutignon, M.; Mézailles, N.; Nebra, N. *Angew. Chem. Int. Ed.* **2017**, *56* (42), 12898–12902.

Chapitre 2 : Synthesis and Reactivities of New NCN-Type Pincer Complexes of Nickel

Article 1

Jean-Philippe Cloutier, Boris Vabre, Berline Moungang-Soumé and Davit Zargarian*

Département de chimie, Université de Montréal, Montréal (Québec), Canada H3C 3J7

Organometallics **2015, *34* (1), 133–145.**

2.1 ABSTRACT

This report describes the preparation, characterization and reactivities of a new family of Ni(II) complexes based on the tridentate NCN-type pincer ligands 1,3-bis(pyrazole),5-R-C_6H_3 (R= H, OMe), which were prepared by Ullman coupling of 1,3-diiodobenzene or 1,3-dibromo,5-methoxy-benzene with pyrazole. Refluxing these ligands in xylene with (*i*-PrCN)$NiBr_2$ and NEt_3 gave the complexes (NCN^{pz})NiBr (**1**) and (MeO-NCN^{pz})NiBr (**2**) via C-H nickelation. The aryloxide derivative (NCN^{pz})Ni(OAr) (Ar= 2,6-*t*-Bu_2-4-Me-OC_6H_2), **3**, was prepared by treating the bromo precursor **1** with NaOAr, whereas the analogous reaction with NaOEt gave instead the protonated or ethoxy-functionalized ligand NC(H)N^{pz} (major) and NC(OEt)N^{pz} (minor). The new complexes **1-3** were fully characterized, including solid state structures. Attempted oxidation of these complexes failed to give the target trivalent derivatives, leading instead to intractable, deeply-colored Ni-containing solids, various ligand-derived side-products, or an unusual I_2 adduct. For example, treatment of **1** or **2** with *N*-bromosuccinimide gave sparingly soluble dark solids that appear to be paramagnetic, whereas **3** reacted with Br_2 to give short-lived dark intermediates that decomposed over seconds to give ArOH. Reaction of the bromo complexes with aq. H_2O_2 (30%) gave the functionalized ligands Br-NC(OH)N^{pz} and NC(OH)N^{pz} (from **1**) or MeO-NC(OH)N^{pz} (from **2**), whereas **1** reacted with I_2 to generate (NCN^{pz})NiBr·I_2, an iodine adduct displaying weak Br—I interactions. Heating **1** in EtOH in air generated NC(OEt)N^{pz}, and this ligand derivatization could be extended to other alcohols (MeOH, *i*-PrOH, CF_3CH_2OH) and amines (morpholine, cyclohexylamine, aniline). Possible mechanistic scenarios for the observed oxidative, Ni-promoted C_{ipso}-X bond formation reactions are discussed in the context of relevant literature precedents.

2.2 INTRODUCTION

Transition metal complexes featuring the NCN-type pincer ligands have proven to be highly versatile in diverse areas of applications, including catalysis and materials.[1] NCN ligands have also played a prominent role in the context of organonickel chemistry. For instance, a variety of mononuclear, divalent species (NCN)NiX or $[(NCN)NiL]^+$ are known to promote Heck type cross coupling[2] and Michael additions,[3] whereas polynuclear dendrimers composed of (NCN)Ni structural units have displayed important materials properties.[4] Another important characteristic of NCN ligands is their capacity to

stabilize trivalent nickel species that catalyze atom transfer radical additions and polymerizations.[5] Complexes featuring Ni(III)-C bonds are also of interest for the important roles they are believed to play in hydrocarbon oxidation,[6] various coupling reactions,[7] and in many bioinorganic and enzymatic reactions, including the C–H activation step involved in the anaerobic oxidation of methane by methanotrophic archaea.[8]

van Koten's group introduced the (NCN)Ni family of complexes in the early 1980's[9] and has driven most of the major developments in this area, including the elaboration of multiple synthetic routes for the preparation of a large variety of NCN-Ni complexes. The two main synthetic strategies employed for this purpose involve (a) oxidative addition of halogenated NCN ligands, NC(X)N (X= Br, I), to zerovalent nickel precursors, or (b) transmetallation of a lithiated ligand, NC(Li)N, first to Au(I) and then to a Ni(II).[9b, 10] While these the synthetic routes generally lead to good yields of the target (NCN)NiX complexes, they involve manipulation of air- and moisture-sensitive reagents (e.g., RLi, $Ni(COD)_2$) and require the use of elaborate (halogenated) pre-ligands and relatively expensive gold precursors. In contrast, a number of pincer-Ni compounds can be prepared more conveniently through direct C-H nickelation of the ligand by simple Ni(II) (e.g., PCP,[11] POCOP,[12] POCN,[13] PIMCOP[14]). Given many of the unique characteristics of NCN-Ni systems, it would be desirable to develop simple synthetic routes to this family of complexes involving a direct C-H nickelation strategy. Just such an approach was reported in 2011: the group of Gong and Song showed that 1,3-phenylene-based NC(H)N ligands featuring imidazole donor moieties react directly with $NiCl_2$ to give (NCN^{im})NiCl (Scheme 1), the first NCN-type complex of nickel prepared by C-H nickelation.[15]

Scheme 2.1. Reactivities of NC(H)N^{im}- and NC(H)N^{pz}-type ligands with Ni(II) salts.

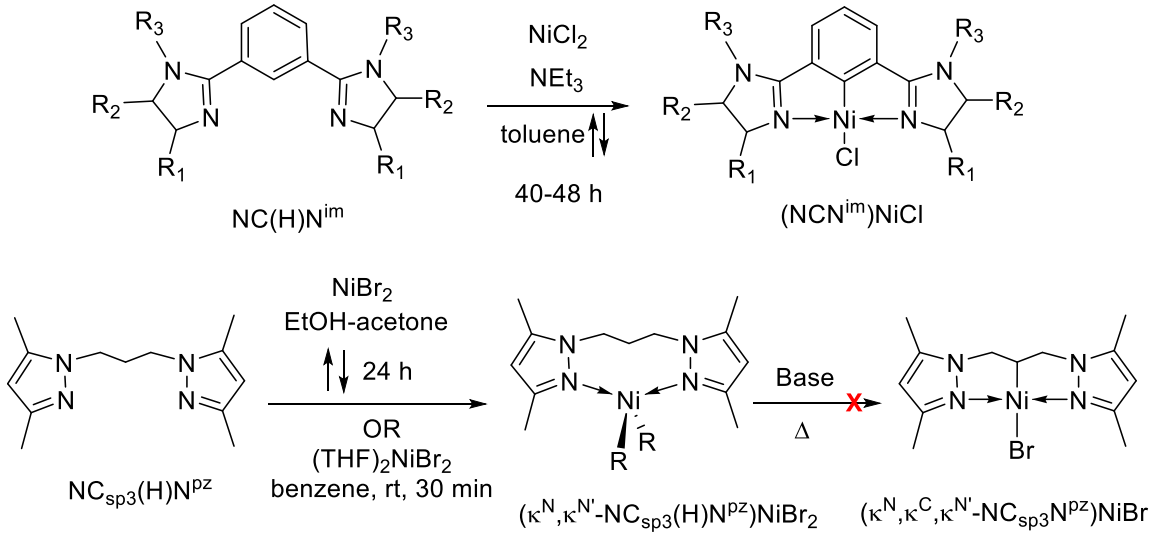

Our long-standing interest in organonickel chemistry[16] and pincer-type Ni complexes,[17] as well as the great promise of NCN ligands for developing the chemistry of Ni(III) complexes, inspired us to explore the efficient synthesis of new families of NCN-Ni complexes via C-H nickelation. An initial effort in this direction showed that reaction of 1,3-bis(3,5-dimethylpyrazolyl)propane with $NiBr_2$ (EtOH-aceton, reflux, 24 h) or $(THF)_2NiBr_2$ (benzene or toluene, rt, 30 min) gives the blue, tetrahedral complex ($\kappa^N,\kappa^{N'}$-$NC_{sp3}(H)N^{pz}$)$NiBr_2$, which could not be induced to undergo the required C-H nickelation to yield the target pincer compound ($\kappa^N,\kappa^C,\kappa^{N'}$-$NC_{sp3}N^{pz}$)NiBr (Scheme 1).[18] This finding prompted us to modify our approach by using different ligands and Ni precursors. Thus, we studied the C-H nickelation of ligands based on a 1,3-phenylene backbone, which is usually more prone to undergo the requisite C-H nickelation, using $(MeCN)_nNiBr_2$[19] or (*i*-PrCN)$NiBr_2$,[20] which had been shown to be excellent precursors for C-H nickelation of a variety of pincer ligands.

The present report describes the preparation of (R-NCN^{pz})NiBr (R= H, **1**; MeO, **2**) via direct C-H nickelation. Spectroscopic and solid state characterization of **1**, **2**, and the aryloxide derivative (NCN^{pz})Ni(OAr) (Ar= 2,6-*t*-Bu_2, 4-Me-C_6H_2; **3**) has allowed us to compare the main structural features of these complexes to previously reported NCN-Ni complexes. Attempts to oxidize these new complexes did not lead to the target Ni(III) derivatives, revealing instead unexpected and uncommon reactivities that allow a functionalization of NCN^{pz} ligands by fairly facile C-O and C-N bond formation reactions, as described below.

2.3 RESULTS AND DISCUSSION

The synthetic methodology used for the preparation of the 1,3-bis(pyrazolyl)arene ligands **a** and **b** and their nickelation is shown in Scheme 2. Ligand **a** is a known substance that can be prepared using a Cu-catalyzed Ulmann coupling of pyrazole with dihalobenzenes.[21] A modified version of this coupling methodology allowed the preparation of the new ligand 1,3-bis(pyrazolyl),5-methoxy-benzene, **b**, from 1,3-dibromo-5-methoxybenzene, which was, in turn, obtained from methylation of commercially available 3,5-dibromophenol using MeI and K_2CO_3. Treating **a** and **b** with (*i*-PrCN)$NiBr_2$[22] in refluxing xylene over 2 days gave the target complexes **1** and **2** in 50% and 24% yields, respectively (Scheme 2.2). Both complexes are stable in air and are quite robust thermally: **1** can be heated to 250 °C without decomposition, and **2** starts decomposing at ~190 °C.

Scheme 2.2. Synthetic routes to ligands a and b and complexes 1 and 2.

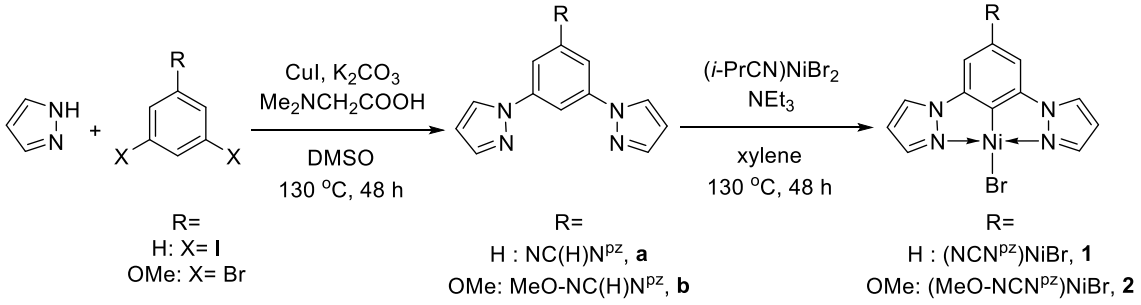

The ^{1}H NMR spectrum of **a** matches reported data,[21] and **b** displayed the expected ^{1}H resonances, namely: three doublets and two triplets for the aromatic protons, plus a singlet for O*CH*$_3$. Nickelation of these ligands was most readily evident from a few features of the ^{1}H NMR spectra for **1** and **2**. First, the ligand signal due to H2, the proton *ortho* to both pyrazole moieties, was absent in the spectra of the complexes. In addition, there were notable changes in the multiplicities and chemical shifts of some protons upon metallation. For instance, the signal for H7 shifted downfield by ca. 0.10 ppm in **1** and 0.15 ppm in **2**, whereas the remaining protons in both complexes shifted upfield, by about 0.7 ppm for H3 and 0.06-0.1 ppm for all others. Multiplicities of the methoxy and pyrazole protons remained unchanged, but H4 changed from a multiplet to a triplet and H3 changed from a multiplet to a doublet (in **1**) or doublet to singlet (in **2**). Overall, the ^{1}H NMR spectra of **1** and **2** display 4 resonances for the 8 aromatic protons that are pairwise equivalent thanks to the C_2 axis bisecting these structures and overlapping C4, C1, Ni, and Br atoms. Moreover, a triplet was detected for H4 in **1** and a singlet for O*CH*$_3$ in **2**. The ^{13}C{^{1}H} NMR

spectra display 5 singlets for the 5 pairwise equivalent carbon nuclei off the C_2 axis, in addition to *ipso*-C, *para*-C, and O*C*H$_3$.

Single crystals suitable for X-ray analysis were obtained by slow recrystallization of **1** and **2** from warm THF; Figure 1 shows the solid-state structures of these complexes and Table S1 (Supporting Information) lists the crystal data and details of data collection. The Ni center in in both compounds adopts a square planar geometry, and the solid-state structures are virtually flat as inferred from the near coplanarity (angle <1°) of the two fused 5-membered nickelacycles defining the (NCN)Ni moiety. The smaller-than-ideal N-Ni-N angles of 162° observed in **1** and **2** are due to the small bite angle of the NCN ligand, a phenomenon observed in other NCN-Ni systems, including van Koten's phebox- or imine-based (NCN)NiBr systems.[23] The Ni-Br bond distances in the latter complexes are somewhat shorter relative to **1** and **2** (2.36 and 2.34 vs. 2.37 and 2.38 Å, respectively), whereas the Ni-C and Ni-N bond distances are fairly comparable in these complexes (Ni-C: 1.83 and 1.82 vs. 1.85 and 1.82 Å, respectively; Ni-N: 1.91 and 1.90 vs. 1.94 and 1.91 Å, respectively).[23]

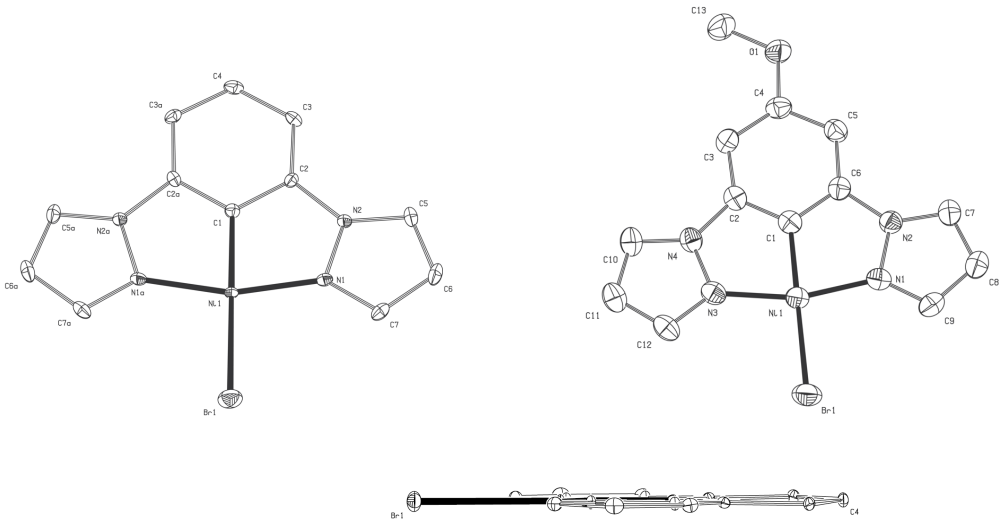

Figure 2.1. Molecular structures of **1** (top left) and **2** (top right), and a side-view of **1** (bottom). The asymmetric unit of **2** contains two molecules, only one of which is shown. Thermal ellipsoids are shown at the 50% probability level, and hydrogen atoms are omitted for clarity. Selected bond distances (Å) and angles (°) are listed below. **1:** Ni1-Br1= 2.3680(9); Ni-N1= 1.908(3); Ni-C1= 1.825(5); C1-Ni1-Br1= 180.000(1); N1a-Ni1-N1= 162.07(17). **2:** Ni11-Br11= 2.3846(7); Ni11-N11= 1.902(3); Ni11-N13= 1.898(3); Ni11-C17= 1.822(4); N13-Ni11-N11= 162.00(13); C17-Ni11-Br11= 177.05(11).

Cyclic volatammetry meausrements and chemical oxidation attempts on complexes 1 and 2. As mentioned earlier, one of the main characteristics of the tertiary amine-based (NCN^{NR2})NiX complexes pioneered by van Koten was their highly electron-rich character and tendency to stabilize trivalent species. With the new NCN^{pz} complexes **1** and **2** in hand, we investigated their redox properties prior to testing their reactivity toward chemical oxidants. Cyclic voltammetry measurements conducted on our compounds showed that their redox profiles are quite different from those of their tertiary amine-based counterparts (Figure 2.28): **1** showed a quasi-reversible Ni^{II}/Ni^{III} redox couple at 452 mV, whereas **2** showed an irreversible oxidation at a higher potential (E_{ox}= 545 mV),[24] both values being much higher than the $E_0^{½}$ value for van Koten's (NCN^{NMe2})NiBr.[25] Comparison of these oxidation potentials to the corresponding values measured for closely related ECE-Ni pincer complexes[26,27,28] reveals the order of electron richness summarized in Figure 3. It is noteworthy that the methoxy-substituted system in **2** appears to be *less* susceptible to oxidation relative to **1**; this is in contrast to our previous observation that (*para*-MeO-POCOP)NiBr is *more* susceptible (by ca. 200 mV) to undergo a Ni^{II}/Ni^{III} oxidation relative to its unsubstituted derivative.[28] We speculate that the observed higher oxidation potential of **2** may be due to a less efficient conjugation in this molecule brought about by the slight planar distortion that is presumably caused by the methoxy substituent.

Figure 2.2. Relative redox potentials of different pincer complexes**.**

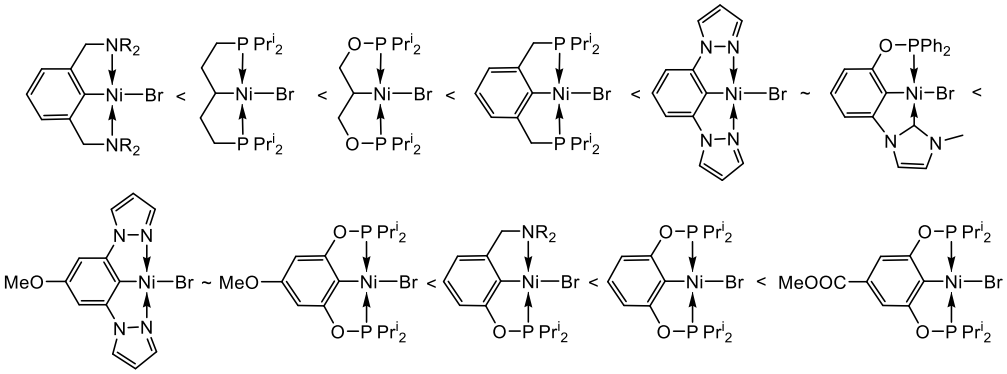

Even though the new (NCN^{pz})NiBr complexes **1** and **2** appear to be less electron-rich than most (ECE)NiX systems that are known to give isolable trivalent species (e.g., (NCN^{NR2})NiX, ($PC_{sp3}P$)NiBr, and ($POC_{sp3}OP$)NiBr), we were encouraged that they appeared to be more electron-rich than the related (POCN)NiBr that are known to stabilize trivalent species.[13] Therefore, we proceeded to test the capacity of our ligands to stabilize trivalent compounds by treating **1** and **2** with slight excess of Br_2, *N*-bromosuccinimide (NBS), or $CuBr_2$, oxidants that have proven competent for generation of trivalent Ni

species from some of the pincer-type Ni(II) complexes studied by our group.[26, 29] In all cases, we observed the same color changes as noted previously during the oxidation attempts on other (ECE)NiX systems: the reaction mixture turned dark immediately and a deeply-colored solid precipitated out of the solution. These sparingly soluble compounds appeared to be very similar to the trivalent species previously isolated by our group.[26, 29] For instance, the deep purple samples prepared by dissolving the solids in question in pyridine or acetonitrile proved NMR-silent, consistent with the anticipated paramagnetism of the trivalent derivatives, and displayed UV-vis spectral patterns similar to those of fully characterized octahedral (NCN^{NMe2})$NiBr_2$(L).[9c] Unfortunately, all attempts to obtain analytically pure samples and grow crystals suitable for X-Ray analysis were unsuccessful. A crude sample obtained from the attempted oxidation of **2** with NBS registered a magnetic susceptibility of 2.96, which is much higher than the value anticipated for a single unpaired electron and suggests that we are dealing with high-nuclearity species.

An unexpected result was obtained when we treated complex **1** with iodine in anticipation of oxidizing the Ni center (Scheme 2.3). Addition of one equivalent of iodine to a THF solution of **1** generated a deep orange mixture from which precipitated an orange-brown solid over 20 min. In contrast to the dark solids obtained from the above-noted oxidation attempts, the solid obtained from the iodine reaction was soluble in CD_2Cl_2 and $CDCl_3$ and displayed well-resolved NMR spectra, attesting to its diamagnetic character. Curiously, the ^1H NMR spectrum of this orange solid was virtually identical to the spectral pattern of the starting material, yet the color of the sample was still orange-brown (as opposed to yellow for **1**). Fortunately, recrystallization (from CH_2Cl_2) gave single crystals that allowed us to identify this product as the iodine adduct **1·I₂** shown in Figure 2.

Scheme 2.3. Chemical oxidation attempts on 1

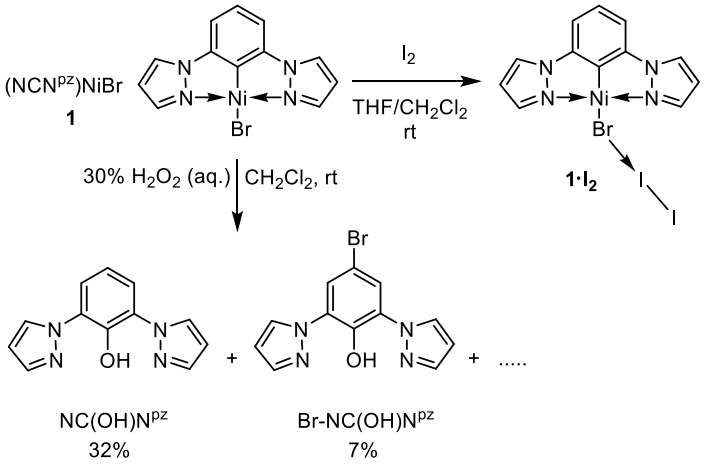

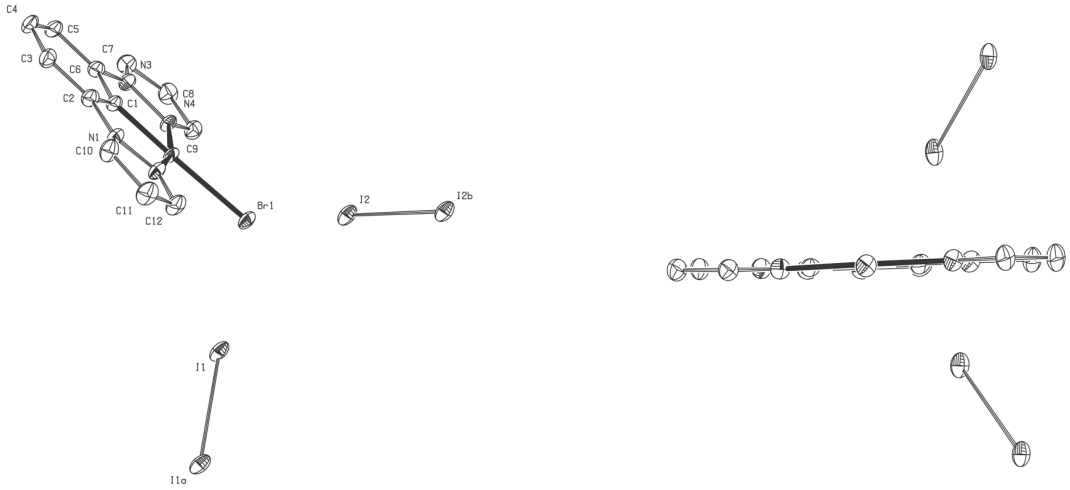

Figure 2.3. Molecular structures of **1·I₂**, sideview (left) and plane view (right). Thermal ellipsoids are shown at the 50% probability level, and hydrogen atoms are omitted for clarity. Selected bond distances (Å) and angles (°): Ni1-Br1= 2.3744(5); Ni-N2= 1.905(3); Ni-N4= 1.901(3); Ni-C1= 1.827(3); I1-I1a= 2.7233(4); I2-I2b= 2.7322(4); Br1-I1= 3.2406(4); Br1-I2= 3.2110(6); C1-Ni1-Br1= 178.23(10); N2-Ni1-N4= 163.11(12); Ni1-Br1-I1= 115.60; Ni1Br1-I2= 114.21; Br1-I1-I1a= 177.12; Br1-I2-I2a= 169.64; I1-Br1-I2= 92.36.

In its solid state, **1·I₂** exhibits Br-I interactions with two iodine molecules, thus creating a one-dimensional zig-zag chain parrallel to the c axis. Interlocking of four of these chains results in pi-stacking of the (NCN^{pz})NiBr units parallel to the c axis with a 3.3 Å distance. Although most structural features of the (NCN^{pz})NiBr unit are largely unperturbed in the solid structure of **1·I₂**, close inspection of some parameters reveals slight but meaningful differences compared to **1**. For instance, the somewhat longer Ni-Br bond (2.3744(5) vs. 2.3680(9) Å), the slightly larger N2-Ni-N4 bite angle (ca. 163° vs 162°), and the I-I bond distance that is slightly longer than in free iodine (avg. 2.727(4) vs 2.715(6) Å)[30] are all consistent with the partial transfer of electron density from Br to I_2. Similar observations are often encountered in transition metal halides engaged in non-covalent type halogen bonds.[31,32] Although there are many examples of such transition metal-halogen—halogen interactions in the literature,[33] to our knowledge **1·I₂** is only the second complex to display Ni-X—halogen bonding.[34] On the other hand, van Koten has reported the complex (NCN)PdI·I_2 (Chart 2)[35] that is very closely analogous to **1·I₂**. The solid-state structure of this compound shows two iodine molecules interacting with the Pd-I moiety and forming nearly linear outer PdI-I-I angles of 172-176° and virtually perpendicular inner I_2-(PdI)-I_2 angles. The

average PdI—I_2 distance in this compound is 3.280 Å, which is nearly 17% shorter than the sum of van der Waals (vdW) radii (3.96 Å), whereas the I-I distance in the iodine molecules is ca. 2.760(1) Å.

Figure 2.4. Pincer complexes featuring halogen bonding.

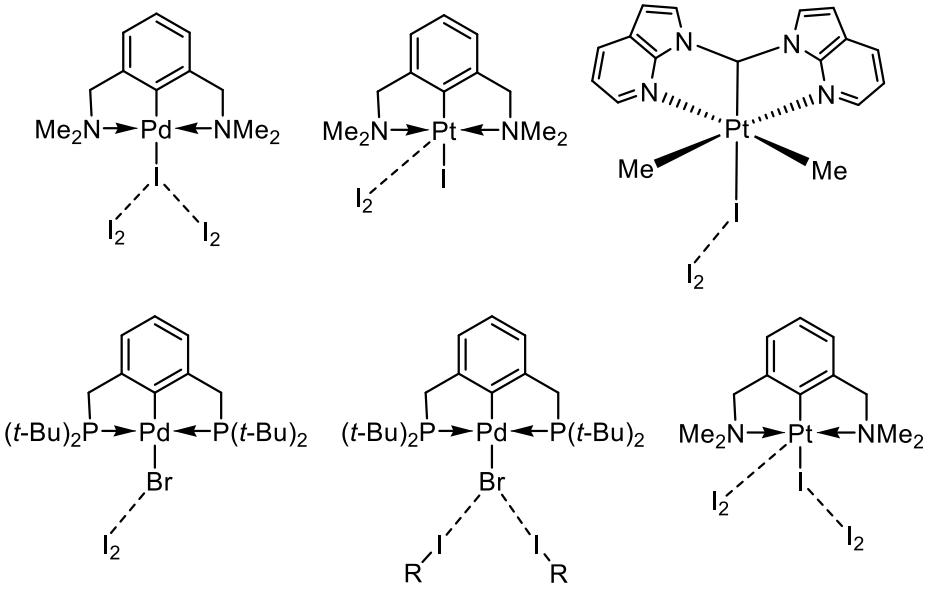

Figure 2.4 shows other pincer-M complexes (M= Pd, Pt) that feature halogen bonds similar to that observed in **1·I₂**. For instance, (NCN^{NMe2})PtI·I_2[36] and (NCN^{BAM})Pt($Me)_2$I·I_2 (BAM= Bis(7-azaindol-1-yl)methyl))[37] show interaction with one iodine only, whereas (PCP)PdX (X= Cl, Br, I)[38] show interaction with one iodine or two electron-poor hydrocarbyl iodides. Wendt et al. have argued that the strong trans influence of the central aryl moiety in the latter compounds elevates the energy of the halide lone pairs, thus promoting their non-covalent interactions with I_2 or iodides. Indeed, the Br—I_2 distance in (PCP)PdBr·I_2 represents a nearly 24% shortening relative to the anticipated value for the sum of Br and I vdW radii (3.83 Å); by comparison, we observe ~ 16% compression in **1·I₂**. Another interesting example of pincer-type complexes featuring non-covalent interactions with I_2 is (NCN)PtI($I_2)_2$.[39] This complex has the unique distinction of displaying two different hydrogen bonds with I_2, one involving a lone pair on the iodide moiety the other involving a Pt-based HOMO, and van Koten et al. have characterized this compound as a model for the initial stage of dihalide oxidative addition to Pt(II).

Reactivities of 1 and 2 with hydrogen peroxide. Following the unsuccessful oxidation attempts described above, we sought a different chemical oxidant for the preparation of trivalent derivatives. The absence in **1** and **2** of oxidation susceptible donor moieties such as phosphines or phosphinites opens up

the possibility of using a stronger oxidant such as hydrogen peroxide. Thus, as a final attempt to oxidize our (NCN)NiBr complexes, we tested their reactivities with this oxidant. Addition of an excess of H_2O_2 (30% solution in water) to a CH_2Cl_2 solution of **1** brought about an immediate color change from yellow to deep purple. The intense color of the reaction reaction mixture turned gradually to pale orange (ca. 12h at rt), indicating that the in-situ generated product has limited thermal stability. All attempts at arresting this deep purple species before it decomposed proved unsuccessful, giving intractable dark solids that have remained unidentified. Thus, we turned our attention to isolating and identifying the product(s) of decomposition in the hopes of clues to the nature of the oxidation process. For this purpose, the pale orange final reaction mixture of an oxidation reaction using H_2O_2 was further diluted with water and extracted with CH_2Cl_2, followed by column chromatography of the organic layer on silica. This work-up procedure afforded two products arising from the oxidative degradation of **1**, namely NC(OH)N^{pz} (32%) and Br-NC(OH)N^{pz} (7%), as shown in Scheme 3. Control experiments confirmed that the Ni center plays a crucial role in this reaction: reaction of NC(H)N^{pz}, **a**, with H_2O_2 or NBS did not furnish any of the observed products.

The functionalized derivatives of ligand **a** have been characterized by NMR and MS analyses. For instance, the ^{1}H NMR of NC(OH)N^{pz} is consistent with its C_{2v} symmetry and displays a triplet and a doublet (^3J= 8 Hz) for the mutually coupled protons of the central ring, whereas the ^{1}H NMR of Br-NC(OH)N^{pz} displays a singlet only for the symmetry related protons of the central ring. Perhaps the most interesting feature in these spectra is the downfield signals due to the acidic O*H* proton (at 12.32 ppm for NCN^{pz}-OH and 12.43 ppm for Br-NC(OH)N^{pz}). Isolation of a suitable single crystal for the latter substance has allowed us to examine its solid-state structure by X-ray diffraction studies. The molecular structure thus elucidated (Figure 3) shows the O---H---N interaction responsible for the downfield NMR signals; the observed O-H and N-H distances are 0.827 and 1.78 Å, respectively.

Figure 2.5. Molecular structures of Br-NCN^{pz}-OH. Thermal ellipsoids are shown at the 50% probability level, and hydrogen atoms are omitted for clarity. See the CIF file for complete structural parameters and Table 2.2 for selected bond distances.

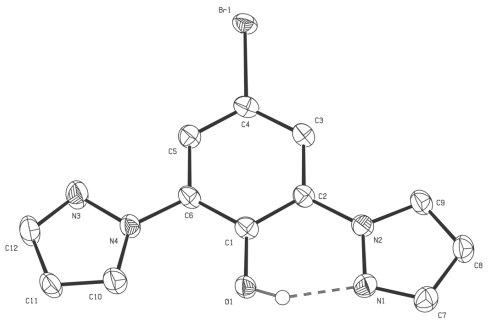

Complex **2** reacted in a similar manner to give the hydroxylated product, MeO-NC(OH)N^{pz}, but no bromination product was observed. It is worth noting that the yellow to deep purple color change observed for **1** was not detected in the reaction of **2**, suggesting that this phenomenon is related to the bromination step, which presumably involves aromatic intermediates featuring unpaired electrons. Two tests were conducted to probe the nature of this reaction. First, we repeated the treatment of **1** with H_2O_2 in the presence of 1.2 equiv of TEMPO; this experiment yielded only NC(OH)N^{pz}, implying that free radicals are likely involved in the formation of Br-NC(OH)N^{pz}. Second, it was established that neither of the above functionalization products was observed when a THF mixture of **1** and NaOH was refluxed for 18 h; the only tractable product of this experiment was the protonated ligand NC(H)N^{pz}. We conclude that an in-situ generated Ni-OH derivative is insufficient for this functionalization reaction, the oxidizing character of H_2O_2 being an essential requirement.

The above-noted oxidatively-induced functionalization of the NCNpz ligand in **1**, hydroxylation at the *ipso* position and bromination at the *para* position, are reminiscent of analogous reactivities reported in the literature. For instance, Hillhouse has demonstrated that $L_2Ni(II)(R)(X)$ species (X= OR', NR'$_2$) can be induced to undergo reductive elimination of R-X in the presence of external oxidants such as O_2, I_2, and $(AcCp)_2Fe^+$ that can generate reactive Ni(III) intermediates.[40] A very recent report has also shown that a pincer-like complex of Ni(II) can promote bromination of aromatic substrates in the presence of strong oxidants such as $PhI(OAc)_2$ or $(C_6F_5)I(OCOCF_3)_2$.[41] On the other hand, van Koten's group has reported a number of studies documenting the CuX_2–induced (X= Cl, Br) *p*-chlorination and *p*-bromination of NCN ligands in the trivalent pincer complexes $[(NCN)Ru(tpy)]^{2+}$ (NCN= 2,6-bis[(dimethylamino)methyl]-phenyl) or 2,6-bis(2-pyridyl)phenyl); tpy= 2,2′:6′,2″-terpyridine). [42] Mechanistic probes of these halogenations have established that a first-order oxidation of the divalent Ru center precedes the halogenation. Moreover, depending on reaction conditions, the oxidized species can undergo a C-C bond formation that leads to a dimerization of the trivalent complex.[43] Similar reactivities, including dimerization, have been observed with the PCP-analogue of these complexes.[44,45] These observations imply that the spin density in the paramagnetic species $[(pincer)Ru(tpy)]^{2+}$ generated by the one-electron oxidation of the pincer complexes is partially localized on the *para* position of the phenylene ligand. We speculate that a similar phenomenon is at play in our NCN^{pz}-Ni systems that might explain the

observed bromination reaction, the irreversible electrochemical oxidation, and also the unstable products of chemical oxidation.

Preparation of (NCN)Ni(OR) and oxidation attempts. Previous studies in our laboratory have shown that the nature of X ligands in pincer-type complexes (EXE)NiX has a dramatic influence on the oxidation potential of these species. For instance, the oxidation half-cell potential values, $E^0_{½}$, are much larger for (POCN)NiBr than their amido derivatives,[46] and the same trend has been observed with ($POC_{sp3}OP$)NiX (OR < Br) and (PCP)NiX (X = NH_2, OH, CN).[47] In light of the generally greater thermal stability of Ni-OR derivatives, we elected to prepare (NCN^{pz})Ni(OR) and attempt their oxidation, as shown in Scheme 2.4 and described below.

Scheme 2.4. Reactivities of 1 with $[OR]^-$.

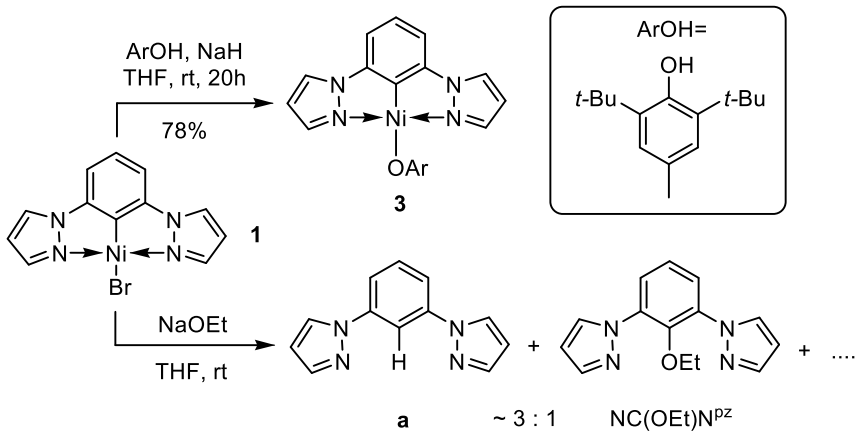

As illustrated in Scheme 4, complex **1** reacted very differently with different sources of OR^-: treatment with the in-situ deprotonated BHT (butylated hydroxytoluene, 2,6-(*t*-Bu)$_2$,4-Me-C_6H_2OH) gave the anticipated simple Ni-OAr derivative **3**, whereas NaOEt gave instead the protio ligand **a** as the major product, as well as the ethoxide-functionalized compound $NC(OEt)N^{pz}$. Although no intermediate species was detected during the latter reactions, we speculate that the observed side-products are derived from decomposition of the unstable intermediate (NCN^{pz})Ni(OEt). For instance, □-H elimination of the latter would give acetaldehyde and (NCN)Ni(H), which would collapse by reductive elimination to give **a**,[48] whereas direct reductive elimination would generate the ethoxy functionalized product $NC(OEt)N^{pz}$ by C-O bond formation.[49,50] The analogous reaction with KO(*t*-Bu) did allow the observation of a more

persistent intermediate, but the detected species decomposed to intractable materials before it could be identified with confidence.

That the above-observed reactions with alkoxide salts are, in fact, even more complex than they appear was revealed by the following observations. First, when the reaction with NaOEt was conducted under rigorously oxygen-free conditions, we obtained ligand **a** only, the ethoxy-functionalized product not being detected at all; the analogous reaction with KO(*t*-Bu) led to a complex mixture from which no tractable compound could be isolated or identified. Second, simply refluxing an ethanol solution of **1** in air (without any base or source of ethoxide) led to exclusive formation of the C-O coupling product, NC(OEt)N^{pz}; the same reactivity was observed with complex **2**. Although these observations do not provide a clear mechanistic picture for this reactivity, they have encouraged us to seek a novel methodology for functionalization of the pyrazole-based NCN ligands under study (vide infra).

The aryloxide derivative **3** was isolated as a bright orange powder that proved to be much more soluble in standard solvents relative to its precursor **1**. This new derivative was found to be highly stable at higher temperature, decomposition of solid-state samples starting above 220 °C. The ^{1}H and ^{13}C{^{1}H} NMR spectra of **3** were in accordance with the proposed structure of this complex. For instance, we observed five aromatic signals each integrating for two protons, indicating the pairwise equivalence of the symmetry-related NCN^{pz} and BHT aryl protons. In addition, the signal due to the *para*-H on the central aryl moiety of NCN^{pz} is a triplet, and there is only one signal for the 18 equivalent protons of the *t*-Bu moieties, implying a low energy barrier for the rotation of BHT about the Ni-O and C-O axes. Finally, all of the NCN^{pz} protons shift upfield by 0.5-1.28 ppm as the bromo precursor is converted to the BHT derivative.

The solid-state structure of **3** was confirmed by X-ray diffraction studies conducted on single crystals obtained from recrystallization using Et_2O at rt (Figure 2.6). The geometry around the Ni center in this complex is distorted square planar (N-Ni-N= 163°) and most structural parameters are similar to the corresponding values in **1** and **2**. The BHT ring is nearly perpendicular to the coordination plane (88°). The Ni-O distance in **3** is similar to the corresponding distance in ($POC_{sp3}OP$)Ni(OMes) (ca. 1.88 Å vs 1.89 Å; Mes= 2,4,6-$(Me)_3C_6H_2$).[51]

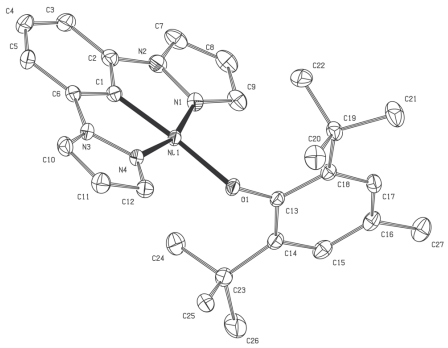

Figure 2.6. Molecular view of 3a. The unit cell contains three molecules, only one of which is shown here. Selected bond distances (Å) and angles (°): Ni1-O1 = 1.8827(14); Ni1-N4 = 1.8990(17); Ni1-N1 = 1.9143(17); Ni1-C1= 1.822(2); N1-Ni1-N14 = 162.64(7); C1-Ni1-O1 = 173.37(8); Ni1-O1-C13= 129.68(12).

Cyclic voltammetry measurements carried out on **3** confirmed the much lower oxidation potential of this aryloxide derivative relative to its bromo precursor (Figure 2.28); indeed, **3** appears to undergo a one-electron irreversible oxidation at a potential lower than the redox couple of ferrocene (-73 mV). Observation of such a facile oxidation seemed to bode well for the prospects of preparing trivalent derivatives by chemical oxidation, but treatment of **3** with Br_2, I_2 or H_2O_2 failed to yield the target products. For instance, reaction with 0.5 equivalent of Br_2 led to generation of **1** and free BHT, whereas the reaction with excess H_2O_2 gave the hydroxylated ligand, $NC(OH)N^{pz}$, and protonated BHT (Scheme 2.5). Evidently, the lower oxidation potential engendered by the presence of the aryloxide moiety does not translate into a stable and isolable trivalent derivative, implying an inherent aspect of this system that renders such pentacoordinate, 17-electron derivatives inaccessible.

Scheme 2.5. Attempted oxidation of 3.

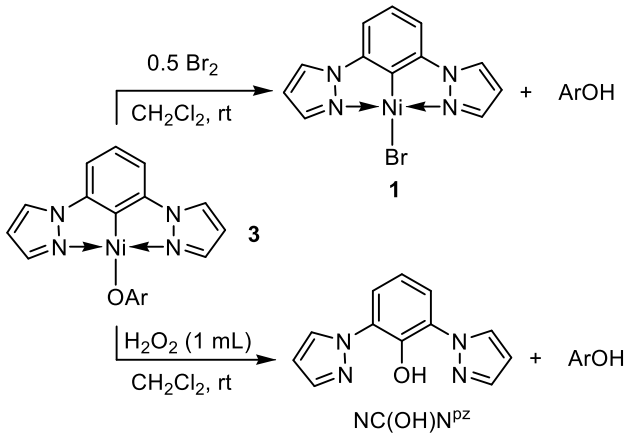

Functionalization of NCN^{pz} via alcoholysis and aminolysis of 1. As mentioned earlier, **1** and **2** react with EtOH to yield ethoxide-functionalized derivatives of the NCN^{pz} and MeO-NCN^{pz} ligands, respectively; these observations inspired us to explore the scope of this unusual reaction, as described below; the preliminary studies undertaken to date were conducted with complex **1** only.

Refluxing **1** with 99% EtOH for 24 h *while exposing the mixture to ambient air* led to the formation of NC(OEt)N^{pz} in ca. 77% yield, whereas using 95% EtOH gave the same yield but the ethoxylation reaction proceeded much faster (Table 2.1, Entry 1). The analogous reactions with MeOH and *i*-PrOH were more sluggish, but in the presence of added water (5% by volume) we obtained after 18 h 65 and 70% yields, respectively (Entries 2 and 3). Small and variable quantities of the protonated ligand **a** were also detected in the reactions with MeOH. Interestingly, alcohols featuring more acidic O-H moieties resulted in either no reaction at all (PhOH and $PhCH_2OH$) or a much lower yield (CF_3CH_2OH, Entry 4); for the latter reaction, the addition of 5% water had no impact on the yield or reaction time.

To our delight, the functionalization could be extended to amines, but C-N bond formations proceeded in generally lower yields. For instance, the secondary amine morpholine gave 41% yield (Entry 5) and the primary amines cyclohexyl amine and aniline gave 10% and 32% yields, respectively (Entries 5 and 6), whereas *p*-F-benzyl amine and ethanolamine did not react at all. As was the case with the alcoholoysis reaction using CF_3CH_2OH, addition of water had no impact on the aminolysis of **1**.

The C-O and C-N bond formation reactions observed with complex **1** are somewhat analogous to a recently reported Pd-catalyzed amination of alkenes in the presence of O_2,[52] and even more so to the stoichiometric intra- or intermolecular C-N bond formation between involving a dicationic Cu(III) species featuring a tetradentate macrocyclic ligand.[53] Heating this complex in the absence of a "nucleophilic" substrate leads to the intramolecularly *N*-functionalized ligand arising via an apparent trans C-N reductive elimination reaction between the aryl-Cu moiety and the tertiary amine moiety in the coordination sphere (Scheme 2.6). The product of intermolecular *N*-functionalization is obtained at rt in the presence of weakly nucleophilic amide-type substrates possessing a fairly acidic N-*H* bond (pK_a< 17; e.g., pyridone, phthalimide, sulfanamide, etc.), whereas less acidic substrates give a mixture of the two products. Evidently, the intermolecular C-N bond formation reactions promoted by this Cu(III) system require acidic substrates, in contrast to the reactivity of complex **1** toward alcohols or amines.

Table 2.1. Functionalization of NCN^{pz}

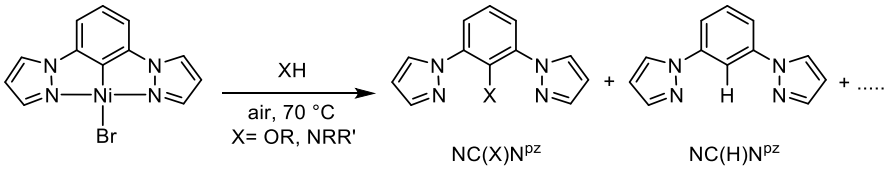

Entry	XH	Time (h)	%Yield of $NC(X)N^{pz}$ GC/MS(isolated)
1	EtOH (95%)	2	77 (68)
2	MeOH (95%)	18	65 (48)
3	*i*-PrOH (95%)	18	70 (68)
4	CF_3CH_2OH	24	15
5	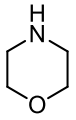	4	41 (29)
6	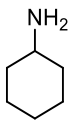	24	10

7	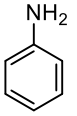	24	32

Reaction conditions: Complex **1** **(**0.072mmol), XH (10 mL), and 1-bromo-3,5-dimethoxybenzene (internal standard) were stirred at 70 °C for the required time. In all cases, yields were determined by GC/MS using a previously prepared calibration curve based on NC(OEt)N^{pz}. In some cases, the product was isolated following a standard chromatographic work-up.

Scheme 2.6. Cu(III)-promoted C-N bond formation.

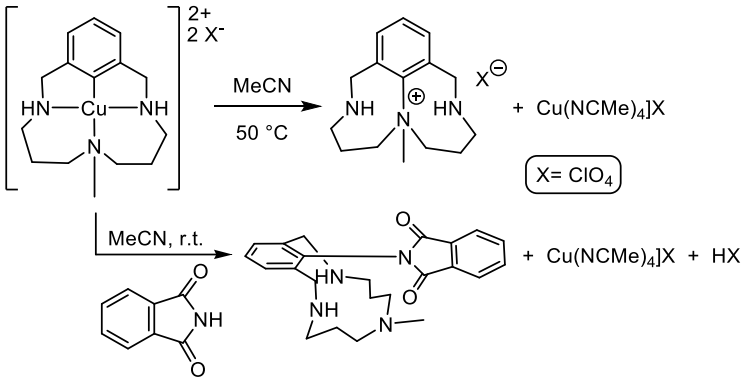

As stated earlier, the alcoholysis and aminolysis reactions described above appear to require an aerobic condition: conducting these reactions using degased substrates and under a nitrogen purge gave traces only of the functionalized product as well as protonated ligand. It occurred to us that other mild oxidants might also promote this reaction, and to test this idea we treated the iodine adduct **1•I2** with MeOD in an NMR tube; the sample was kept at rt and under a nitrogen atmosphere. ^{1}H NMR analysis confirmed the complete conversion to NC(OMe)N^{pz} over 5 min, implying a dramatic acceleration of the methanolysis reaction which required refluxing over several hours under aerobic conditions.

2.4 CONCLUSION

This study has led to the elaboration of a convenient, C-H nickelation-based synthetic route for the preparation of the first two members of a new family of pyrazole-based NCN complexes using a readily available Ni(II) precursor. Access to complexes **1** and **2** has allowed us to evaluate their oxidation potentials and assess their propensity toward oxidation of the nickel center. The results presented in this report do not bode well for the prospects of stable and isolable high-valent species, but the chemical

oxidation attempts undertaken in the course of this work have revealed potentially useful C-O and C-N bond formation reactions that facilitate oxidative, Ni-promoted alcoholysis and aminolysis of 1,3-bis(pyrazole)benzne. Although the scope of these reactions remains rather narrow so far and they require stoichiometric quantities of Ni(II), we are hopeful that with a better understanding of the complex pathways involved in these reactions it might be possible to elaborate more efficient, practical, and catalytic methodologies for functionalizing a wide range of these aromatic substrates.

2.5 EXPERIMENTAL SECTION

Materials and methods. Unless otherwise indicated, all manipulations were carried out using standard Schlenk and glove box techniques under a dry nitrogen atmosphere using solvents which were dried to water contents of less than 10 ppm (determined using a Mettler-Toledo C20 coulometric Karl Fischer titrator) by passage through activated aluminum oxide columns (MBraun SPS). The following starting materials were purchased from commercial sources and used without further purification: Aldrich: 1,3-diiodobenzene; 3,5-dibromophenol, pyrazole, methyliodide, CuI, N,N-dimethylglycine, Ni powder, Br_2, I_2, *i*-PrCN, 2,6-*t*-Bu_2-4-Me-C_6H_2OH (BHT), *t*-BuOK, N-bromosuccinimide and morpholine; American Chemicals: NEt_3 and H_2O_2; Acros: *c*-$C_6H_{11}NH_2$). $NiBr_2$(NCiPr) was synthesized according to a literature procedure.[28]

The NMR spectra were recorded on the following spectrometers: Bruker AV400rg (^{1}H at 400 MHz) and Bruker ARX400 (^{1}H at 400 MHz and $^{13}C\{^1H\}$ at 100.56 MHz). Chemical shift values are reported in ppm (δ) and referenced internally to the residual solvent signals (^{1}H and ^{13}C: 7.26 and 77.16 ppm for $CDCl_3$; 7.16 and 128.06 ppm for C_6D_6). Coupling constants are reported in Hz. The elemental analyses were performed by the Laboratoire d'Analyse Élémentaire, Département de chimie, Université de Montréal.

(5-methoxy-1,3-phenylene)bis(1H-pyrazole), b. A dried Schlenk flask was charged with 3,5-dibromo-1-methoxybenzene (1.13 g, 4.25 mmol), pyrazole (0.868 g, 12.8 mmol), K_2CO_3 (3.52 g, 25.5 mmol), CuI (0.032 mg, 0.170 mmol) and N,N-dimethylglycine (0.029 g, 0.286 mmol). The system was purged 3 times with N_2 and 15 mL of DMSO was added. This mixture was then heated at 130 °C for 96 h and then cooled to rt. Water (30 mL) and ethyl acetate (30 mL) were then added to the final mixture and the resulting

mixture partitioned. The organic layer was extracted with ethyl acetate (3 x 15 mL) and washed with brine. The combined ethyl acetate fractions was evaporated next and the residue purified by column chromatography (silica get; eluent: 20:80 to 40:60 mixtures of ethyl acetate: hexanes). Evaporation of the combined fractions gave the final product as a slightly yellow solid. (0.171 g, 46%).^{1}H NMR (CDCl3, 400MHz), δ 7.99 (2H, d, J_{HH} = 2.5, H5), 7.74 (2H, d, J_{HH} = 1.6, H7), 7.64 (1H, t, J_{HH} = 1.9, H1), 7.22 (2H, d, J_{HH} = 1.9, H3), 6.49 (2H, t, J_{HH} = 1.9, H6), 3.93 (3H, s, H8). ^{13}C NMR $CDCl_3$, δ 161.42 (1C, s, C4), 142.01 (2C, s, C2), 141.47 (2C, s, C7), 127.19 (2C, s, C5), 108.13 (2C, s, C6), 102.98 (2C, s, C3), 102.23 (1C, s, C1), 56.02 (1C, s, C8). MS: m/z= 240; the mass spectrum is shown in SI (Figure S23).

{□$^{□}$□□^{C},□^{N}-**2,6-(pyrazole)$_2$-C$_6$H$_3$**}**NiBr, 1.** An oven-dried Schlenk was taken inside the glovebox and charged with $NiBr_2$(NC(*i*-Pr)) (1.64 g, 5.71 mmol), ligand **a** (1.00 g, 4.76 mmol), and NEt_3 (0.927 mL, 0.673 g, 6.67 mmol). The vessel was then taken out of the glovebox and 10 mL of *m*-xylene added against a flow of N_2. The resulting mixture was then refluxed for 36 h, cooled down to rt, and evaporated under reduced pressure. The resulting solid residue was stirred with distilled water (3 x 20 mL, in air) and filtered on a Buchner filter, the solid residue being washed consecutively with 3 x 20 mL each of cold MeOH and hexanes. The yellow powder thus obtained was then extracted with THF, concentrated under reduced pressure, and allowed to crystallize to give the target complex as oranges crystals (0.720 g, 44%). ^{1}H NMR $CDCl_3$, δ 7.95 (2H, d, J_{HH} = 2.2, H5), 7.85 (2H, d, J_{HH} = 2.7, H7), 7.18 (1H, t, J_{HH} = 7.8, H4), 6.85 (2H, d, J_{HH} = 7.8, H3), 6.35 (2H, t, J_{HH} = 2.4, H6). ^{13}C NMR DMSO-d6, δ 144.07 (2C, s, C5), 142.74 (2C, s, C2), 137.34 (1C, s, C1), 128.58 (2C, d, C7), 126.87 (1C, s, C4), 108.66 (2C, s, C6), 108.57 (2C, s, C3). Anal Calc for $C_{12}H_9BrN_4Ni$ (347,82): C, 41.44; N, 16.11; H, 2.61. Found: C, 41.41; N, 16.16; H, 2.53.

{□$^{□}$□□^{C}**,**□^{N}**-2,6-bis(pyrazole),4-MeO-C$_6$H$_2$**}**NiBr, 2.** The above procedure was followed using $NiBr_2$(NC(*i*-Pr)) (1.06 g, 3.68 mmol), ligand **b** (0.632 g, 2.63 mmol), and NEt_3 (0.513 mL, 0.373 g, 3.69 mmol) in xylene (10 mL). The target complex **2** was obtained as orange crystals (0.235 mg, 24%). ^{1}H NMR $CDCl_3$, δ 7.89 (2H, d, J_{HH} = 2.0, H5), 7.81 (2H, d, J_{HH} = 2.7, H7), 6.46 (2H, s, H3), 6.34 (2H, t, J_{HH} = 2.4, H6), 3.87 (3H, s, H8). ^{13}C NMR $CDCl_3$, δ 159.82 (1C,s C4), 144.50 (2C, s, C5), 142.68 (2C,s C2), 127.92 (1C,s, C1), 125.59 (2C, s, C7), 107.85 (2C, s, C6), 94.76 (2C, s, C3), 56.19 (1C,s, C8). Anal Calc for $C_{12}H_9BrN_4Ni$ (377,85): C, 41.32; N, 14.83; H, 2.93. Found: C, 41.23; N, 14.78; H, 2.86.

{□$^{□}$□□^{C},□^{N}-**2,6-(pyrazole)$_2$-C$_6$H$_3$**}**NiBr.I$_2$, 1•I2 .** A CH_2Cl_2 solution of I_2 (0.073 g, 0.288 mmol, in 10 mL) was added dropwise to a THF solution of **1** (0.100 g, 0.288 mmol, in 30 mL). The mixture turned from yellow to deep orange and an orange powder precipitated after 20 min. The final mixture was filtered

after an additional 2 h of stirring to give the crude product as an orange solid (57 mg, 33%). Recrystallization from warm CH_2Cl_2 gave orange crystals after standing overnight. Gradual sublimation of iodine circumvented an accurate elemental analysis of this compound. The ^{1}H NMR and UV-vis spectra of this adduct were virtually identical to the corresponding spectra of **1** (See Figures S1 and S31).

{$k^N k^C$, k^N-2,6-(pyrazole)$_2$-C$_6$H$_3$}Ni(BHT), 3. A dry Schlenk flask purged with N_2 was charged with **1** (0.200g, 0.575mmol), BHT (0,127 g, 0,575 mmol), and THF (30 mL). NaH (0.022 g, 0.96 mmol) was then added slowly to this mixture against a flow of N_2. The final mixture was left to stir for 20 h at rt. The resulting orange solution was evaporated under vacuum and the yellow residue extracted with dry Et_2O (5 x 10 mL). Evaporation to dryness gave a bright orange powder (0.280g, 78% Yield). ^{1}H NMR C_6D_6, δ 7.39 (2H, s, H10), 6.88 (2H, d, J_{HH} = 2.1, H5), 6.67 (1H, t, J_{HH} = 7.8, H4), 6.57 (2H, d, J_{HH} = 2.4, H7), 6.05 (2H, d, J_{HH} = 7.8, H3), 5.47 (2H, t, J_{HH} = 2.4, H6), 2.63 (3H, s, H12), 2.19 (18H, s, H14). ^{13}C NMR C_6D_6, δ 167.6 (1C, s, C8), 143.97 (2C, s, C2), 141.18 (2C, s, C5), 140.64 (2C, s, C9), 139.88 (1C, s, C1), 126.30 (2C, s, C10), 124.77 (1C, s, C4), 124.36 (2C, s, C7), 121.82 (1C, s, C11), 107.23 (2C, s, C6), 106.91 (2C, s, C3), 36.22 (2C, s, C13), 32.37 (6C, s, C14), 22.09 (1C, s, C12). Anal Calc for $C_{27}H_{32}N_4NiO$ (487.26): C, 66.55; N, 11.50; H, 6.62. Found: C, 66.16; N, 11.30; H, 6.58.

4-Bromo-2,6-di(1*H*-pyrazol-1-yl)phenol and **2,6-di(1*H*-pyrazol-1-yl)phenol.** A Schlenk flask was charged with **1** (0,050 g, 0,144 mmol), CH_2Cl_2 (30 mL), and H_2O_2 (1 mL of 30% solution in water, 9.79 mmol), and stirred for 18 h. The initial yellow color of the mixture turned deep purple 20 min, but this color faded gradually such that the final mixture was yellowish. Addition of H_2O (20 mL) followed by extraction with CH_2Cl_2 (3 x 20 mL) and evaporation of the combined organic layers gave an oily residue which was purified by column chromatography (silica; eluent: $CHCl_3$). Evaporation of the first and second fractions collected gave the minor and major components of the product mixture, respectively, as white powders (6 mg, 7%; 22 mg, 32%).

Characterization data for **4-Bromo-2,6-di(1*H*-pyrazol-1-yl)phenol:** ^{1}H NMR $CDCl_3$, δ 12.43 (1H, s, H8), 8.21 (2H, d, J_{HH} = 2.4 H5), 7.75 (2H, d, H7), 7.71 (2H, s, H3), 6.52 (2H, t, J_{HH} = 2.1, H6).^{13}C NMR $CDCl_3$, δ 140.91 (1C, s, C1), 140.10 (2C, s, C7), 129.75 (2C, s, C5), 129.09 (2C, s, C2), 121.84 (2C, s, C3), 111.05 (1C, s, C4), 107.37 (2C, s, C6). LRMS : expected mass ($M+H^+$) = 305.0 ; 307.0 ; Found ($M+H^+$) = 305.1 ; 307.1

Characterization data for **2,6-di(1*H*-pyrazol-1-yl)phenol:** ^{1}H NMR $CDCl_3$, δ 12.32 (1H, s, H8), 8.20 (2H, d, J_{HH} = 2.3 H5), 7.75 (2H, s, H7), 7.55 (2H, d, J_{HH} = 8.1, H3), 7.01 (1H, t, J_{HH} = 8.1, H4), 6.51 (2H, t, J_{HH} = 2.0, H6). ^{13}C NMR $CDCl_3$, δ 142.07 (1C, s, C1), 139.72 (2C, s, C7), 129.62 (2C, s, C5), 128.38 (2C, s, C2), 119.47 (2C, s, C3), 119.42 (1C, s, C4), 106.91 (2C, s, C6). LRMS : expected Mass ($M+H^+$) = 227.1 ; Found ($M+H^+$) = 227.2.

(2-methoxy-1,3-phenylene)bis(1H-pyrazole). A round bottom flask was charged with **1** (0.040 g, 0.116 mmol), MeOH (30 mL) and distilled water (1.5 mL) and the mixture stirred at reflux for 24 h. The resulting pale yellow mixture was left to cool to rt and evaporated. The residue was extracted with diethyl ether (3 x 20 mL), evaporated, and the solid mixture purified by column column chromatography (silica; eluent: 20/80 ethylacetate/hexane) to give both the protonated ligand **a** and the functionalized ligand (13 mg, 48% Yield). ^{1}H NMR (CDCl3, 400MHz), δ 8.10 (2H, d, J_{HH} = 2.4, H5), 7.75 (2H, d, J_{HH} = 1.6, H7), 7.69 (2H, d, J_{HH} = 8.0, H3), 7.32 (1H, t, J_{HH} = 8.0, H4), 6.49 (2H, t, J_{HH} = 2.0, H6), 3.28 (3H, s, H8).^{13}C NMR $CDCl_3$, δ 144.85 (1C, s, C1), 140.98 (2C, s, C7), 134.97 (2C, s, C2), 131.28 (2C, s, C5), 125.09 (1C, s, C4), 124.18 (2C, s, C3), 107.40 (2C, s, C6), 60.94 (1C, s, C8). GCMS 240m/z.

(2-ethoxy-1,3-phenylene)bis(1H-pyrazole). A round bottom flask was charged with **1** (0.150 g, 0.431 mmol) and 95% ethanol (40 mL), and the mixture stirred for 5h at reflux. The resulting pale yellow solution is left to cool to rt and then evaporated. The solid residue was then purified by column chromatography on silica with acetone as eluent. The combined fractions were evaporated to yield the desired product as an oil (47 mg, 68% yield). ^{1}H NMR $CDCl_3$, δ 8.13 (2H, d, J_{HH} = 2.4, H5), 7.75 (2H, d, J_{HH} = 1.6, H7), 7.69 (2H, d, J_{HH} = 8.1, H3), 7.32 (1H, t, J_{HH} = 8.1, H4), 6.49 (2H, t, J_{HH} = 2.1, H6), 3.39 (2H, q, H8), 0.96 (3H, t, H9).^{13}C NMR $CDCl_3$, δ 143.81 (1C, s, C1), 140.93 (2C, s, C5), 135.41 (2C, s, C2), 131.39 (2C, s, C7), 125.06 (1C, s, C4), 124.16 (2C, s, C3), 107.17 (2C, s, C6), 70.00 (1C, s, C8), 15.05 (1C, s, C9). GCMS 254 m/z.

1,1'-(2-isopropoxy-1,3-phenylene)bis(1H-pyrazole). The procedure used above was repeated with (0.040 g, 0.115 mmol) of **1** in *i*-propanol to the target product as an oil (22 mg 70% Yield). ^{1}H NMR $CDCl_3$, δ 8.11 (2H, d, J_{HH} = 2.4, H5), 7.74 (2H, d, J_{HH} = 1.5, H7), 7.67 (2H, d, J_{HH} = 8.1, H3), 7.32 (1H, t, J_{HH} = 8.1, H4), 6.48 (2H, t, J_{HH} = 2.1, H6), 3.38 (1H, sept, J_{HH} = 6.1, H8), 0.82 (6H, d, J_{HH} = 6.1 H9).^{13}C NMR $CDCl_3$, δ 142.6 (1C, s, C1), 140.88 (2C, s, C7), 136.0 (2C, s, C2), 125.0 (2C, s, C5), 124.97 (1C, s, C4), 124.28 (2C, s, C3), 106.9 (2C, s, C6), 29.86 (1C, s, C8), 21.58 (2C, s, C9). GCMS 268 m/z.

4-(2,6-di(1H-pyrazol-1-yl)phenyl)morpholine. The procedure used above for the preparation of 1,1'-(2-ethoxy-1,3-phenylene)bis(1H-pyrazole) was repeated with **1** (34 mg, 0.098 mmol,) and morpholine (20 mL) to give an off-white solid after evaporation (8 mg, 29%). ^{1}H NMR $CDCl_3$, δ 7.75 (2H, d, J_{HH} = 1.8, H5), 7.73 (2H, d, J_{HH} = 1.8, H7), 7.41 (2H, d, J_{HH} = 7.8, H3), 7.24 (1H, t, J_{HH} = 7.5, H4), 6.47 (2H, t, J_{HH} = 1.9, H6), 3.38 (4H, t, J_{HH} = *4.6*, H8), 2.51 (4H, t, J_{HH} = *4.6*, H9).^{13}C NMR $CDCl_3$, δ 142.7 (1C, s, C1), 140.81 (2C, s, C7), 138.2 (2C, s, C2), 131.80 (2C, s, C5), 129.0 (1C, s, C4), 124.34 (2C, s, C3), 106.83 (2C, s, C6), 67.13 (2C, s, C8), 50.06 (2C, s, C9). GCMS 295 m/z.

Supporting Information Available. NMR, UV-vis, and GC/MS spectra; cyclic voltammetry traces; data collection and structure resolution procedures, and tables of crystal data and collection/refinement parameters. Free of charge at http://pubs.acs.org. Complete details of the X-ray analyses reported herein have been deposited at *The Cambridge Crystallographic Data Centre* (CCDC 1027168 (**1**), 1027169 (**2**), 1027126 (**1•I2**), 1027124 (**3**), 1027125 (**Br-NC(OH)N^{pz}**)). This data can be obtained free of charge via www.ccdc.cam.ac.uk/data_request/cif, or by emailing data_request@ccdc.cam.ac.uk, or by contacting The Cambridge Crystallographic Data Centre, 12, Union Road, Cambridge CB2 1EZ, UK; fax: +44 1223 336033.

Acknowledgement. The authors are grateful to: NSERC of Canada for a Discovery Grant to D.Z.; Université de Montréal (FESP) for graduate fellowships to J.-P.C.; Dr. Michel Simard and Prof F. Hein Schaper for his valuable assistance with crystallography; Dr. Christine Lepetit for discussions regarding theoretical treatments of halogen bonds; Prof. O. Wendt (Lund University) for valuable discussions on the formation of **1·I$_2$**.

2.6 SUPPORTING INFORMATION

Figure 2.7 ^{1}H NMR of NCN^{pz}NiBr-CDCl$_3$

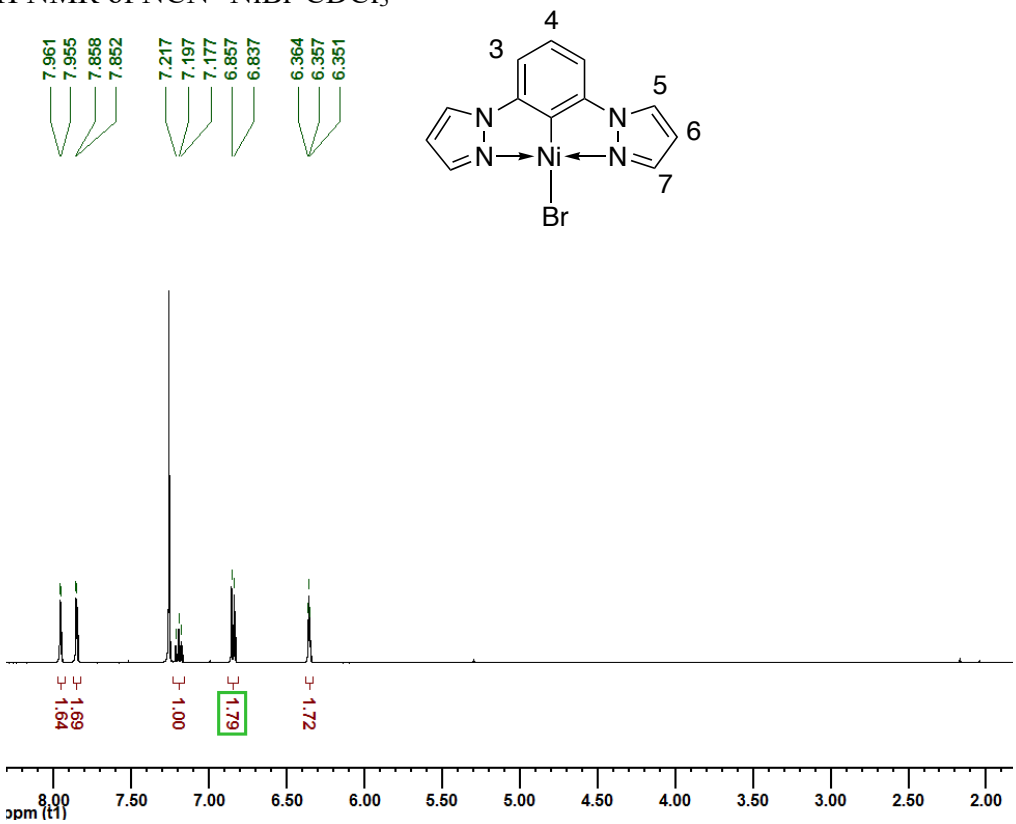

^{1}H NMR (CDCl3, 400MHz), δ 7.95 (2H, d, J_{HH} = 2.2, H^{5}), 7.85 (2H, d, J_{HH} = 2.7, H^{7}), 7.20 (1H, t, J_{HH} = 7.8, H^{4}), 6.85 (2H, d, J_{HH} = 7.8, H^{2}), 6.36 (2H, t, J_{HH} = 2.4, H^{6})

Figure 2.8 ^{13}C NMR of NCN^{pz}NiBr – DMSO-d6

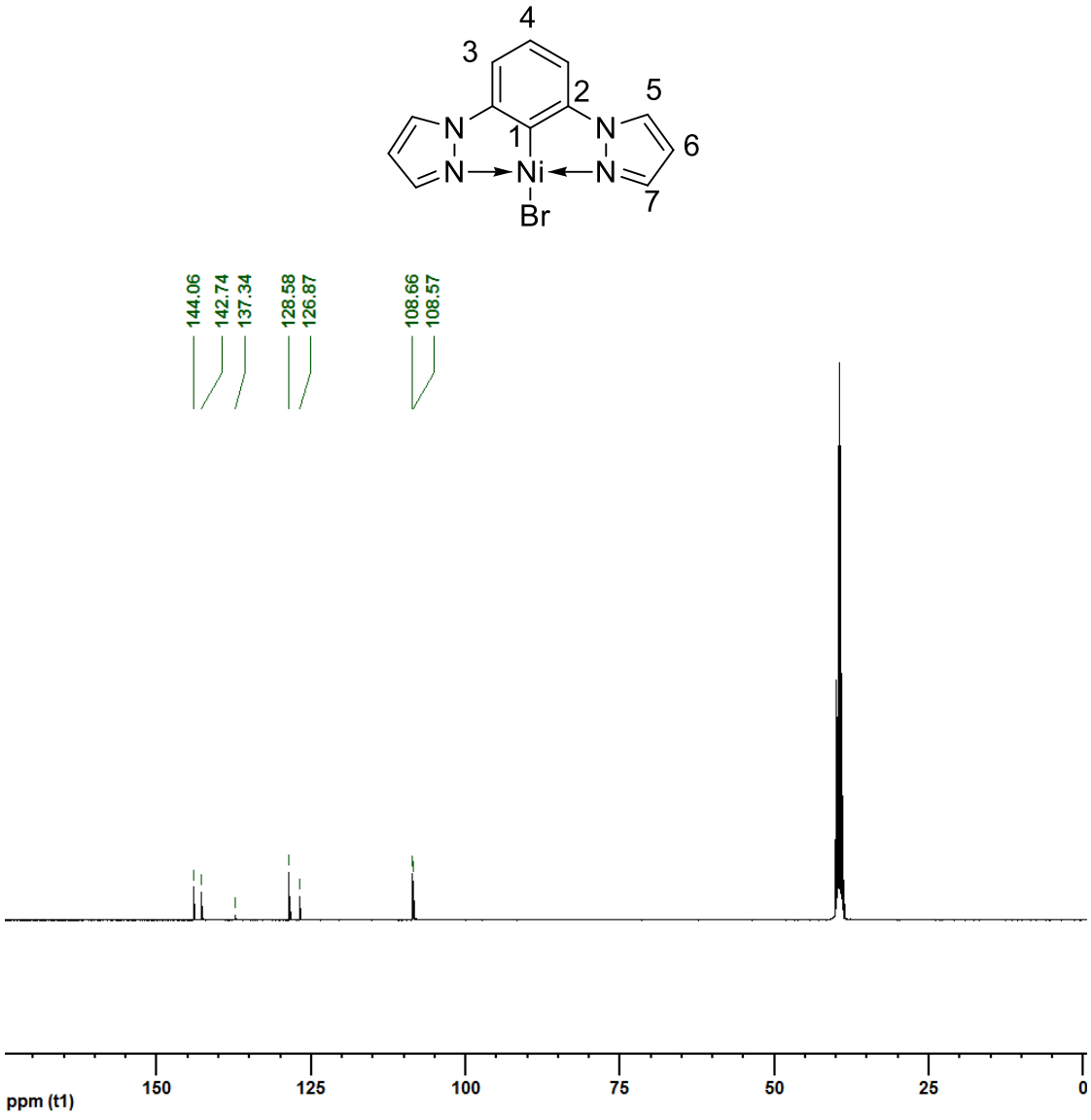

^{13}C NMR (DMSO-d6, 400MHz), δ 144.07 (2C, s, C5), 142.74 (2C, s, C2), 137.34 (1C, s, C1), 128.58 (2C, d, C7), 126.87 (1C, s, C4), 108.66 (2C, s, C3), 108.57 (2C, s, C6)

Figure 2.9. ^{1}H NMR of OMe-NCN (ligand b) – $CDCl_3$

^{1}H NMR (CDCl3, 400MHz), δ 7.99 (2H, d, J_{HH} = 2.5, H5), 7.74 (2H, d, J_{HH} = 1.6, H7), 7.64 (1H, t, J_{HH} = 1.9, H1), 7.22 (2H, d, J_{HH} = 1.9, H3), 6.49 (2H, t, J_{HH} = 1.9, H6), 3.93 (3H, s, H8).

Figure 2.10 ^{13}C NMR of OMe-NCN (ligand b) - $CDCl_3$

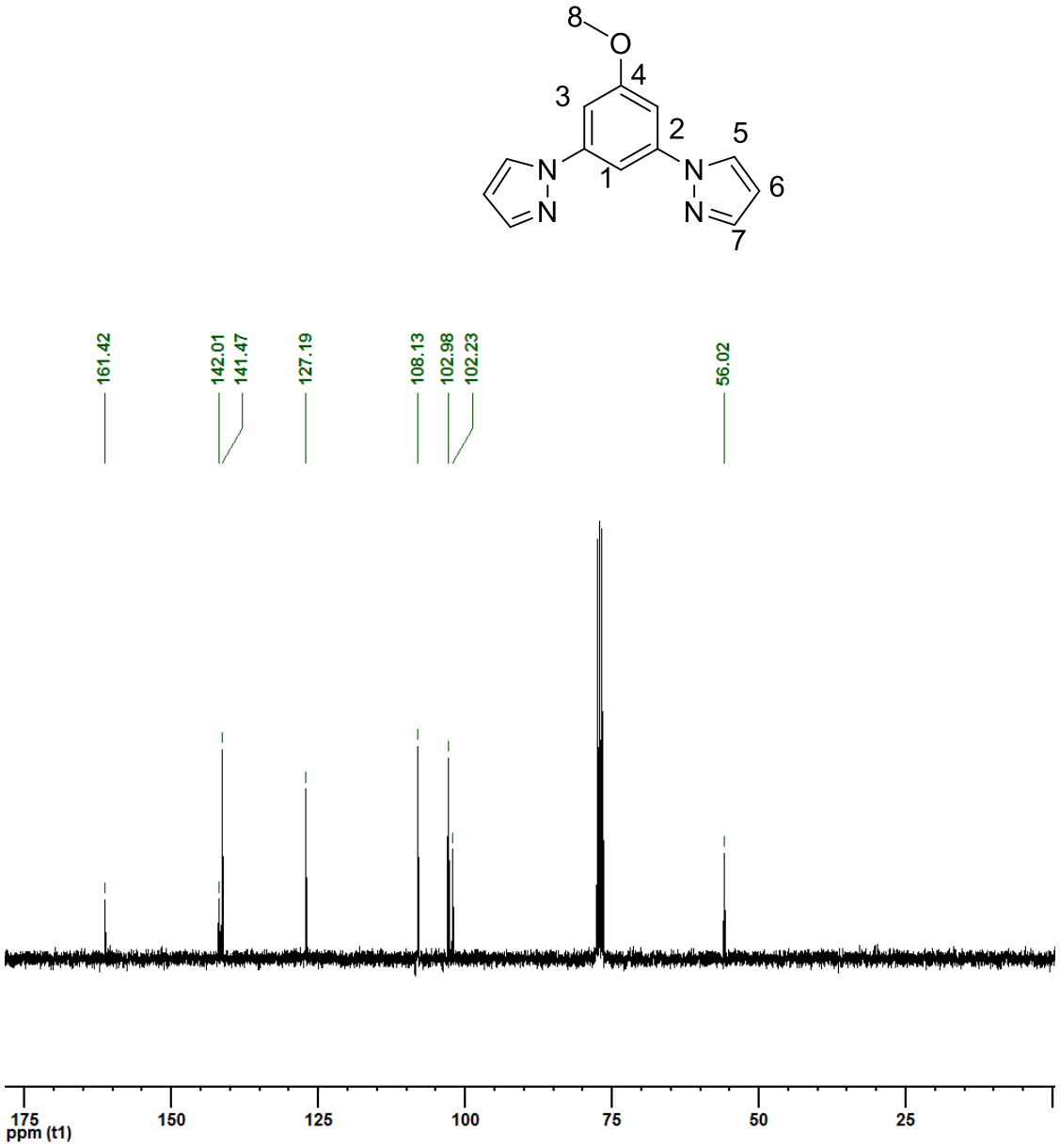

^{13}C NMR (CDCl3, 400MHz), δ 161.42 (1C, s, C4), 142.01 (2C, s, C2), 141.47 (2C, s, C7), 127.19 (2C, s, C5), 108.13 (2C, s, C6), 102.98 (2C, s, C3), 102.23 (1C, s, C1), 56.02 (1C, s, C8).

Figure 2.11. ^{1}H NMR of OMe-NCN^{pz}NiBr (2) – $CDCl_3$

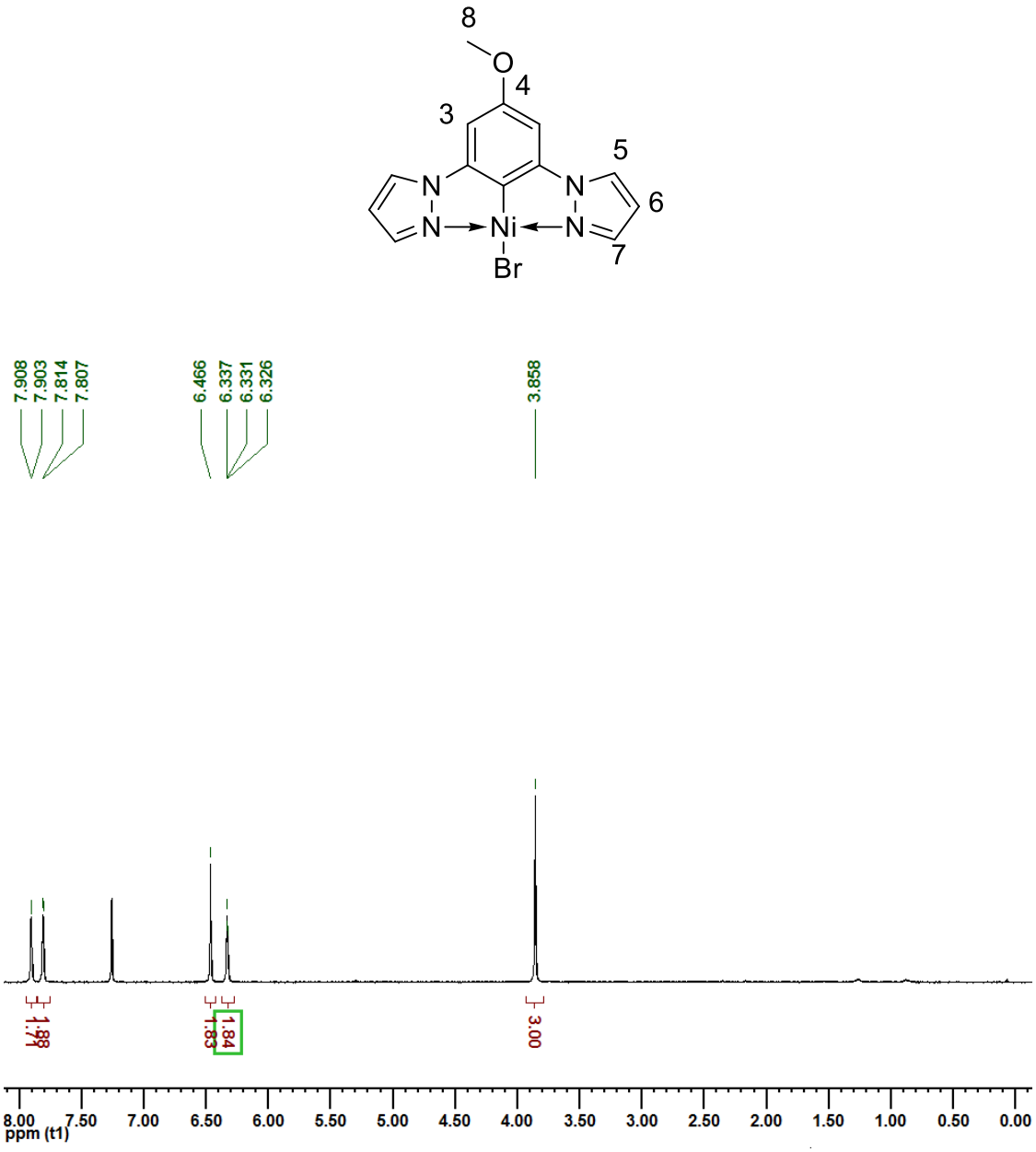

^{1}H NMR (CDCl3, 400MHz), δ 7.89 (2H, d, J_{HH} = 2.0, H5), 7.81 (2H, d, J_{HH} = 2.7, H7), 6.46 (2H, s, H3), 6.34 (2H, t, J_{HH} = 2.4, H6), 3.87 (3H, s, H8).

Figure 2.12. ^{13}C NMR of OMe-NCN^{pz}NiBr (2) – $CDCl_3$

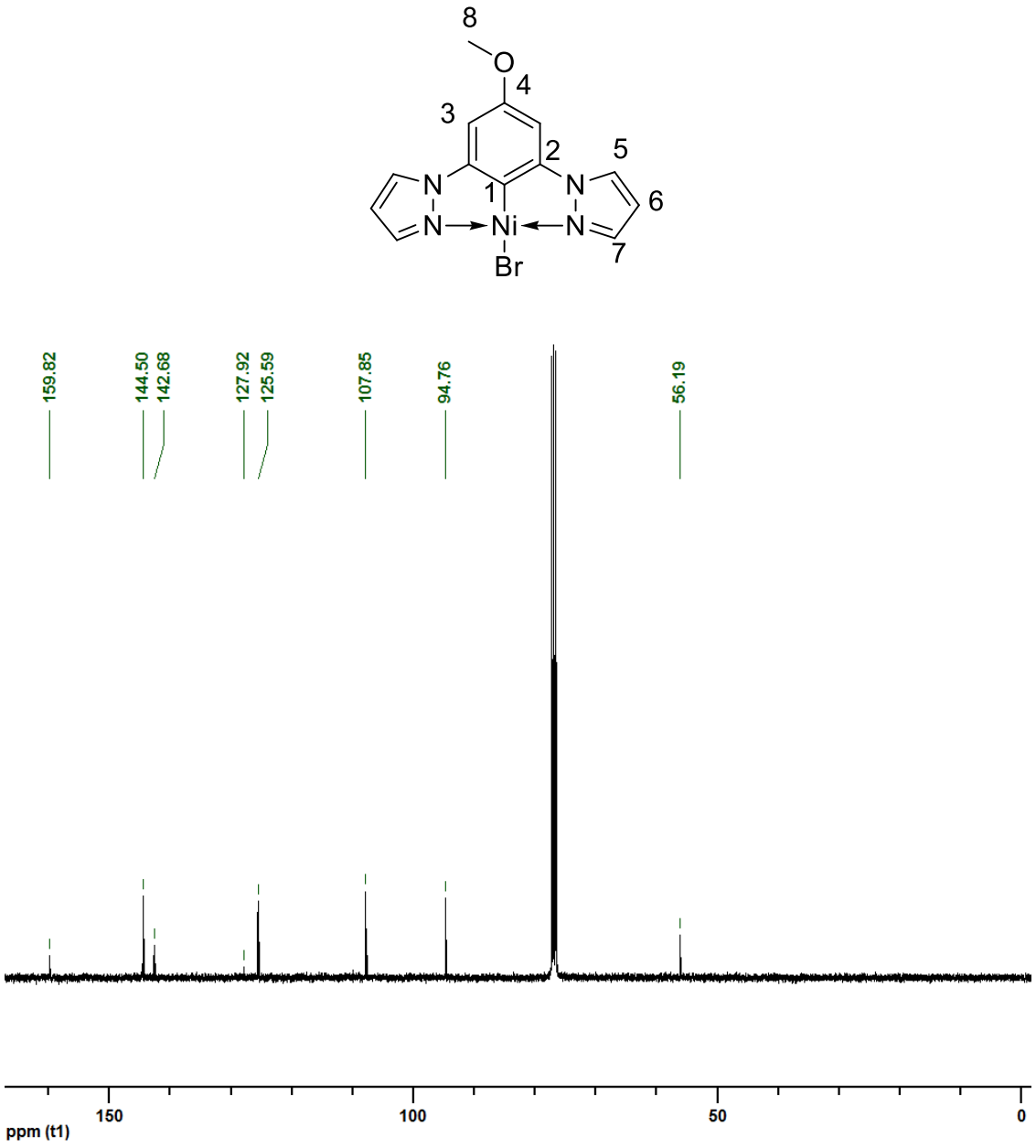

^{13}C NMR (CDCl3, 400MHz), δ 159.82 (1C,s C4), 144.50 (2C, s, C5), 142.68 (2C,s C2), 127.92 (1C,s, C1), 125.59 (2C, s, C7), 107.85 (2c, s, C6), 94.76 (2C, s, C3), 56.19 (1C,s, C8).

Figure 2.13. ^{1}H NMR of NCN-OH – $CDCl_3$

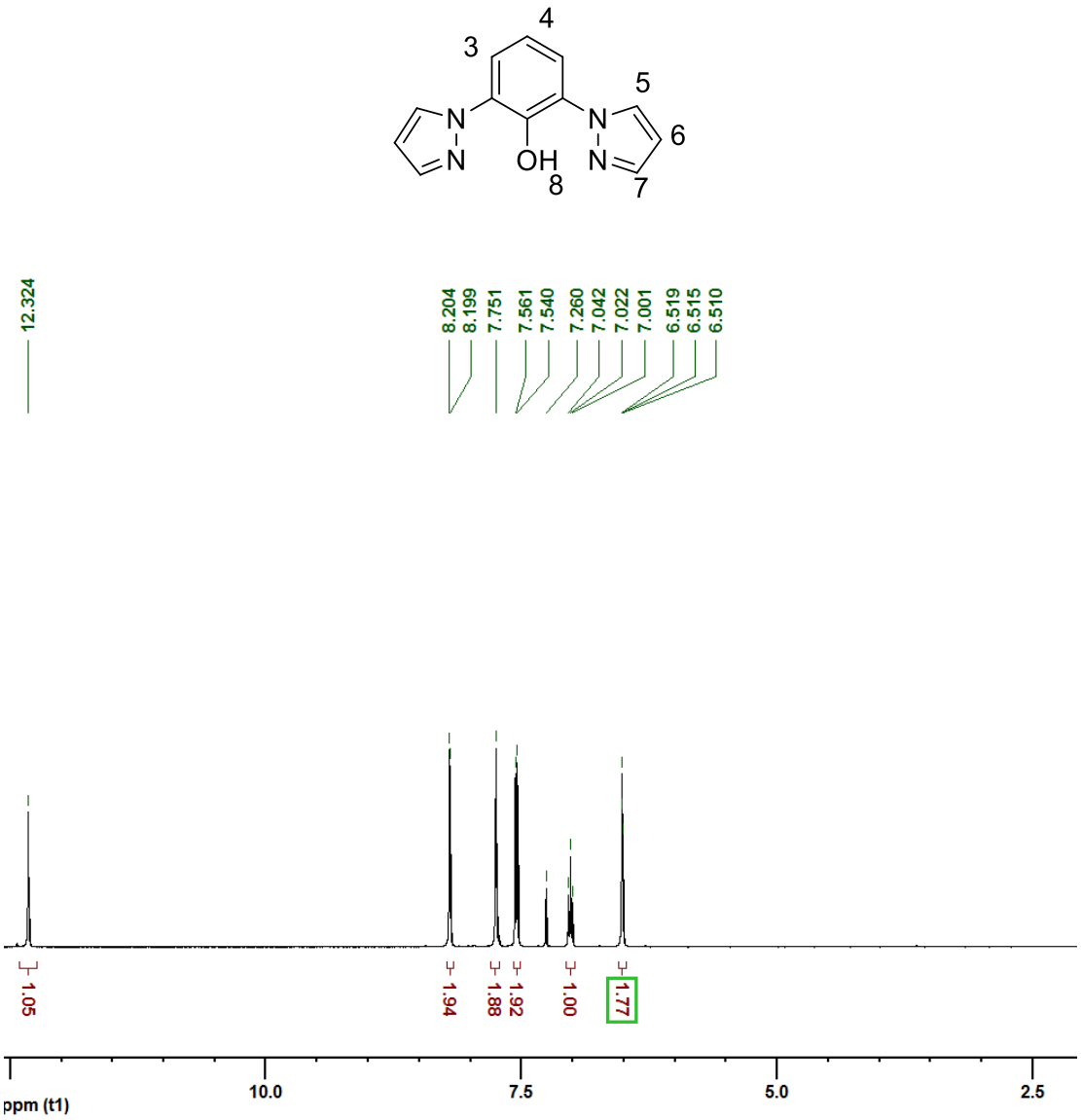

^{1}H NMR ($CDCl_3$, 400MHz), δ 12.32 (1H, s, H^8), 8.20 (2H, d, J_{HH} = 2.3 H^5), 7.75 (2H, s, H^7), 7.55 (2H, d, J_{HH} = 8.1, H^3), 7.01 (1H, t, J_{HH} = 8.1, H^4), 6.51 (2H, t, J_{HH} = 2.0, H^6).

Figure 2.14. ^{13}C NMR of NCN-OH – $CDCl_3$

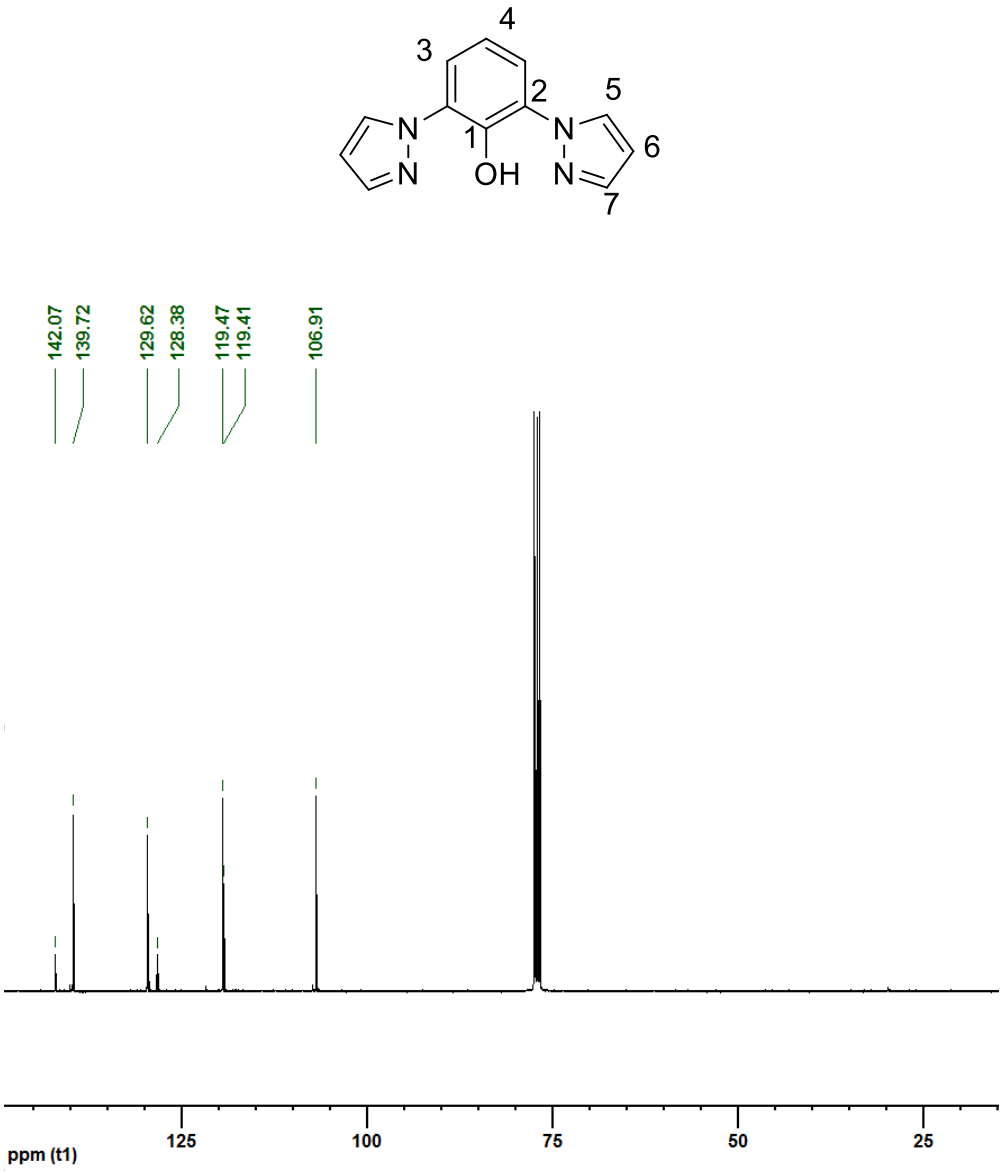

^{13}C NMR ($CDCl_3$, 400MHz), δ 142.07 (1C, s, C^1), 139.72 (2C, s, C^7), 129.62 (2C, s, C^5), 128.38 (2C, s, C^2), 119.47 (2C, s, C^3), 119.42 (1C, s, C^4), 106.91 (2C, s, C^6)

Figure 2.15. ^{1}H NMR of Br-NCN-OH – $CDCl_3$

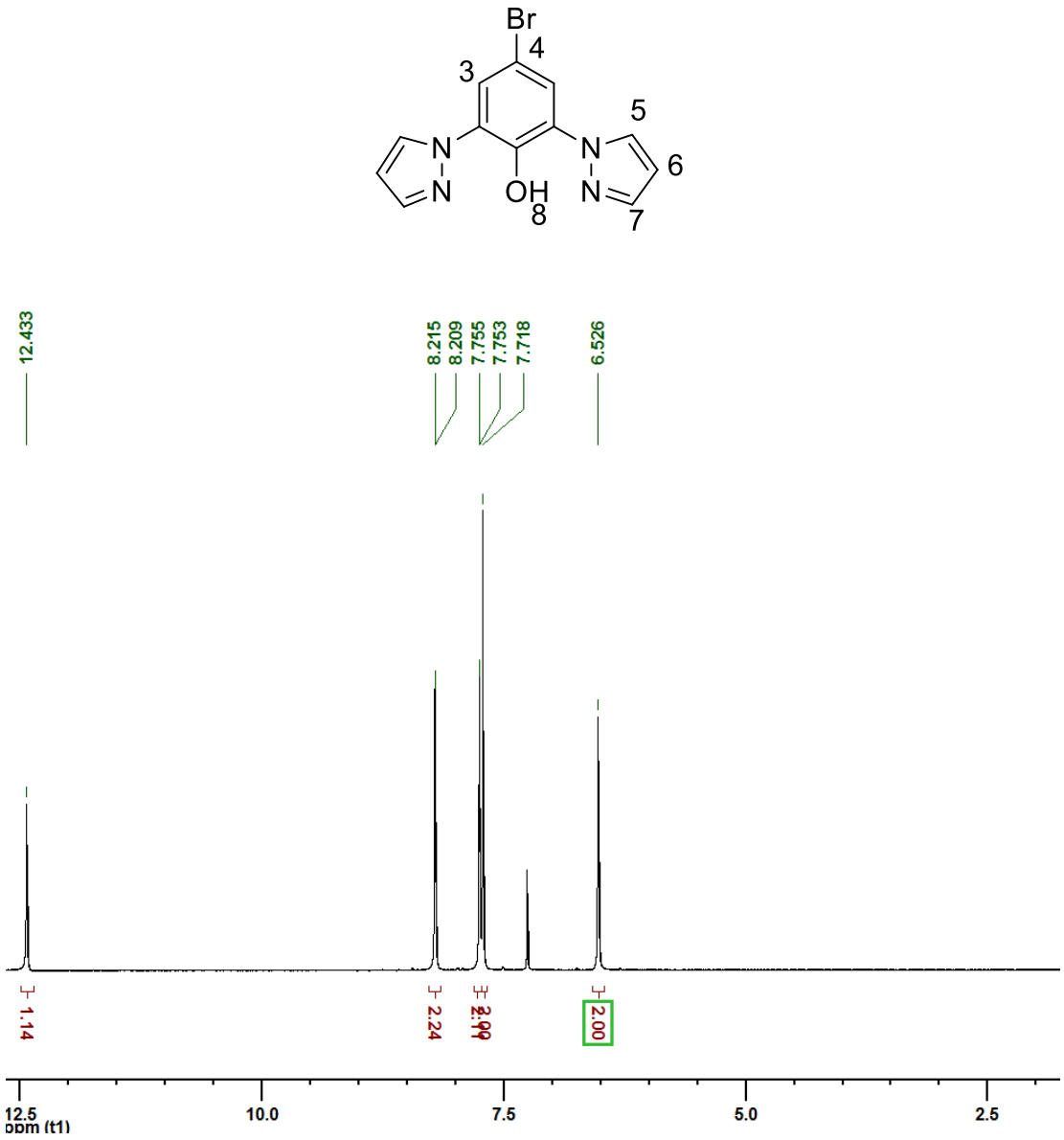

^{1}H NMR ($CDCl_3$, 400MHz), δ 12.43 (1H, s, H^{8}), 8.21 (2H, d, J_{HH} = 2.4 H^{5}), 7.75 (2H, d, H^{7}), 7.71 (2H, s, H^{3}), 6.52 (2H, t, J_{HH} = 2.1, H^{6}).

Figure 2.16. ^{13}C NMR of Br-NCN^{-}OH – $CDCl_3$

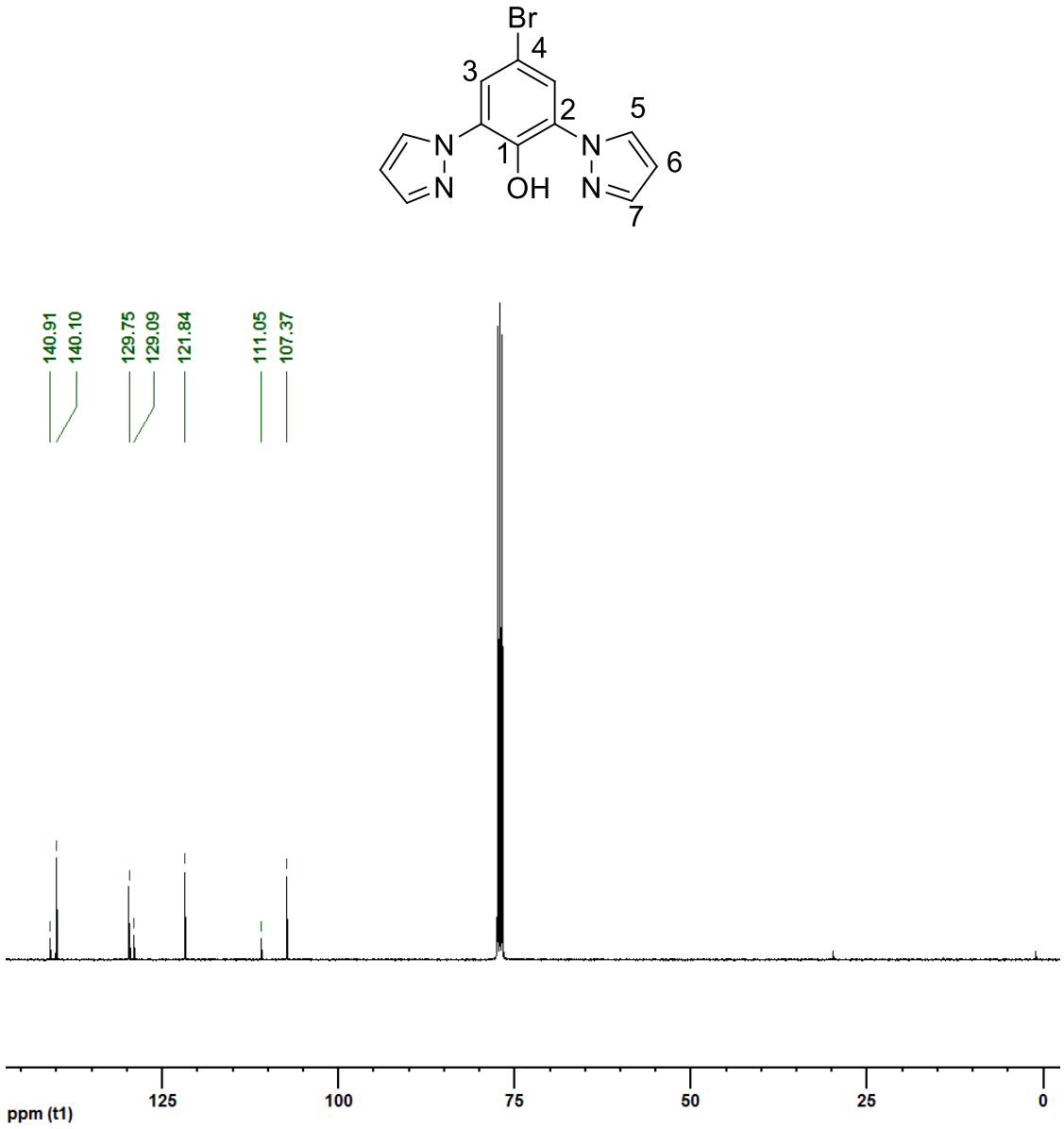

^{13}C NMR ($CDCl_3$, 400MHz), δ 140.91 (1C, s, C^1), 140.10 (2C, s, C^7), 129.75 (2C, s, C^5), 129.09 (2C, s, C^2), 121.84 (2C, s, C^3), 111.05 (1C, s, C^4), 107.37 (2C, s, C^6).

Figure 2.17. ^{1}H NMR of NCN-NiBHT – $CDCl_3$

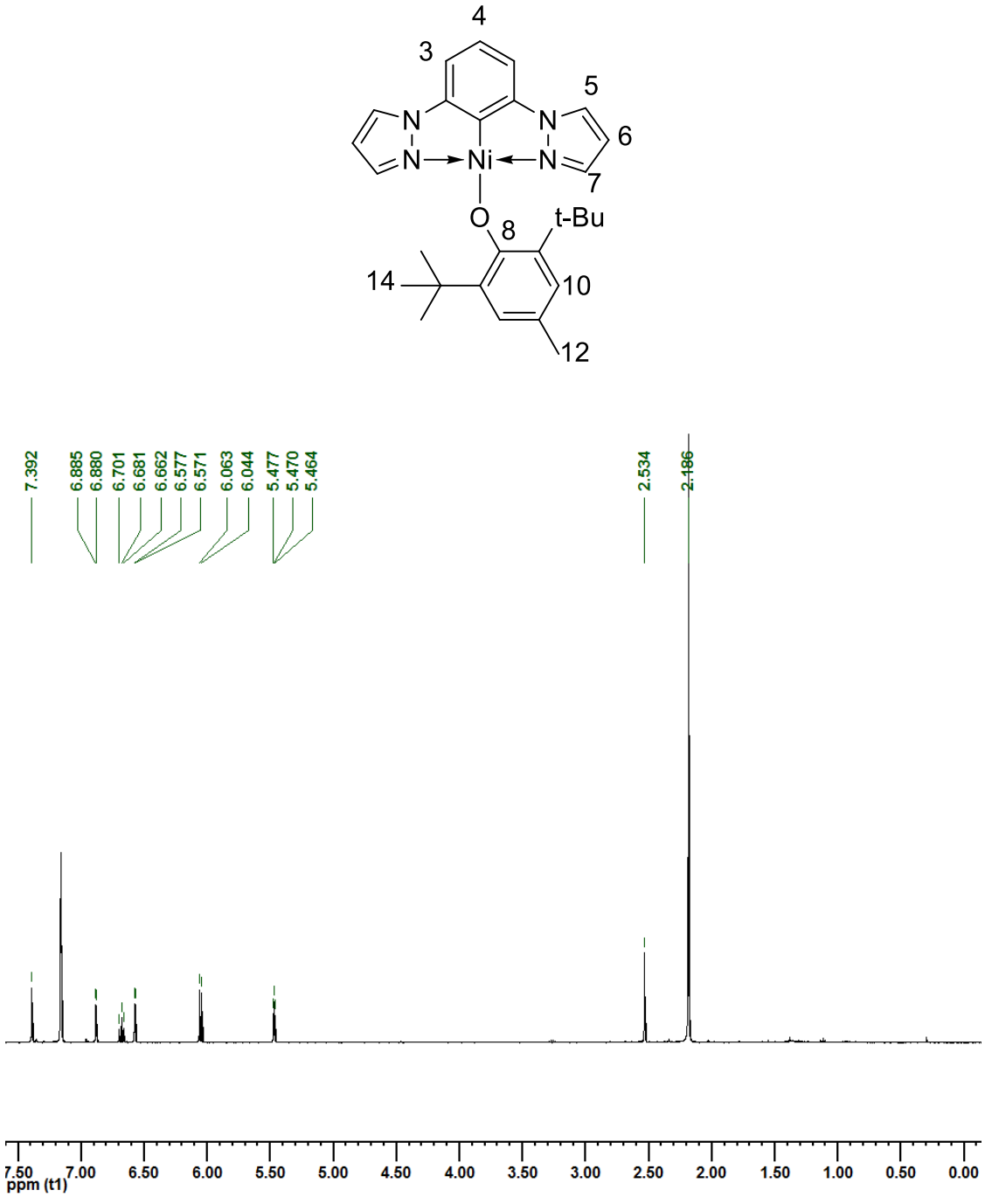

^{1}H NMR (C_6D_6, 400MHz), δ 7.39 (2H, s, H^{10}), 6.88 (2H, d, J_{HH} = 2.1, H^{5}), 6.67 (1H, t, J_{HH} = 7.8, H^{4}), 6.57 (2H, d, J_{HH} = 2.4, H^{7}), 6.05 (2H, d, J_{HH} = 7.8, H^{3}), 5.47 (2H, t, J_{HH} = 2.4, H^{6}), 2.63 (3H, s, H^{12}), 2.19 (18H, s, H^{14}).

Figure 2.18. ^{13}C NMR of NCN-NiBHT – $CDCl_3$

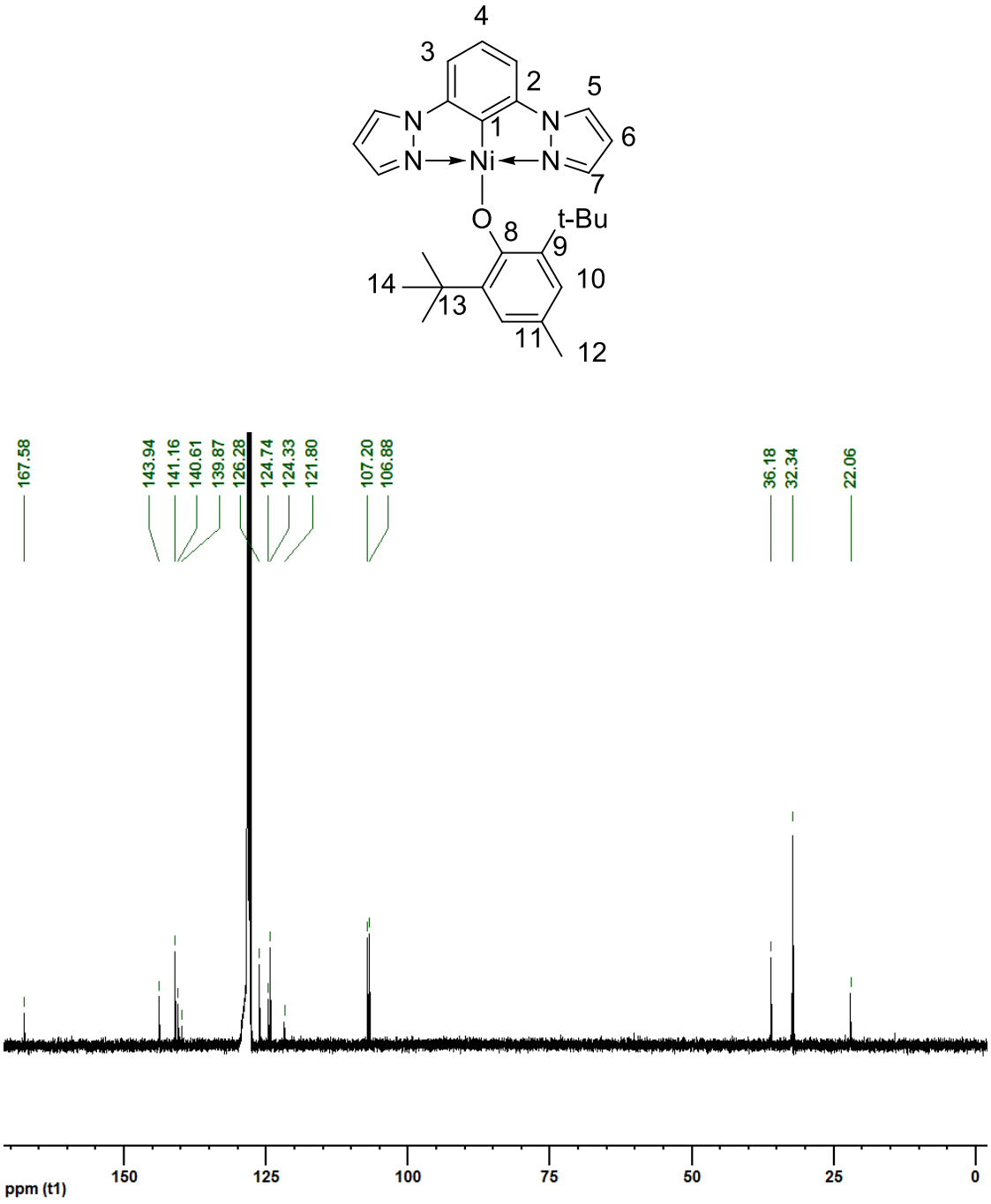

^{13}C NMR (CDCl3, 400MHz), δ 167.6 (1C, s, C8), 143.97 (2C, s, C2), 141.18 (2C, s, C5), 140.64 (2C, s, C9), 139.88 (1C, s, C1), 126.30 (2C, s, C10), 124.77 (1C, s, C4), 124.36 (2C, s, C7), 121.82 (1C, s, C11), 107.23 (2C, s, C3), 106.91 (2C, s, C6), 36.22 (2C, s, C13), 32.37 (6C, s, C14), 22.09 (1C, s, C12).

Figure 2.19. ^{1}H NMR of NCN-OMe – $CDCl_3$

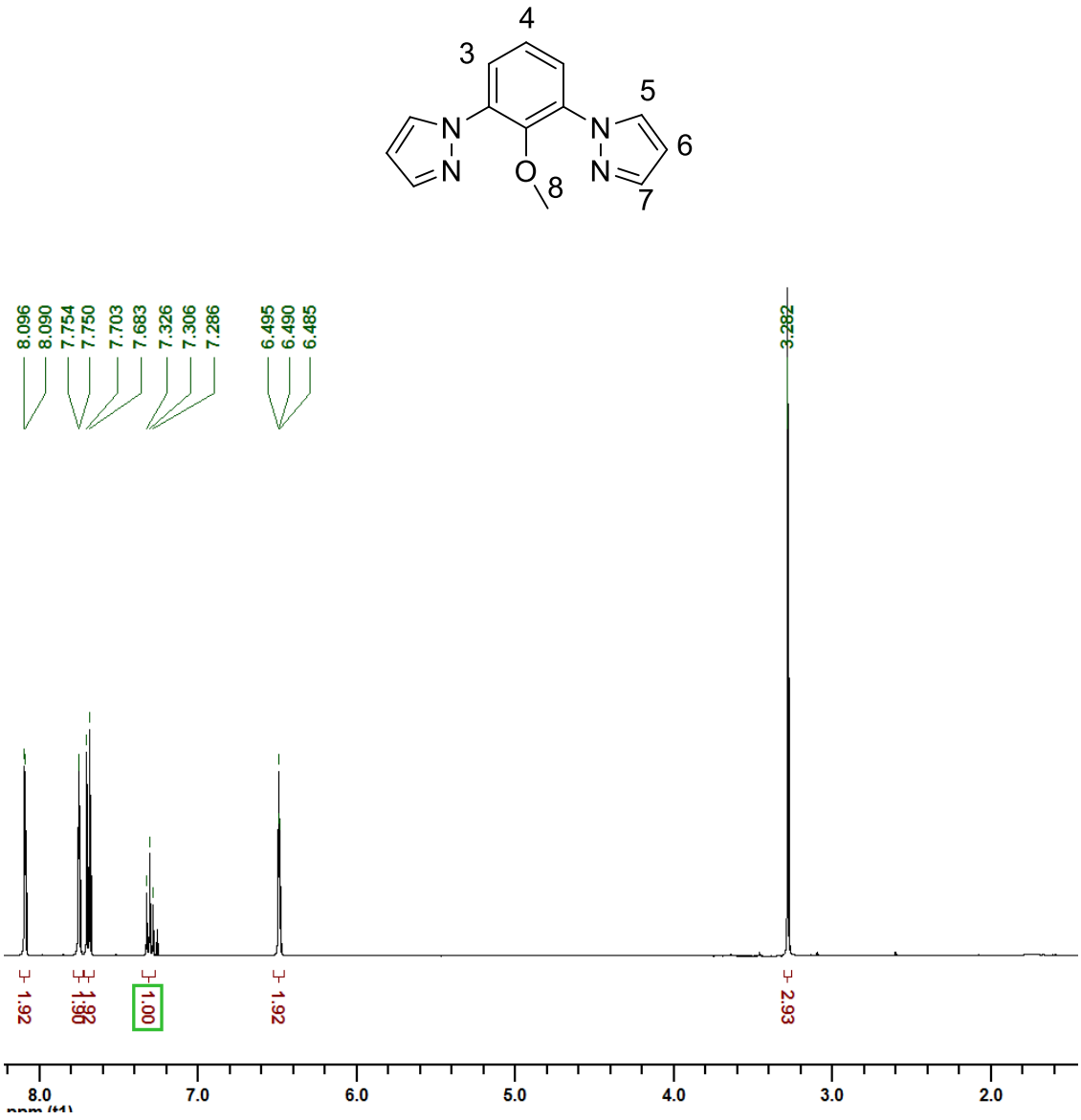

^{1}H NMR (CDCl3, 400MHz), δ 8.10 (2H, d, J_{HH} = 2.4, H^5), 7.75 (2H, d, J_{HH} = 1.6, H^7), 7.69 (2H, d, J_{HH} = 8.0, H^3), 7.32 (1H, t, J_{HH} = 8.0, H^4), 6.49 (2H, t, J_{HH} = 2.0, H^6), 3.28 (3H, s, H^8).

Figure 2.20. ^{13}C NMR of NCN-OMe – $CDCl_3$

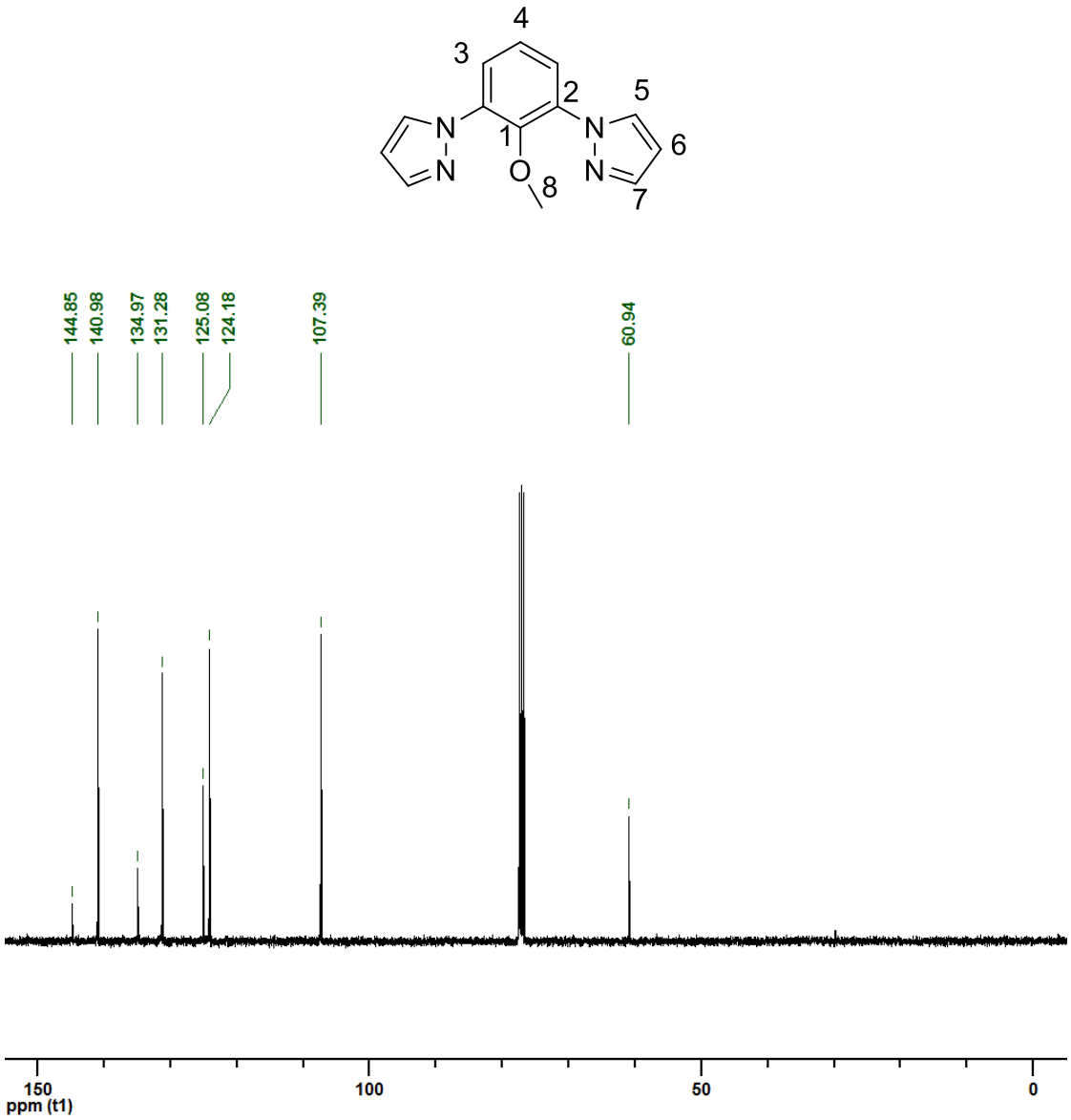

^{13}C NMR (CDCl3, 300MHz), δ 144.85 (1C, s, C^1), 140.98 (2C, s, C^7), 134.97 (2C, s, C^2), 131.28 (2C, s, C^5), 125.09 (1C, s, C^4), 124.18 (2C, s, C^3), 107.40 (2C, s, C^6), 60.94 (1C, s, C^8).

Figure 2.21. ^{1}H NMR of NCN-OEt – $CDCl_3$

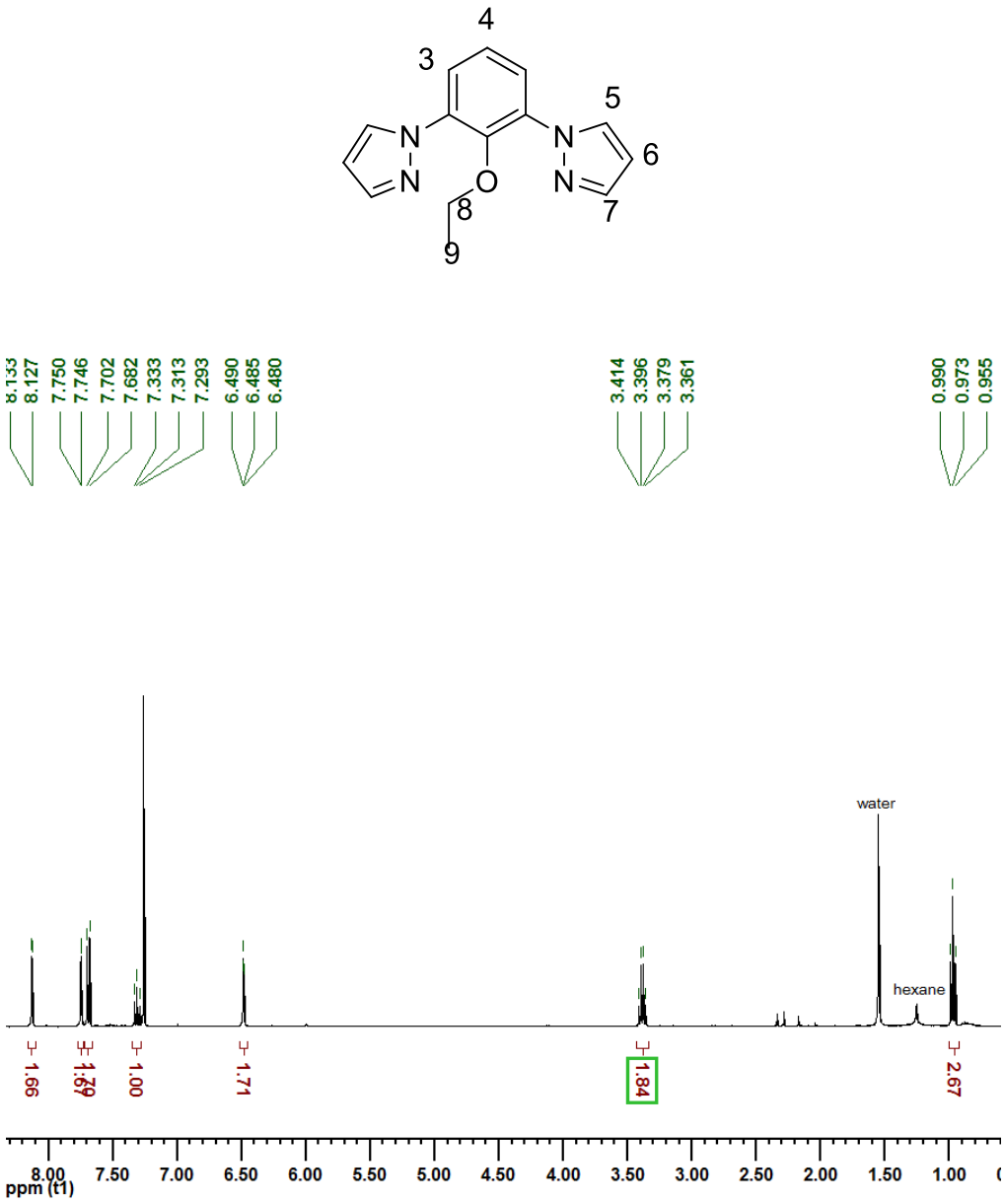

^{1}H NMR (CDCl3, 400MHz), δ 8.13 (2H, d, J_{HH} = 2.4, H^5), 7.75 (2H, d, J_{HH} = 1.6, H^7), 7.69 (2H, d, J_{HH} = 8.1, H^3), 7.32 (1H, t, J_{HH} = 8.1, H^4), 6.49 (2H, t, J_{HH} = 2.1, H^6), 3.39 (2H, q, H^8), 0.96 (3H, t. H^9).

Figure 2.22. ^{13}C NMR of NCN-OEt – $CDCl_3$

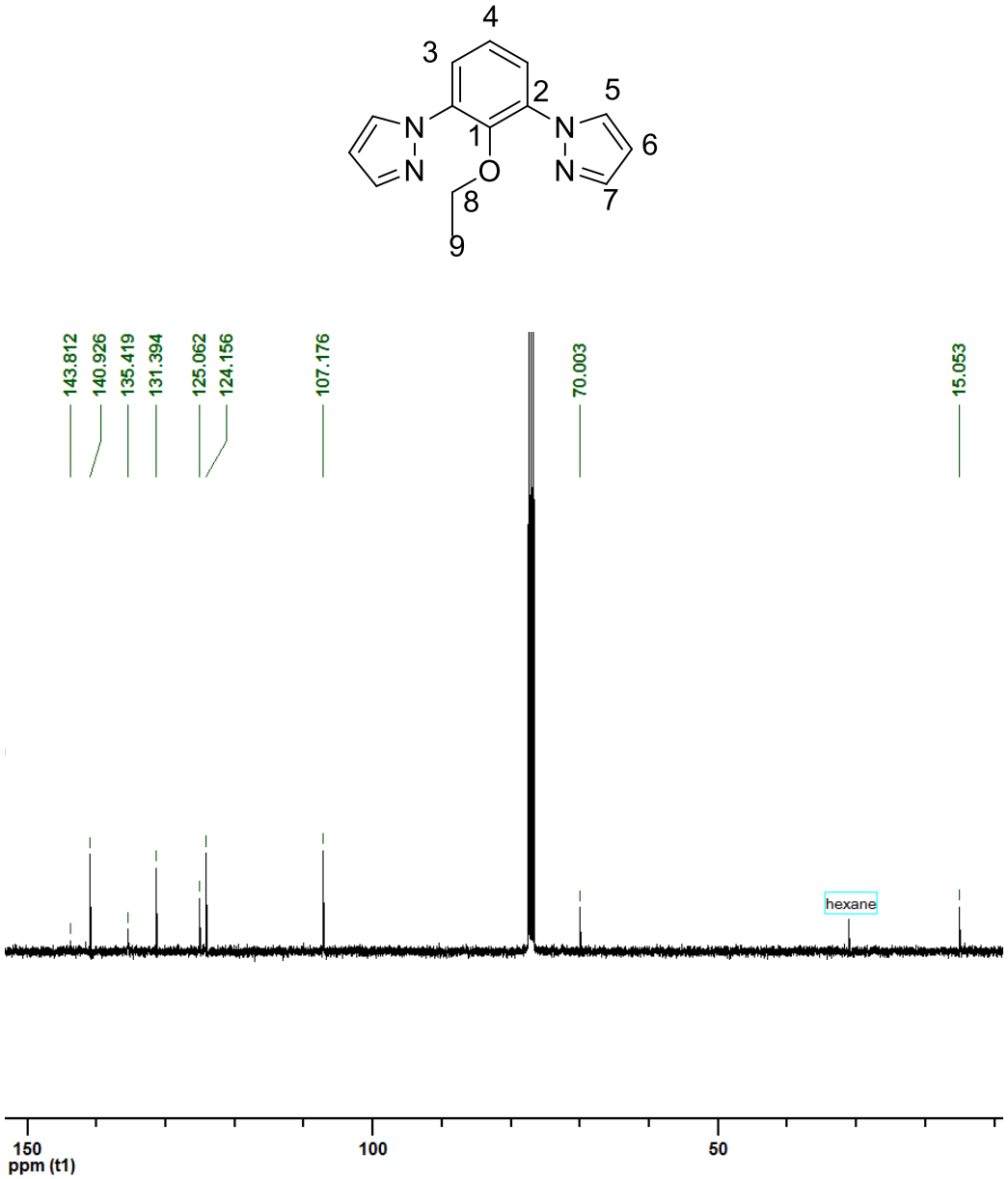

^{13}C NMR (CDCl3, 300MHz), δ 143.81 (1C, s, C^1), 140.93 (2C, s, C^5), 135.41 (2C, s, C^2), 131.39 (2C, s, C^7), 125.06 (1C, s, C^4), 124.16 (2C, s, C^3), 107.17 (2C, s, C^6), 70.00 (1C, s, C^8), 15.05 (1C, s, C^9).

Figure 2.23. ^{1}H NMR of NCN-OiPr – $CDCl_3$

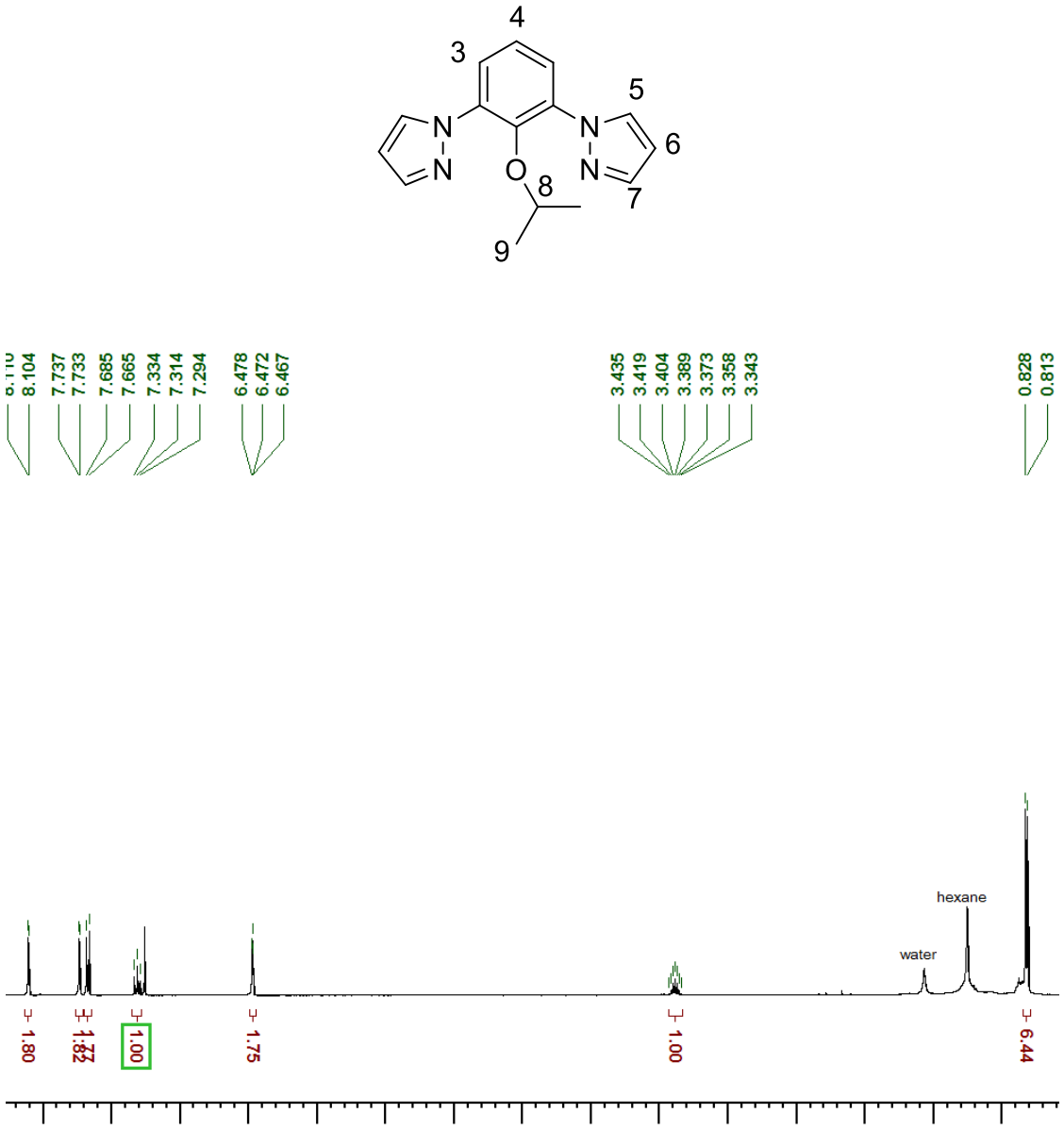

^{1}H NMR (CDCl3, 400MHz), δ 8.11 (2H, d, J_{HH} = 2.4, H^{5}), 7.74 (2H, d, J_{HH} = 1.5, H^{7}), 7.67 (2H, d, J_{HH} = 8.1, H^{3}), 7.32 (1H, t, J_{HH} = 8.1, H^{4}), 6.48 (2H, t, J_{HH} = 2.1, H^{6}), 3.38 (2H, sept, J_{HH} = 6.1, H^{8}), 0.82 (3H, d, J_{HH} = 6.1 H^{9}).

Figure 2.24. ^{13}C NMR of NCN-OiPr – $CDCl_3$

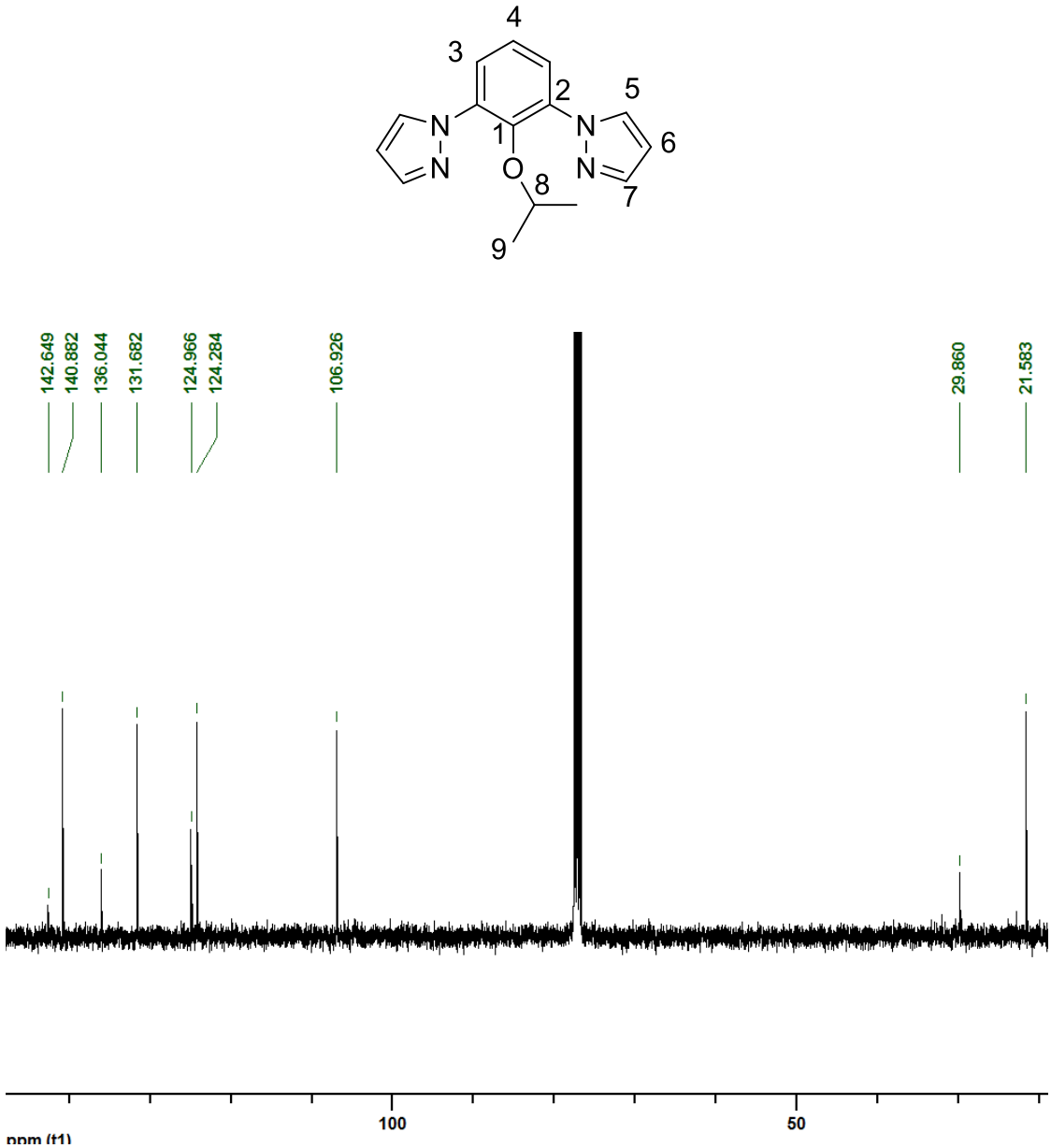

^{13}C NMR (CDCl3, 400MHz), δ 142.6 (1C, s, C^1), 140.88 (2C, s, C^7), 136.0 (2C, s, C^2), 125.0 (2C, s, C^5), 124.97 (2C, s, C^4), 124.28 (2C, s, C^3), 106.9 (2C, s, C^6), 29.86 (1C, s, C^8), 21.58 (2C, s, C^9).

Figure 2.25. ^{1}H NMR of NCN-Morpholine – $CDCl_3$

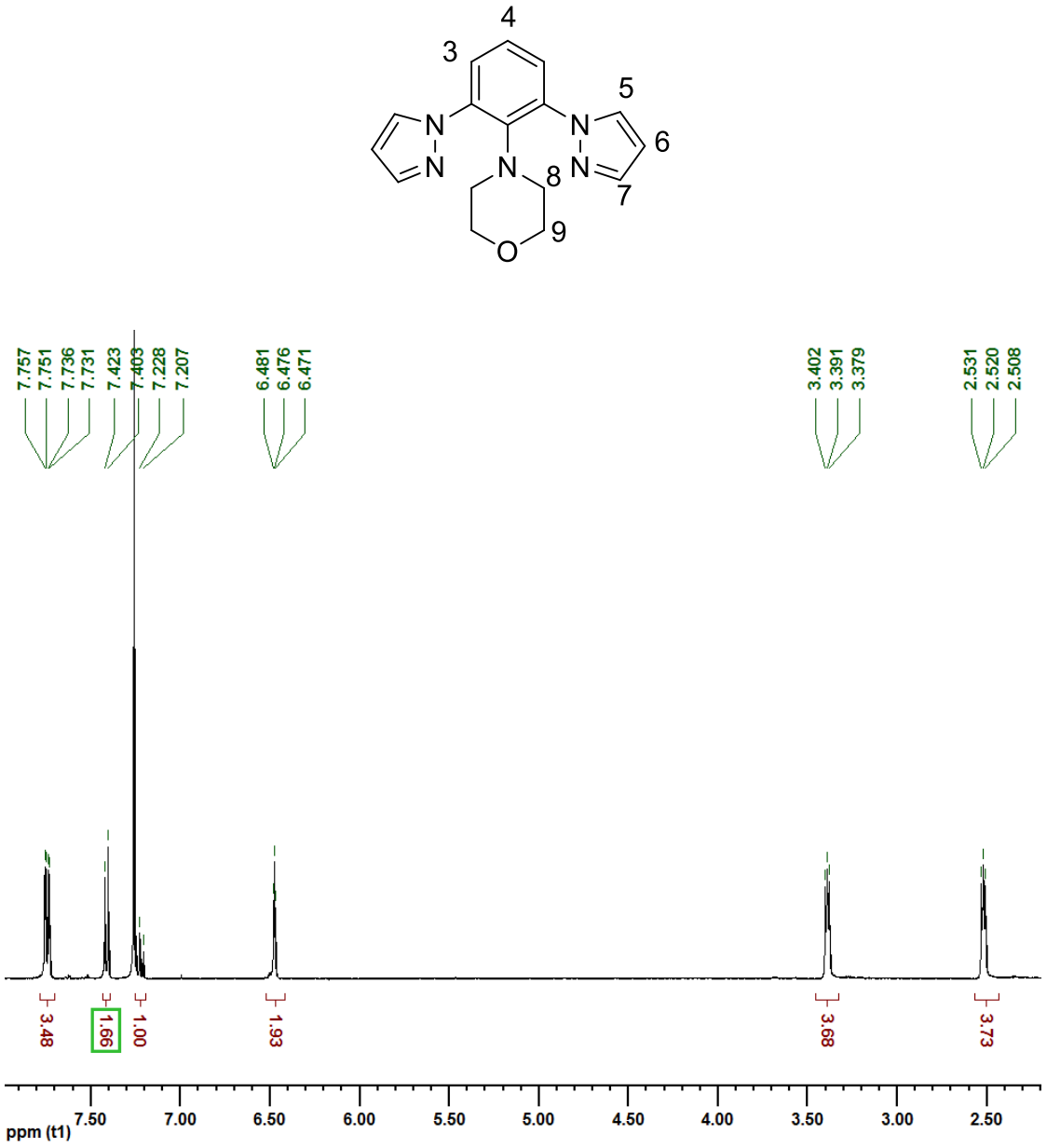

^{1}H NMR (CDCl3, 400MHz), δ 7.75 (2H, d, J_{HH} = 1.8, H^5), 7.73 (2H, d, J_{HH} = 1.8, H^7), 7.41 (2H, d, J_{HH} = 7.8, H^3), 7.24 (1H, t, J_{HH} = 7.5, H^4), 6.47 (2H, t, J_{HH} = 1.9, H^6), 3.38 (4H, t, J_{HH} = *4.6*, H^8), 2.51 (4H, t, J_{HH} = *4.6*, H^9).

Figure 2.26. ^{13}C NMR of NCN-Morpholine – $CDCl_3$

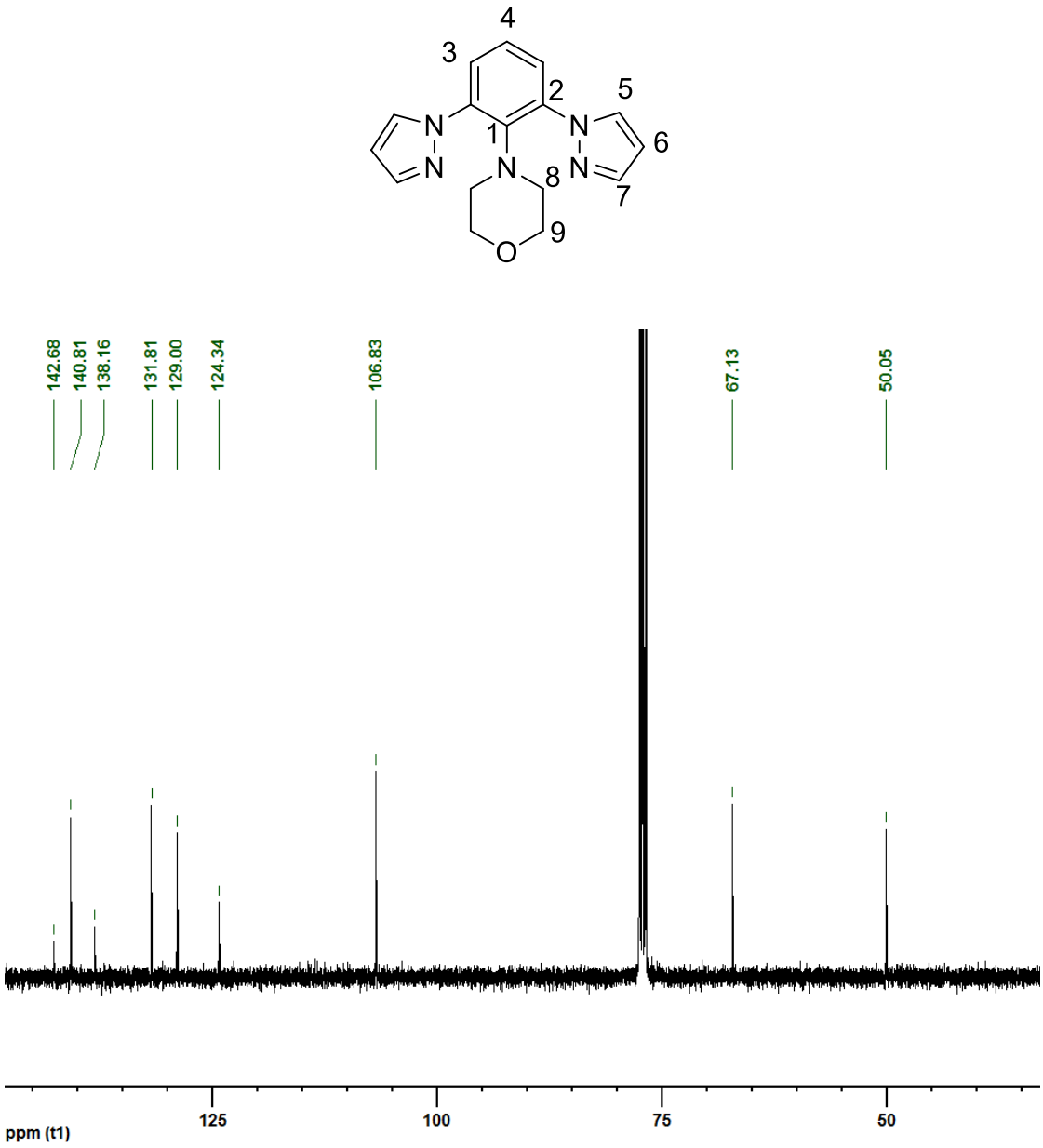

^{13}C NMR (CDCl3, 400MHz), δ 142.7 (1C, s, C^1), 140.81 (2C, s, C^7), 138.2 (2C, s, C^2), 131.80 (2C, s, C^5), 129.0 (2C, s, C^3), 124.34 (2C, s, C^6), 106.83 (1C, s, C^4), 67.13 (2C, s, C^8), 50.06 (2C, s, C^9).

Figure 2.27. ^{1}H NMR of crude OMe-NCN^{pz}-OH – $CDCl_3$

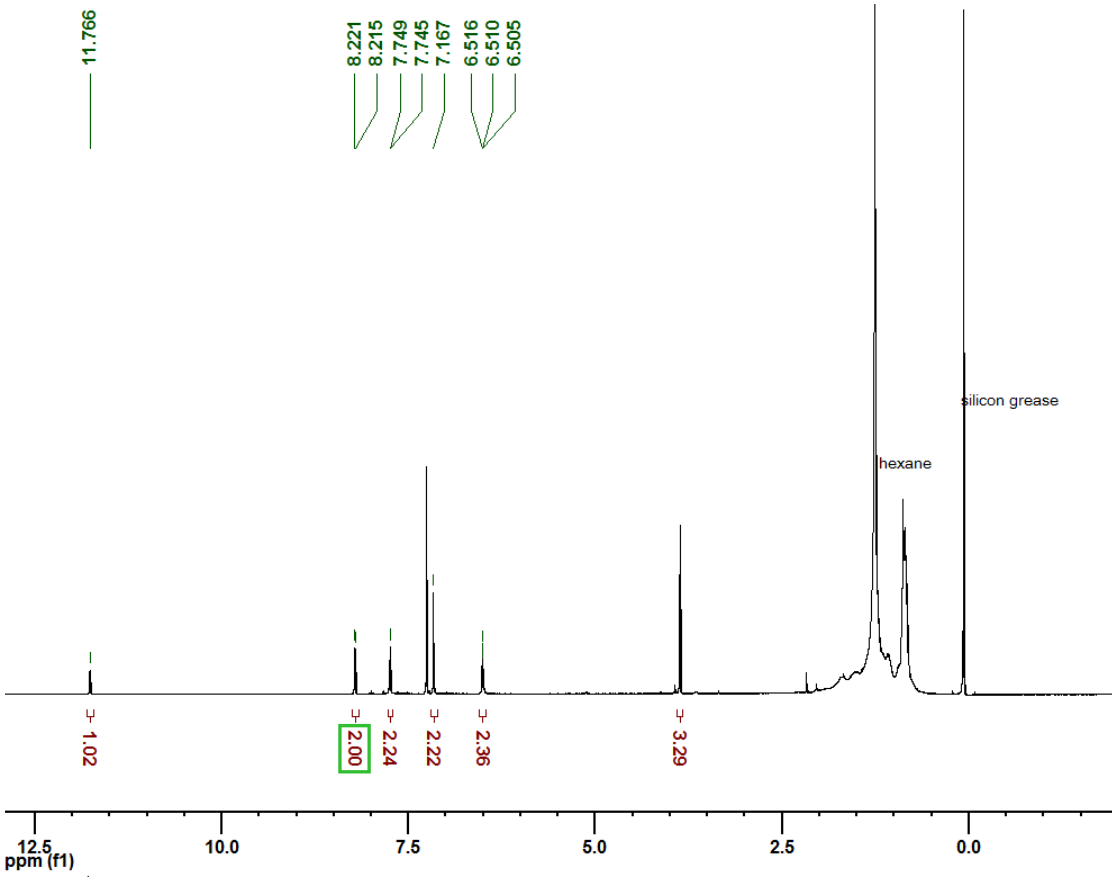

Figure 2.28. Cyclic voltammetry of 1 and 2 and 3. The measurements were carried out at 298K on CH_2Cl_2 solutions containing a concentration of 0.1M of [Bu_4N] [BF_6] and 1mM of sample

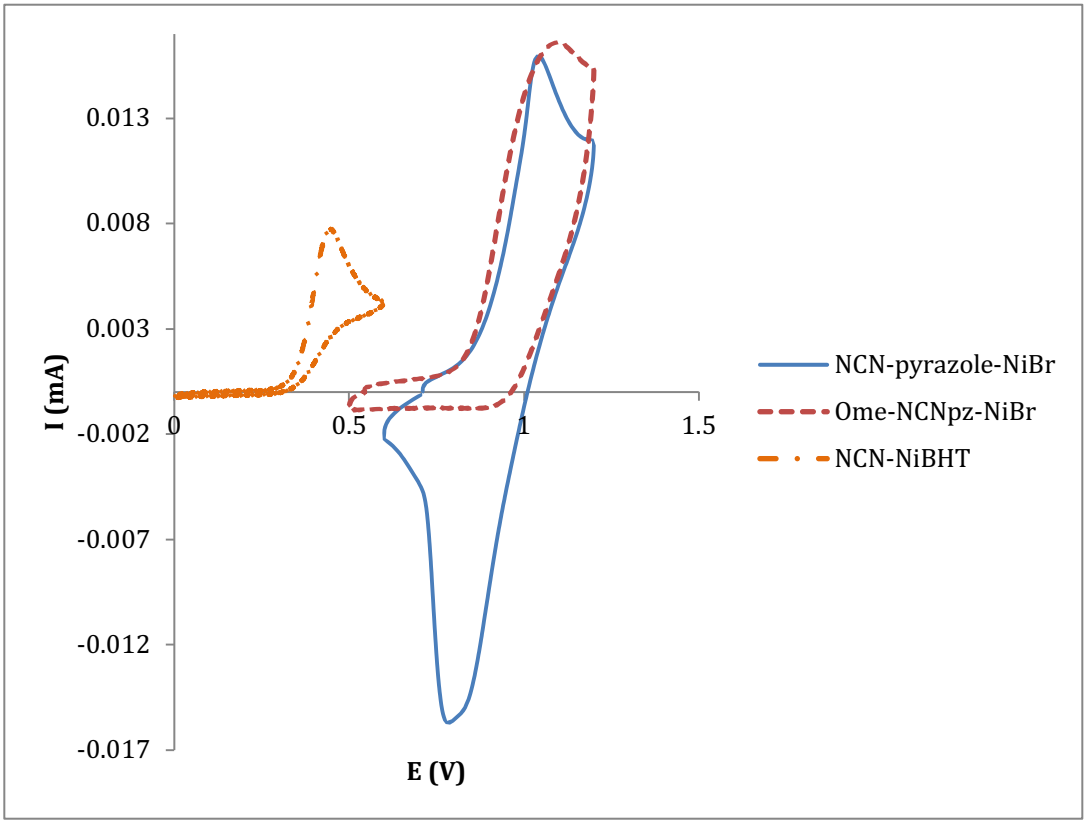

Figure 2.29. Mass spectrum of ligand b

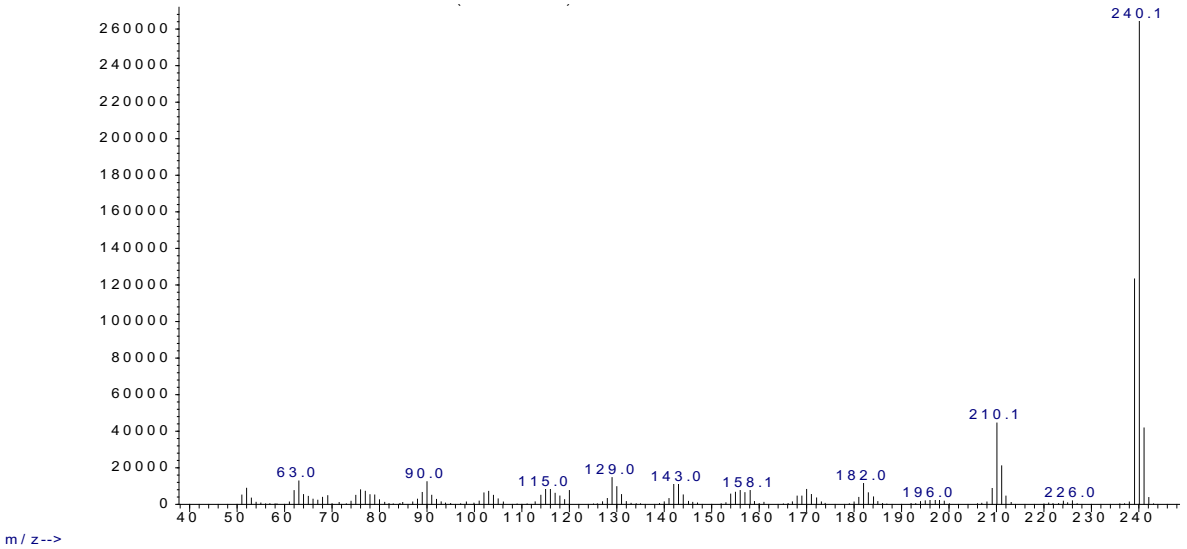

Figure 2.30. Mass spectrum of NCN-OMe

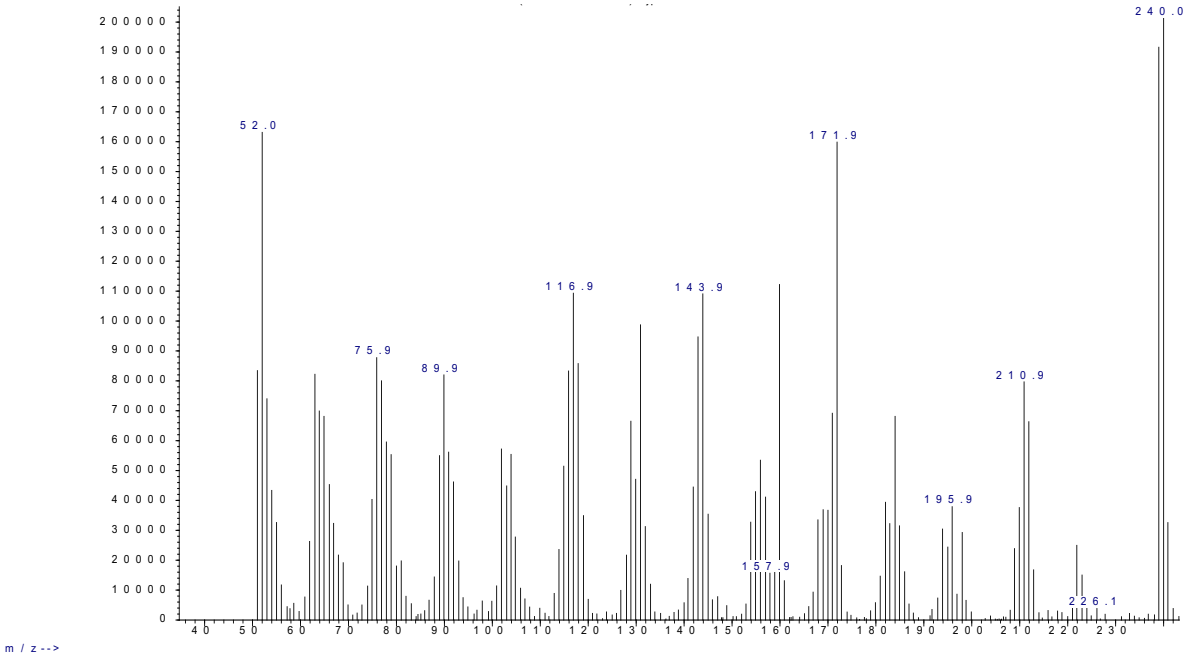

Figure 2.31. Mass spectrum of NCN-OEt

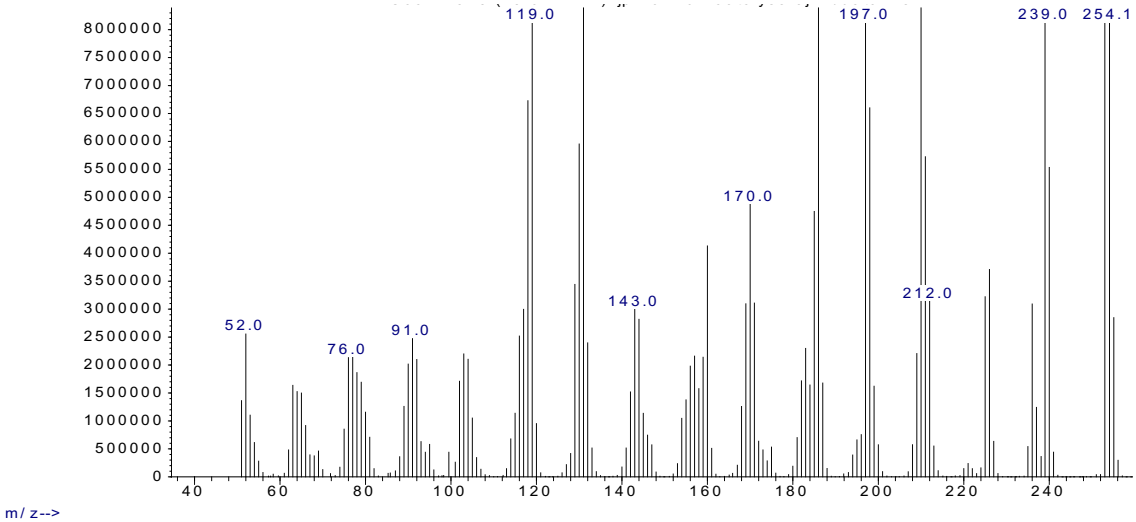

Figure 2.32. Mass spectrum of NCN-OiPr

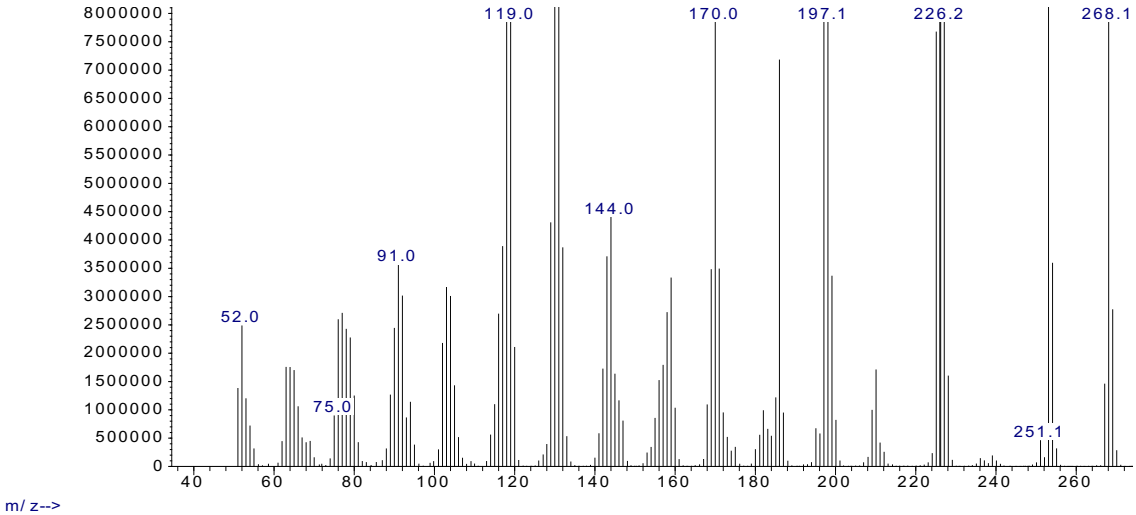

Figure 2.33. Mass spectrum of NCN-OCH_2CF_3

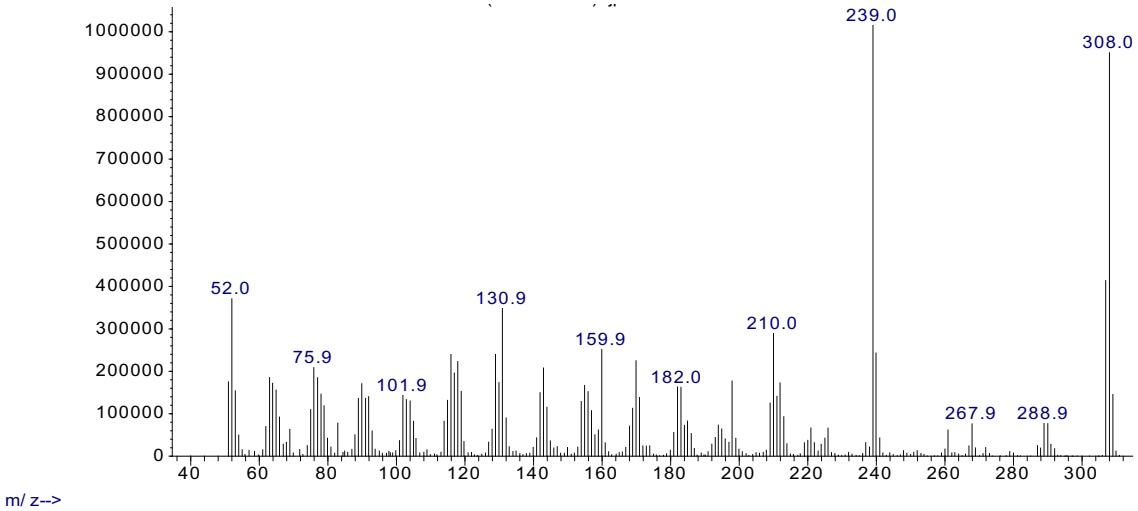

Figure 2.34. Mass spectrum of NCN-Morpholine

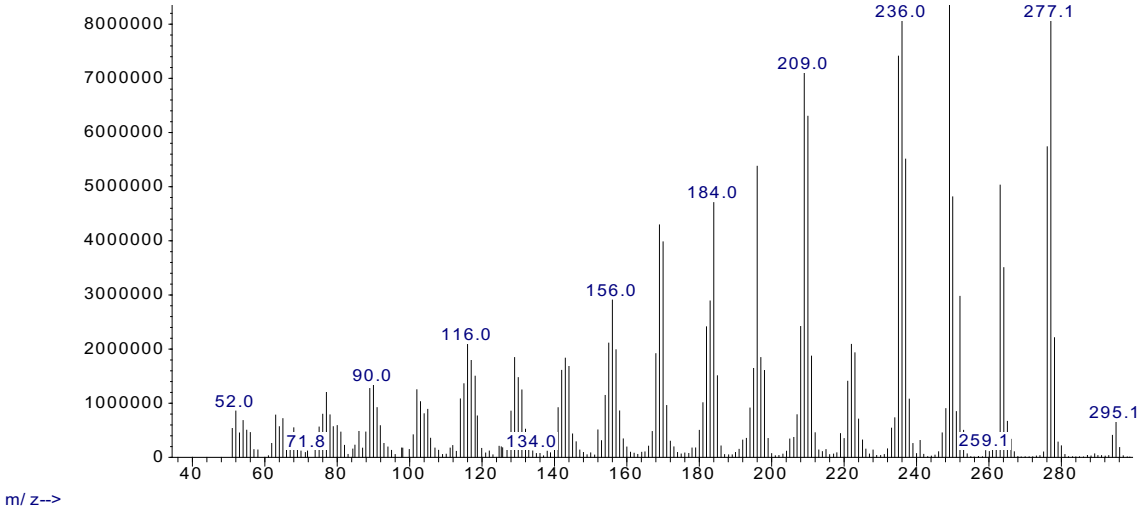

Figure 2.35. Mass spectrum of NCN-Cyclohexylamine

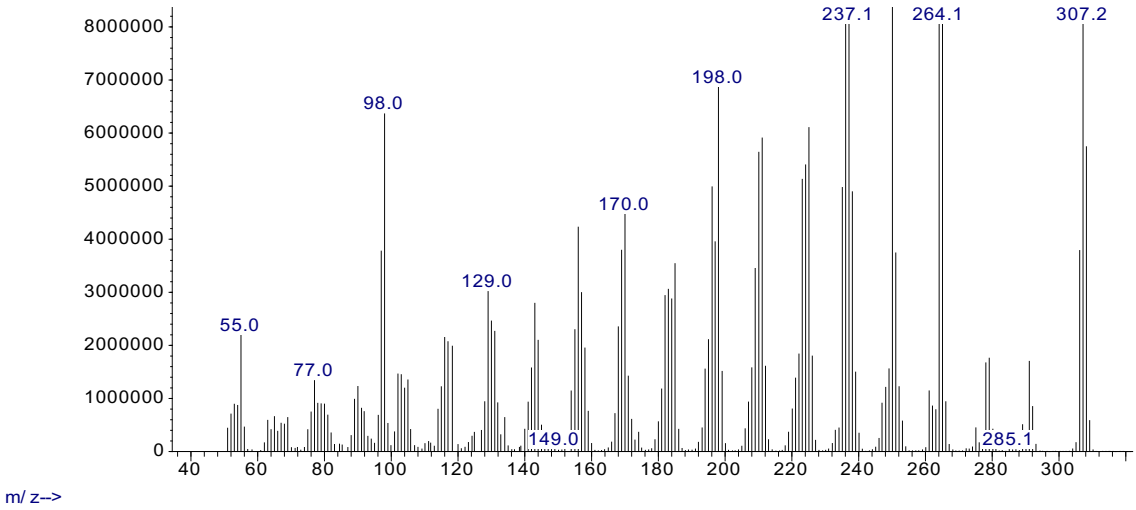

Figure 2.36. UV-vis spectrum of the putative NCN-NiBr2 in pyridine

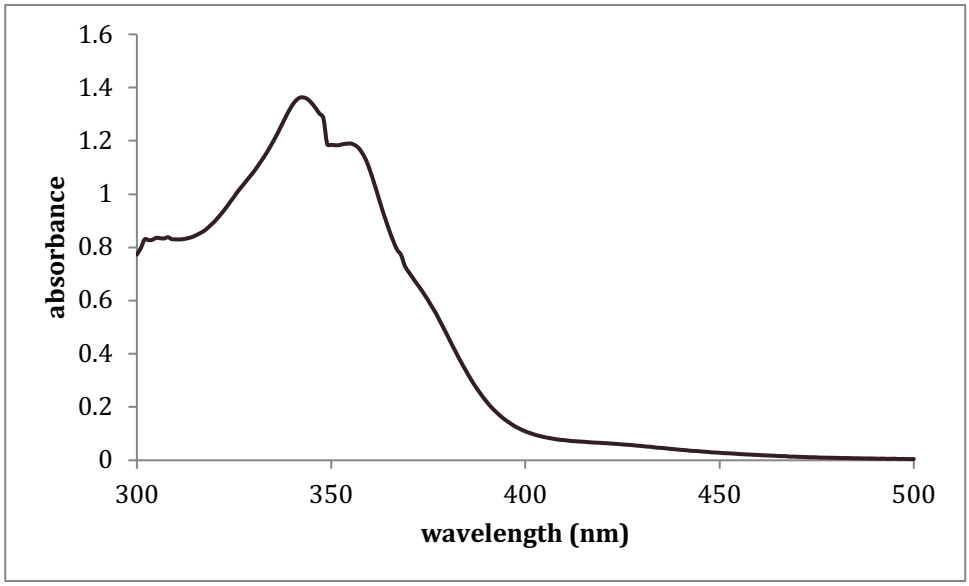

Figure 2.37. UV-vis spectrum of 1 and 1-$(I_2)_2$. Measurements were made in $CHCl_3$ at a concentration of 0.01 mM.

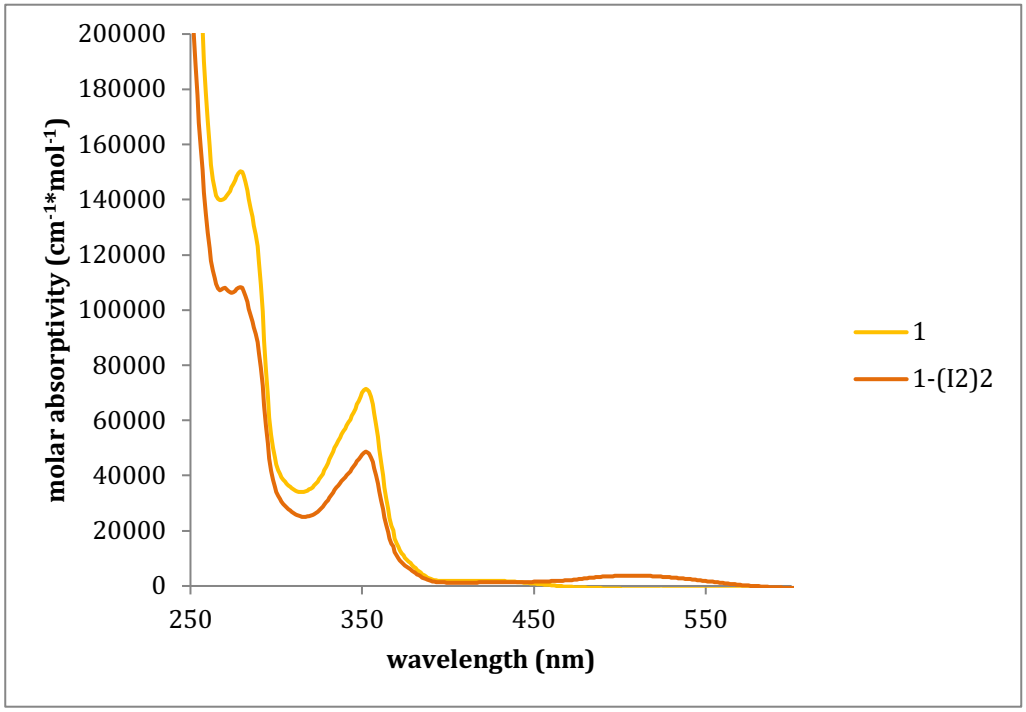

Table 2.2. Crystal Data Collection and Refinement Parameters for Complexes.

	1	**2**	**1-$(I_2)_2$**	**4**	**5**
chemical formula	C12H9BrN4Ni	C13H11BrN4NiO	C12H9BrN4Ni,2(I)	C27H32N4NiO	C12H9BrN4O
Fw	347.85	3039.02	601.65	487.27	305.14
***T* (K)**	100	150(2)	100	100	296(2)
wavelength (Å)	1.54178	1.54178	1.34139	1.54178	1.54178
space group	C2/c	P 21/c	C2/c	P-1	P 2_1 2_1 2
***a* (Å)**	10.52515(13)	7.1063(3)	16.4329(6)	9.3981(2)	15.0595(5)
***b* (Å)**	15.0444(2)	16.9237(7)	17.7994(7)	17.2030(3)	19.1216(6)
***c* (Å)**	7.40691(9)	22.9341(9)	13.2743(5)	23.6482(4)	3.95930(10)
α (deg)	90	90.00	90	99.585(1)	90
β (deg)	99.0692(4)	96.534(2)	126.4370(11)	98.417(1)	90
γ (deg)	90	90.00	90	98.959(1)	90

Z	4	1	8	6	4
***V* (Å^3)**	1158.19(2)	2740.25(19)	3123.7(2)	3665.23(12)	1140.13(6)
ρ_{calcd} (g cm^{-3})	1.995	1.842	2.559	1.325	1.778
μ (mm^{-1})	6.333	5.480	29.814	1.343	4.870
θ range (deg)	5.88 − 71.42	3.25 − 69.56	3.623 − 59.753	1.925 − 71.075	3.736 − 70.452
R1[a] [I > 2σ(I)]	0.0349	0.0397	0.0258	0.0604	0.0243
wR2[b] [I > 2σ(I)]	0.0957	0.1207	0.0696	0.1614	0.0640
R1 [all data]	0.0349	0.0403	0.0266	0.0625	0.0243
wR2 [all data]	0.0957	0.1212	0.0706	0.1648	0.0641
GOF	1.130	1.067	1.111	1.031	1.092

[a] $R_1=\Sigma(||F_o|-|F_c||)/\Sigma|F_o|$

[b] $wR_2=\{\Sigma[w(F_o^2-F_c^2)^2]/\Sigma[w(F_o^2)^2]\}^{½}$

Figure 2.38. Structure and Bond distances for 5

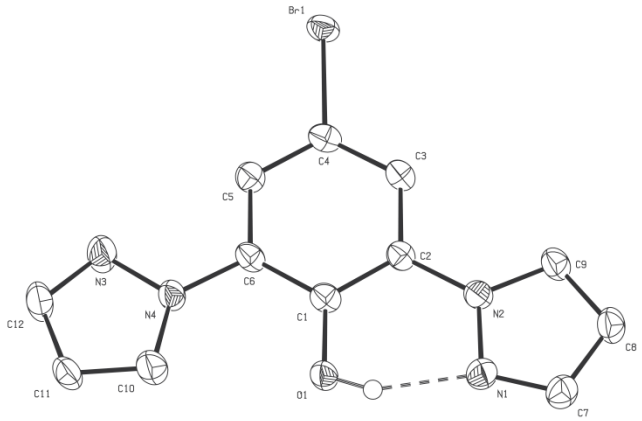

Molecular structure of Br-NCN^{pz}-OH. Thermal ellipsoids are shown at the 50% probability level, and hydrogen atoms are omitted for clarity. Bond distances and angles for pyrazole and benzene ring are available in cif file.

Table 2.3. Selected bond distances for Br-NC(OH)N^{pz}

bond	Distance (Å)
C4-Br1	1.897(3)
C6-N4	1.424(4)
C2-N2	1.417(4)
C1-O1	1.354(4)
O1-H	0.83(6)
H-N1	1.78(6)

2.7 REFERENCES

[1] For a historical review of NCN-type pincer complexes see: Albrecht, M.; van Koten, G. Angew. Chem. Int. Ed. 2001, 40, 3750.

[2] Mitsudo, K.; Imura, T.; Yamaguchi, T.; Tanaka, H. *Tetrahedron Lett.* **2008**, *49*, 7287.

[3] Fossey, J. S.; Richards, C. J. *J. Organomet. Chem.* **2004**, *689*, 3056.

[4] (a) Knapen, J. W. J.; van der Made, A. W.; de Wilde, J. C.; van Leeuwen, P. W. N. M.; Wijkens, P.; Grove, D. M.; van Koten, G. *Nature* **1994**, *372*, 659. (b) Gossage, R. A.; Jastrzebski, T. B. H.; van Ameijde, J.; Mulders, S. J. E.; Brouwer, A. J.; Liskamp, R. M. J.; van Koten, G. *Tetrahedron Lett.* **1999**, *40*, 1413. (c) Kleij, A. W.; Gossage, R. A.; Klein Gebbink, R. J. M.; Brinkmann, N.; Reijerse, E. J.; Kragl, U.; Lutz, M.; Spek, A. L.; van Koten, G. *J. Am. Chem. Soc.* **2000**, *122*, 12112. (d) Pathmamanoharan, C.; Wijkens, P.; Grove, D. M.; Philipse, A. P. *Langmuir* **1996**, *12*, 4372. (e) van de Kuil, L. A.; Grove, D. M.; Zwikker, J. W.; Jenneskens, L. W.; Drenth, W.; van Koten, G. *Chem. Mater.* **1994**, *6*, 1675.

[5](a) van de Kuil, L. A.; Grove, D. M.; Gossage, R. A.; Zwikker, J. W.; Jenneskens, L. W.; Drenth, W.; van Koten, G. *Organometallics* **1997**, *16*, 4985. (b) Grove, D. M.; van Koten, G.; Verschuuren, A. H. M. *J. Mol. Catal.* **1988**, *45*, 169. (c) Grove, D. M.; Verschuuren, A. H. M.; van Koten, G. *J. Organomet. Chem.* **1989**, *372*, C1. (d) van de Kuil, L. A.; Grove, D. M.; Gossage, R. A.; Zwikker, J. W.; Jenneskens, L. W.; Drenth, W.; van Koten, G. *Organometallics* **1997**, *16*, 4985. (e) van de Kuil, L. A.; Veldhuizen, Y. S. J.; Grove, D. M.; Zwikker, J. W.; Jenneskens, L. W.; Drenth, W.; Smeets, W. J. J.; Spek, A. L.; van Koten, G. *Recl. Trav. Chim. Pays-Bas* **1994**, *113*, 267. (f) Granel, C.; Dubois, Ph. Jérôme, R.; Teyssié, Ph. *Macromolecules* **1996**, *29*, 8576.

[6] Yoon, H.; Wagler, T. R.; O'Connor, K. J.; Burrows, C. J. *J. Am. Chem. Soc.* **1990**, *112*, 4568.

[7] (a) Madhira, V. N.; Ren, P.; Vechorkin, O.; Hu, X.; Vicic, D. A. *Dalton Trans*. **2012**, *41*, 7915–7919.

(b) Zhang,C.-P.; Wang, H.; Klein, A.; Biewer, C.; Stirnat, K.; Yamaguchi, Y.; Xu, L.; Gomez-Benitez, V.; Vicic, D. A. *J. Am. Chem. Soc.* **2013**, *135*, 8141−8144. (c) Zheng, B.; Tang, F.; Luo, J.; Schultz, J. W.; Rath, N. P.; Mirica, L. M. *J. Am. Chem. Soc.* **2014**, *136*, 6499−6504.

[8] (a) Cammack, R. *Adv. Inorg. Chem.* **1988**, *32*, 297. (b) Lancaster, Jr., J. R. (ed.) "*Bioinorganic Chemistry of Nickel*," VCH, New York, 1988. (c) Halcrow, M. A.; Christou, G. *Chem. Rev.* **1994**, *94*, 2421. (d) Ermler, U.; Grabarse, W.; Shima, S.; Goubeaud, M.; Thauer, R. K. *Science* **1997**, 278, 1457. (e) Evans, D. J. *Coord. Chem. Rev.* **2005**, 249, 1582. (f) Yang, N.; Reiher, M.; Wang, M.; Harmer, J.; Duin, E. C. *J. Am. Chem. Soc.* **2007**, 129, 11028. (g) Dey, M.; Telser, J.; Kunz, R. C.; Lees, N. S.; Ragsdale, S. W.; Hoffman, B. M. *J. Am. Chem. Soc.* **2007**, 129, 11030. (h) Ragsdale, S. W. *J. Biol. Chem.* **2009**, 284, 18571. (i) Scheller, S.; Goenrich, M.; Mayr, S.; Thauer, R. K.; Jaun, B. *Angew. Chem. Int. Ed.* **2010**, 49, 8112. (j) Scheller, S.; Goenrich, M.; Boecher, R.; Thauer, R. K.; Jaun, B. *Nature* **2010**, 465, 606.

[9] (a) Grove, D. M.; van Koten, G.; Zoet, R. *J. Am. Chem. Soc.* **1983**, 105, 1379. (b) Grove, D. M.; van Koten, G.; Ubbels, H. J. C.; Zoet, R. *Organometallics* **1984**, *3*, 1003. (c) Grove, D. M.; van Koten,G.; Mul, W. P.; van der Zeijden, A. A. H.; Terheijden, J. *Organometallics* **1986**, *5*, 322.

[10] (a) Albrecht, M.; Dani, P.; Lutz, M.; Spek, A. L.; Van Koten, G. *J. Am.Chem.Soc.* **2000**, *122*, 11822. (b) Contel, M.; Stol, M.; Casado, M. A.; van Klink, G. P. M.; Ellis, D. D.; Spek, A. L.; van Koten, G. *Organometallics* **2002**, *21*, 4556.

[11] (a) Moutlon, C. J.; Shaw, B. L. *Dalton Trans.* **1976**, 1020. (b) Rimml, H.; Venanzi, L. M. *J. Organomet. Chem.* **1983**, *259*, C6. (c) Rimml, H.; Venanzi, L. M. *J. Organomet. Chem.* **1984**, *260*, C52. (d) Kennedy, A.R.; Cross, R. J.; Muir, K. W. *Inorganica Chim. Acta* **1995**, *231*, 195. (e) Cámpora, J.; Palma, P.; del Río, D.; Álvarez, E. *Organometallics* **2004**, *23*, 1652. (f) van der Boom, M. E.; Liou, S.-Y.; Shimon, L. J. W.; Ben-David, Y.; Milstein, D. *Inorganica Chim. Acta* **2004**, *357*, 4015. (g) Groux, L.F.; Bélanger-Gariépy, F.; Zargarian, D. *Can. J. Chem*. **2005**, *83*, 634. (h) Castonguay, A.; Beauchamp, A. L.; Zargarian, D. *Inorg. Chem.* **2009**, *48*, 3177.

[12] (a) Gómez-Benítez, V.; Baldovino-Pantaleón, O.; Herrera-Álvarez, C.; Toscano, R. A.; Morales-Morales, D. *Tetrahedron Lett.* **2006**, 47, 5059. (b) Pandarus, V.; Zargarian, D. *Chem. Commun*. **2007**, 978. (c) Chakraborty, S.; Krause, J. A.; Guan, H. *Organometallics* **2009**, *28*, 582. (d) Zhang, J.; Medley, C. M.; Krause, J. A.; Guan, H. *Organometallics* **2010**, *29*, 6393. (e) Lefèvre, X.; Durieux, G.; Lesturgez,

S.; Zargarian, D. *J. Mol. Catal. A.* **2010**, *335*, 1. (f) Salah, A.; Offenstein, C.; Zargarian, D. *Organometallics* **2011**, *30*, 5352. (g) Hao, J.; Vabre, B.; Mougang-Soumé, B.; Zargarian, D. *Chem. Eur. J.* **2014**, *20*, 12544.

[13] (a) Spasyuk, D. M.; Zargarian, D.; van der Est, A. *Organometallics* **2009**, *28*, 6531. (b) Zhang, B.-S.; Wang, W.; Shao, D.-D.; Hao, X.-Q.; Gong, J.-F.; Song, M.-P. *Organometallics* **2010**, *29*, 2579. (c) Yang, M.-J.; Liu, Y.-J.; Gong, J.-F.; Song, M.-P. *Organometallics* **2011**, *30*, 3793. (d) Sanford, J.; Dent C.; Masuda, J.; Xia, A. *Polyhedron* **2011**, *30*, 1091.

[14] Vabre, B.; Canac, Y.; Duhayon, C.; Chauvin, R.; Zargarian, D. *Chem. Commun.***2012**, *48*, 10446**.**

[15] Shao, D.-D.; Niu, J.-L.; Hao, X.-Q.; Gong, J.-F.; Song, M.-P. *Dalton Trans.* **2011**, *40*, 9012.

[16] Zargarian, D. *Coord. Chem. Rev.* **2002**, *233-234*, 157.

[17] Zargarian, D.; Castonguay, A.; Spasyuk, D. M. *Top. Organomet. Chem.* **2013***, 40*, 131-174. Eds. G. van Koten and D. Milstein. Springer-Verlag, Berlin Heidelberg. (i) Vabre, B.; Lambert, M. L.; Petit, A.; Ess, D. H.; Zargarian, D. *Organometallics* **2012**, *31*, 6041.

[18] Pandarus, V.; Castonguay, A.; Zargarian, D. *Dalon. Trans.* **2008**, 4756.

[19] (a) Castonguay, A.; Spasyuk, D. M.; Madern, N.; Beauchamp, A. L.; Zargarian, D. *Organometallics* **2009**, *28*, 2134. (b) Lefèvre, X.; Spasyuk, D. M.; Zargarian, D. *J. Organomet. Chem.* **2011**, *696*, 864. (c) Salah, A.; Zargarian, D. *Dalton Trans.* **2011**, *40*, 8977.

[20] (a) Vabre, B.; Lambert, M. L.; Petit, A.; Ess, D. H.; Zargarian, D. *Organometallics* **2012**, *31*, 6041. (b) Vabre, B.; Lindeperg, F.; Zargarian, D. *Green Chem.* **2013**, *15*, 3188. (c) (l) Vabre, B.; Petiot, P.; Declercq, R.; Zargarian, D. *Organometallics* **2014**, *33*, xxxx.

[21] Develay, S.; Blackburn, O.; Thompson, A. L.; Williams, J. A. G. *Inorg. Chem.***2008**, *47*, 11129–11142.

[22] Vabre, B.; Lambert, M. L.; Petit, A.; Ess, D. H.; Zargarian, D. *Organometallics* **2012**, *31*, 6041–6053.

[23] Stol, M.; Snelders, D. J. M.; Godbole, M. D.; Havenith, R. W. A.; Haddleton, D.; Clarkson, G.; Lutz, M.; Spek, A. L.; van Klink, G. P. M.; van Koten, G. *Organometallics* **2007**, *26*, 3985–3994.

[24] All potentials are referenced to the Fe^{2+}/Fe^{3+} redox couple for ferrocene measured under identical conditions.

[25] According to van Koten (Grove, D. M.; van Koten, g.; Mul, P.; Zoet, R.; van der Linden, J. G. M.; Legters, J.; Schmitz, J. E. J.; Murrall, N. W.; Welch, A. J. *Inorg. Chem.* **1988**, *27,* 2466), the E^0_{ox} for $(NCN^{NMe}{}_2)NiBr$ is 240 mV and the E^0_{red} for $(NCN)NiBr_2$ is 50 mV, both values being measured in acetone and referenced to Ag/AgCl. Under these conditions, the $E^0_{½}$ potential for Fc/Fc^+ is given as 630 mV, which means that the $E^0_{½}$ value for our pyrazole-based complex **1** is nearly 1 V higher than that of van Koten's $NCN^{NMe}{}_2$ analogue.

[26] Pandarus, V.; Zargarian, D. *Organometallics* **2007**, *26*, 4321–4334.

[27] Vabre, B.; Canac, Y.; Duhayon, C.; Chauvin, R.; Zargarian, D. *Chem. Comm.* **2012**, *48*, 10446.

[28] Vabre, B.; Spasyuk, D. M.; Zargarian, D. *Organometallics* **2012**, *31*, 8561.

[29] Castonguay, A.; Beauchamp, A. L.; Zargarian, D. *Organometallics* **2008**, *27*, 5723.

[30] Bolhuis, F. van; Koster, P. B.; Migchelsen, T. *Acta Cryst.* **1967**, *23*, 90.

[31] Halogen bonds are a subset of so-called "□-hole" bonds consisting of highly directional, electrostatically-driven interactions between a region of positive electrostatic potential (e.g., □ * orbital of I_2) and a negative site (e.g., lone pair of a charge-neutral Lewis base or anion). For a discussion of the theoretical underpinnings of halogen bonds see: (a) Politzer, P.; Murray, J. S.; Clark, T. *Phys. Chem. Chem. Phys*, **2010**, *12*, 7748. (b) Politzer, P.; Murray, J. S.; Clark, T. *Phys.Chem. Chem. Phys.* **2013**, *15*, 11178.

[32] Some halogen bonds are considered to be comparable in energy to H-bonds and have been used for the elaboration of supramolecular assemblies. For a selection of reports on this topic see: (a) Zordan, F.;

Brammer, L.; Sherwood, P. *J. Am. Chem. Soc.* **2005**, *127*, 5979. (b) Metrangolo, P.; Resnati, G. *Science* **2008**, *321*, 918. (c) Rissanen, K. *Cryst. Eng. Comm.* **2008**, *10*, 1107.

[33] (a)Le Bras, J.; Amouri, H.; Vaissermann, J. *Inorg. Chem.* **1998**, *37*, 5056–5060. (b) Tebbe, K.-F.; Grafe-Kavoosian, A.; Freckmann, B. Z. Naturforsch., B: *Chem. Sci.* **1996**, 51, 999. (c) Ambrosetti, R.; Baratta, W.; Dell'Amico, D. B.; Calderazzo, F.; Marchetti, F. Gazz. *Chim. Ital.* **1990**, 120, 511. (d) Wieczorrek, C. *Acta Crystallogr.* **2000**, C56, 1085. (e) Masuhara, N.; Nakashima, S.; Yamada, K. *Chem. Lett.* **2005**, 34, 1352. (f) Belicchi, M. F.; Fava, G. G.; Pelizzi, C. *Acta Crystallogr*. **1981**, B37, 924. (g) Gray, L. R.; Gulliver, D. J.; Levason, W.; Webster, M. *Inorg. Chem.* **1983**, 22, 2362. (h) Chaviara, A. T.; Tsipis, A. C.; Cox, P. J.; Bolos, C. A. *Eur. J. Inorg. Chem.* **2005**, 3491.

[34] For the only other Ni complex displaying Ni-I—I interactions see : Blanchard, S.; Neese, F.; Bothe, E.; Bill, E.; Wehermuller, T.; Wieghardt, K. *Inorg. Chem.* **2005**, *44*, 3636.

[35] Mills, A. M.; van Beek, J. A. M.; van Koten, G.; Spek, A. L. *Acta Crystallogr.* **2002**, *C58*, m304.

[36] Van Beek, J. A. M.; Van Koten, G.; Smeets, W. J. J.; Spek, A. L. *J. Am. Chem. Soc.* **1986**, *108*, 5010–5011.

[37] Zhao, S.-B.; Wang, R.-Y.; Wang, S. *Organometallics* **2009**, *28,* 2572.

[38] Johnson, M. T.; Džolić, Z.; Cetina, M.; Wendt, O. F.; Öhrström, L.; Rissanen, K. *Cryst. Growth Des.* **2012**, *12*, 362

[39] Gossage, R. A.; Ryabov, A. D.; Spek, A. L.; Stufkens, D. J.; van Beek, J. A. M.; van Eldik, R.; van Koten, G. *J. Am. Chem. Soc.* **1999**, *121*, 2488.

[40] (a) Koo, K.; Hillhouse, G.L. *Organometallics* **1996***, 15,* 2669. (b) Koo, K.; Hillhouse, G.L. *Organometallics* **1995***, 14,* 4421. (c) Han, R.; Hillhouse, G.L. *J. Am. Chem. Soc.* **1997**, *119,* 8135. (d) Lin, B. L.; Clough, C. R.; Hillhouse, G.L. *J. Am. Chem. Soc.* **2002**, *124,* 2890.

[41] Bhattacharya, M.; Cluff, D. B.; Das, S. *Inorganica Chimica Acta* **2014**, *423*, 238. It is worth noting that the mechanistic evidence presented in this report does not support the involvement of free radicals in the

bromination reactions under discussion. For instance, the presence of TEMPO does not hinder substrate bromination, in contrast to what is observed in our system.

[42] Wadman, S. H.; Havenith, R. W. A.; Lutz, M.; Spek, A. L.; Klink, G. P. M. van; Koten, G. van. *J. Am. Chem. Soc.* **2010**, *132*, 1914–1924.

[43] (a) Sutter, J.-P.; Grove, D. M.; Beley, M.; Collin, J.-P.; Veldman, N.; Spek, A. L.; Sauvage, J.-P.; van Koten, g. *Angew. Chem. Int. Ed. Eng.* **1994**, *33*, 1282. (b) Steenwinkel, P.; Grove, D. M.; Veldman, N.; Spek, A. L.; van Koten, G. *Organometallics* **1998**, *17,* 5647.

[44] Gagliardo, M.; Amijs, C. H. M.; Lutz, M.; Spek, A. L.; Havenith, R. W. A.; Hartl, F.; van Klink, G. P. M.; van Koten, G. *Inorg. Chem.* **2007**, *46*, 11133.

[45] Similar cases of (electrophilic) substitution (halogenation and nitration) at the *para* position with respect to a metalated aromatic carbon have also been observed with non-pincer complexes: (a) Coudret, C.; Fraysse, S.; Launay, J.-P. *Chem. Commun*. **1998**, 663. (b) Clark, A. M.; Rickard, C. E. F.; Roper, W. R.; Wright, L. J. *Organometallics* **1999**, *18,* 2813. (c) Clark, A. M.; Rickard, C. E. F.; Roper, W. R.; Wright, L. J. *J. Organomet. Chem.* **2000***, 598*, 262. (d) Arm, K. J.; Williams, J. A. G. *Chem. Commun.* **2005**, 230. (e) Ghosh, R.; Emge, T. J.; Krogh-Jespersen, K.; Goldman, A. S. *J. Am. Chem. Soc.* **2008**, *130*, 11317.

[46] Spasyuk, D. M.; Zargarian, D. *Inorg. Chem.* **2010**, *49*, 6203–6213.

[47] Schmeier, T. J.; Nova, A.; Hazari, N.; Maseras, F. *Chem. Eur. J.* **2012**, *18*, 6915–6927.

[48] (a)Although it might be conceptually difficult to envisage such a reductive elimination reaction given the mutually trans relationship between the hydride and the central aryl moiety of NCN, it should be noted that such a reaction has been observed previously with ($PC_{sp3}P$)Ni(*n*-Bu) (Castonguay, A.; Sui-Seng, C.; Zargarian, D.; Beauchamp, A. L. *Organometallics* **2006**, *25*, 602–608), whereas the closely related complex (POCsp3-OP)NiEt is stable to decomposition (ref. [26]).

[49] Reductive elimination to form C-O bonds is generally thought to be less facile compared to the analogous reactions forming C-H or C-C bonds; nevertheless, there are a few precedents for this reactivity with Ni (see ref. [40]) and many more with high-valent species such as Ir(III), Pd(III), Pd(IV), and Pt(IV):

(a) Driver, M. S.; Hartwig, J. F. *J. Am. Chem. Soc.* **1997**, *119*, 8232. (b) Rosini, G. P.; Wang, K.; Patel, B.; Goldman, A. S. *Inorg. Chim. Acta* **1998**, *270*, 537–542. (c) Williams, B. S.; Holland, A. W.; Goldberg, K. I. *J. Am. Chem. Soc.* **1999**, *121*, 252. (d) Williams, B. S.; Holland, A. W.; Goldberg, K. I. *J. Am. Chem. Soc.* **1999**, *121,* 252. (e) Williams, B. S.; Goldberg, K. I. *J. Am. Chem. Soc.* **2001**, *123,* 2576. (f) Yamashita, M.; Vicario, J. V. C.; Hartwig, J. F. *J. Am. Chem. Soc.* **2003**, *125,* 16347. (g) Canty, A.J.; Denney, M. C.; Skelton, B. W.; White, A. H. *Organometallics* **2004**, *23,* 1122. (h) Canty, A.J.; Denney, M. C.; van Koten, G.; Skelton, B. W.; White, A. H.; *Organometallics* **2004**, *23,* 5432. (i) Khusnutdinova, J. R.; Zavalij, P. Y.; Vedernikov, A. N. *Organometallics* **2007**, *26,* 3466. (j) Pawlikowski, A. V.; Getty, A. D.; Goldberg, K. I. *J. Am. Chem. Soc.* **2007**, *129*, 10382. (k) Racowski, J. M.; Dick, A. R.; Sanford, M. S. *J. Am. Chem. Soc.* **2009**, *131*, 10974. (l) Powers, D. C.; Benitez, D.; Tkatchouk, E.; Goddard III, W .A.; Ritter, T. *J. Am. Chem. Soc.* **2010**, *132*, 14092. (m) Marquard, S. L.; Hartwig, J. F. *Angew. Chem. Int. Ed.* **2011**, *50*, 7119. (n) Hayashi, Y.; Wada, S.; Yamashita, M.; Nozaki, K. *Organometallics* **2012**, *31*, 1073. (o) Peng, H.; Yuan, Z.; Wang, H.-Y.; Guo, Y.-L.; Liu, G. *Chem. Sci.* **2013**, *4*, 3172. (p) Camasso, N. M.; Pérez-Temprano, M. H.; Sanford, M. S. *J. Am. Chem. Soc.* **2014**, *136*, 12771.

[50] For mini-reviews on the topic of C-heteroatom reductive elimination reactions see : (a) Hartwig, J. F. *Inorg. Chem.* **2007**, *46*, 1936. (b) Vedernikov, A. N. *Chem. Commun.,* **2009**, 4781.

[51] Hao, J.; Mougang-Soumé, B.; Vabre, B.; Zargarian, D. *Angew. Chemie Int. Ed.* **2014**, *53*, 3218–3222.

[52] Ji, X.; Huang, H.; Wu, W.; Li, X.; Jiang, H. *J. Org. Chem***. 2013**, *78*, 11155–11162.

[53] Huffman, L. M.; Stahl, S. S. *J. Am. Chem. Soc.* **2008**, *130*, 9196–9197.

Chapitre 3 : Functionalization o3f the Aryl Moiety in the Pincer Complex (NCN)$Ni^{III}Br_2$: Insights on Ni^{III}-Promoted Carbon-Heteroatom Coupling

Article 2

Jean-Philippe Cloutier and Davit Zargarian*

Département de chimie, Université de Montréal, Montréal (Québec), Canada H3C 3J7

Organometallics **2018, *37* (9), 1446–1455**.

3.1 ABSTRACT

This report describes the C-O, C-N, and C-halogen functionalization of the Ni^{III}-Ar moiety stabilized within a pincer framework that serves as a model system for studying C-heteroatom coupling reactions promoted by high-valent Ni compounds. Treating van Koten's pincer complex (NCN)$Ni^{III}Br_2$ under a nitrogen atmosphere with water, 1° or 2° alcohols, 1° amines, HCl, or HBr results in hetero-functionalization at the *ipso*-C of the pincer ligand's aryl moiety. The yields of these hetero-functionalizations are generally < 50%, which has been attributed to the occurrence of a comproportionation reaction between the trivalent precursor and a Ni^{I} species arising from the reductive elimination step in the functionalization process. Other side-reactions include a C-OH coupling with residual water and C-H coupling (net protonation) that is prevalent with mineral acids, some alcohols, and aqueous NH_3. Kinetic measurements have established that the reaction with MeOH is first order with respect to [(NCN)$Ni^{III}Br_2$], and a kinetic isotope effect of 0.47 has been obtained for functionalization with CH_3OH / CD_3OD. These and other observations have allowed us to propose two different mechanistic postulates for the involvement of trivalent intermediates in the functionalization reactions under discussion. Tetravalent species such as [(NCN)$Ni^{IV}Br_2$]$^+$ can be generated *in-situ* under strongly oxidative conditions and they do promote C-Br coupling, but such species play no role in the C-heteroatom coupling reactions under non-oxidative conditions.

3.2 INTRODUCTION

The past few decades have witnessed a steady rise in the number of reports on new catalytic methodologies for the coupling/functionalization of both activated C-X and "inert" C-H bonds. A more recent trend is the move to develop catalytic protocols based on abundant 3d metals. From a mechanistic viewpoint, 3d metals boast reactivity features that are often distinct from those of their 4d and 5d counterparts, including the prevalence of single-electron redox processes and involvement of odd-electron intermediates in key steps of the catalytic cycle. These considerations warrant further mechanistic investigations of 3d metal-catalyzed coupling processes so that the new insights thus gained may pave the way to more efficient and sustainable synthetic methodologies.

Classical 3d metal-catalyzed coupling reactions that exemplify the above-alluded reactivity features include Ni-catalyzed C-C coupling methodologies such as Kumada-Corriu, Suzuki, and Negishi coupling reactions, many of which are thought to proceed through Ni^{III} intermediates.[1] The analogous Ni-promoted C-heteroatom coupling reactions have been studied less extensively, but these, too, are believed to involve high-valent species.[2] In this context, Hillhouse was among the first to demonstrate that C-N and C-O coupling reactions proceed via Ni^{III} species (Scheme 3.1).[3]

Scheme 3.1. Literature precedents on aerobic-oxidation induced C-X bond formation.

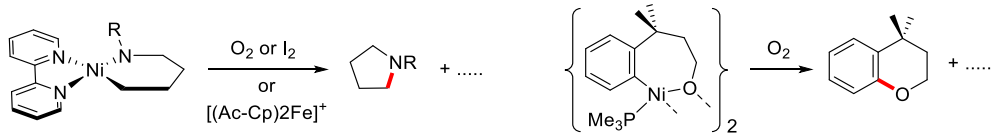

Hillhouse's findings inspired a number of research groups to investigate the fundamental reactivities of high-valent Ni complexes and test their potential in stoichiometric and catalytic C-heteroatom coupling reactions. Notable examples of these investigations include systematic studies reported by Mirica[4] and Sanford[5] on C-N, C-O and C-halogen coupling reactions using authenticated Ni^{III} and Ni^{IV} model compounds (Figure 3.1).[6] In this context, a very recent report by the groups of Canty and Sanford[7] has demonstrated that Ni^{IV} species appear to be more reactive than their Pd^{IV} homologues toward C-C and C-heteroatom bond formation.[8]

Figure 3.1. Examples of authenticated Ni^{III} and Ni^{IV} complexes relevant to C-heteroatom coupling reactions.

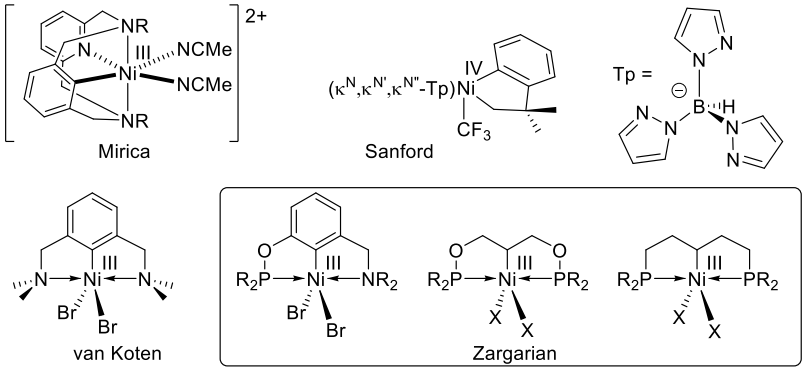

Other important milestones in the area of Ni^{III}-catalyzed C-heteroatom coupling include reports by the groups of MacMillan and Molander, which have shown that photolytically generated, cationic Ni^{III} intermediates catalyze the coupling of alcohols and thiols with aryl halides.[9] These and other recent developments in the organometallic chemistry of high-valent Ni complexes[10] are certain to further invigorate research efforts in this field with the ultimate objective of supplanting Pd in C-heteroatom coupling reactions.

Our group's studies of Ni^{III} complexes evolved from a long-standing interest in organonickel chemistry,[11] but it was van Koten's seminal reports on pincer-backboned trivalent Ni complexes $(NCN)Ni^{III}X_2$ (NCN = $\kappa^N,\kappa^C,\kappa^N$-1,3$(CH_2NMe_2)C_6H_3$; X = Br, I, NO_3, NO_2)[12] that prompted us to investigate the chemistry of this family of complexes. To complement the rigid *m*-phenylene backbone of these complexes and their peripheral hard donor moieties, we prepared a number of PCP- and POCOP-variants based on less rigid non-aromatic backbones and featuring soft donor moieties, as well as new complexes featuring the hybrid POCN-type ligands (Figure 3.1).[13] However, these trivalent complexes did not show promising reactivity in C-heteroatom coupling, promoting only Kharasch-type additions of CCl_4 to olefins.[13b]

Next, we focused on nickel complexes featuring NCN^{pz}-type ligands, close analogues of van Koten's NCN platform featuring pyrazole donor moieties. We showed that $(NCN^{pz})Ni^{II}Br$ reacts with water, alcohols, and amines under mild oxidative conditions of ambient air to promote C-O and C-N coupling with the aryl moiety of the ligand (eq. 1).[14] This ligand functionalization reaction was reminiscent of the above-cited work by Hillhouse's group,[3] with the important difference that in the latter case both C- and O/N-based ligands were pre-assembled on the Ni^{II} center (unimolecular coupling), whereas $(NCN^{pz})Ni^{II}Br$ reacts with external substrates (bimolecular coupling).

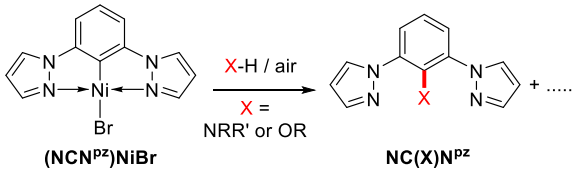

$(NCN^{pz})NiBr$ **$NC(X)N^{pz}$** (1)

As was the case in Hillhouse's system, the trivalent intermediates generated from oxidation of our $(NCN^{pz})Ni^{II}Br$ complexes could not be isolated and authenticated. This shortcoming prompted us to launch follow-up studies using different ligand platforms that might give access to sufficiently stable

trivalent intermediates capable of serving as suitable models for probing the mechanism of the C-heteroatom coupling reactions. Screening tests showed that van Koten's original NCN ligand platform was a suitable candidate for these purposes, which was an intriguing finding since Canty and van Koten had shown in 2004 that the Pt^{IV} complex (NCN)Pt(O_2CPh)$_3$ was stable to C-O bond formation involving the aryl moiety of the NCN ligand.[15] This led us to systematically investigate the reactivities of van Koten's compound in hetero-functionalization of the Ni-Ar moiety.

The present report describes the reactivities of (NCN)$Ni^{III}Br_2$ with water, alcohols, and amines to promote C-O and C-N coupling reactions under inert atmosphere. Significantly, this trivalent precursor also reacts with strong mineral acids HBr and HCl to give halogen-functionalization of the NCN ligand, a counter-intuitive reactivity likely arising from the electrophilic character of the Ni-C bond in this high-valent compound. The results reported herein serve to illustrate the stark contrast between the reactivities of various trivalent organonickel species generated *in-situ* from (NCN)$Ni^{III}Br_2$ relative to their divalent counterparts and the (NCN)Pt^{IV} complex alluded to above.[15]

3.3 RESULTS AND DISCUSSION

1. Synthesis of (NCN)Ni^{II}Br, 1, and (NCN)$Ni^{III}Br_2$, 2. van Koten's group has reported different methods for the preparation of the divalent pincer complexes (NCN)$Ni^{II}X$,[16] and has used them as convenient precursors to the thermally stable trivalent species (NCN)$Ni^{III}X_2$.[12] For instance, the divalent complex (Me_3Si-NCN)NiCl bearing a *p*-trimethylsilyl substituent on the central phenylene ring has been prepared by treating the lithium salt of the proligand with the Ni^{II} precursor $(PEt_3)_2NiCl_2$.[17] We used a revised version of this protocol (Scheme 3.2) to prepare complex (NCN)Ni^{II}Br, **1**, which was then oxidized by $CuBr_2$ to give the target trivalent complex (NCN)$Ni^{III}Br_2$, **2**.[12]

Scheme 3.2. Syntheses of complexes 1 and 2.

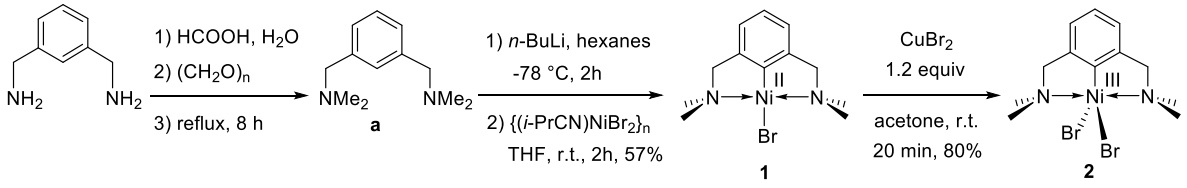

2. Anaerobic reactions of 2 with water, alcohols, and amines. Screening studies showed that the trivalent complex **2** reacts with protic substrates XH under anaerobic conditions to give C-O and C-N functionalization of the NCN ligand (Scheme 3.3, Table 3.1).

Scheme 3.3. Functionalization of (NCN)$Ni^{III}Br_2$, 2, with water, alcohols, and amines.

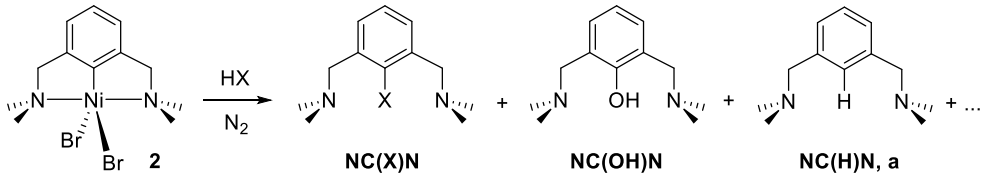

Table 3.1. Functionalization of the NCN ligand in 2[a]

Entry	Substrate HX	Conditions	Yield		
			NC(X)N	NC(OH)N	**a**
1	H_2O	r.t., 3 d	-----	53%	-----
2		70 °C, 24 h	-----	36%	21%
3	MeOH	r.t., 7 h	23%	-----	-----
4		65 °C, 7 h	33%	5%	-----
5	*i*-$PrNH_2$	r.t., 2 h	31%	9%	-----
6	EtOH	70 °C, 24 h	27%	-----	8%
7	CF_3CH_2OH	70 °C, 12 h	24%	-----	8% [b]
8	*i*-PrOH	70 °C, 12 h	37%	-----	15%
9	*t*-BuOH	70 °C, 24 h	-----	22%	-----
10	*i*-Pr_2NH	r.t., 15 min	-----	32%	-----
11	NH_3 (28% in H_2O)	r.t., 2 h	24%	15%	15%
12	$MeNH_2$ (33% in EtOH)	r.t., 5 min	31% [c]	4%	-----
13	Me_2NH (40% in H_2O)	r.t., 15 min	-----	11%	-----
14	$H_2NCH_2CH_2OH$	r.t., 1 h	24% [c]	-----	13%

(a) See SI for experimental and operational details and for additional comments on yields.

(b) This reaction also generated 8% of the C-Br coupling product NC(Br)N.

(c) This is the yield for the C-N coupling product.

Inspection of the results listed in Table 3.1 indicates that the success of the functionalization reactions depends on the nature of XH, C-O coupling being fairly sluggish with water or alcohols compared to C-N coupling with amines. For instance, stirring **2** in water at r.t. gave a 53% yield of

NC(OH)N over three days, whereas the analogous reactions with MeOH and *i*-PrNH$_2$ gave, respectively, a 23% yield of NC(OMe)N over 7 h vs a 31% yield of NC(*i*-PrNH)N in 2 h only (entries 1, 3, and 5). The latter reaction also generated 9% of NC(OH)N, presumably due to a competitive side-reaction with residual water (*vide infra*).

The much slower rates of C-O coupling with water and MeOH prompted us to test the impact of heating on these functionalization reactions. For the reaction of **2** with MeOH, heating did improve the yield of the desired NC(OMe)N from 23% at r.t. to 33% at 65 °C (entry 4), but the higher temperature also gave 5% NC(OH)N. For the reaction of **2** with water, however, heating to 70 °C led to a lower yield of NC(OH)N and generated significant quantities of the proligand **a** (entry 2). The latter side-product is believed to be due to protonolysis of in-situ generated (NCN)Ni^{II}Br (*vide infra*). It should be noted, however, that the proligand **a** was also generated in the reactions with EtOH, CF_3CH_2OH, and *i*-PrOH (entries 6-8).

Based on the observations reported by Mirica's group on Ni^{III} promoted ligand functionalizations,[18] we suspected that a different side-reaction is responsible for the formation of proligand **a** in the reactions with alcohols. Our suspicions were confirmed by these observations: the anaerobic reaction of the divalent complex **1** with NaOEt gave proligand **a** as the only product, whereas the analogous reaction with trivalent **2** gave both **a** and NC(OEt)N (Scheme 3.4).

Scheme 3.4. Reactions of 1 and 2 with NaOR.

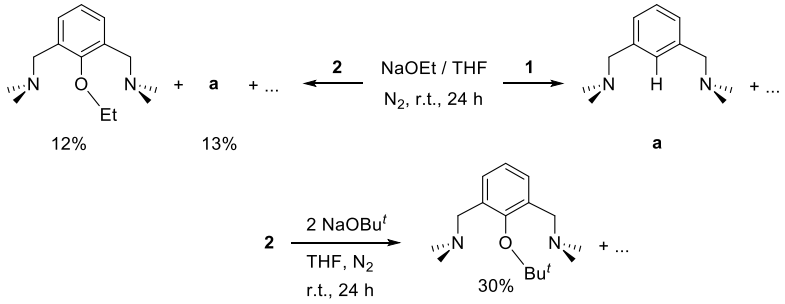

The above observations confirmed that C-OEt coupling requires a trivalent precursor, whereas the net protonolysis giving the proligand **a** arises from a divalent species. We suspect that the latter side-reaction originates from (NCN)Ni^{II}-OEt, a divalent ethoxy intermediate generated *in-situ* during the C-OEt functionalization reaction. □-H Elimination from the Ni^{II}-OEt moiety would give a thermally

unstable hydride species that would, in turn, give **a** via reductive elimination. Consistent with this assertion, the direct reaction of **2** with the □-H free salt NaO(*t*-Bu) gave only NC(OBu^t)N, none of the proligand **a** or NC(OH)N being detected.

In contrast to the success of the C-O(*t*-Bu) coupling from the reaction with NaO(*t*-Bu), the analogous reaction of **2** with *t*-BuOH gave only NC(OH)N (entry 9). A similar result was observed with *i*-Pr$_2$NH (entry 10), which implied that sterics can hinder the functionalization reaction, presumably because of the weak nucleophilicity of these bulky substrates. Comparing the results of these two reactions to those with *t*-BuOH and water allows two other conclusions. First, the observation that NC(OH)N is generated in the reaction with *t*-BuOH but not NaO(*t*-Bu) supports the above-mentioned proposal that the formation of the C-OH coupling side-product with various alcohols and amines is due to residual moisture. Second, C-OH coupling is clearly much more facile with the residual moisture in *i*-Pr$_2$NH vs. the reaction of **2** with pure water (32% over 15 min vs 53% over 3 d) or with the residual moisture in *t*-BuOH (22% over 24 h at 70 °C).

The acceleration of C-OH coupling with water in the presence of amines was also noted when we treated **2** with deoxygenated NH$_4$OH (28% aqueous ammonia): running this reaction at ambient temperature over 2 h gave NC(NH$_2$)N as the major product (ca. 24%) as well as 15% each of NC(OH)N and the proligand **a** (entry 11). The formation of significant quantities of **a** in this case implies that NH_4^+ can protonate the in-situ generated divalent species fairly readily, an assertion which was supported by the observation that treating the divalent species **1** with aqueous ammonia (under anaerobic conditions) gave **a** as the only tractable product (Scheme 3.5).

Scheme 3.5. Reactions of 1 and 2 with aq. NH$_3$.

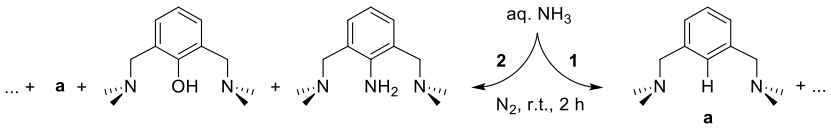

Three other C-N vs. C-O functionalization tests were conducted, as follows. Functionalization of **2** with a 30% EtOH solution of MeNH$_2$ turned out to be even faster than the analogous reaction with aqueous ammonia, requiring only 5 min to give NC(NMeH)N as the major product in addition to a minor amount of NC(OH)N (31% and 4%, respectively; entry 12 in Table 3.1). It is significant that no C-OEt

functionalization was detected in this reaction even though it was conducted in EtOH as solvent; evidently, C-X functionalization follows the order MeNH > OH > OEt. The functionalization with a 40% aqueous solution of the more sterically demanding Me_2NH was also quite fast, but gave only NC(OH)N (entry 13), presumably because of the greater steric bulk of this substrate. Finally, the reaction of **2** with ethanolamine, a substrate that features a primary amine and a primary alcohol in the same molecule, gave the C-$NHCH_2CH_2OH$ coupling product (24%) as well as **a** (13%), but not the C-$OCH_2CH_2NH_2$ coupling product (entry 14).

3. C-halogen functionalization of NCN in (NCN)$Ni^{III}Br_2$, 2. Having established that a pre-formed trivalent complex such as **2** can react under inert atmosphere with the protic substrates water, alcohols, and primary amines to promote C-N and C-O coupling, we wondered whether the analogous C-halogen coupling might also be possible with hydrohalides. To be sure, there are precedents for Ni^{III}-promoted C-halide coupling: Sanford's group has reported that trivalent intermediates generated in-situ by oxidation of the divalent precursors $L_2Ni^{II}(Ar)(halide)$ or $L_2Ni^{II}(Ar)_2$ promote C-C and C-halide bond formation reactions,[19] whereas Mirica's group has shown that the authenticated trivalent species $[L_4Ni(Ar)Br]^+$ promotes reductive elimination of Ar-Br.[4b] Moreover, the detection of minor amounts of the C-Br coupling product NC(Br)N in the reaction of **2** with trifluoroethanol at 70 °C (Table 3.1, entry 7) hinted that such reactivity is feasible and encouraged us to explore this idea.

Treating **2** with hydrohalides confirmed that C-halide coupling is feasible and fairly efficient, but protonation (C-H coupling) is a major side-reaction. For instance, treating the trivalent complex **2** with 0.9 M HBr at r.t. and over 30 min gave nearly equal yields of the desired C-Br coupling product (34%) and proligand **a** (31%), in addition to traces of unidentified degradation products (Scheme 6).[20] To probe the importance of acid concentration for this reaction, we repeated the reaction with 48% HBr, which gave a higher yield of the C-Br at the expense of **a** (43:22 vs. 34:31). The reaction with 36% HCl was even faster, requiring only 5 min to give a mixture of the halo-functionalized products NC(Cl)N (36%) and NC(Br)N (<5%), as well as the proligand **a** (22%).

Scheme 3.6. Reactivity of 2 with HBr and HCl.

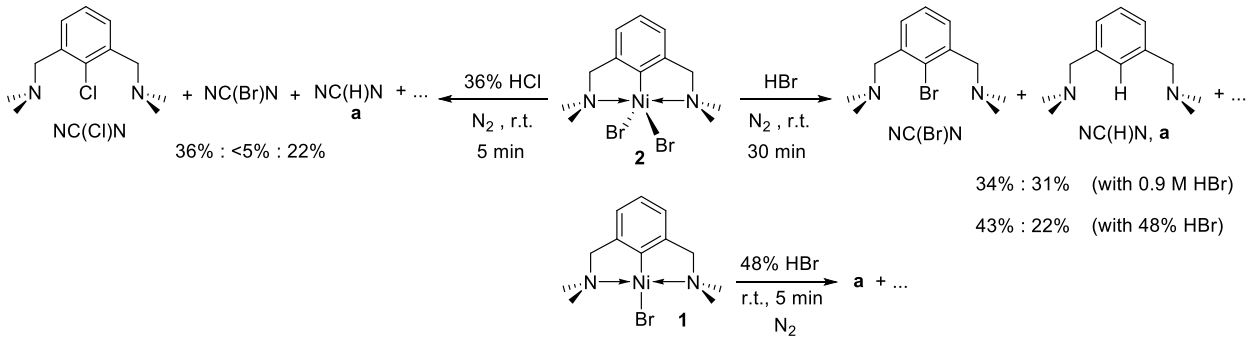

The observed Brønsted-acid triggered C-halide coupling reactivity of **2** is in stark contrast to the protonolysis of the Ni-aryl moiety in the divalent complex **1** (Scheme 3.6): the latter reaction results in an immediate bleaching of the mixture and generates only the proligand **a**, which was obtained in near quantitative yields after basic extraction. It is worth emphasizing here that no C-X coupling product is detected from the reaction of **1** with HCl, HBr, or other acids. Thus, we conclude that the reactivity of (NCN)Ni$^{(n+1)}$Br$_n$ with hydrohalides depends on the oxidation state of the Ni center: the divalent complex **1** (n = 1) leads to protonolysis of the Ni^{II}-aryl moiety exclusively, whereas both halogenation and protonolysis occur with the trivalent species **2** (n = 2). A similar case of such dual reactivity has been reported by Roddick for the reactions of *trans*-{PMe(C$_2$F$_5$)$_2$}$_2$Pt(X)Me with different HX: HOTf leads to elimination of Me-H, i.e., protonolysis), whereas the more oxidizing acid HOSO$_2$F generates Me-OSO$_2$F, i.e., C-X coupling presumably via a Pt^{IV}-Me intermediate (Scheme 3.7).[21]

Scheme 3.7. Literature precedents for C-X bond formation triggered by reaction with Brønsted acids HX.

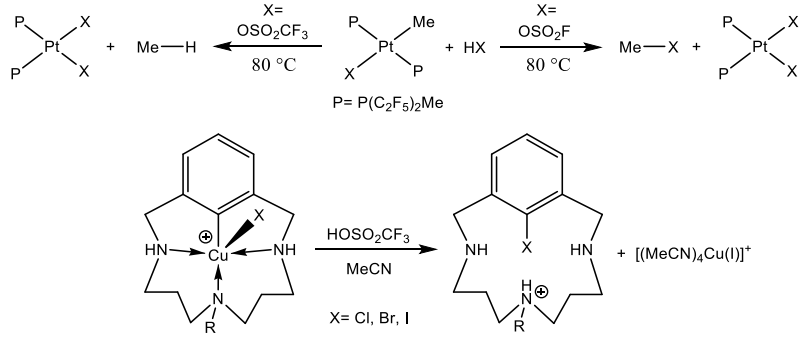

Ar-halide coupling observed with **2** is also reminiscent of the analogous reactivity reported for the Cu^{III} complex shown in Scheme 3.7.[22] Protonation of the tertiary amine ligand moiety in this compound compromises its thermal stability and leads to C-halide bond formation. That the observed reactivity does not involve the weakly coordinating conjugate base triflate implies that the functionalization reaction

proceeds via reductive elimination. To determine if a similar scenario governs the Ni^{III} system under discussion, we treated **2** with aqueous HBF_4, which led to C-Br coupling (ca. 40%) as well as protonolysis (ca. 26% of **a**; Scheme 3.8). We infer from this observation that C-X functionalization in this system is an inner-sphere event that favors Ni-bound anions such as chloride and bromide over unbound anions and nucleophiles such as H_2O that cannot be deprotonated under low pH conditions. Interestingly, C-Br coupling in **2** can also take place, albeit to a small extent, under non-acidic conditions and in the presence of aqueous Br^- (Scheme 3.8). In contrast, no C-Br coupling takes place when **2** is treated with 20 equivalents of Bu_4NBr in MeCN, showing that an aqueous medium is essential for this reactivity and suggesting that C-OH coupling likely precedes C-Br coupling.

Scheme 3.8. Reaction of 2 with HBF_4 or H_2O/KBr**.**

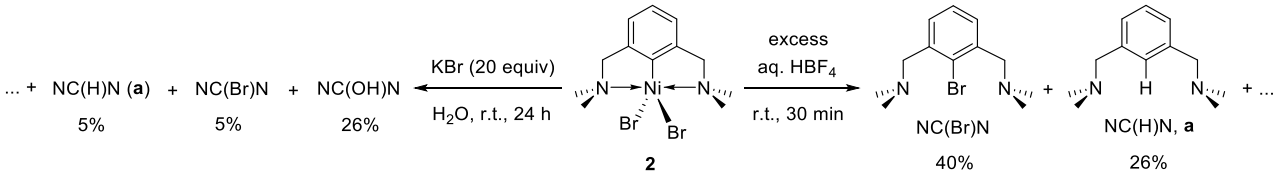

4. Insights on the C-X bond forming step. The results presented in the preceding sections have established that the trivalent species **2** reacts with HX and leads to C-O, C-N and C-halogen functionalization of the central aryl moiety of the NCN ligand, giving NC(X)N; in contrast, no functionalization takes place in the analogous reactions with the divalent complex **1**. Based on these observations, it would seem reasonable to assume *a priori* that the hetero-functionalization reactions under discussion must involve Ni^{III} intermediates, as opposed to Ni^{IV} species, because (a) these functionalizations proceed in the absence of added oxidants, and (b) the oxidation potential of **2** is relatively high (E°' for $Ni^{IV/III}$ is 0.69 V vs. $Fc^{+1/0}$ in MeCN; see Fig. 3.42 in SI). These considerations notwithstanding, we felt compelled to question whether the observed functionalizations of **2** might in fact involve *in-situ* generated tetravalent intermediates, because strong evidence has been presented in recent literature in support of the viability of Ni^{IV} intermediates in C-C and C-X bond forming reactions (*vide infra*). For instance, we wondered if tetravalent species might be generated by disproportionation of **2**; this scenario seemed feasible in principle, because the requisite conversion of two equivalents of **2** into a Ni^{II} and a Ni^{IV} species in such a mechanism would also explain the generally <50% yields observed. The following experiments were, therefore, undertaken to probe this question.

First, we made kinetic measurements to determine the order of [**2**] in the C-OMe coupling reaction with MeOH. Thus, UV-vis spectroscopy was used to monitor the time profile of a reaction between **2** and a large excess of MeOH (7000-8000 equiv). These measurements showed a first order decay for [**2**], indicating a pseudo-first-order reaction with respect to Ni^{III}; this finding argues against the involvement of a bimolecular disproportionation reaction in the formation of NC(OMe)N from **2** and MeOH.

Next, we probed the question of whether oxidative conditions might facilitate functionalization of **2**, regardless of whether or not tetravalent species might be accessible in standard conditions of functionalization. For this purpose, we selected to examine the bromo-functionalization of **2**, because this reaction does not occur in the absence of external sources of bromide or under non-oxidative conditions. Indeed, Sanford's group has shown that the thermal reaction of **2** under inert atmosphere is very sluggish, requiring heating to 150° or higher temperatures (Scheme 3.9).[23] As oxidants, we tested NO^+ and the triarylaminium radical cation $[N(4\text{-}Br\text{-}C_6H_4)_3]^+$ (magic blue), both of which possess formal potentials E°' that are comparable to that of **2** : 0.87 and 0.67 V, respectively, vs. 0.69 V for **2**.[24] We were intrigued to find that C-Br coupling was fairly facile in the presence of NO^+: stirring an acetonitrile solution of **2** with $NOBF_4$ at ambient temperature gave 26% of NC(Br)N in 15 min. The analogous C-Br functionalization also proceeded with the aminium radical cation, but heating to 50 °C was required in this case (47% yield over 24 h). It should be noted that these reactions did not generate any of the usual side-products NC(OH)N or NC(H)N.

Scheme 3.9. Thermolytic and oxidative decomposition of 2.

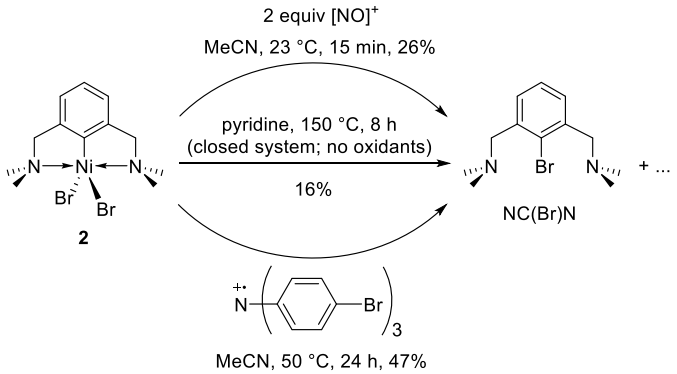

The more facile C-Br bond formation under oxidative conditions relative to the results of Sanford's thermal reaction demonstrates that **2** is less stable under oxidative conditions. We propose that the

oxidation-induced C-Br coupling reactions shown in Scheme 3.9 proceeds by an inner-sphere reductive elimination from a transient tetravalent intermediate akin to [**2**]$^{+}$. As mentioned earlier, there are some literature precedents for the involvement of tetravalent intermediates in Ni-promoted C-X and C-C bond formation reactions. For instance, Mirica's group has shown that both C-O[4a] and C-C[6a,b] reductive eliminations take place in authenticated Ni^{III} species, but some of their observations indicate that these reactions proceed more readily and with higher yields under oxidative conditions, implicating in-situ generated Ni^{IV} species in these C-O and C-C bond forming.

The competence of Ni^{IV} precursors in C-C bond formation has also been demonstrated clearly by Sanford's group.[5a] Particularly relevant to this discussion are the reports by the groups of Sanford and Canty that compare ease of C-C and C-X coupling with tri- and tetravalent precursors. They showed, for instance, that in-situ oxidation of the trivalent compound (Tp)Ni(Ph)(CF_3) (Tp = tris(pyrazolyl)borate) facilitates reductive elimination of Ph-CF_3, presumably through a tetravalent intermediate.[5b] These authors have also proposed C-X bond formation promoted by Ni^{IV} species proceeds via nucleophilic attack of an unbound X^- on the Ni^{IV}-C bond of an octahedral species (an outer-sphere S_N2 mechanism) as opposed to a reductive elimination (an inner-sphere mechanism).[7,25]

To further examine the impact of oxidative conditions on the functionalization of **2** with protic reagents, we probed in more detail the reaction with MeOH. First, we noted that conducting the reaction of **2** in MeOH <u>in air</u> gave the highest yield of C-OMe coupling product obtained in this study: 52% of NC(OMe)N was obtained over 2d, in addition to 10% of the C-OH coupling product NC(OH)N, i.e., a 62% combined C-O functionalization yield (Scheme 3.10). It should be recalled that aerobic oxidation of **2** is not feasible, which rules out the involvement of tetravalent species here. As a second test, we conducted the reaction of **2** with MeOH at room temperature and <u>under N_2</u>, which gave significant quantities (~46%) of the divalent complex **1** (Scheme 3.10); by comparison, no trace of **1** was observed in the analogous aerobic reaction.

Scheme 3.10. Aerobic and non-aerobic reaction of 2 with MeOH.

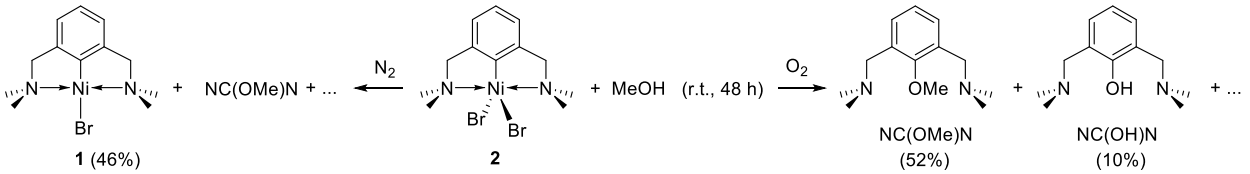

The above results can be reconciled with the postulate that the reductive elimination step that gives the product of C-OMe coupling also generates Ni^{I} intermediates that undergo a comproportionation reaction with **2** (or other trivalent species present in the reaction mixture) to give **1**. This would, of course, consume one equivalent of the trivalent precursor, thereby limiting the maximum functionalization yield to 50%. Such an unproductive side-reaction can be circumvented when an alternative pathway is available for the oxidation of the in-situ generated monovalent species, for instance when the reaction is conducted in air; this would explain the enhanced yield of the C-OMe coupling product in air.[26]

5. Mechanistic proposals for C-heteroatom functionalization of the aryl moiety in 2. Putting together the observations described in the preceding sections has allowed us to envisage a mechanistic scenario for the observed ligand functionalization reactions of **2** with the protic substrates HX. A simplified version of this mechanism for the reactions with amines, alcohols, or water is illustrated in Scheme 3.11 and explained below; a different sequence of steps will be invoked for the analogous functionalization with hydrohalides (*vide infra*).

Scheme 3.11. Proposed mechanism for the functionalization of 2 with amines, alcohols, or water.

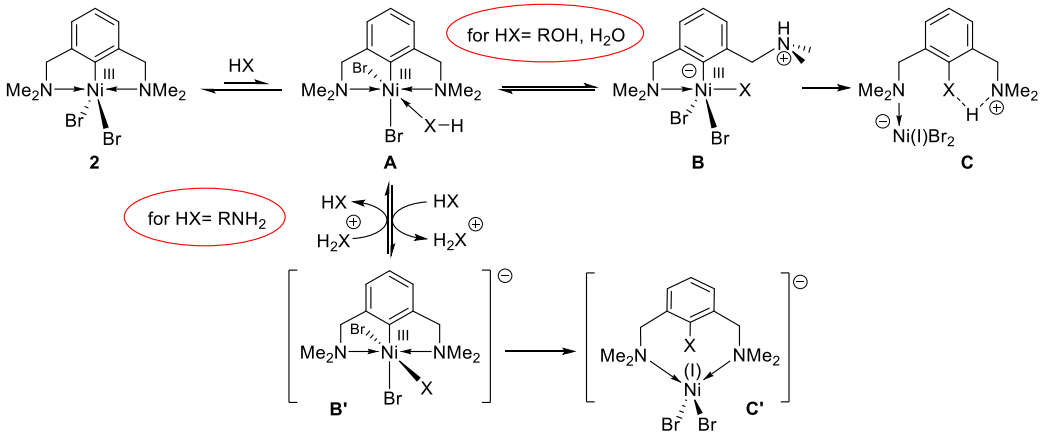

The functionalization reactions would begin by substrate coordination to the electrophilic Ni^{III} center in precursor **2**, converting this penta-coordinate, 17-electron precursor to the octahedral, 19-

electron species **A**. This should be an uphill process on both electronic and steric grounds,[27] and the resulting equilibrium should have a very small K_{eq}, which is consistent with the observed requirement for a very large excess of the weakly nucleophilic or sterically hindered XH (*vide supra*).

Coordination of XH to the trivalent center in **A** would activate the X-H bond and facilitate the crucial H^+-transfer step. In the case of reactions with the weakly basic substrates water and alcohols, deprotonation would be assured by the NMe_2 moiety of the pincer arm to give **B**, whereas in the case of reactions with primary amines the H^+-transfer might be assisted by additional molecules of substrate instead of the pincer arm, giving **B'**. Such acceleration of the H^+-transfer step would also explain the above-noted facile C-OH coupling in the presence of *i*-Pr_2NH, NH_3, and Me_2NH (entries 10, 11, and 13 in Table 3.1). Also consistent with this assertion, addition of NEt_3 to aqueous or MeOH solutions of **2** accelerated the formation of the C-O coupling products. For instance, whereas reaction of pure water gives little or no functionalization over 2-3 h, the presence of just 1 equiv of NEt_3 led to a 24% yield of NC(OH)N in 1 h, implying that expediting the H^+-transfer step greatly influences the overall functionalization rate.

To confirm the impact of the H^+-transfer step on the functionalization rate, we measured the kinetics of the reaction of **2** with CH_3OH and CD_3OD, as follows. UV-vis spectra were recorded for 0.81 x 10^{-3} M solutions of **2** in CH_3OH or CD_3OD, at r. t. and under pseudo-first-order conditions (substrate : Ni^{III} ratio > 1: 500). Monitoring the disappearance of the absorption band at 553 nm allowed us to extract the observed rate constants for the functionalization reaction (Figure 3.2). Observation of non-unity isotope effects indicated that the H^+-transfer step has a significant influence on reaction rates, likely occurring before the rate determining step. Running these experiments in triplicate yielded an inverse $k_{obs}(H) / k_{obs}(D)$ value of 0.47, which implied that we are dealing with an equilibrium isotope effect (EIE). In other words, the H^+-transfer step(s) must take place over one or more equilibria that lead to the final and rate determining C-X bond formation step.

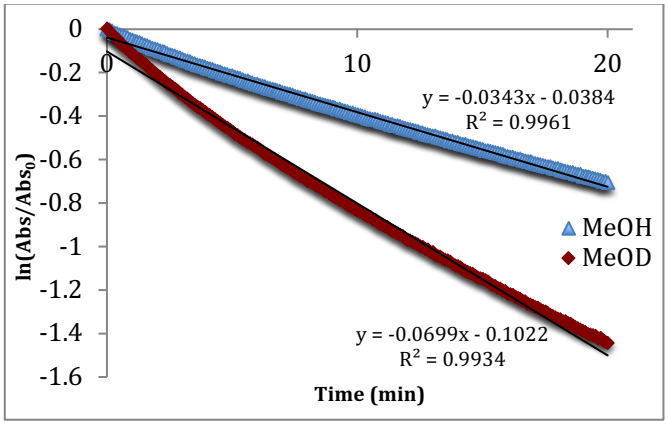

Figure 3.2. Kinetic profile for the functionalization of a 0.81 mM solution of 2 in MeOH/MeOD. The slope corresponds to the observed rate constant.

Continuing our discussion of the mechanistic proposal shown in Scheme 3.11, generation of a Ni-X moiety in species **B** and **B'** by deprotonation of the coordinated substrate HX sets the stage for a reductive elimination that gives the C-X functionalized product and generates an anionic Ni^{I} species. These products likely remain bound to each other in the form of species **C** and **C'**. These monovalent adducts would then undergo a net comproportionation reaction with the trivalent precursor **2 (**or related trivalent species generated during the course of the reaction). Such comproportionation can be viewed as the transfer of a Br radical from the trivalent species to its monovalent partner, generating the divalent NCN complex **1** and a second divalent adduct of the functionalized product. This unproductive consumption of a trivalent species would explain the generally low (<50%) functionalization yields observed throughout this work, and this proposal is consistent with the observation that functionalization with MeOH is higher-yielding under aerobic conditions.

The above mechanistic scheme needs to be modified slightly to account for the much more facile and rapid functionalization reactions observed with the mineral acids HCl and HBr. We propose that these reactions begin with a direct protonation of one or both of the chelating amine moieties,[28] followed by coordination of one or two halide atoms at the liberated coordination sites around the trivalent Ni center, as shown in Scheme 3.12. The loss of chelation would render the Ni-aryl moiety much more susceptible to reductive elimination. It is also noteworthy that monovalent species generated in-situ after the halogen-functionalization step would be readily oxidized, either as above (comproportionation with **2**) or in direct reaction with the mineral acids HX.

Scheme 3.12. Proposed mechanism for the C-halogen functionalization of 2 with HBr or HCl.

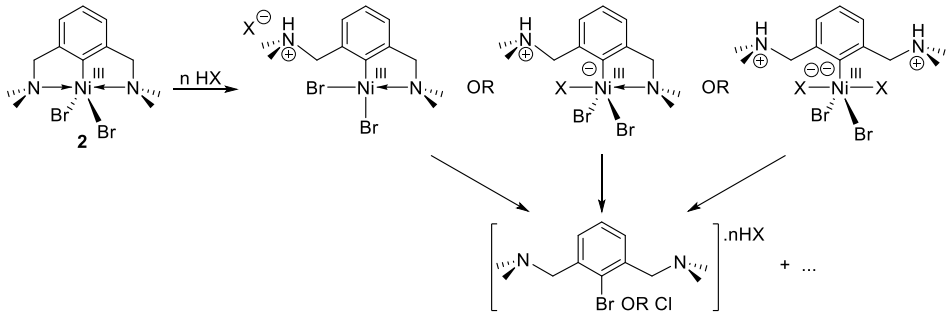

The mechanistic scenarios shown in Schemes 3.11 and 3.12 do not depict the side-reactions responsible for the commonly observed side-product NC(H)N, **a**. As stated earlier, we believe that the formation of the proligand **a** in the reaction with EtOH arises from a □-H elimination from the Ni^{II}-OEt intermediate, while its formation in other cases (reaction of **2** with H_2O, NH_4OH, HCl, HBr, and KBr/H_2O) likely occurs by protonation of the in-situ generated divalent species $(NCN)Ni^{II}Br$.

3.4 SUMMARY AND CONCLUDING REMARKS

The results discussed in this report show that the reaction of water, aliphatic alcohols, and primary aliphatic amines with $(NCN)NiBr_2$, **2**, leads to the direct hetero-functionalization of the Ni^{III}-bound aryl moiety in this authenticated trivalent pincer complex. The main findings of this study are in line with those of recent reports by the groups of Mirica and Sanford on C-C and C-heteroatom coupling reactions involving thermally stable Ni^{III} complexes, and also support our proposal that in-situ generated trivalent species are involved in the analogous hetero-functionalization of the pyrazole-based pincer complex $(NCN^{pz})NiBr$ [14] for which thermally stable trivalent derivatives have proven to be hitherto inaccessible. Moreover, halo-functionalization of **2** is observed upon treatment with Brönsted acids HX, as well as with strong oxidants NO^+ or aminium radical cations, but the latter reactions are thought to involve tetravalent intermediates.

That the observed C-X coupling reactions are generally low-yielding is believed to be due, primarily, to the unproductive consumption of the trivalent precursor in a comproportionation reaction with monovalent species generated *in-situ* via the C-X reductive elimination step. This comproportionation

side-reaction leads to the divalent species (NCN)NiBr, which is eventually converted to a tetravalent hydride derivative that, in turn, gives the proteo form of the pincer ligand via C-H reductive elimination. Another common side-product arises from C-OH coupling due to reaction of the trivalent precursor with substrate residual moisture.

From a mechanistic viewpoint, the results discussed in this report have established the importance of the following factors for C-X functionalization rates. Destabilization of the pincer complex **2** due to Brönsted acid-induced protonation/dechelation of one or both of the chelating NMe_2 donor moieties results in rapid C-Br and C-Cl coupling reactions (on the order of minutes). Functionalization is also fast (2 h or less) with primary amines, because the greater nucleophilicity of these substrates favors their coordination to the Ni^{III} center, while their basicity facilitates the crucial H^+-transfer step that generates the requisite Ni^{III}-NRH moiety. The importance of these factors is evident in (a) the sluggish reactivity of sterically hindered amines and alcohols, and (b) the much faster C-O functionalization rates in the presence of amines.

An important mechanistic issue that remains to be established unequivocally is whether C-X bond formation proceeds via an inner-sphere reductive elimination or an outer-sphere S_NAr-type nucleophilic attack on the aryl moiety of the trivalent species. Sanford and Canty have presented evidence in favor of outer-sphere mechanisms dominating the hetero-functionalization reactions promoted by coordinatively saturated Ni^{III} compounds.[5a,7] In the reaction of non-acidic substrates HX with the coordinatively unsaturated complex **2**, we believe that the nucleophilic attack is more likely to occur on the Ni^{III} center (i.e., coordination), followed by H^+-transfer to generate the requisite Ni^{III}–X and finally Ar-X reductive elimination. In the case of reaction with Brönsted acids, the functionalization appears to favor the more strongly coordinating conjugate base, thus also favoring the inner-sphere reductive elimination scenario. The successful functionalization of the aryl moiety in **2** following treatment with the weak nucleophile *t*-BuO^- also argues against an outer-sphere nucleophilic attack in this system. Nevertheless, future investigations will seek to shed more light on this question.

Experimental and operational details for the syntheses of complexes **1** and **2**, functionalization reactions and characterization of various products, and kinetic studies. The Supporting Information is available free of charge on the ACS Publications website at DOI: 10.1021/acs.organomet.8b00103.

AUTHOR INFORMATION

Corresponding author. *E-mail: zargarian.davit@umontreal.ca.

Notes. The authors declare no competing financial interest.

Acknowledgements. The authors gratefully acknowledge the financial support provided by NSERC of Canada (Discovery grant to D.Z.), Université de Montréal (research award to J.-P. C.) and GCCC/ CCVC (travel award to J.-P. C.). Mr Loïc Mangin is thanked for stimulating discussions at various stages of this work.

3.5 SUPPORTING INFORMATION

General. Unless otherwise indicated, all manipulations were carried out using standard Schlenk and glove box techniques under a dry nitrogen atmosphere using solvents dried by passage through activated aluminum oxide columns (MBraun SPS) to water contents of less than 10 ppm (determined using a Mettler-Toledo C20 coulometric Karl Fischer titrator). The reagents and substrates used in the functionalization reactions, as well as the starting materials used for the syntheses reported in this report, were purchased from Aldrich and used without further purification. 1,3-Bis(aminomethyl)benzene was used in the Eschweiler-Clarke reaction[29] to give the proligand 1,3-$(Me_2NCH_2)_2C_6H_4$ (NC(H)N or **a**), which was then used to prepare the divalent complex {1,3-$(Me_2NCH_2)_2C_6H_3$}NiBr ((NCN)NiBr or **1**). Literature procedures were used to prepare the nickel precursor $NiBr_2\{NC(i\text{-}Pr)\}_n$[30].

The NMR spectra were recorded on the following spectrometers: Bruker AV400rg (^{1}H at 400 MHz) and Bruker ARX400 (^{1}H at 400 MHz and $^{13}C\{^1H\}$ at 100.56 MHz). Chemical shift values are reported in ppm (δ) and referenced internally to the residual solvent signals (^{1}H and ^{13}C: 7.26 and 77.16 ppm for $CDCl_3$; 7.16 and 128.06 ppm for C_6D_6) or externally. Coupling constants are reported in Hz. The elemental analyses were performed by the Laboratoire d'Analyse Élémentaire, Département de chimie, Université de Montréal.

Synthesis of (NCN)Ni^{II}Br, 1. This compound was prepared following a revised procedure reported for the synthesis of a closely related derivative (see ref. 16 in the main manuscript). An oven-dried Schlenk flask was charged with the proligand **a** (2.00 g, 10.4 mmol) and hexanes (15 mL). The mixture was cooled to -78 °C and *n*-BuLi (11.4 mmol, 4.6 mL) was added dropwise. The resulting red mixture was warmed

to r.t. and left to stir for 2 h. Evaporation of the solvent followed by addition of THF (15 mL) gave a deep red solution, which was cannula-transferred onto a suspension of $NiBr_2\{NC(i\text{-}Pr)\}_n$ (4.53 g, 12.5 mmol) THF, and stirred at r.t. for 2 h. The resulting dark brown solution was evaporated under vacuum and the product extracted with 3 x 20 mL Et_2O. The orange solution was filtered through a pad of silica gel (5 cm) and the filtrate concentrated to ~ 5 mL to precipitate an orange solid. Addition of hexanes (60 mL) to the filtrate completed the precipitation, and filtration and washing with hexanes (3 x 10 mL) gave a bright orange powder (1.96 g, 57 %). ^{1}H NMR C_6D_6, δ 6.96 (1H, t, J_{HH} = *7.4,* H_1), δ 6.39 (2H, d, J_{HH} = *6.9,* H_2), δ 3.11 (4H, s, H_3), δ 2.53 (12H, s, H_4). Anal Calc for $C_{12}H_{19}BrN_2Ni$ (329.89): C, 43.69; N, 8.49; H, 5.81. Found: C, 43.64; N, 8.39; H, 5.77.

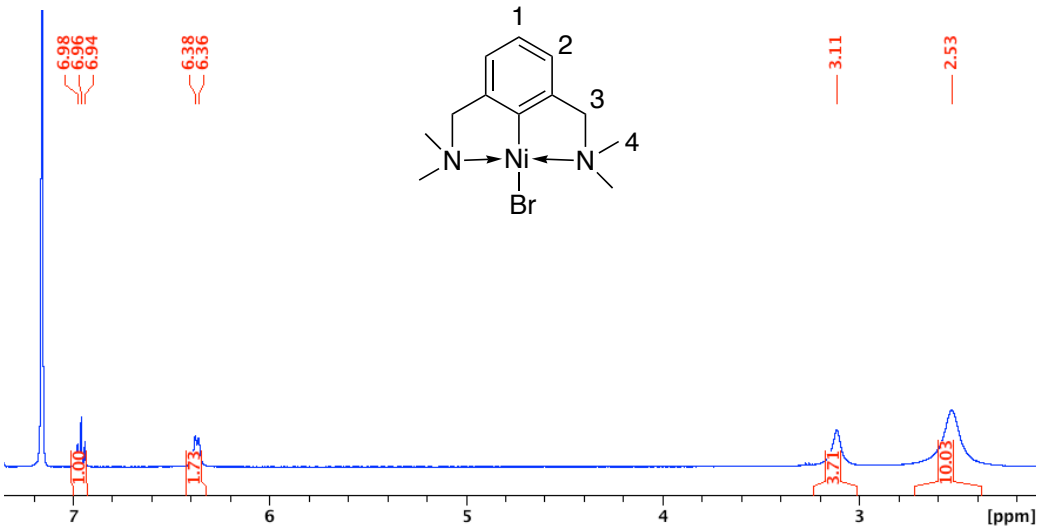

Figure 3.4. ^{1}H NMR (C_6D_6) of complex 1. δ 6.96 (1H, t, J_{HH} = *7.4,* H_1), δ 6.39 (2H, d, J_{HH} = *6.9,* H_2), δ 3.11 (4H, s, H_3), δ 2.53 (12H, s, H_4)

Synthesis of (NCN)Ni^{III}Br$_2$, 2. This compound was prepared using a reported procedure (see ref. 12 in the main manuscript), and has been used in the functionalization reactions. An oven-dried Schlenk flask was charged with **1** (0.500 g, 1.52 mmol) and acetone (10 mL) followed by addition of $CuBr_2$ (0.406 g, 1.82 mmol). The dark solution was left to stir for 15 min. The solution was then canula filtered to remove CuBr and the residue was washed with 3 x 10 mL of acetone. The combined filtrate and washings were evaporated to dryness under vacuum yielding a dark solid. This solid was extracted with 3 x 10 mL DCM and the resulting dark green extracts were evaporated to give **2** as a dark-green solid (0.549 g, 88 % yield).

General procedure for the functionalization of 2. These reactions were conducted by stirring complex **2** (100 mg, 0.244 mmol) in neat substrate (10 mL). The reaction mixtures were evaporated and worked up by base extraction, and the yields were determined by ^{1}H NMR using 1-bromo-3,5-dimethoxybenzene as standard (0.013 g, 0.061 mmol). The results are listed in Table 1 and discussed throughout the main manuscript.

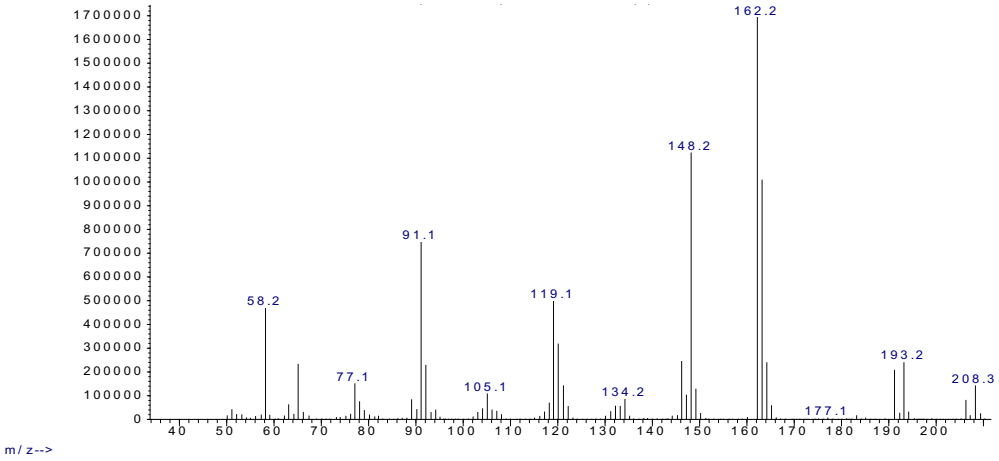

Figure 3.5. Mass spectrum of NC(OH)N

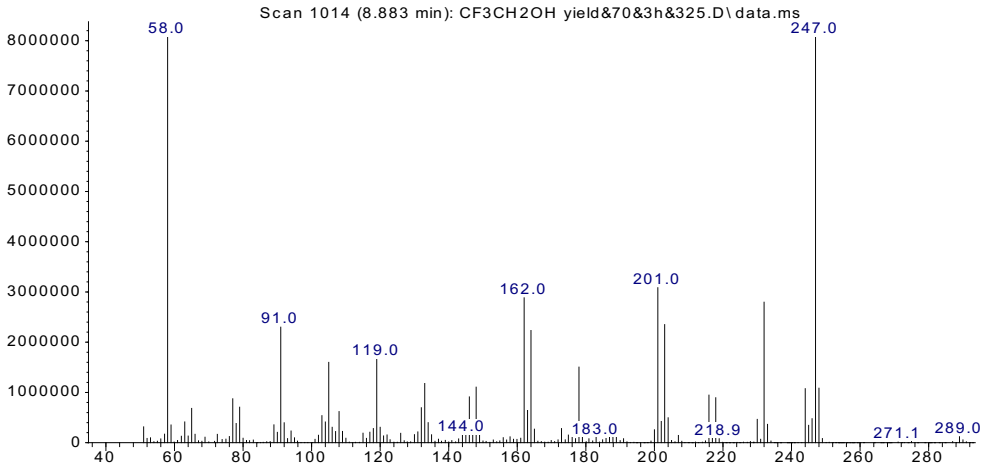

Figure 3.6. Mass spectrum of $NC(OCH_2CF_3)N$

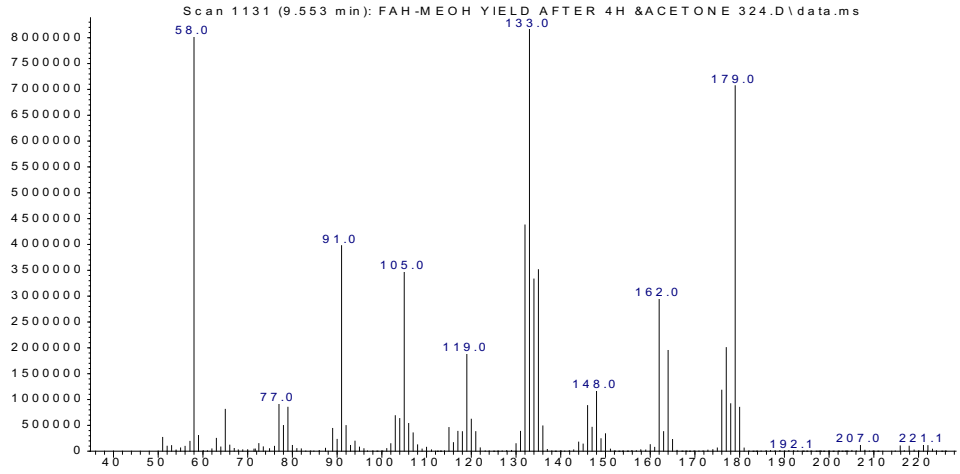

Figure 3.7. Mass spectrum of NC(OMe)N

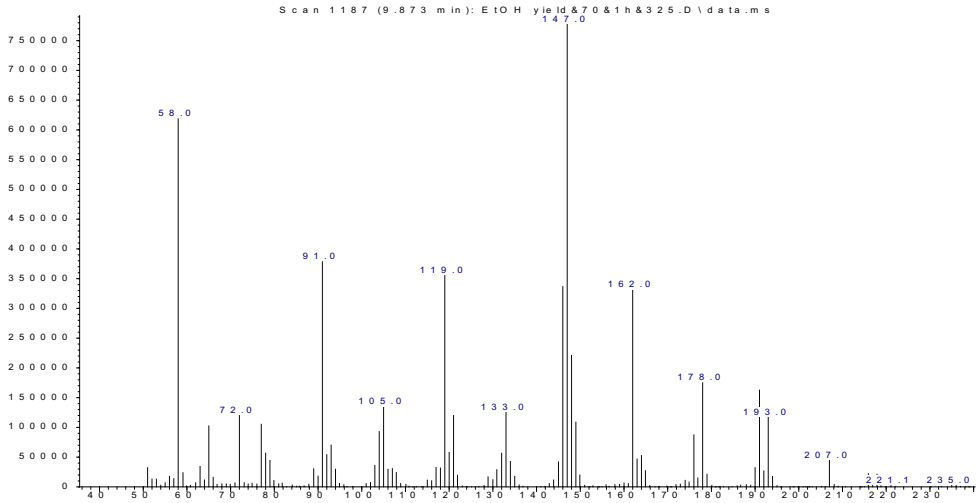

Figure 3.8. Mass spectrum of NC(OEt)N

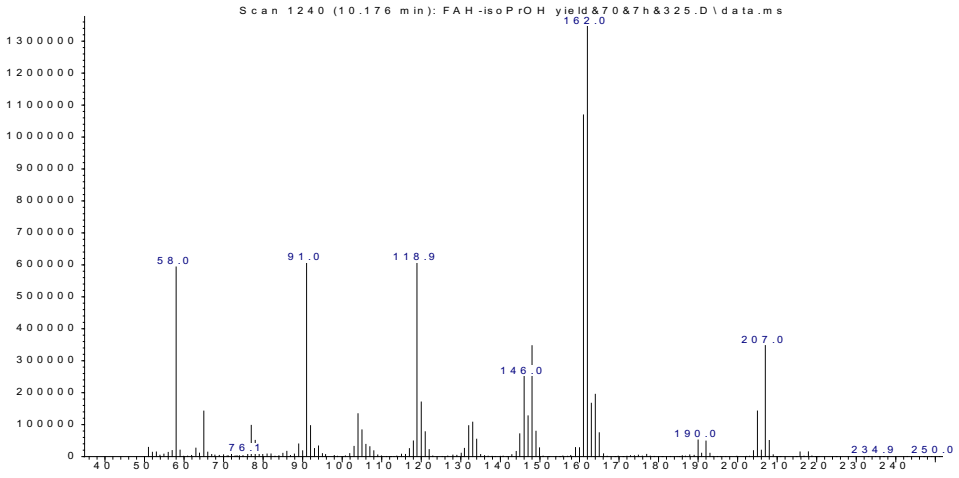

Figure 3.9. Mass spectrum of NC(*i*-PrO)N

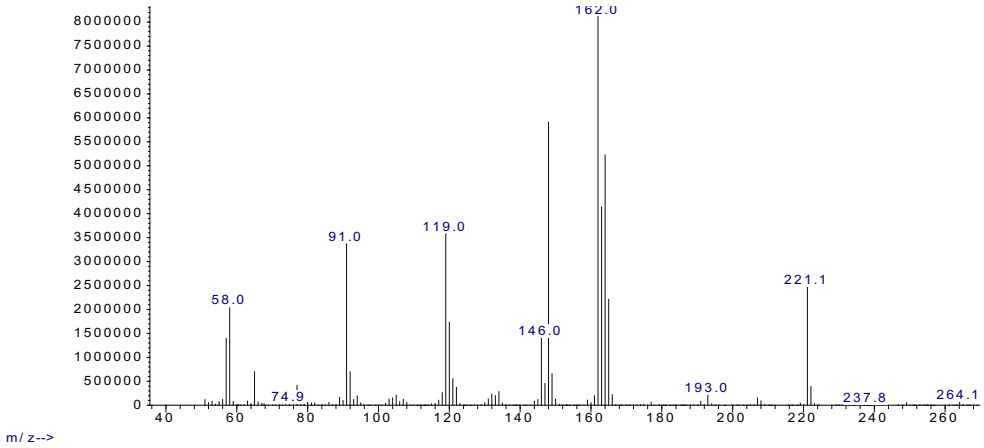

Figure 3.10. Mass spectrum of NC(*t*-BuO)N

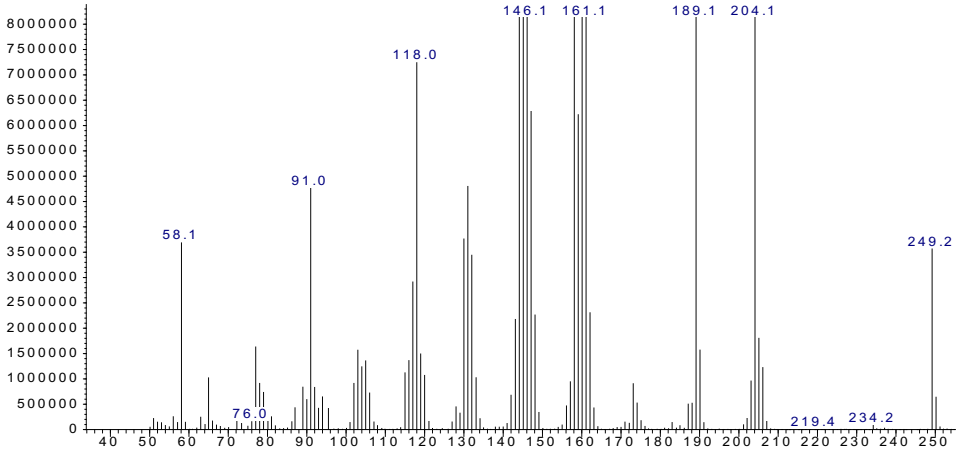

Figure 3.11. Mass spectrum of NC(*i*-PrNH)N

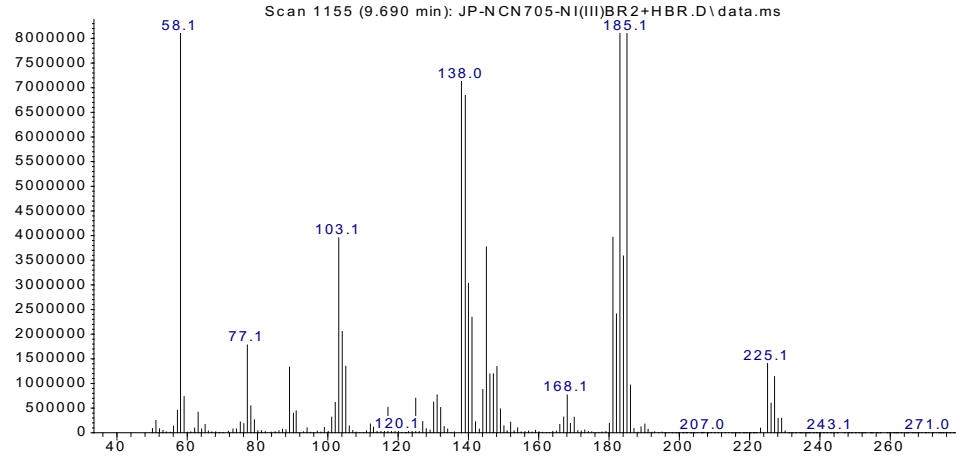

Figure 3.12. Mass spectrum of NC(Br)N

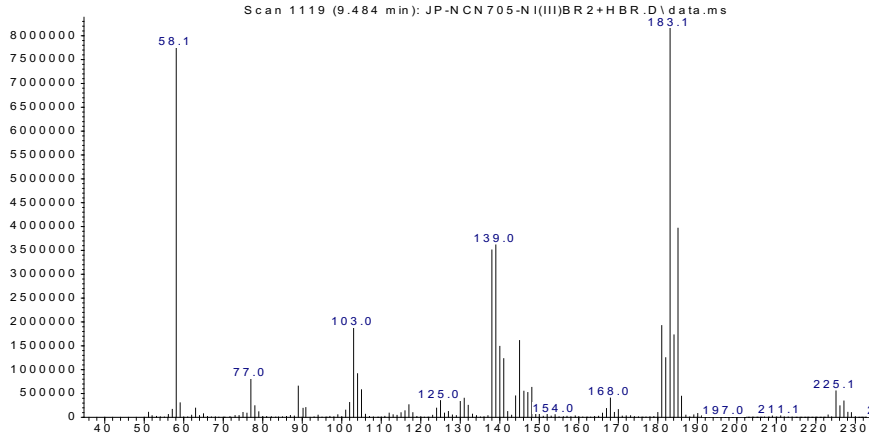

Figure 3.13. Mass spectrum of NC(Cl)N

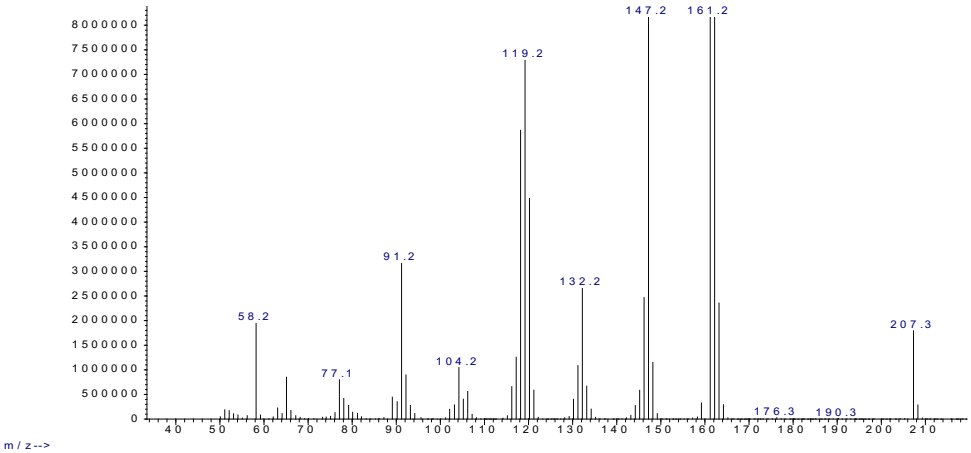

Figure 3.14. Mass spectrum of $NC(NH_2)N$

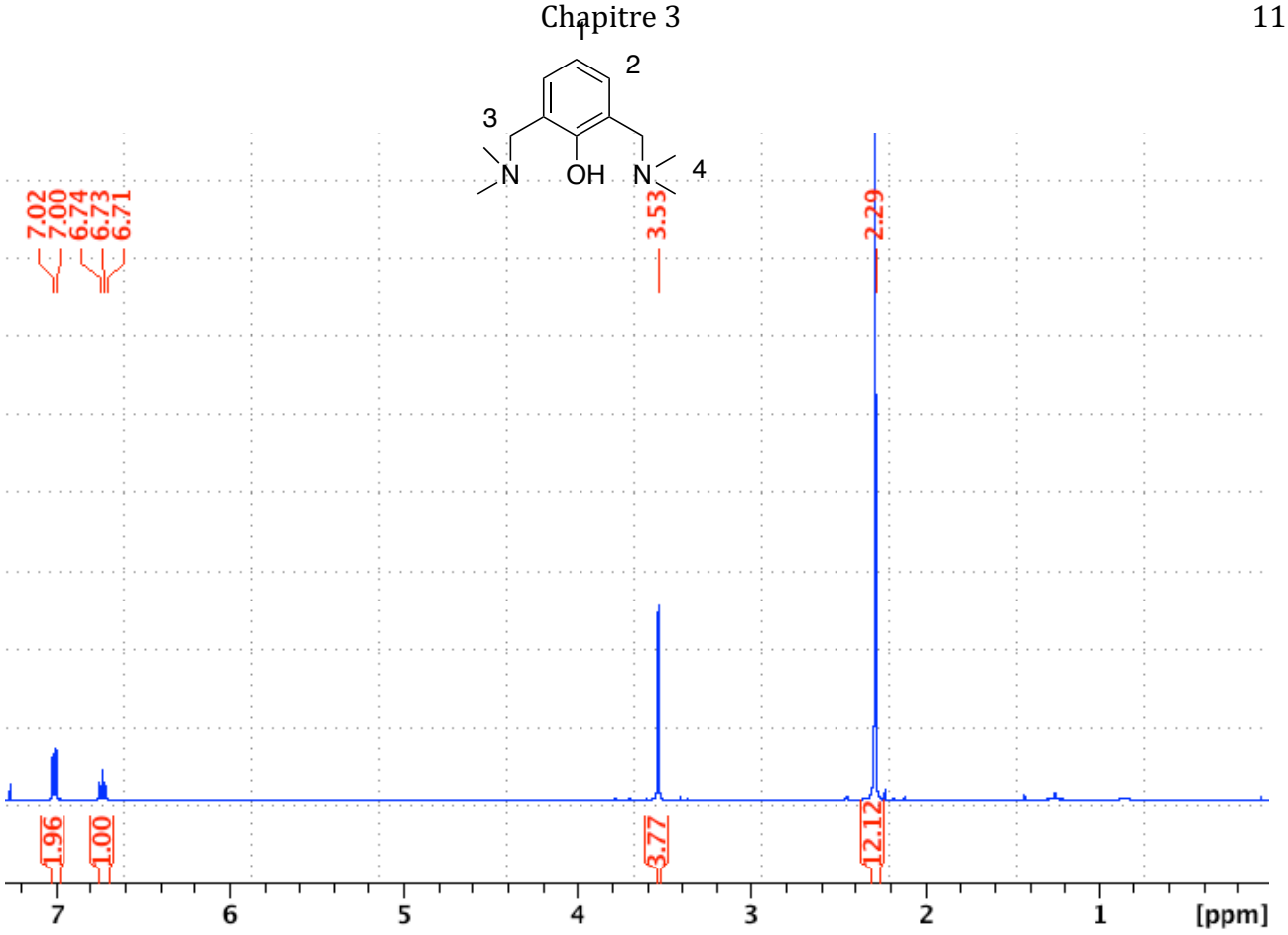

Figure 3.15. NC(OH)N ^{1}H NMR $CDCl_3$, δ 7.01 (2H, d, J_{HH} = *7.5,* H_2), δ 6.73 (1H, t, J_{HH} = *7.5,* H_1), δ 3.53 (4H, s, H_3), δ 2.29 (12H, s, H_4), -*OH* proton signal was not detected.

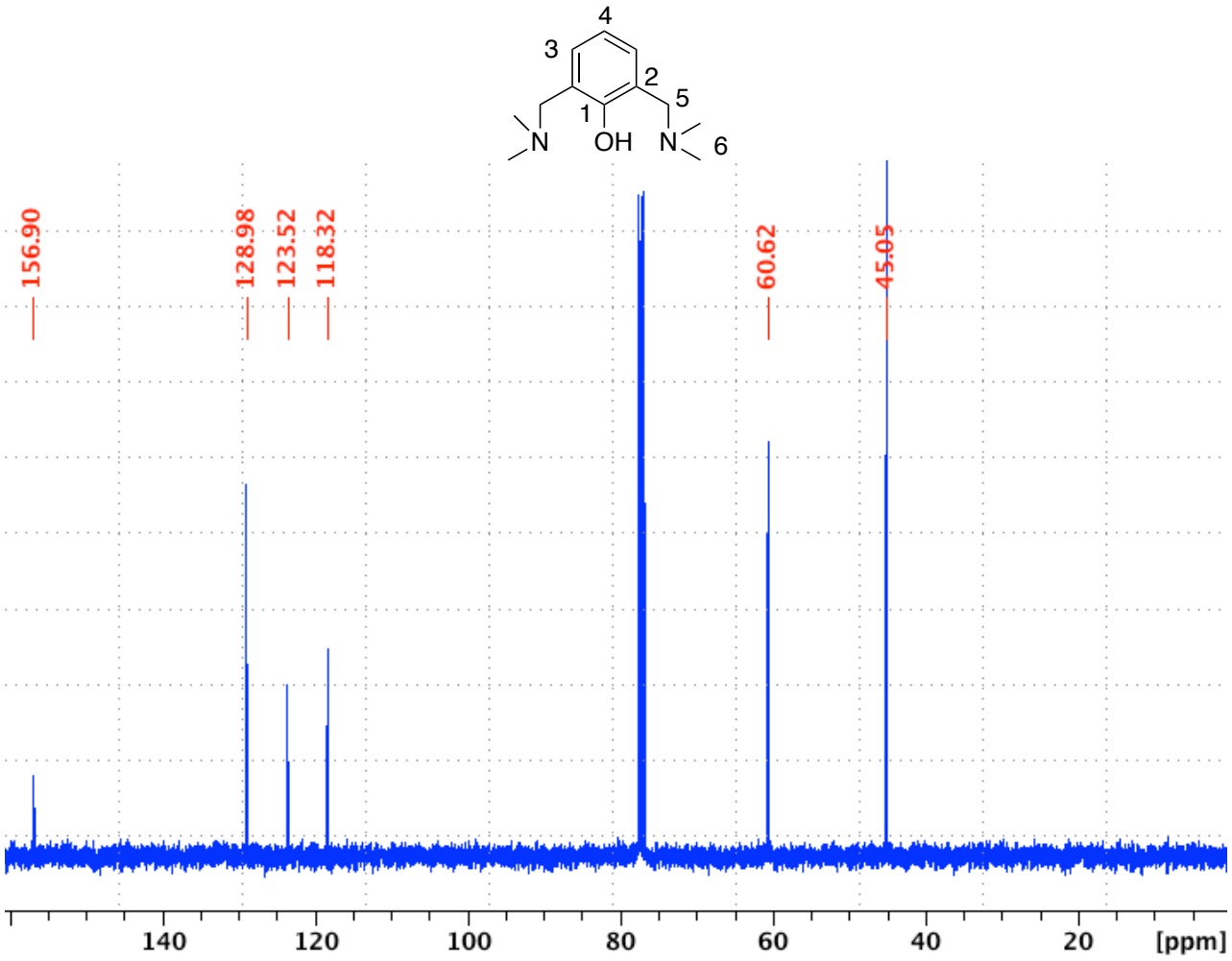

Figure 3.16. NC(OH)N ^{13}C NMR $CDCl_3$, δ 156.90 (1C, s, C_1), δ 128.98 (2C, s, C_3), δ 123.52 (2C, s C_2), δ 118.32 (1C, s, C_4), δ 60.62 (1C, s, C_7), δ 45.05 (2C, s, C_5)

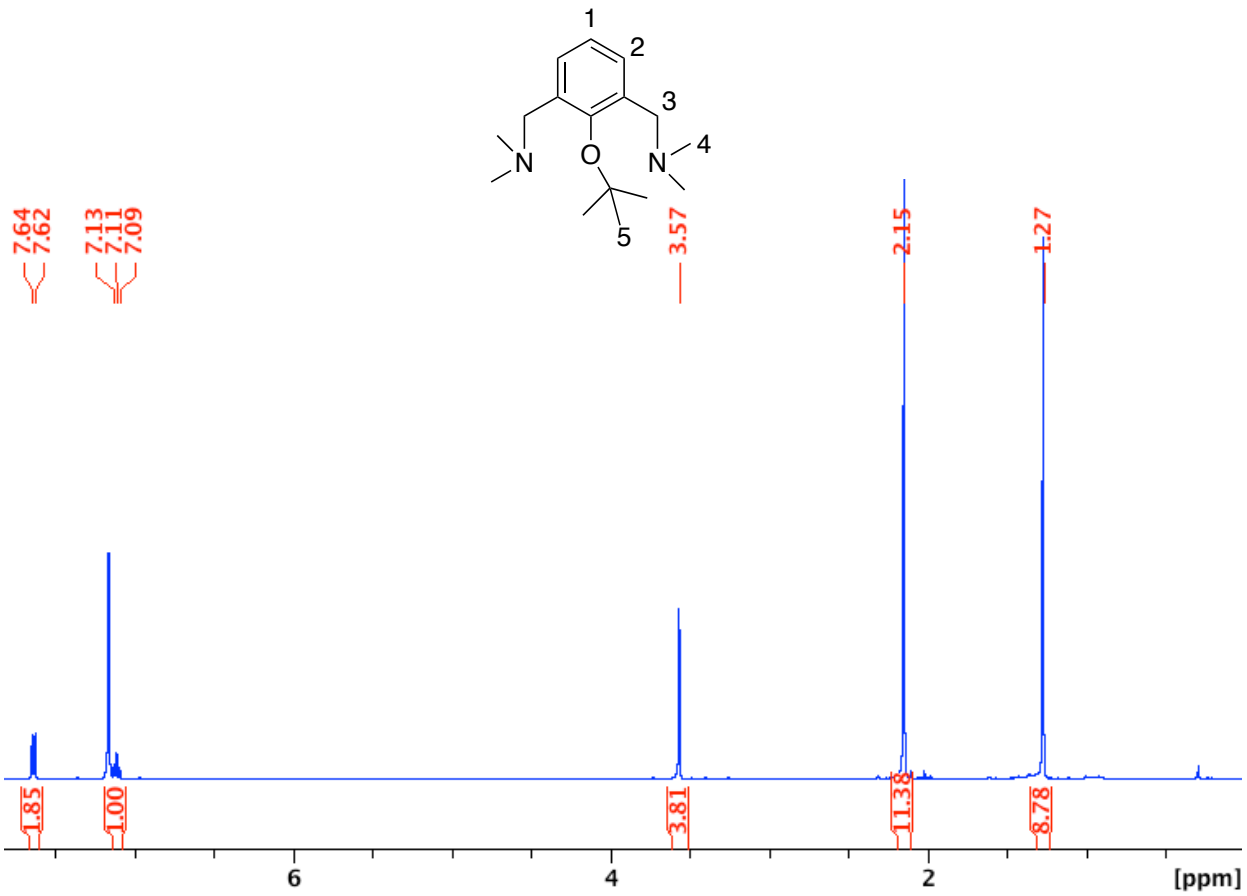

Figure 3.17. NC(OtBu)N ^{1}H NMR C_6D_6, δ 7.63 (2H, d, J_{HH} = *7.5,* H_2), δ 7.11 (1H, t, J_{HH} = *7.5,* H_1), δ 3.57 (4H, s, H_3), δ 2.15 (12H, s, H_4), δ 1.27 (9H, s, H_5)

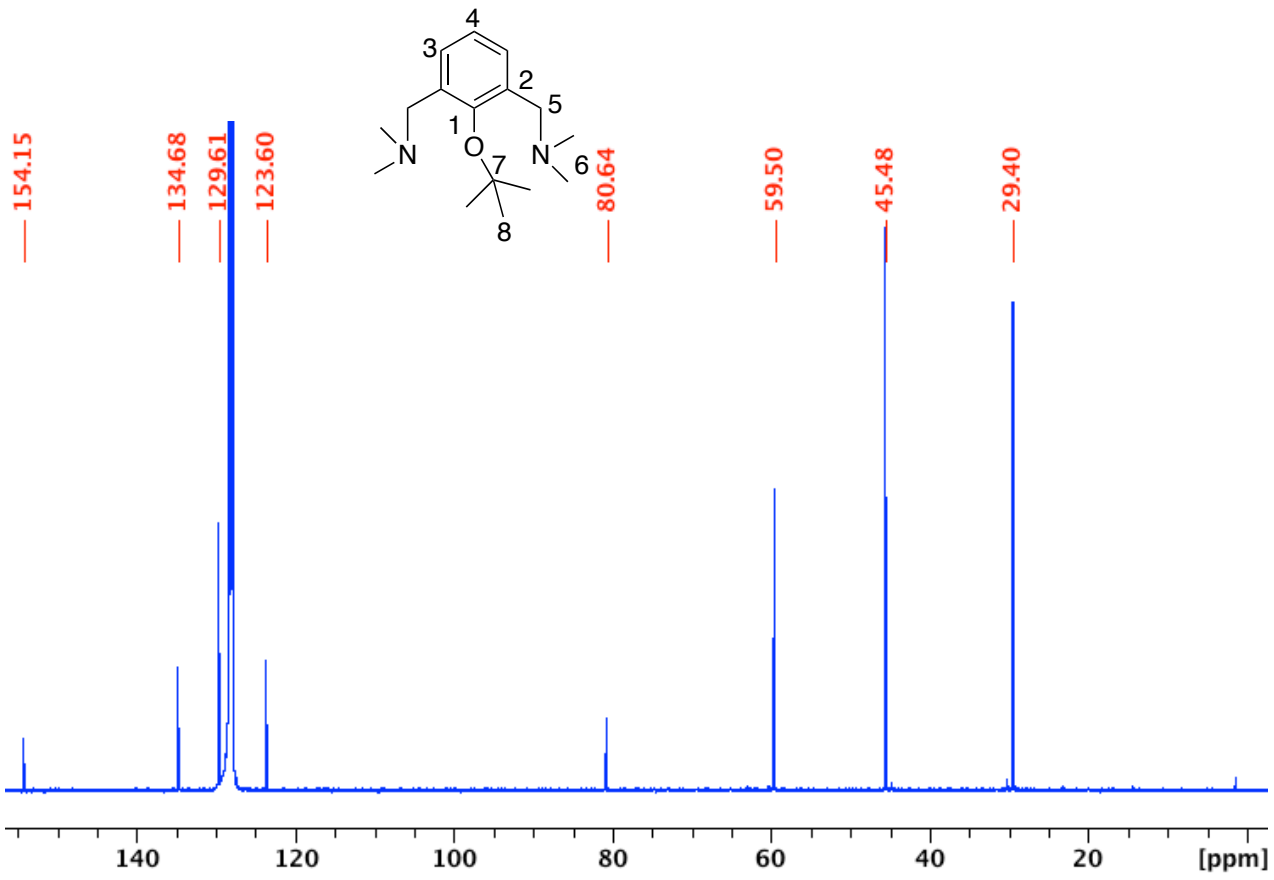

Figure 3.18. NC(OtBu)N ^{13}C NMR C_6D_6, δ 154.15 (1C, s, C_1), δ 134.68 (2C, s, C_3), δ 129.61 (2C, s C_2), δ 123.60 (1C, s, C_4), δ 80.64 (1C, s, C_7), δ 59.50 (2C, s, C_5), δ 45.48 (4C, s, C_6), δ 29.40 (3C, s, C_8).

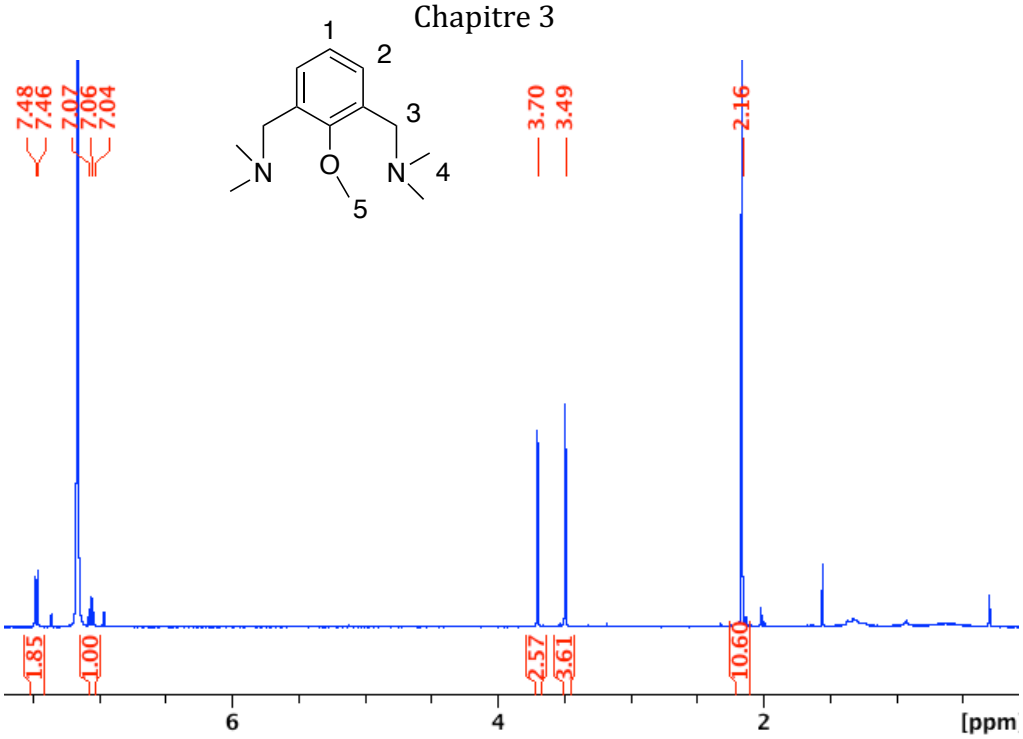

Figure 3.19. NC(OMe)N ^{1}H NMR C_6D_6, δ 7.47 (2H, d, J_{HH} = *7.6,* H_2), δ 7.05 (1H, t, J_{HH} = *7.6,* H_1), δ 3.70 (3H, s, H_5), δ 3.49 (4H, s, H_3), δ 2.16 (12H, s, H_4).

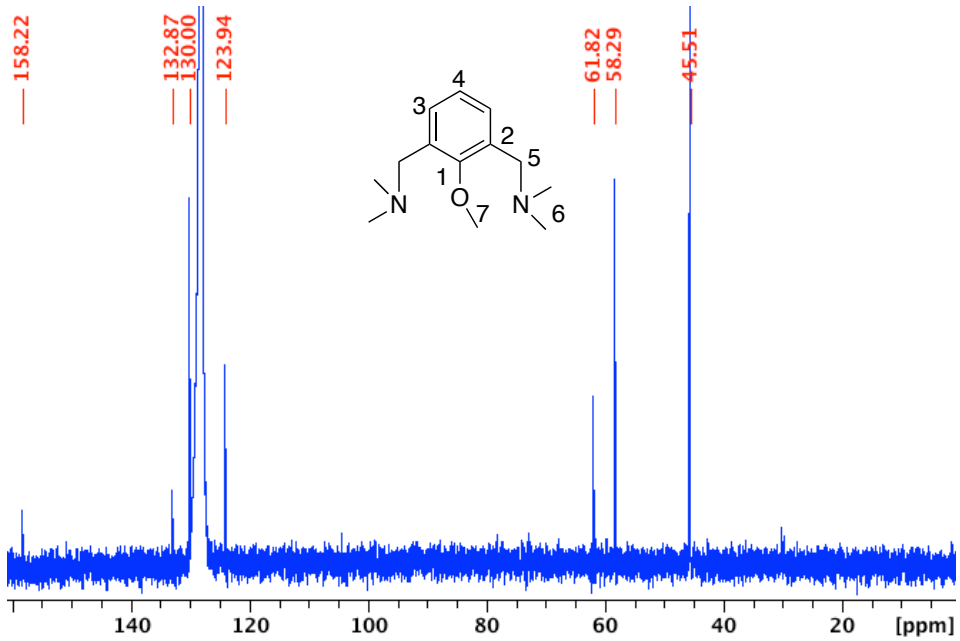

Figure 3.20. NC(OMe)N ^{13}C NMR C_6D_6, δ 158.22 (1C, s, C_1), δ 132.87 (2C, s, C_3), δ 130.00 (2C, s C_2), δ 124.94 (1C, s, C_4), δ 61.82 (1C, s, C_7), δ 58.29 (2C, s, C_5), δ 45.51 (4C, s, C_6)

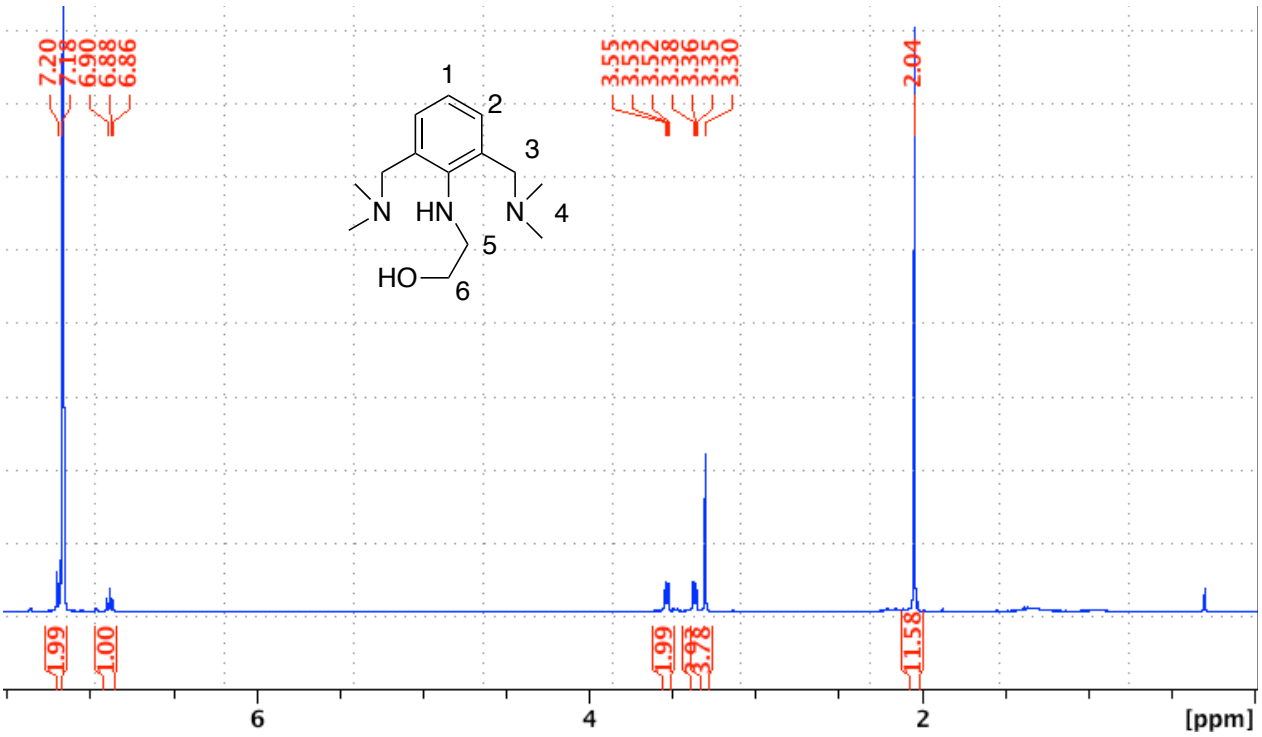

Figure 3.21. NC(ethanolamine)N ^{1}H NMR C_6D_6, δ 7.19 (2H, d, J_{HH} = *7.5,* H_2), δ 6.88 (1H, t, J_{HH} = *7.5,* H_1), δ 3.53 (2H, vt, J_{HH} = *4.7,* H_6), δ 3.36 (2H, vt, J_{HH} = *4.7,* H_5), δ 3.30 (4H, s, H_3), δ 2.04 (12H, s, H_4).

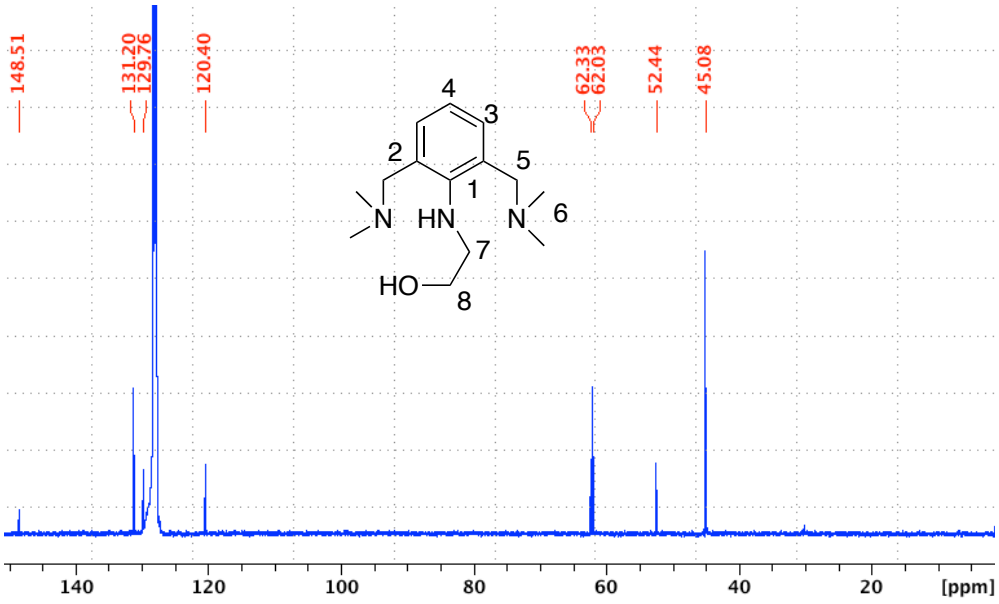

Figure 3.22. NC(ethanolamine)N ^{13}C NMR C_6D_6, δ 148.51 (1C, s, C_1), δ 131.20 (2C, s, C_3), δ 129.76 (2C, s C_2), δ 120.40 (1C, s, C_4), δ 62.33 (1C, s, C_8), δ 62.03 (2C, s, C_5), δ 52.44 (1C, s, C_7), δ 45.08.44 (4C, s, C_6).

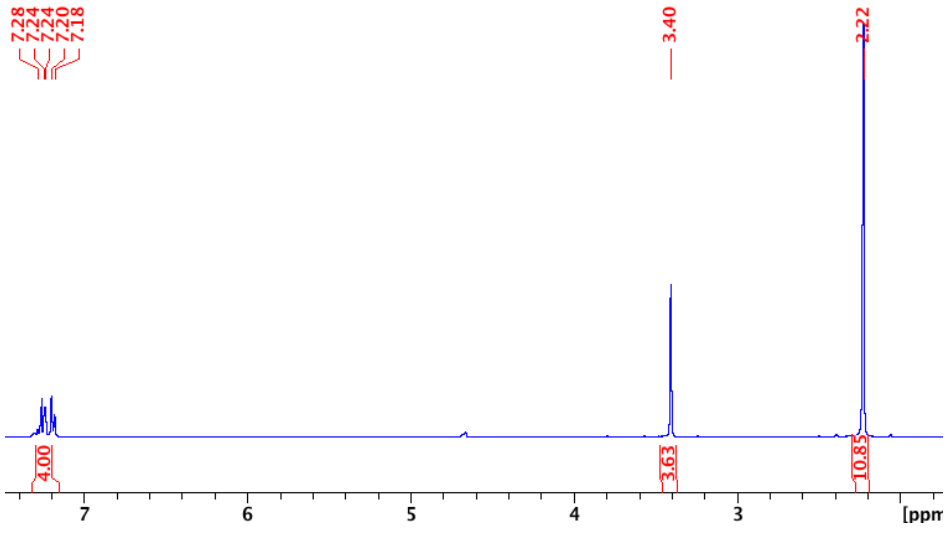

Figure 3.23. ^1H NMR spectrum of **NC(H)N** in $CDCl_3$.

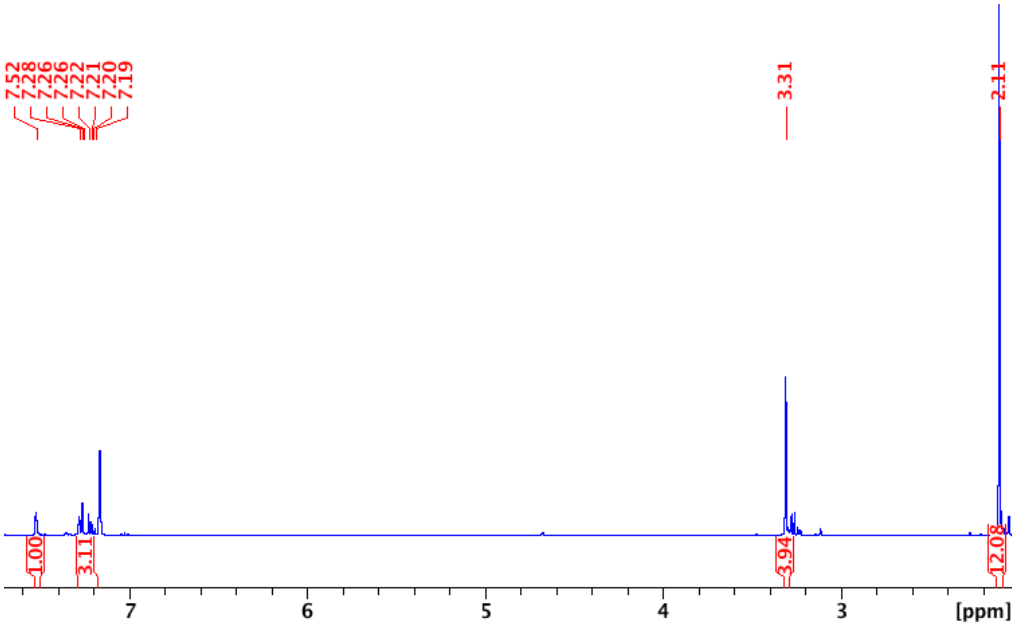

Figure 3.24. ^{1}H NMR spectrum of **NC(H)N** in C_6D_6**.**

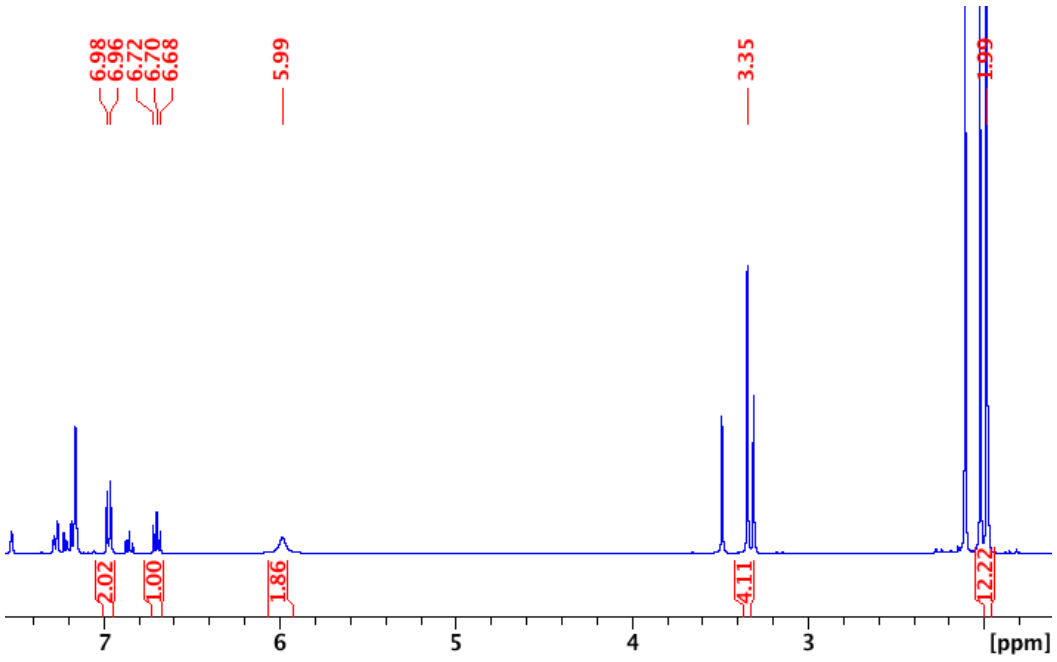

Figure 3.25. ^{1}H NMR spectrum of reaction with NH_4OH 28% in C_6D_6. The integrated signals correspond to the **NC(NH_2)N** product. The other products are **NC(OH)N** and **NC(H)N**.

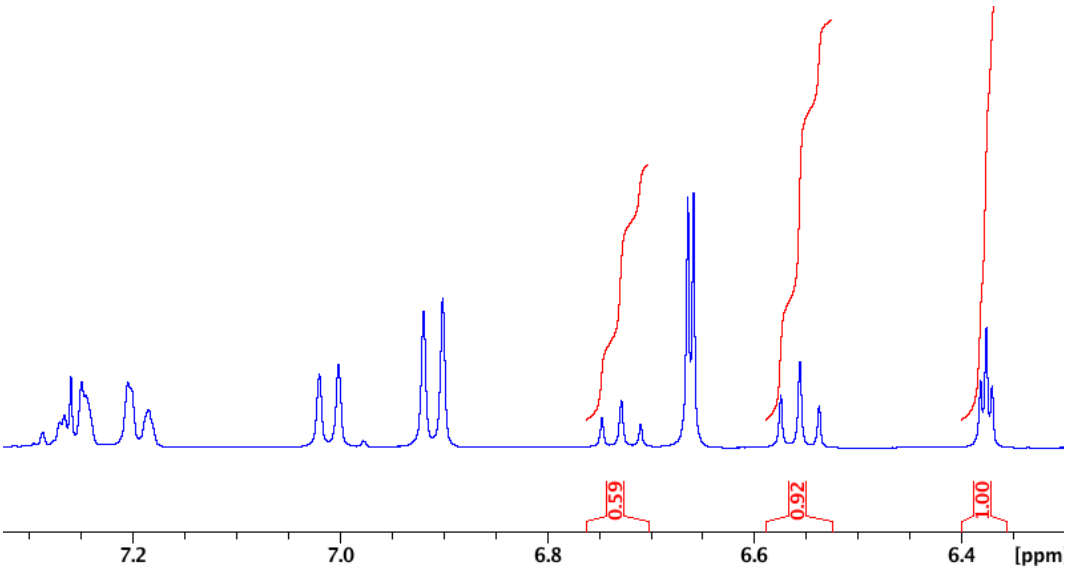

Figure 3.26. ^{1}H NMR spectrum of reaction with NH_4OH 28% in $CDCl_3$ with internal standard (integrated to 1.00). The integrated signals correspond to the **NC(NH₂)N** (major) and **NC(OH)N** (minor)

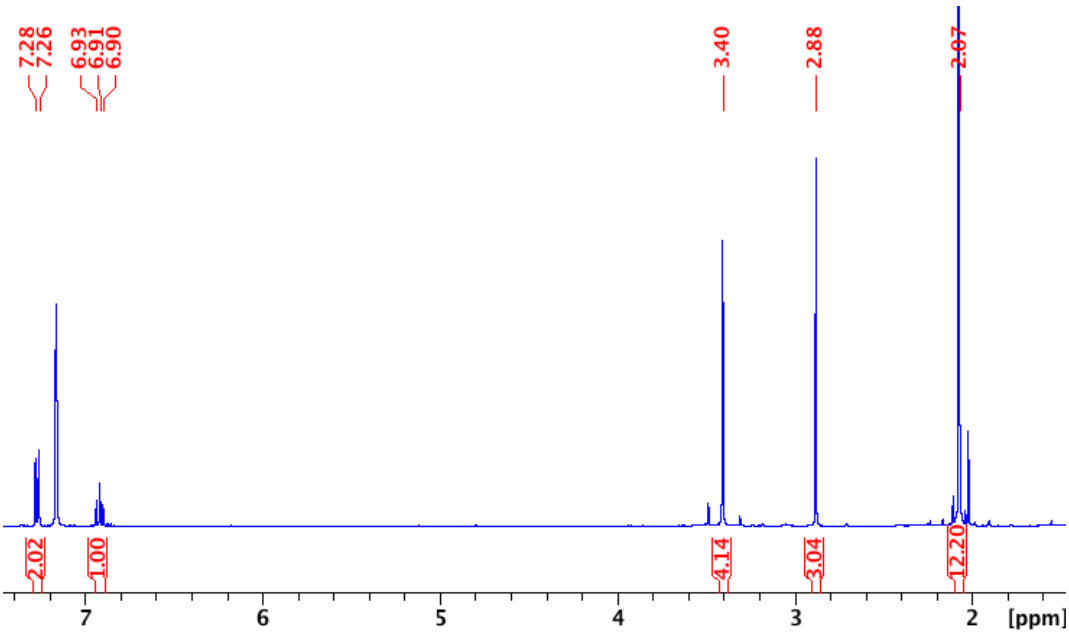

Figure 3.27. ^{1}H NMR spectrum of reaction with $MeNH_2$ 33% in C_6D_6. The integrated signal corresponds to the **NC(NMeH)N** product.

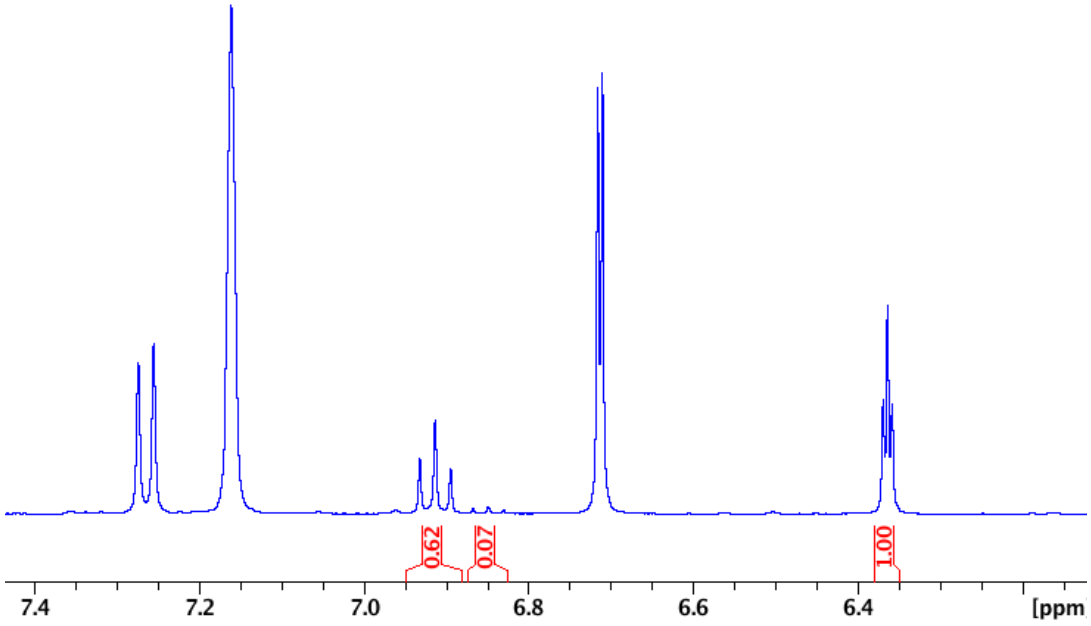

Figure 3.28. ^{1}H NMR spectrum of reaction with $MeNH_2$ 33% with internal standard (integrated to 1.00) in C_6D_6. The integrated signals correspond to the **NC(NMeH)N** (major) and **NC(OH)**N (minor).

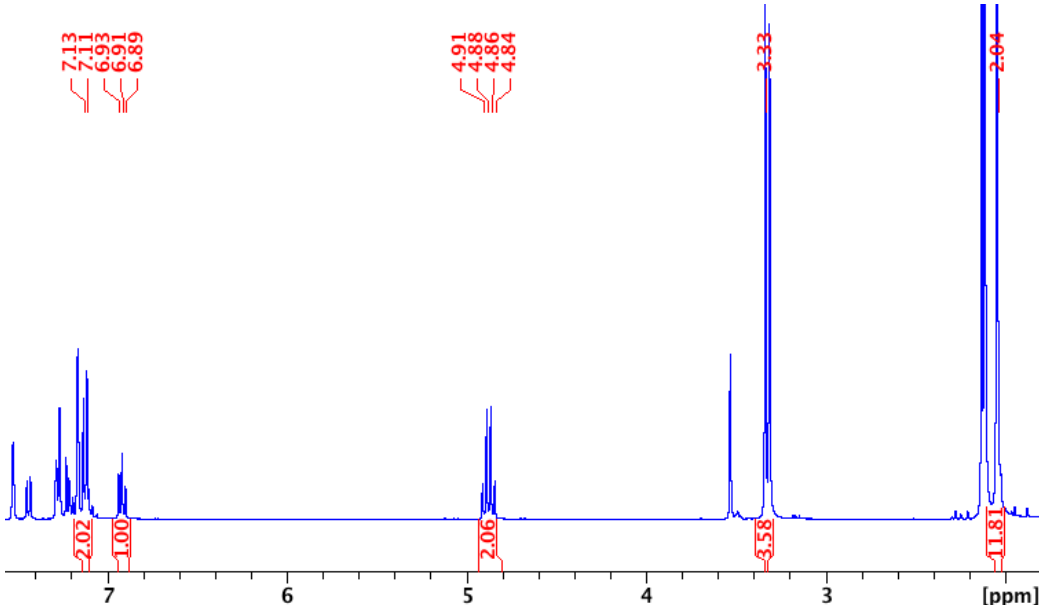

Figure 3.29. ^{1}H NMR spectrum of reaction with CF_3CH_2OH in C_6D_6. The integrated signal correspond to **NC(OCH$_2$CF$_3$)N**. The other signals correspond to NC(H)N and NC(Br)N.

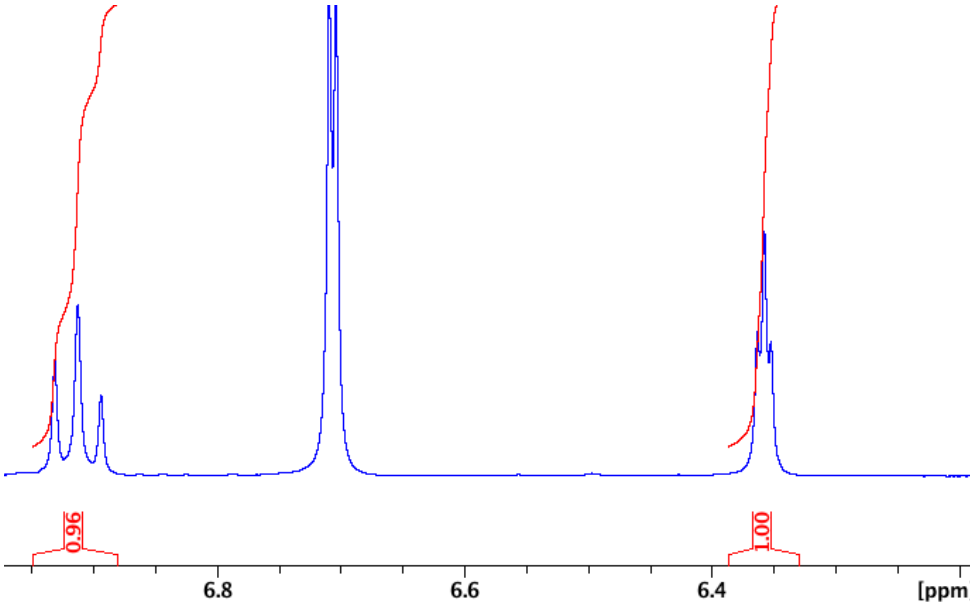

Figure 3.30. ^{1}H NMR spectrum of reaction with **CF_3CH_2OH** with internal standard in C_6D_6 (integrated to 1.00).

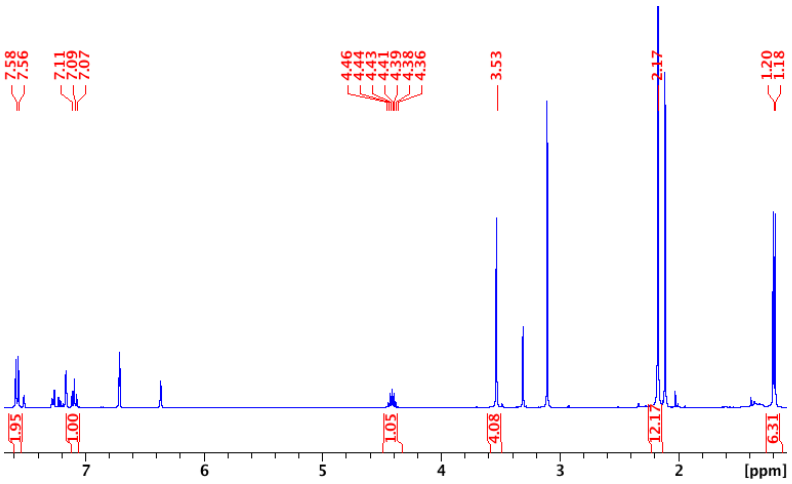

Figure 3.31. ^{1}H NMR spectrum of reaction with iPrOH in C_6D_6. The integrated signals correspond to NC(O*i*-Pr)N. The other signals correspond to NC(H)N.

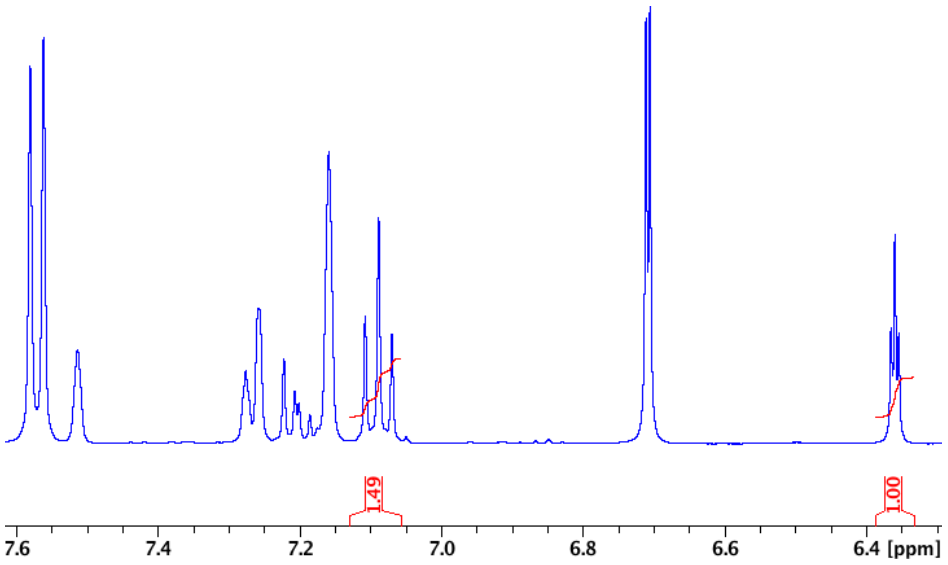

Figure 3.32. ^{1}H NMR spectrum of reaction with **iPrOH** with internal standard in C_6D_6 (integrated to 1.00). The other signals correspond to NC(H)N.

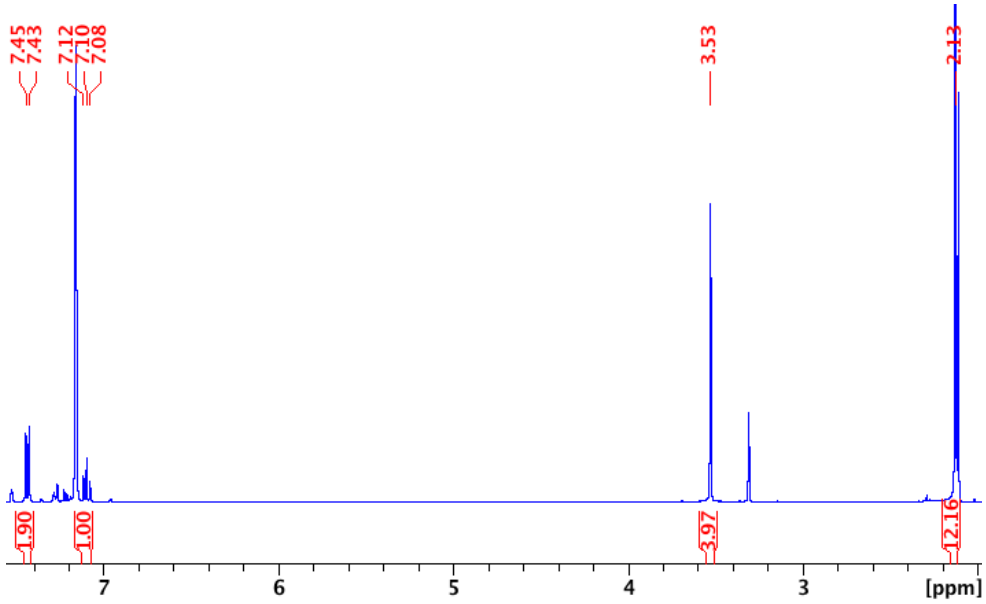

Figure 3.33. NC(Br)N ^{1}H NMR spectrum of reaction with **HBr** 48% in C_6D_6. The other signal correspond to NC(H)N

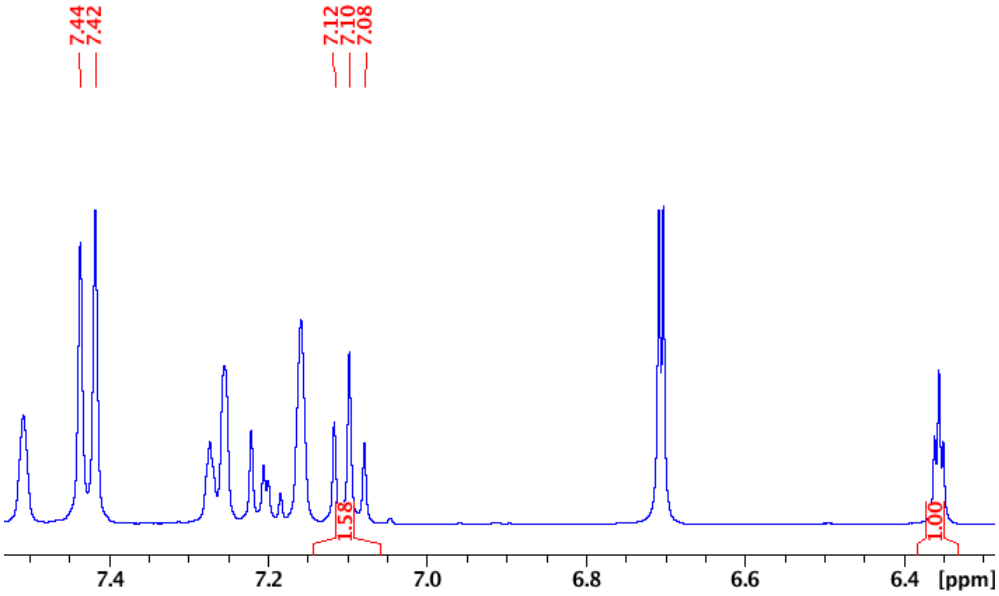

Figure 3.34. ^{1}H NMR spectrum of reaction with **HBr** 48% with internal standard in C_6D_6 (integrated to 1.00). The other signals correspond to NC(H)N.

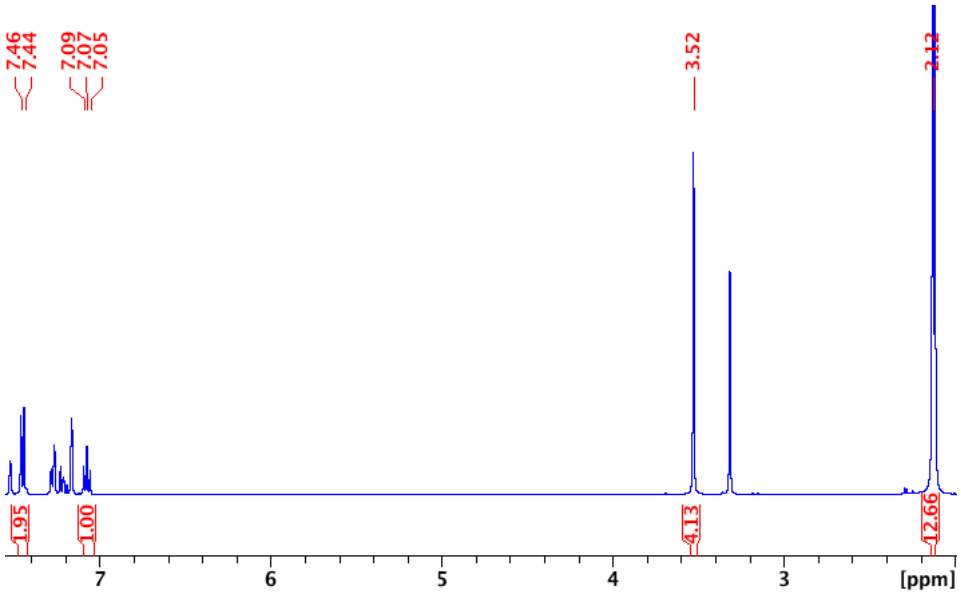

Figure 3.35. ^{1}H NMR spectrum of reaction with **HCl** 36% in C_6D_6. The other signals correspond to NC(H)N**.**

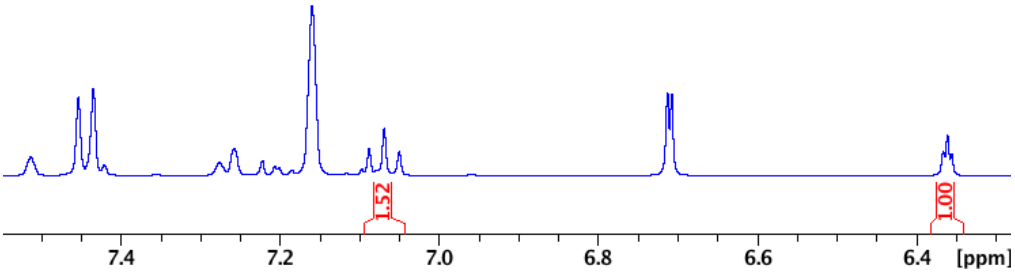

Figure 3.36. ^{1}H NMR spectrum of reaction with **HCl** 36% with internal standard in C_6D_6 (integrated to 1.00). The other signals correspond to NC(H)N.

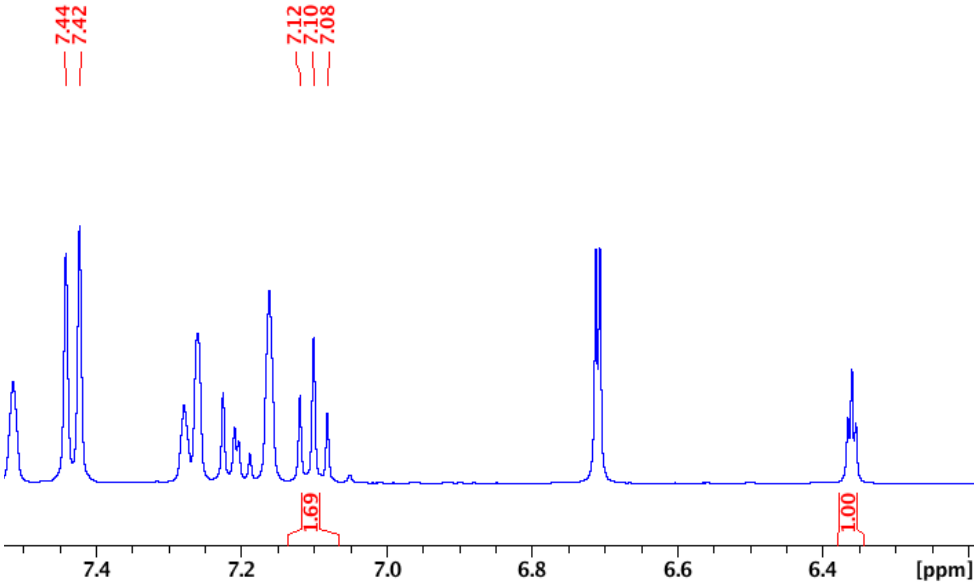

Figure 3.37. ^{1}H NMR spectrum of reaction with HBF_4 48% with internal standard in C_6D_6 (integrated to 1.00). The other signals correspond to NC(H)N.

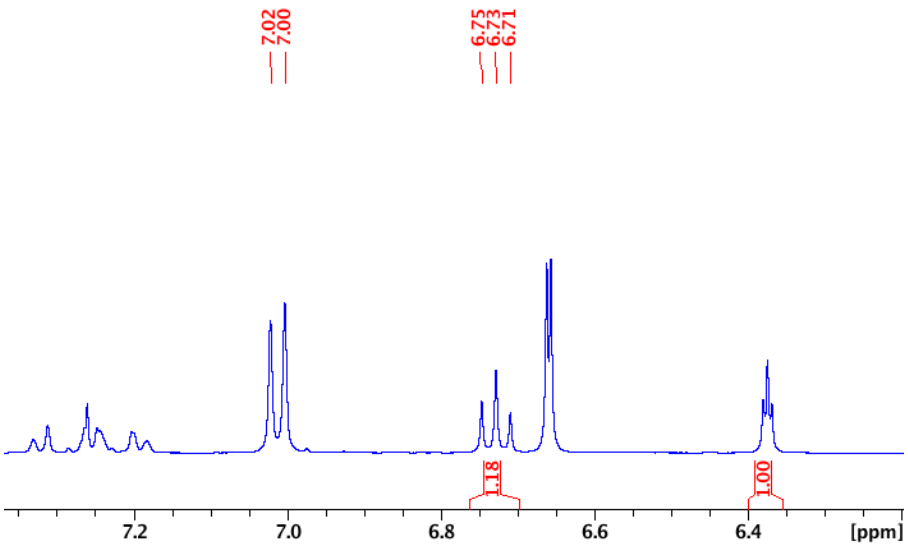

Figure 3.38. ^{1}H NMR spectrum of reaction with **H_2O and KBr** with internal standard in $CDCl_3$ (integrated to 1.00). The other signals correspond to NC(H)N.

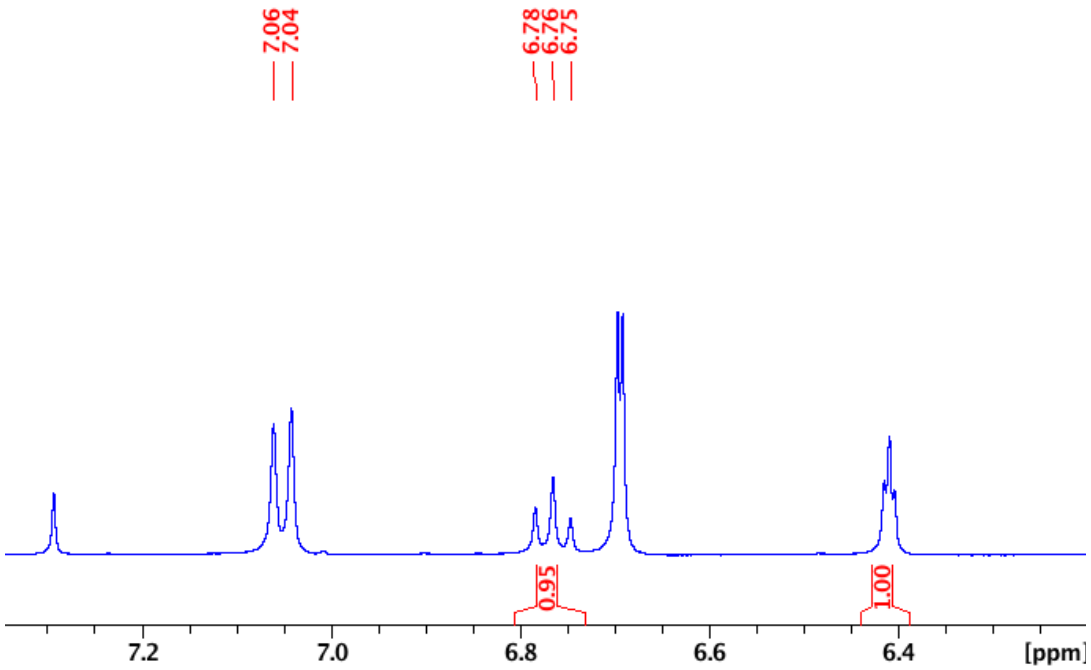

Figure 3.39. ^{1}H NMR spectrum of reaction with **H_2O and NEt_3** with internal standard in $CDCl_3$ (integrated to 1).

General procedure for the reaction of 2 with the radical $[N(4\text{-}Br\text{-}C_6H_4)_3][SbCl_6]$ and $[NO][BF_4]$(Table 1). These reactions were conducted by stirring complex **2** (50 mg, 0.122 mmol) in MeCN (5 mL). The reaction mixtures were evaporated and worked up by base extraction, and the yields were determined by ^{1}H NMR using 1-bromo-3,5-dimethoxybenzene as standard (0.013 g, 0.061 mmol).

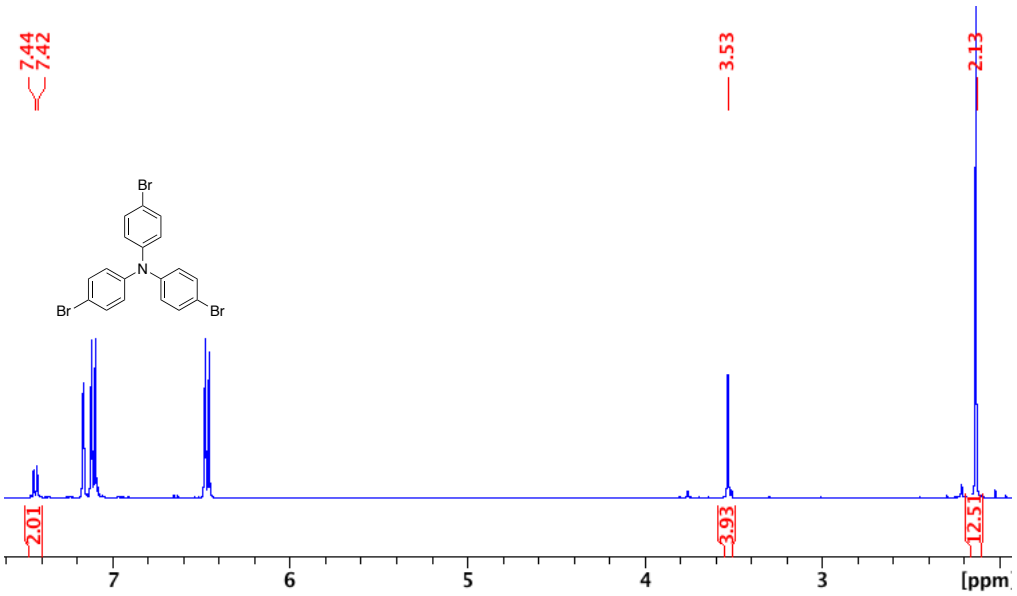

Figure 3.40. ^{1}H NMR spectrum of reaction with **$[N(4\text{-}Br\text{-}C_6H_4)_3][SbCl_6]$** in C_6D_6.

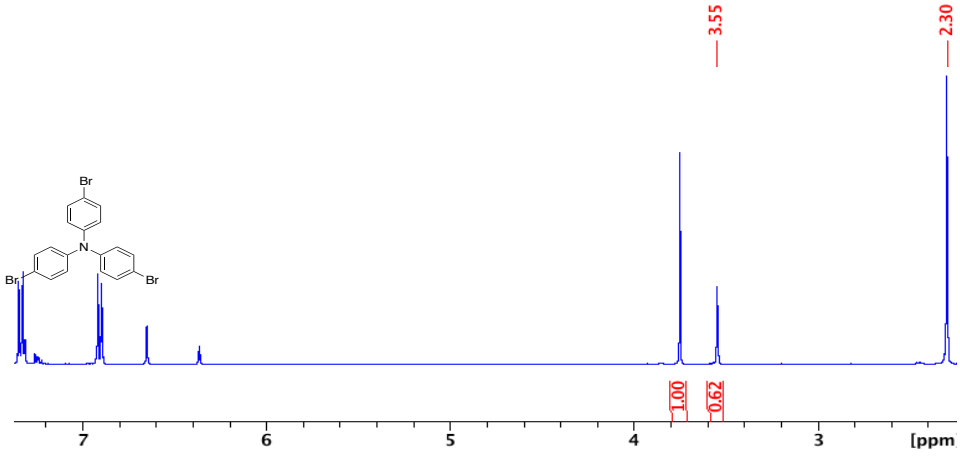

Figure 3.41. ^{1}H NMR spectrum of reaction with $[N(4\text{-}Br\text{-}C_6H_4)_3][SbCl_6]$ with internal standard in $CDCl_3$ (integrated to 1.00).

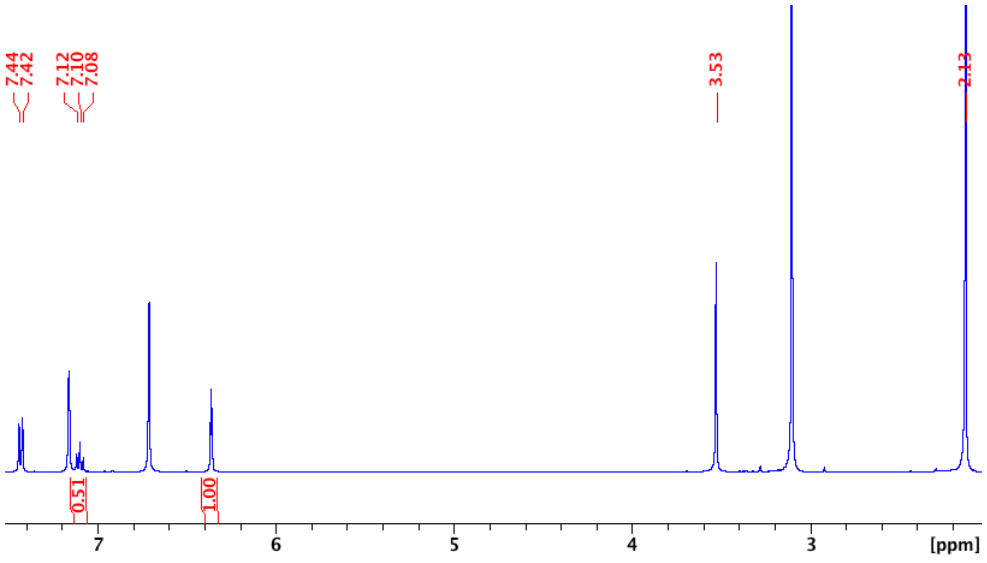

Figure 3.42. ^{1}H NMR spectrum of reaction with **[NO][BF$_4$]** with internal standard in C_6D_6 (integrated to 1.00).

Ni^{III}/Ni^{IV}

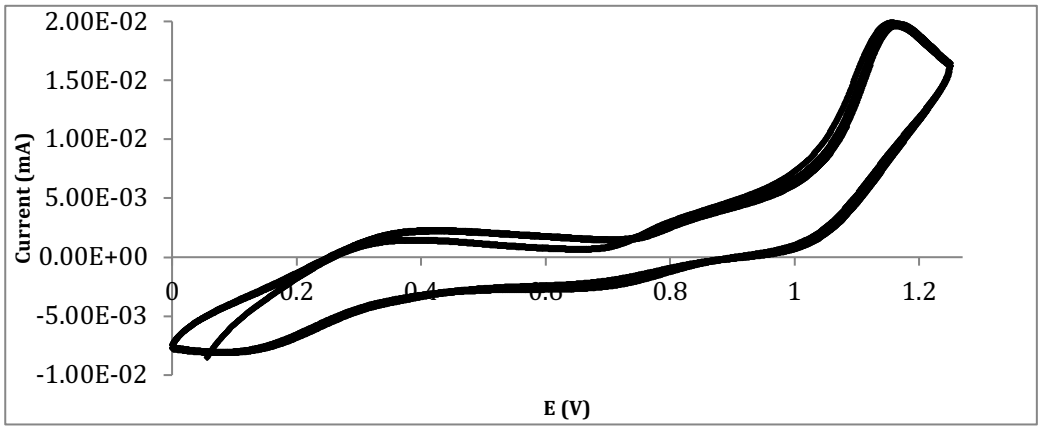

Figure 3.43. Cyclovoltammetry of 2 (1 mM) in MeCN with $[NtBu_4][PF_6]$ (100 mM). Scan rate 100 mV/s.

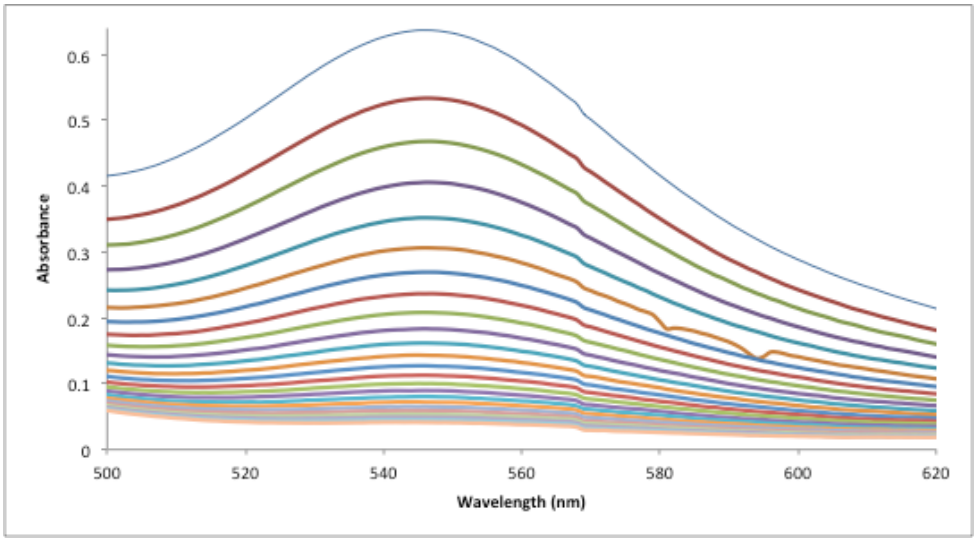

Figure 3.44. Time profile of the absorbance at 553 nm for the reaction of 2 (0.81 mM) in neat MeOH. The reaction was followed for 2 h**.**

3.6 REFERENCES

[1] For recent reviews on Ni-catalyzed C-C coupling reactions see: (a) Tasker, S. Z.; Standley, E. A.; Jamison, T. F., Recent Advances in Homogenous Nickel Catalysis. *Nature* **2014**, *509*, 299-309. (b)

Vedernikov, A. N., Mechanism of the Kumada-Corriu Cross-Coupling Catalysed by Low-Coordinate Bis(amido)-Nickel Complexes: Identification of Ni(I)-Ni(III) Catalytic Intermediates. *ChemCatChem*. **2014**, *6*, 2490-2492. For recent reports on Ni(III)-catalyzed Negishi-, Suzuki-, and Kumada-Corriu-type C-C coupling reactions see: (c) Phapale, V. B.; Buñuel, E.; García-Iglesias, M.; Cárdenas, D. J., Ni-Catalysed Cascade Formation of $C(sp^3)$-$C(sp^3)$ bonds by Cyclization and Cross-Coupling Reactions of Iodoalkanes with Alkyl Zinc Halides. *Angew. Chem. Int. Ed.* **2007**, *46*, 8790-8795. (d) Zultanski, S.; Fu, G., Nickel-Catalysed Carbon-Carbon Bond-Forming Reactions of Tertiary alkyl Halides: Suzuki Arylations. *J. Am. Chem. Soc.* **2013**, *134*, 624-627. (e) Guisán-Ceinos, M.; Soler-Yanes, R.; Collado-Sanz, D.; Phapale, V. B.; Buñuel, E.; Cárdenas, D. J., Ni-Catalysed Cascade Cyclization Alkyl-Alkyl Cross-Coupling. *Chemistry Eur. J.* **2013**, *19*, 8405-10. For one of the earliest mechanistic studies pointing to the involvement of trivalent nickel species in C-C bond formation reactions see: (f) Tsou, T. T.; Kochi, J. K., Mechanism of Oxidative Addition. Reaction of Nickel(0) complexes with Aromatic Halides. *J. Am. Chem. Soc.* **1979**, *101*, 7547-7560. On the other hand, Vicic has shown that in some cases the oxidation state of the Ni center in the catalytically active intermediates can depend on the redox properties of the auxiliary ligands. See: (g): Jones, G. D.; Martin, J. L.; McFarland, C.; Allen, O. R.; Hall, R. E.; Haley, A. D.; Brandon, R. J.; Konovalova, T.; Desrochers, P. J.; Pulay, P.; Vicic, D. A., Ligand Redox Effects in the Synthesis, Electronic Structure, and Reactivity of an Alkyl-Alkyl Cross-Coupling Catalyst. *J. Am. Chem. Soc.* **2006**, *128*, 13175-13183.

[2] (a) For an example of C-B coupling reactions purported to involve trivalent species see: Dudnik, A. S.; Fu, G. C., Nickel-Catalysed Coupling Reactions of Alkyl Electrophiles, Including Unactivated Tertiary Alkyl Halides, To Generate Carbon-Boron Bonds. *J. Am. Chem. Soc.* **2012,** *134* (25), 10693-7. (b) For C-N coupling reactions purported to involve tri- or tetravalent species see: Yokota, A.; Aihara, Y.; Chatani, N., Ni(II)-Catalysed Direct Arylation of C-H Bonds in Aromatic Amides Containing an 8-Aminoquinoline Moiety as a Directing Group. *J. Org. Chem.* **2014,** *79* (24), 11922-32.

[3] (a) (a) Koo, K.; Hillhouse, G. L., Carbon-Nitrogen Bond Formation by Reductive Elimination from Nickel(II) Amido Alkyl Complexes. *Organometallics* **1995,** *14* (9), 4421-4423. (b) Han, R.; Hillhouse, G. L., Carbon−Oxygen Reductive-Elimination from Nickel(II) Oxametallacycles and Factors That Control Formation of Ether, Aldehyde, Alcohol, or Ester Products. *J. Am. Chem. Soc.* **1997,** *119* (34), 8135-8136. (c) Lin, B. L.; Clough, C. R.; Hillhouse, G. L., Interactions of Aziridines with Nickel Complexes: Oxidative-Addition and Reductive-Elimination Reactions that Break and Make C−N Bonds. *J. Am. Chem. Soc.* **2002,** *124* (12), 2890-2891.

[4] (a) Zhou, W.; Schultz, J. W.; Rath, N. P.; Mirica, L. M., Aromatic Methoxylation and Hydroxylation by Organometallic High-Valent Nickel Complexes. *J. Am. Chem. Soc.* **2015,** *137* (24), 7604-7. (b) Zhou, W.; Zheng, S.; Schultz, J. W.; Rath, N. P.; Mirica, L. M., Aromatic Cyanoalkylation through Double C-H Activation Mediated by Ni(III). *J. Am. Chem. Soc.* **2016,** *138* (18), 5777-80.

[5] (a) Camasso, N. M.; Sanford, M. S., Design, synthesis, and carbon-heteroatom coupling reactions of organometallic nickel(IV) complexes. *Science* **2015,** *347* (6227), 1218-20. (b) Bour, J. R.; Camasso, N. M.; Meucci, E. A.; Kampf, J. W.; Canty, A. J.; Sanford, M. S., Carbon-Carbon Bond-Forming Reductive Elimination from Isolated Nickel(III) Complexes. *J. Am. Chem. Soc.* **2016,** *138* (49), 16105-16111.

[6] Similar studies have also been reported for the analogous C-C bond formation reactions promoted by high-valent Ni complexes. For a few pertinent examples see: (a) Watson, M. B.; Rath, N. P.; Mirica, L. M., Oxidative C-C Bond Formation Reactivity of Organometallic Ni(II), Ni(III), and Ni(IV) Complexes. *J. Am. Chem. Soc.* **2017,** *139* (1), 35-38. (b) Schultz, J. W.; Fuchigami, K.; Zheng, B.; Rath, N. P.; Mirica, L. M., Isolated Organometallic Nickel(III) and Nickel(IV) Complexes Relevant to Carbon-Carbon Bond Formation Reactions. *J. Am. Chem. Soc.* **2016,** *138* (39), 12928-12934.

[7] Camasso, N. M.; Canty, A. J.; Ariafard, A.; Sanford, M. S., Experimental and Computational Studies of High-Valent Nickel and Palladium Complexes. *Organometallics* **2017,** *36* (22), 4382-4393.

[8] For the synthesis and reactivities of related Ni^{IV} species see: (a) Martinez, G. E.; Ocampo, C.; Park, Y. J.; Fout, A. R., Accessing Pincer Bis(carbene) Ni(IV) Complexes from Ni(II) via Halogen and Halogen Surrogates. *J. Am. Chem. Soc.* **2016,** *138* (13), 4290-3. (b) Chong, E.; Kampf, J. W.; Ariafard, A.; Canty, A. J.; Sanford, M. S., Oxidatively Induced C-H Activation at High Valent Nickel. *J. Am. Chem. Soc.* **2017,** *139* (17), 6058-6061. (c) D'Accriscio, F.; Borja, P.; Saffon-Merceron, N.; Fustier-Boutignon, M.; Mezailles, N.; Nebra, N., C-H Bond Trifluoromethylation of Arenes Enabled by a Robust, High-Valent Nickel(IV) Complex. *Angew Chem Int Ed Engl* **2017,** *56* (42), 12898-12902.

[9] (a) Terrett, J. A.; Cuthbertson, J. D.; Shurtleff, V. W.; MacMillan, D. W., Switching on elusive organometallic mechanisms with photoredox catalysis. *Nature* **2015,** *524* (7565), 330-4. (b) Jouffroy, M.; Kelly, C. B.; Molander, G. A., Thioetherification via Photoredox/Nickel Dual Catalysis. *Org Lett* **2016,** *18* (4), 876-9. (c) Welin, E. R.; Le, C.; Arias-Rotondo, D. M.; McCusker, J. K.; MacMillan, D. W., Photosensitized, energy transfer-mediated organometallic catalysis through electronically excited

nickel(II). *Science* **2017,** *355* (6323), 380-385.

[10] (a) Kogut, E.; Wiencko, H. L.; Zhang, L.; Cordeau, D. E.; Warren, T. H., A terminal Ni(III)-imide with diverse reactivity pathways. *J. Am. Chem. Soc.* **2005,** *127* (32), 11248-9. (b) Chiou, T. W.; Liaw, W. F., Mononuclear nickel(III) complexes [Ni(III)(OR)(P(C_6H_3-3-$SiMe_3$-2-S)$_3$)](-) (R = Me, Ph) containing the terminal alkoxide ligand: relevance to the nickel site of oxidized-form [NiFe] hydrogenases. *Inorg. Chem.* **2008,** *47* (17), 7908-13. (c) Lee, C.-M.; Chen, C.-H.; Liao, F.-X.; Hu, C.-H.; Lee, G.-H., Mononuclear Ni ^{III} −Alkyl Complexes (Alkyl = Me and Et): Relevance to the Acetyl-CoA Synthase and Methyl-CoM Reductase. *J. Am. Chem. Soc.* **2010,** *132* (27), 9256-9258. (d) Lipschutz, M. I.; Yang, X.; Chatterjee, R.; Tilley, T. D., A structurally rigid bis(amido) ligand framework in low-coordinate Ni(I), Ni(II), and Ni(III) analogues provides access to a Ni(III) methyl complex via oxidative addition. *J. Am. Chem. Soc.* **2013,** *135* (41), 15298-301. (e) Biswas, S.; Weix, D. J., Mechanism and selectivity in nickel-catalyzed cross-electrophile coupling of aryl halides with alkyl halides. *J. Am. Chem. Soc.* **2013,** *135* (43), 16192-7. (f) Zhang, C. P.; Wang, H.; Klein, A.; Biewer, C.; Stirnat, K.; Yamaguchi, Y.; Xu, L.; Gomez-Benitez, V.; Vicic, D. A., A five-coordinate nickel(II) fluoroalkyl complex as a precursor to a spectroscopically detectable Ni(III) species. *J. Am. Chem. Soc.* **2013,** *135* (22), 8141-4. (g) Hwang, S. J.; Anderson, B. L.; Powers, D. C.; Maher, A. G.; Hadt, R. G.; Nocera, D. G., Halogen Photoelimination from Monomeric Nickel(III) Complexes Enabled by the Secondary Coordination Sphere. *Organometallics* **2015,** *34* (19), 4766-4774.

[11] (a) Fontaine, F.-G.; Kadkhodazadeh, T.; Zargarian, D., Nickel indenyl complexes as precatalysts for dehydropolymerization of phenylsilane. *Chemical Communications* **1998,** (12), 1253-1254. (b) Groux, L. F.; Zargarian, D., Aminoalkyl-Substituted Indenylnickel(II) Complexes (η^3:η^0-Ind(CH_2)2NMe_2)Ni(PR_3)X and [(η^3:η^1-Ind(CH_2)2NMe_2)Ni(PR_3)][BPh_4]: Influence of the Phosphine in Ligand Exchange and Polymerization Reactions. *Organometallics* **2003,** *22* (23), 4759-4769. (c) Groux, L. F.; Zargarian, D., Aminoalkyl-Substituted Indenyl−Nickel Compounds: Tuning Reactivities as a Function of the Pendant, Hemilabile Moiety. *Organometallics* **2003,** *22* (15), 3124-3133.

[12] (a) Grove, D. M.; Van Koten, G.; Zoet, R.; Murrall, N. W.; Welch, A. J., Unique stable organometallic nickel(III) complexes; syntheses and the molecular structure of [Ni[C_6H_3(CH_2NMe_2)$_2$-2,6]I_2]. *J. Am. Chem. Soc.* **1983,** *105* (5), 1379-1380. (b) Grove, D. M.; Van Koten, G.; Mul, P.; Zoet, R.; Van der Linden, J. G. M.; Legters, J.; Schmitz, J. E. J.; Murrall, N. W.; Welch, A. J., Syntheses and characterization of

unique organometallic nickel(III) aryl species. ESR and electrochemical studies and the x-ray molecular study of square-pyramidal [Ni{$C_6H_3(CH_2NMe_2)$2-o,o'}I_2]. *Inorg. Chem.* **1988,** *27* (14), 2466-2473.

[13] (a) Pandarus, V.; Zargarian, D., New pincer-type diphosphinito (POCOP) complexes of NiII and NiIII. *Chem Commun* **2007,** (9), 978-80. (b) Pandarus, V.; Zargarian, D., New Pincer-Type Diphosphinito (POCOP) Complexes of Nickel. *Organometallics* **2007,** *26* (17), 4321-4334. (c) Castonguay, A.; Beauchamp, A. L.; Zargarian, D., Preparation and Reactivities of PCP-Type Pincer Complexes of Nickel. Impact of Different Ligand Skeletons and Phosphine Substituents. *Organometallics* **2008,** *27* (21), 5723-5732. (d) Spasyuk, D. M.; Zargarian, D.; van der Est, A., New POCN-Type Pincer Complexes of Nickel(II) and Nickel(III). *Organometallics* **2009,** *28* (22), 6531-6540. (e) Spasyuk, D. M.; Gorelsky, S. I.; van der Est, A.; Zargarian, D., Characterization of Divalent and Trivalent Species Generated in the Chemical and Electrochemical Oxidation of a Dimeric Pincer Complex of Nickel. *Inorg. Chem.* **2011,** *50* (6), 2661-2674. (f) Zargarian, D.; Castonguay, A.; Spasyuk, D. M., ECE-Type Pincer Complexes of Nickel. **2013,** *40*, 131-173. (g) Mougang-Soumé, B.; Belanger-Gariépy, F.; Zargarian, D., Synthesis, Characterization, and Oxidation of New POCNimine-Type Pincer Complexes of Nickel. *Organometallics* **2014,** *33* (21), 5990-6002.

[14] Cloutier, J.-P.; Vabre, B.; Moungang-Soumé, B.; Zargarian, D., Synthesis and Reactivities of New NCN-Type Pincer Complexes of Nickel. *Organometallics* **2015,** *34* (1), 133-145.

[15] Canty, A. J.; Denney, M. C.; van Koten, G.; Skelton, B. W.; White, A. H., Carbon−Oxygen Bond Formation at Metal(IV) Centers: Reactivity of Palladium(II) and Platinum(II) Complexes of the [2,6-(Dimethylaminomethyl)phenyl-N,C,N]-(Pincer) Ligand toward Iodomethane and Dibenzoyl Peroxide; Structural Studies of M(II) and M(IV) Complexes. *Organometallics* **2004,** *23* (23), 5432-5439.

[16] One such synthetic method involves the direct oxidative addition of the Br-functionalized proligand 1-Br,2,6-$(CH_2NMe_2)_2$-C_6H_3, NC(Br)N, to the zero-valent precursor $Ni(COD)_2$: (a) Grove, D. M.; Van Koten, G.; Ubbels, H. J. C.; Zoet, R.; Spek, A. L., Organonickel(II) complexes of the tridentate monoanionic ligand o,o'-bis[(dimethylamino)methylphenyl (N-C-N). Syntheses and the x-ray crystal structure of the stable nickel(II) formate [Ni(N-C-N)O_2CH]. *Organometallics* **1984,** *3* (7), 1003-1009. Substituted derivatives of this complex, (R-NCN)NiBr, have also been prepared in a similar fashion: (b) van de Kuil, L. A.; Luitjes, H.; Grove, D. M.; Zwikker, J. W.; van der Linden, J. G. M.; Roelofsen, A. M.;

Jenneskens, L. W.; Drenth, W.; van Koten, G., Electronic tuning of arylnickel(II) complexes by para substitution of the terdentate monoanionic 2,6-bis[(dimethylamino)methyl]phenyl ligand. *Organometallics* **1994,** *13* (2), 468-477.

[17] Kleij, A. W.; Gossage, R. A.; Klein Gebbink, R. J. M.; Brinkmann, N.; Reijerse, E. J.; Kragl, U.; Lutz, M.; Spek, A. L.; van Koten, G., A "Dendritic Effect" in Homogeneous Catalysis with Carbosilane-Supported Arylnickel(II) Catalysts: Observation of Active-Site Proximity Effects in Atom-Transfer Radical Addition. *J. Am. Chem. Soc.* **2000,** *122* (49), 12112-12124.

[18] Mirica et al.[4a] have proposed that treating the trivalent species $[(^{t\text{-Bu}}N_3C)Ni^{III}(NCMe)_2]^{2+}$ with NaOMe leads to a disproportionation reaction to generate the divalent intermediate $(^{t\text{-Bu}}N_3C)Ni^{II}$-OMe that undergoes □-H elimination followed by reductive elimination to give the protonated ligand $^{t\text{-Bu}}N_3C$-H.

[19] Higgs, A. T.; Zinn, P. J.; Sanford, M. S., Synthesis and Reactivity of NiII(Phpy)$_2$(Phpy = 2-Phenylpyridine)†. *Organometallics* **2010,** *29* (21), 5446-5449.

[20] This reaction also gave small amounts of another product that appears to be 3-dimethylaminomethyl-benzaldehyde, 3-(Me_2NCH_2)-$C_6H_4C(O)H$. We speculate that this side-product is generated via one-electron oxidation of the CH_2NMe_2 moiety in the proligand, **a**, by the trivalent precursor, followed by hydrolysis.

[21] Butikofer, J. L.; Parson, T. G.; Roddick, D. M., Adduct Studies and Reactivity of trans-$[(C_2F_5)_2MeP]_2Pt(Me)X$ (X = O_2CCF_3, OTF, OSO_2F). *Organometallics* **2006,** *25* (26), 6108-6114.

[22] Casitas, A.; King, A. E.; Parella, T.; Costas, M.; Stahl, S. S.; Ribas, X., Direct observation of CuI/CuIII redox steps relevant to Ullmann-type coupling reactions. *Chemi. Sci.* **2010,** *1* (3), 326.

[23] Higgs, A. T.; Zinn, P. J.; Simmons, S. J.; Sanford, M. S., Oxidatively Induced Carbon−Halogen Bond-Forming Reactions at Nickel. *Organometallics* **2009,** *28* (21), 6142-6144.

[24] The E°' values for these oxidants are taken from the following sources: (a*)* Connelly, N. G.; Geiger, W. E., Chemical Redox Agents for Organometallic Chemistry. *Chemical Reviews* **1996,** *96* (2), 877-910.; (b) Kochi, J. K., Inner-sphere electron transfer in organic chemistry. Relevance to electrophilic aromatic nitration. *Accounts of Chemical Research* **2002,** *25* (1), 39-47.

The redox potential for **2**, i.e., the $Ni^{IV/III}$ redox couple, was measured as described in SI. All E°' values cited in the text are measured in acetonitrile and have been referenced against the ferrocenium/ferrocence couple (at 0.40 V in acetonitrile against SCE).

[25] Another interesting finding reported by Sanford and Canty is the much greater propensity of cationic vs. charge-neutral Ni^{IV} species to undergo C-C reductive elimination.[7]

[26] Cyclic voltammetry measurements conducted on **2** showed that aerobic oxidation of this species is not likely (E_{ox} (Ni^{IV}/Ni^{III}) = +1.2 V. Thus, we can dismiss the possibility of generating tetravalent intermediates under aerobic conditions.

[27] It should be noted here that the solid state structure of **2** (ref. [12]) shows that the Ni center is out of the equatorial plane while the two NMe_2 moieties are pushed away from the apical Br, presumably due to the greater steric demand of the latter.

[28] Note that protonation of the Ni^{III} center in **2** is not possible, as this would imply the improbable formation of a pentavalent species.

[29] Yamamoto, Y.; Chen, X.; Kojima, S.; Ohdoi, K.; Kitano, M.; Doi, Y.; Akiba, K. *J. Am. Chem. Soc.* **1995,** *117*, 3922-3932.

[30] Vabre, B.; Spasyuk, D. M.; Zargarian, D. *Organometallics* **2012**, *31*, 8561−8570.

Chapitre 4: C-O and C-N Functionalization of Cationic, NCN-Type Pincer Complexes of Trivalent Nickel: Mechanism, Selectivity, and Kinetic Isotope Effect

Article 3

Jean-Philippe Cloutier, Lionel Rechignat, Yves Canac, Daniel H. Ess, and Davit Zargarian

Département de chimie, Université de Montréal, Montréal (Québec), Canada H3C 3J7

Accepted in Inorganic chemistry

4.1 ABSTRACT

This report presents the synthesis of new mono- and dicationic NCN-Ni^{III} complexes and describes their reactivities with protic substrates. (NCN is the pincer-type ligand $\kappa^N, \kappa^C, \kappa^N$-2,6-$(CH_2NMe_2)_2$-$C_6H_3$.) Treating van Koten's trivalent complex (NCN)$Ni^{III}Br_2$ with $AgSbF_6$ in acetonitrile gives the dicationic complex $[(NCN)Ni^{III}(MeCN)_3]^{2+}$, whereas the latter complex undergoes a ligand exchange reaction with (NCN)$Ni^{III}Br_2$ to furnish the related monocationic complex $[(NCN)Ni^{III}(Br)(MeCN)]^+$. These trivalent complexes have been characterized by X-ray diffraction analysis and EPR spectroscopy. Treating these trivalent complexes with methanol and methylamine led, respectively, to C-OCH_3 or C-$NH(CH_3)$ functionalization of the Ni-aryl moiety in these complexes, C-heteroatom bond formation taking place at the *ipso*-C. These reactions also generate the cationic divalent complex $[(NCN)Ni^{II}(NCMe)]^+$, which was prepared independently and characterized fully. The unanticipated formation of the latter divalent species suggested a comproportionation side-reaction between the cationic trivalent precursors and a monovalent species generated at the C-O and C-N bond formation steps; this scenario was supported by direct reaction of the trivalent complexes with the monovalent compound $(PPh_3)_3Ni^{I}Cl$. Kinetic measurements and DFT analysis have been used to investigate the mechanism of these C-O and C-N functionalization reactions and to rationalize the observed inverse kinetic isotope effect in the reaction of $[(NCN)Ni^{III}(Br)(MeCN)]^+$ with CH_3OH/CD_3OD.

4.2 INTRODUCTION

Examples of Ni-promoted carbon-heteroatom coupling reactions are increasingly frequent in the literature.[1] Proposed mechanisms for C-O and C-N bond formation reactions often invoke the involvement of high-valent (Ni^{III} and Ni^{IV}) intermediates. The origins of this idea can be traced to seminal work by Hillhouse's group showing that Ni^{II} alkoxide and amide complexes could undergo C-O and C-N reductive elimination upon oxidation.[2] More recent reports by Mirica have shown that Ni^{III} complexes can promote C-C and C-O functionalization of a Ni^{III}-Ar moiety,[3] whereas authentic Ni^{IV} complexes active in C-C, C-N, C-O and C-S formation were isolated by Sanford and Nebra.[4]

Our group's earlier work[5] has shown that the divalent complex $(NCN^{pz})Ni^{II}Br$ bearing a pyrazine-flanked pincer ligand (NCN^{pz}= 1,3-bis(pyrazole)-C_6H_3) undergoes C-O/C-N functionalization at the aryl moiety of the pincer ligand when treated with alcohols or amines under aerobic conditions, or with H_2O_2

(Scheme 1). That aerobic conditions are essential for the observed C-X coupling reactivities of these compounds with alcohols or amines strongly indicated that these reactions go through high-valent intermediates, but no such species could be isolated.

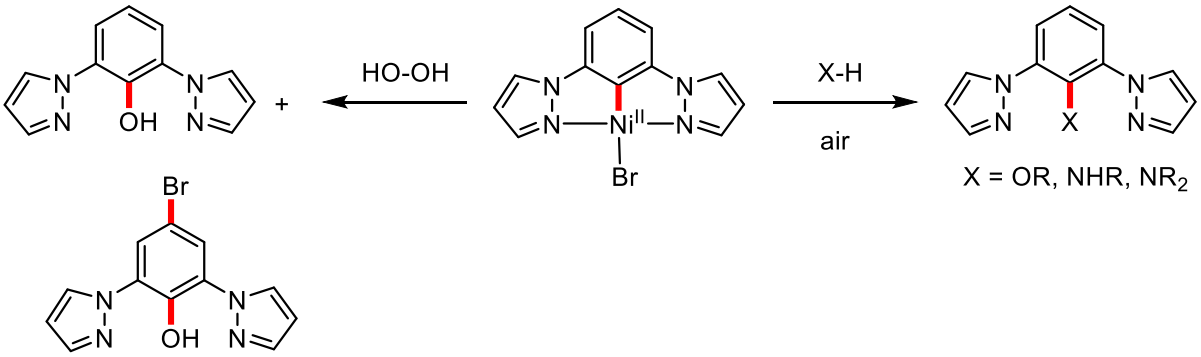

Scheme 4.1. Previous work on C-heteroatom coupling promoted by a Ni^{II} precursor.

In a more recent follow-up study,[6] we reported that analogous C-O and C-N functionalizations take place at the *ipso*-C of the NCN ligand in (NCN)$Ni^{III}Br_2$ (NCN= κ^N, κ^C, κ^N-2,6-$(CH_2NMe_2)_2$-C_6H_3),[7] when this authenticated trivalent complex is treated with water, alcohols, and amines; this system also promoted the more difficult C-halogen functionalization reaction with HCl or HBr.

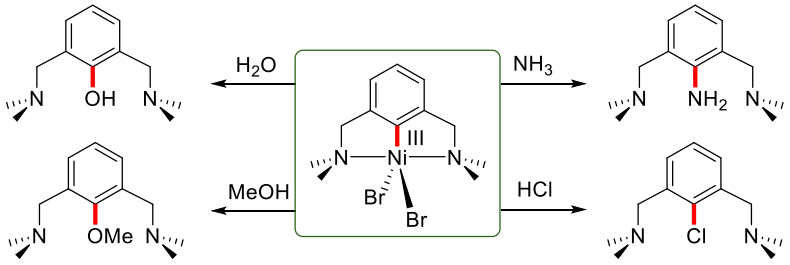

Scheme 4.2. Previous work on C-heteroatom coupling promoted by a Ni^{III} precursor.

The two key steps in the proposed mechanism for these functionalization reactions are the coordination of the protic substrate HX to the trivalent Ni center, followed up by its deprotonation to generate the requisite Ni-X moiety. We reasoned that both of these steps should take place more readily with a more electrophilic, cationic Ni precursor. Indeed, involvement of cationic Ni^{III} intermediates in C-O coupling reactions has been postulated by MacMillan[1a] and demonstrated by Mirica.[3] We were thus inspired to prepare isolable and thermally stable cationic trivalent complexes and investigate their intrinsic reactivities toward protic substrates.

The present work reports the synthesis and characterization of new mono- and dicationic Ni^{III} complexes based on van Koten's NCN ligand and describes their reactions with methanol and methylamine to give C-O and C-N backbone functionalization under mild conditions. We also report a new cationic Ni^{II} capable of promoting aerobic C-O backbone functionalization, albeit slowly. DFT studies have revealed metal-ligand cooperativity in the deprotonation of MeOH and have shown that the C-O coupling step is the result of a reductive elimination process. As was the case in our previous report on the functionalization of the charge-neutral trivalent complex $(NCN)Ni^{III}Br_2$, the yields obtained from the reaction of cationic and dicationic complexes with MeOH under nitrogen never exceed 50%, implying a redox process taking place between the trivalent precursors and monovalent species generated at the reductive elimination step. DFT calculations confirm that this redox process is not only viable but crucial for rendering the C-O bond formation step irreversible. The reductive elimination is rate limiting for both C-O and C-N coupling. The potential energy surface obtained for the reaction with methylamine shows that deprotonation is most likely assured by a second molecule of the substrate. Calculations also explain the observed inverse kinetic isotope effect by showing that coordination of CD_3OD is favoured over that of CH_3OH.

4.3 RESULTS and DISCUSSION

We began our studies by preparing the divalent cation $[(NCN)Ni(NCMe)]^+$, **1**, and testing its reactivity with methanol. This compound was prepared in 64% yield by using silver salts to abstract the Br^- in van Koten's divalent complex $(NCN)Ni^{II}Br$[8] and replacing it with acetonitrile (Scheme 4.3). The ^1H and ^{13}C NMR spectra of the resulting solid were consistent with the anticipated C_{2v} point group symmetry of the target cationic complex. (Some of the signals were also quite characteristic and facilitated monitoring the functionalization reactions; vide infra.) For instance, the ^1H NMR spectrum (C_6D_6) showed the anticipated triplet and doublet signals for the three aromatic protons (6.89 and 6.29 ppm; $^3J_{HH}$ = 7.5) and the two singlets for NCH_2 and NCH_3, at 2.76 and 2.20 ppm, respectively. The latter are shifted upfield by 0.33 ppm compared to the corresponding signals in the charge-neutral bromo precursor, whereas the singlet for Ni-$NCCH_3$ resonates close to the corresponding signal for free acetonitrile in C_6D_6 (0.62 vs 0.58 ppm). The most characteristic $^{13}C\{^1H\}$ signal was due to Ni-$C_{(Ar)}$ (~147 ppm). Single crystal x-ray diffraction studies of **1** confirmed the anticipated square planar structure, which is also shown in Scheme 1; the most pertinent structural parameters are provided in Supporting Information (SI).

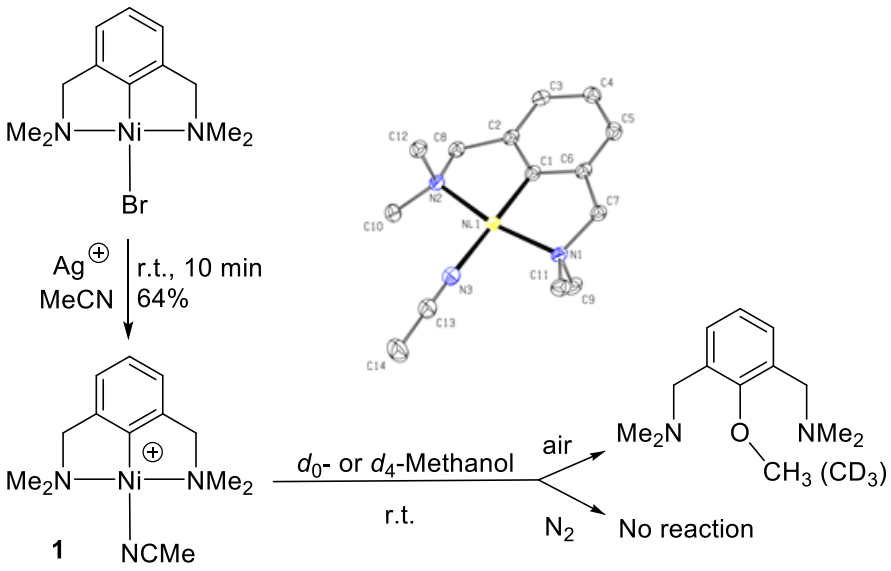

Scheme 4.3. Synthesis of $[(NCN)Ni^{II}(MeCN)]^{+}$ (1) and its reaction with methanol.

With **1** fully characterized, we proceeded to test its reaction with methanol. No reaction took place when **1** was stirred in CH_3OH or CD_3OD at room temperature under N_2, but conducting the same reactions in air led to slow formation of the de-metallated coupling products, $NC(OCH_3)N$ or $NC(OCD_3)N$. For example, the latter was obtained in < 5% after 2 h and ~11% after 24 h. The observation that aerobic functionalization of the Ni-aryl moiety is possible suggested that perhaps O_2 can induce oxidation of the Ni^{II} complex **1** to a dicationic trivalent Ni^{III} intermediate, a species that would be poised for methanol coordination and subsequent C-O coupling. Cyclic voltammetry measurements carried out on cationic **1** showed, not surprisingly, that it has a greater oxidation potential relative to its charge-neutral bromo precursor (724 vs 240 mV, ref. Ag/AgCl; see SI for CV trace), but we surmised that this complex should be prone to oxidation with strong oxidants. Thus, we set out to prepare trivalent analogues of **1** and study their reactivities toward protic substrates.

Synthesis of mono- and dicationic trivalent complexes. We targeted the cationic acetonitrile adducts $[(NCN)Ni^{III}(Br)(NCMe)_n]^{+}$ and $[(NCN)Ni^{III}(NCMe)_m]^{+2}$, because acetonitrile is known to stabilize divalent[9] and trivalent[3] Ni cations. To our surprise, several attempts at oxidizing **1** with $CuBr_2$ or $NOBF_4$ did not give the target mono- and dicationic trivalent species. Thus, we modified our synthetic strategy as follows: instead of oxidizing the divalent cation **1**, we prepared the previously reported charge-neutral, trivalent complex **2**[7] and ionized it subsequently by bromide abstraction in acetonitrile, as shown in Scheme 2.

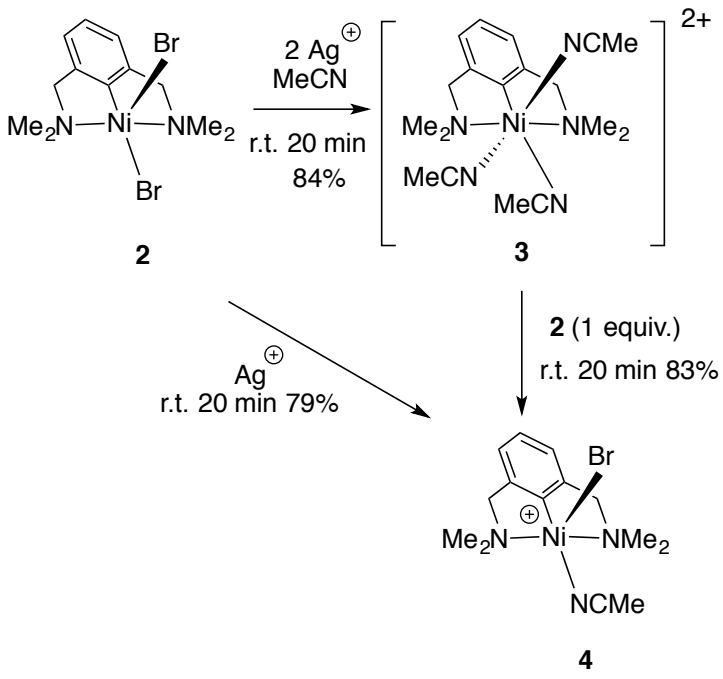

Scheme 4.4. Syntheses of $[(NCN)Ni^{III}(MeCN)_3]^{2+}$ (3) and $[(NCN))Ni^{III}(Br)(MeCN)]^{+}$ (4).

Thus, treating **2** with two equivalents of Ag^+ allowed the isolation of the formally 19-electron octahedral dication $[(NCN)Ni(NCMe)_3]^{2+}$, **3**, as an air-stable red powder in 84% yield (Scheme 4.4). It then occurred to us that this dication might undergo a ligand exchange reaction with its charge-neutral precursor **2** to generate a monocationic trivalent complex. Indeed, treatment of **3** with one equivalent of **2** furnished the monocation **4** as a deep purple solid in 83% yield (Scheme 4.4). The pentacoordinate, formally 17-electron complex **4** can also be obtained directly from the reaction of **2** with one equivalent of Ag^+ in 79% yield. Complexes **3** and **4** were fully characterized, including by single crystal X-ray diffraction analysis (Figures 4.1 and 4.2) and EPR spectroscopy (*vide infra*). To our knowledge, these are the first examples of cationic Ni^{III} complexes featuring monoanionic, meridional ECE-type pincer ligands. Figure 4.1 and 4.2 show the x-ray structures of **3** and **4**, along with selected distances and angles.

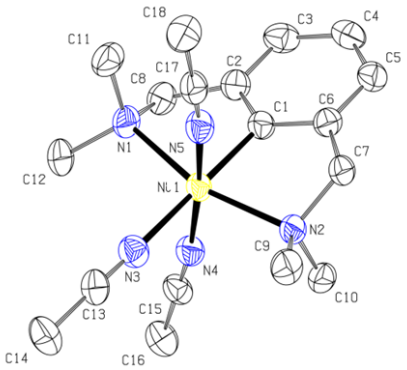

Figure 4.1. X-ray structure of **3**. Thermal ellipsoids are shown at the 50% level. The SbF_6 counter anions and all H atoms are omitted for clarity. Selected bond distances (Å) and angles (°): Ni1-N1 = 2.122(4); Ni1-N2 = 2.099(4); Ni1-N3= 2.003(5); Ni1-N4 = 2.082(5); Ni1-N5= 2.086(5); Ni1-C1= 1.905(5); N1-Ni1-N2 = 161.34(17); C1-Ni1-N3 = 179.2(2); Ni1-N3-C13 = 177.5(5); Ni1-N4-C15 = 170.6(5); Ni1-N5-C17 = 169.4(5).

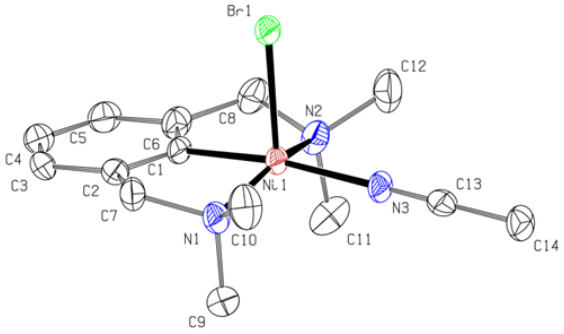

Figure 4.2. X-ray structure of **4**. Thermal ellipsoids are shown at the 50% level. The SbF_6 counter anion and all H atoms are omitted for clarity. Selected bond distances (Å) and angles (°):Ni1-N1 = 2.013(4); Ni1-N2 = 2.011(4); Ni1-C1= 1.873(4); Ni1-N3 = 1.978(4); Ni1-Br1 = 2.4014(8); N1-Ni1-N2 = 156.06(17); C1-Ni1-N3 = 171.56(16); C1-Ni1-Br1 = 90.31(12).

Complex **3** adopts a distorted octahedral geometry in the solid-state, whereas **4** displays a square pyramidal geometry with the Ni atom positioned ca. 0.42 Å out of the basal plane defined by C1, N1, N2 and N3 atoms. The main structural distortions in **3** and **4** are related to the very long axial Ni-N and Ni-Br distances[10] as well as the smaller-than-ideal trans angles N_{NMe2}-Ni-N_{NMe2} that define the bite angle for the NCN ligand (161° in **3** and 156° in **4**). Comparison of the structural parameters in **3** and **4** to structurally related Ni^{III} species reported in the literature shows that the average Ni-NMe_2 distances are comparable to the corresponding distances of the octahedral (NCN)Ni^{III}(py)$(NCS)_2$ (2.110 vs. 2.132 Å)[11] and the penta-coordinate dibromide **2**, (NCN)$NiBr_2$, (2.012 vs. 2.039 Å).[12] The Ni-NCMe distance trans from the aryl moiety in **3** is also comparable to the corresponding distance found in the dicationic octahedral Ni(III) species $[(^{t\text{-Bu}}N_3C)Ni(NCMe)_2]^{2+}$ reported recently by Mirica's group.[3] The Ni-C_{Ar} distance in the latter complex is also close to the corresponding distance in **4** (1.9018(1) vs. 1.873(4) Å).

Complexes **3** and **4** were also analyzed by X-band EPR spectroscopy (Figures 4.3 and 4.4; Table 1). The EPR X-band spectrum of the dicationic Ni complex **3** shows a temperature-independent, broad signal lacking hyperfine structure (Figure 4.3, *left*). The simulated spectrum allowed us to determine three distinct *g* values, which confirmed the expected rhombicity for paramagnetic Ni^{III} complexes (Table 4.1 and Figure 4.3, *right*).[7] The cationic Ni complex **4** is also characterized by an isotropic broad signal at 293

K (Figure 4.4, *top*). In contrast to the relatively unchanged low-temperature spectrum observed for **3**, complex **4** displayed a dramatic change at 120 K with the appearance of an anisotropic signal featuring different hyperfine couplings. The high multiplicity of the frozen EPR spectrum of **4** cannot *a priori* be rationalized by the presence of a single paramagnetic Ni^{III} species. The most likely explanation is that the EPR signal is due to the co-existence of two stereoisomers, **4** and **5**, wherein the Br atom occupies, respectively, either the axial or the equatorial position of the plane defined by the C1, N1, N2 and N3 atoms. More precisely, the EPR spectrum of **4** exhibits high rhombicity with three distinct *g* values for each isomer (**4**: g_x = 2.269; g_y = 2.145; g_z = 2.027; **5**: g_x = 2.307; g_y = 2.090; g_z = 2.077). Hyperfine couplings to the Br atom (I = 3/2) are evidenced along the g_z direction in **4** (A_{Br} = 151.5 G), and along the g_x (A_{Br} = 27.6 G) and g_y (A_{Br} = 60.1 G) directions in **5** (Figure 4.4, *bottom*). On the basis of the best fit between experimental and simulated spectra, we propose that the two stereoisomers **4** and **5** exist in an approximately 3:1 ratio, with the major isomer **4** corresponding to the structure determined by X-ray diffraction analysis (See Figure 2).

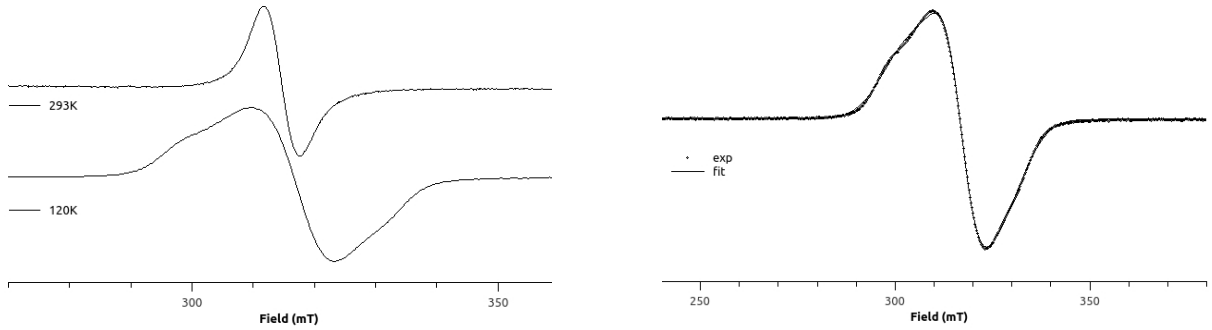

Figure 4.3. Experimental (MeCN, 293 and 120 K, *left*), and simulated (120 K, *right*) X-band EPR spectra of 3.

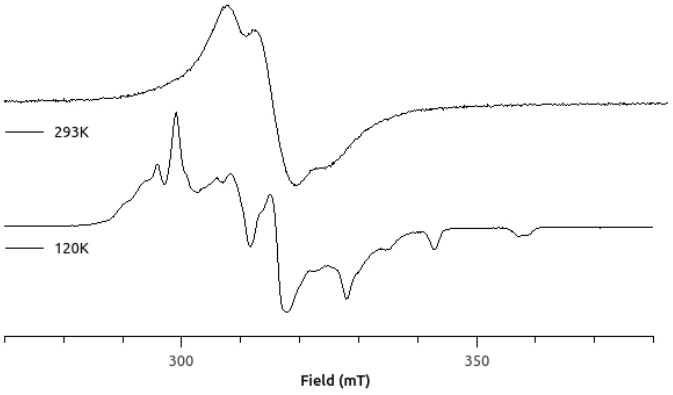

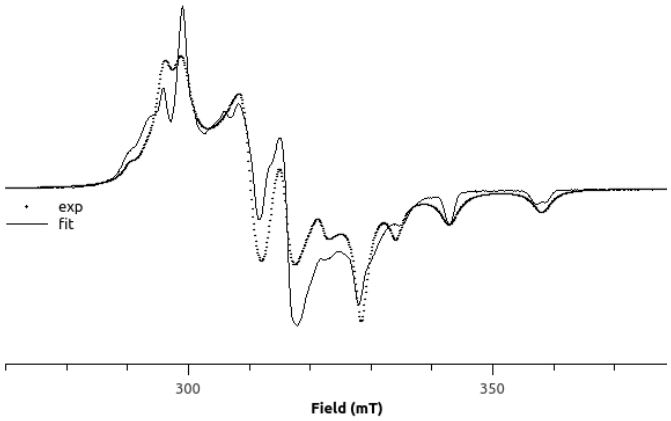

Figure 4.4. Experimental (MeCN/toluene, 293 K, and CH_2Cl_2/toluene, 120 K, *left*), and simulated (120 K, *right*) X-band EPR spectra of 4.

Table 4.1. Data for the experimental and simulated EPR spectra of 3 and 4.

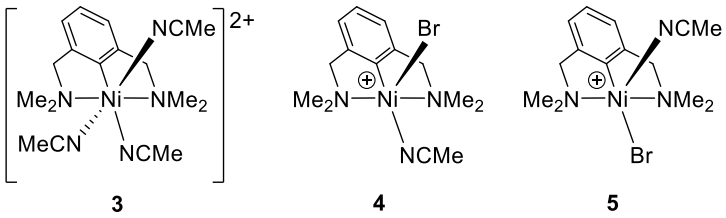

3 **4** **5**

Complex	g_x	g_y	g_z	A_x[a]	A_y[a]	A_z[a]
3	2.247	2.144	2.073			
4	2.269	2.145	2.027			151.5
5	2.307	2.090	2.077	27.6	60.1	

[a] In Gauss.

The EPR spectra of both **3** and **4** revealed *g* values that are higher than the free electron *g* value 2.0023; this indicates the absence of significant ^{14}N coupling, thus supporting the localization of the unpaired spin density in an orbital bearing substantial metal character. This assessment was supported by Density-functional theory (DFT) calculations (using UM06L/6-31G**[Def2-TZVP]), showing Mulliken spin density build-up on the nickel center with a value of 0.97 e/Å^3 for **3** (Figure 4.5). In the case of

complex **4**, the Mulliken spin density values were 0.85 e/Å^3 on Ni and 0.20 e/Å^3 on Br. For complex **4**, the isomer shown in Figure 5, is only ~4 kcal/mol lower in free energy than the alternative isomer **5** with acetonitrile and bromide positions switched; this finding is consistent with the presence of two species identified in the EPR spectrum.

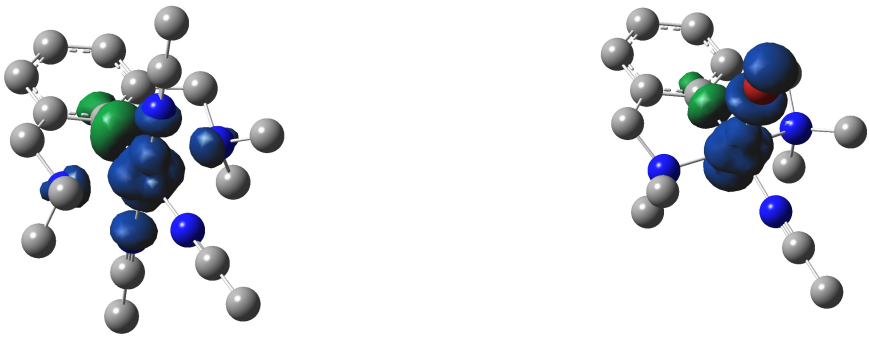

Figure 4.5. Alpha spin density plots for complexes **3** (*left*) and **4** (*right*). Plots generated with an isovalue of 0.004 e/Å^3**.**

Reactivity of the cationic trivalent species 3 and 4. As shown in Scheme 4.5, complexes **3** and **4** reacted readily (r.t.) with methanol and methyl amine to give C-O and C-N aryl-functionalization products. It is worth recalling here that the analogous functionalization of the divalent complex **1** requires aerobic conditions, whereas functionalization of the trivalent complexes **3** and **4** proceeds under a nitrogen atmosphere. The reactions with CD_3OD were monitored by ^{1}H NMR spectroscopy to establish functionalization rates relative to those observed with the cationic divalent species **1**. Given the NMR-silent nature of **3** and **4**, the reaction progress was based on monitoring the aromatic signals of the emerging functionalized product, *i.e.*, the triplet at ~7.3 ppm for *p*-H and/or the doublet at ~7.5 ppm for *m*-H. While the products of the C-NH(CH_3) coupling reactions could be isolated directly, isolation of the C-OCH_3 coupling products required extraction of the final reaction mixture with aqueous base to neutralize the in-situ generated ammonium moiety. The results are discussed below.

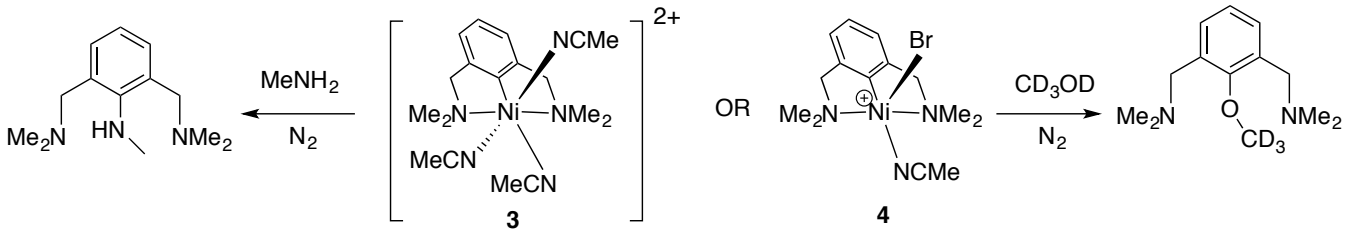

Scheme 4.5. Reactions of **3** and **4** in neat CD_3OD or CH_3NH_2 (33% solution in EtOH).

The C-OCD_3 functionalization of **3** and **4** gave different yields as a function of time and the presence of oxygen. For instance, under anaerobic conditions, we obtained 47% (**3**) and 7% (**4**) functionalization after 10 min; extending the reaction time to 2 h increased the yield for the reaction with **4** (42%), but the yield remained unchanged for the reaction with **3**. Conducting these C-O functionalization reactions under aerobic conditions gave very similar initial yields, 48% with **3** and 42% with **4** over 2 h. Interestingly, however, the yields of these reactions increased significantly with extended reaction times, going from 42% to 67% over 24 h with **4**, and from 48% to 73% over 96 h with **3**. The significance of obtaining higher than 50% yields for these aerobic reactions is discussed below.

An essential observation was made for the reaction of CD_3OD with both mono- and dicationic complexes: in addition to the functionalized product $NC(OCD_3)N$, we detected the formation of the monocationic divalent species $[(NCN)Ni^{II}(NCMe)]^+$, **1**; moreover, these two products formed in a 1:1 ratio. As shown in Scheme 4, we propose that this 1:1 ratio results from a comproportionation reaction between **3** or **4** and a Ni^I species that must be generated in-situ as a side-product of the reductive elimination step that furnishes the C-O coupling product.

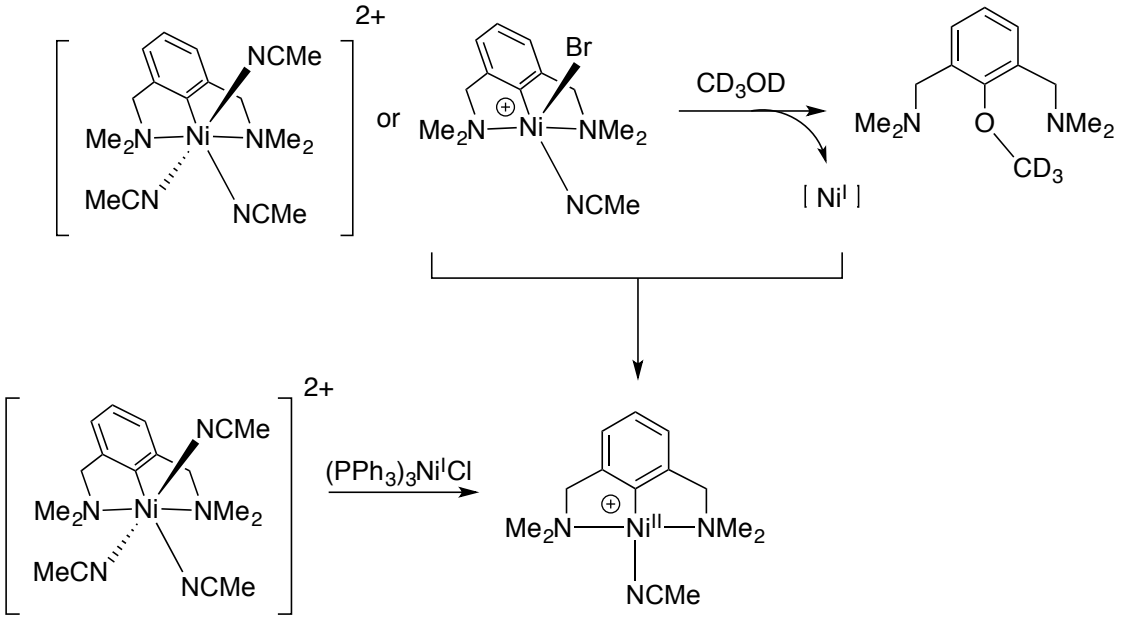

Scheme 4.6. Reactivities of **3** and **4** in support of proposed functionalization mechanism.

To test the above hypothesis involving a comproportionation reaction, we prepared the known monovalent complex $(PPh_3)_3Ni^ICl$[13] and allowed it to react with one equivalent of **3** in CD_3CN; as expected, this reaction generated the divalent cation **1** after 1 h. The signals for the latter were broad at

first but became progressively well-defined after 15 h. (See Figure S25 in SI.) This finding, combined with the observation of a 1:1 ratio for the functionalized product NC(OCD_3)N and **1**, supports the postulated comproportionation reaction between the Ni^{III} precursor and the in-situ generated Ni^{I}. Moreover, we can conclude that this redox process is faster than the functionalization reaction itself, because a rate limiting comproportionation would increase the yield of the functionalization product NC(OMe)N, which turns out not to be the case. Another observation consistent with the proposed comproportionation side reaction is the increase in yield observed with the extended reaction time under air: we believe that the in-situ generated divalent cationic Ni **1** is responsible for giving higher yields of the C-O coupling product.

The kinetics of the functionalization reactions with methanol were measured by ^{1}H NMR (see SI) and UV-visible spectroscopy (Figure 4.6), both approaches revealing a first-order reaction with respect to Ni. Comparison of the rates for reactions conducted under otherwise identical conditions with CH_3OH or CD_3OD allowed us to measure the overall kinetic isotope effect of the C-O coupling reaction. Treating the trivalent monocationic species **4** with neat CH_3OH or CD_3OD and monitoring the decay of complex **4** by UV-vis spectroscopy gave a pseudo-first order time profile with an overall k_H/k_D value of 0.62. This inverse kinetic isotope effect (KIE) is similar to the k_H/k_D value of 0.47 we measured for the reaction of complex **2** with CH_3OH/CD_3OD.[6]

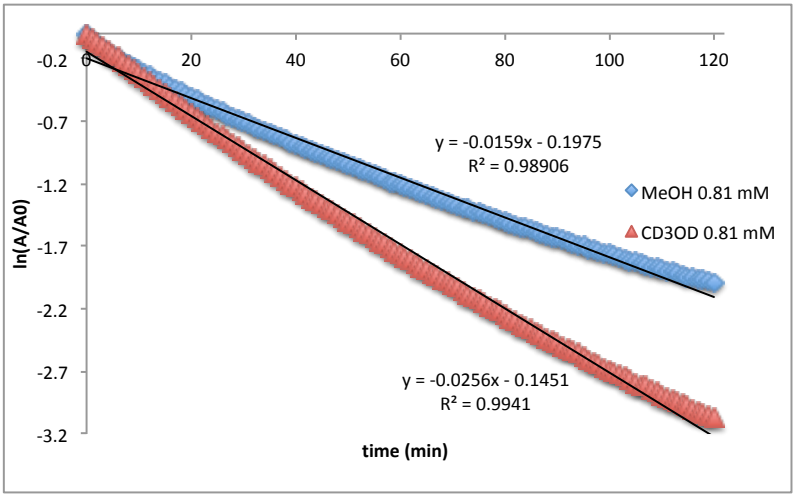

Figure 4.6. UV-visible spectroscopy time course profile for the reaction of a 0.81 mM solution of 4 with CH_3OH/CD_3OD.

The above results allow us to conclude that the C-O coupling is fastest with the dicationic, trivalent complex **3** (47% yield in 10 min), followed by its monocationic analogue **4** (42% yield in 2 h), and finally by the divalent monocation **1** (11% yield over 24 h), which suggests a strong correlation between the electrophilicity of the Ni center, on the one hand, and substrate uptake and reductive elimination rates on the other. Similarly, reactions of **3** and **4** with CH_3NH_2 (used as 33% solution in EtOH at r.t. and under N_2) led to rapid C-N bond formation (over 5 min) with yields of 15% with **3** and 21% with **4**. Running these reactions under aerobic conditions over 2 h gave the same yield for the C-NH(CH_3) coupling product with **3** (16%), but a slightly higher yield was obtained with **4** (29% vs. 21%). The following test confirmed that the poor yields observed in these C-N bond formation reactions are caused by rapid reduction of **3** and **4** by CH_3NH_2: indeed, reacting the dicationic complex **3** with the bulky amine *t*-$BuNH_2$ did not promote C-N functionalization, leading instead to the rapid formation of the divalent complex **1**.[14] It is noteworthy that no C-OEt coupling was observed for the reactions with CH_3NH_2 conducted in EtOH.

Density Functional Calculations: Ni^{III}/Ni^{IV} oxidation potential and Ni^{III} orbital characterization. The above-presented functionalizations of **3** and **4** with CH_3OH and CH_3NH_2 indicate that, contrary to what was observed with C-heteroatom functionalization promoted in air by the divalent precursors **1**, external oxidants are *not* essential for the C-O and C-N functionalization of these cationic Ni^{III} complexes. We have undertaken DFT calculations to improve our understanding of the mechanism of Ni-aryl bond functionalization in trivalent Ni complexes. Before analyzing the reactivities of **3** and **4** with CH_3OH and CH_3NH_2, we sought to verify that our computational approach would accurately model the Ni^{III} and higher oxidation states. For all calculations in Gaussian 09, geometries were optimized with UM06L/6-31G**[Def2-TZVP] with the continuum MeCN SMD solvent model. Final electronic energies, with solvation, were evaluated using the Def2-TZVP basis set. For complex **3**, the M06L calculated Ni^{III}/Ni^{IV} oxidation potential is 1.21 V (calculated at 298 K relative to ferrocene), which is very close to the experimentally measured value of 1.18 V. Other functionals such as M06, B3LYP, and ωB97X-D gave values >0.5 V too large (see SI). For complex **4**, the calculated Ni^{III}/Ni^{IV} oxidation potential is 0.91, which is 0.15 V larger than the experimental value of 0.74 V. Again, other functionals showed significantly larger errors for estimating this oxidation potential.

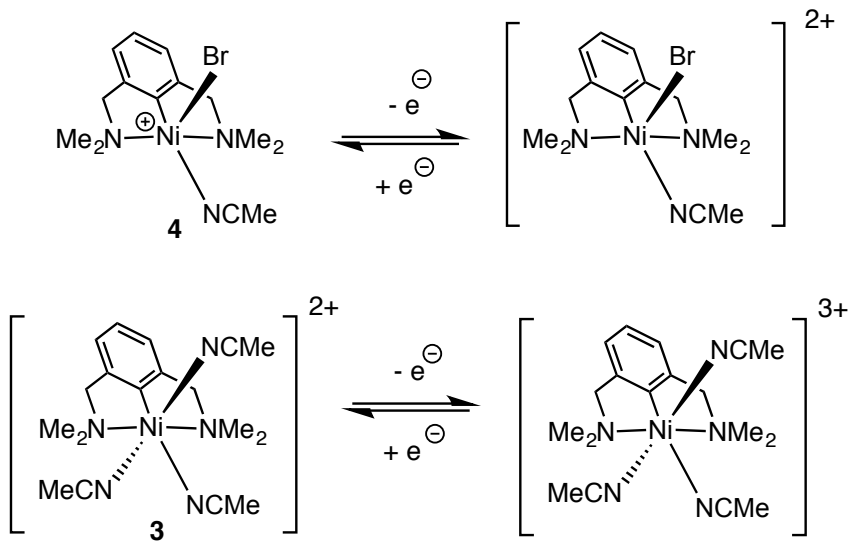

Scheme 4.7. Ni^{III}/Ni^{IV} redox reactions at 298 K.

Figure 4.7 displays the α-spin and β-spin molecular orbitals of the formally 17 electron monocationic complex **4**. Analysis of the α-spin HOMO orbital shows that it is an antibonding combination of the Ni d_z^2 and bromide p_z. This orbital description is consistent with the spin density plot in Figure 5. About 0.4 eV lower in energy than the α-spin HOMO, there are two degenerate α-spin HOMO-1 orbitals with d_{xz} and d_{yz} character and antibonding interactions with bromide p_x and p_y orbitals. The degenerate HOMO-2 orbital set is mainly ligand centered, whereas the degenerate HOMO-3 set is Ni d-orbital based. Although the α-spin orbitals 95 α, 94 α, 93 α, and 91 α are significantly delocalized on the Br atom, they nevertheless provide 4 electrons to the Ni metal center. Similarly, there are three β-spin electrons with Ni d-character, two degenerate β-spin HOMOs and HOMO-3. Similarly to the α-spin manifold, the pair of β-spin HOMOs is delocalized onto the Br atom.

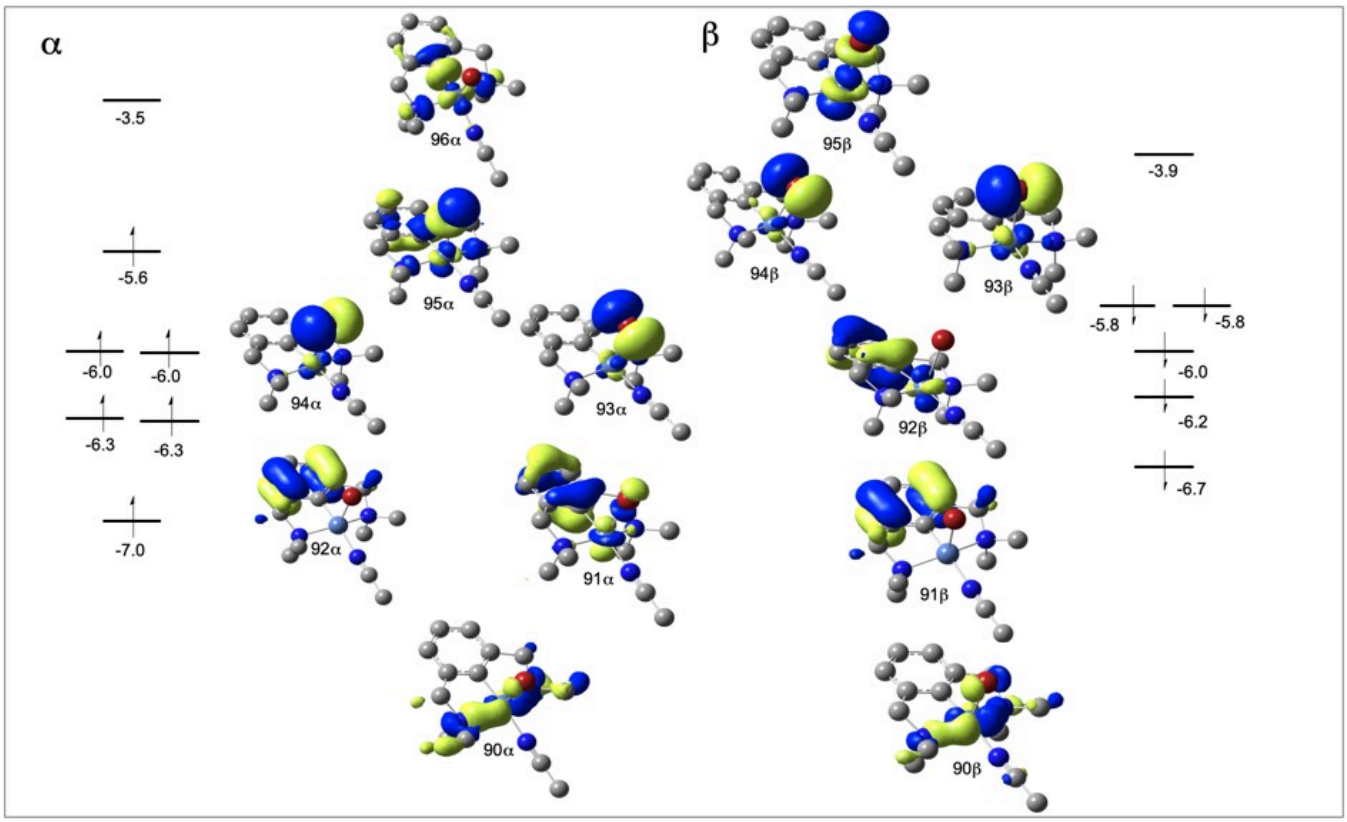

Figure 4.7. UM06L α-spin and β-spin molecular orbitals for monocationic complex 4. Orbital energies reported in eV.

Examining the formally 19-electron dicationic complex **3** in a similar manner yields the MO assignments shown in Figure 4.8. The α-LUMO is composed of the d_{z^2} orbital and is σ antibonding with the phenyl ring. The α-spin HOMO consists of the $d_{x^2-y^2}$ orbital and interacts in an anti-bonding fashion with the p_x orbitals of the nitrogen atoms, as well as with the p_y orbital from the axial acetonitrile's lone pair. The α-HOMO-2 is a mixture between the d_{xz} and the amine lone pairs of the pincer ligand. The two last α-spin metal-based orbitals, located at ~2.0 eV from the α-HOMO, are the d_{yz} and the d_{xy}, both of which are involved in an antibonding interaction with the 3 acetonitrile ligands. The β-spin manifold contains 3 orbitals of metal character (96, 95 and 93) for a total of 7 d electrons.

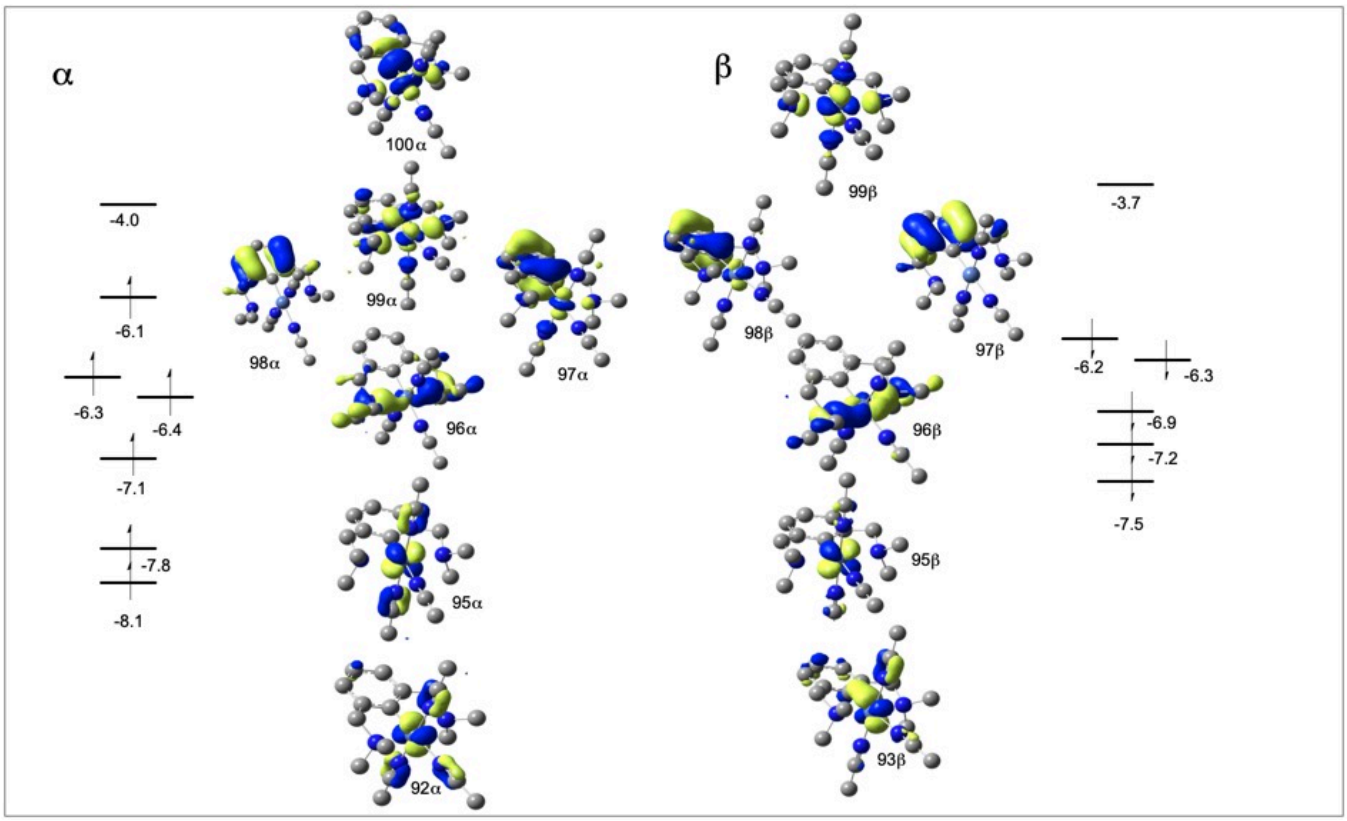

Figure 4.8. UM06L α-spin and β-spin molecular orbitals for dicationic complex 3. Orbital energies reported in eV.

DFT analysis of the mechanism for reactions of 3 and 4 with CH_3OH. Scheme 4.8 shows a simplified mechanistic proposal for Ni-aryl C-O functionalization of **4** involving the following elementary steps: (i) CH_3OH coordination, (ii) proton transfer to the NMe_2 side arm of the pincer ligand, and (iii) formation of C-O bond through reductive elimination.

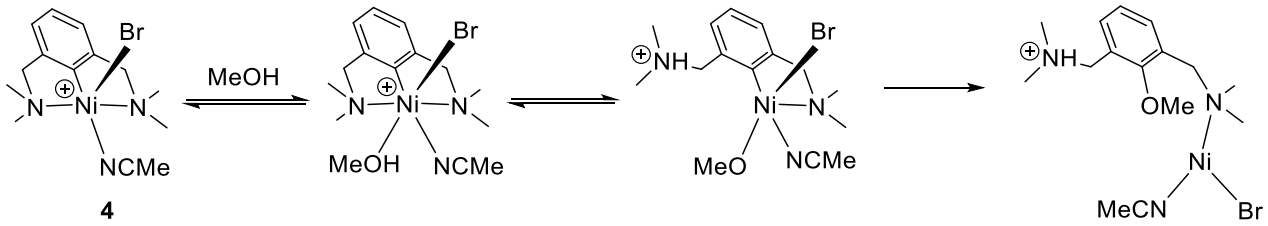

Scheme 4.8. Simplified mechanistic proposal for C-O coupling for reaction between 4 and CH_3OH.

We began by calculating the relative free energies and enthalpies for possible CH_3OH coordination complexes and ligand substitution. As expected, there are a large variety of low-energy complexes. The

hexa-coordinate complex **6** shows that CH_3OH coordination is unfavorable: it is indeed endothermic and endergonic by 1.3 and 7.4 kcal/mol, respectively. The unfavorable coordination of methanol is likely the result of the α-spin HOMO occupation shown in Figure 8; since this MO is antibonding in character, the dative Ni-O coordination interaction is destabilizing. This is confirmed by a relatively long Ni-O(CH_3)H distance of 2.17 Å in **6**. Next, the positional isomer represented by structure **8** (wherein Br and CH_3CN have switched positions) appears slightly more stable than **6**, but the **4→8** conversion is still uphill in free energy. Overall, these calculated structures confirm that acetonitrile is easily replaced by CH_3OH. For example, structure **9** is only 1.3 kcal/mol endergonic relative to **4**.

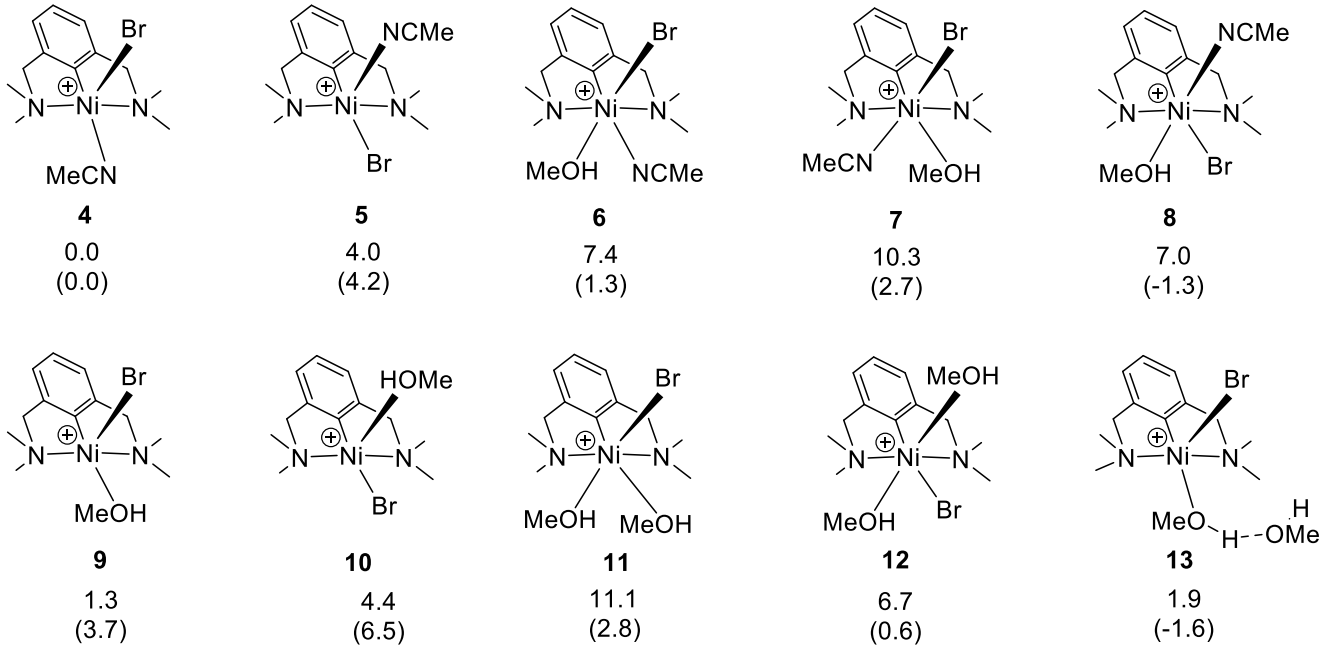

Scheme 4.9. Gibbs free energy (and enthalpy) for CH_3OH coordination and substitution with complex 4. (kcal/mol)

We then performed a comprehensive search for the CH_3OH-to-$NMe_{2(ligand)}$ proton transfer from all of the identified ground states. The lowest energy pathway identified involves starting from ground-state **6** and proceeds through transition-state structure **TS6** (Scheme 4.10). The energy surface of this proton transfer is extremely flat and endothermic/endergonic, and while the resulting intermediate **14** is a potential surface minimum, it is only slightly higher in free energy compared to **TS6**. The 3D structure of **TS6** shows that the Ni-NMe_2 coordination is completely severed prior to proton transfer (Fig. 4.9). Direct deprotonation from adducts **7** and **8** showed transition states located ca. 22-26 kcal/mol higher than the

starting complex **4.** This last observation indicates that deprotonation is less favorable when CH_3OH is *trans* to the phenyl ring or to the MeCN ligand.

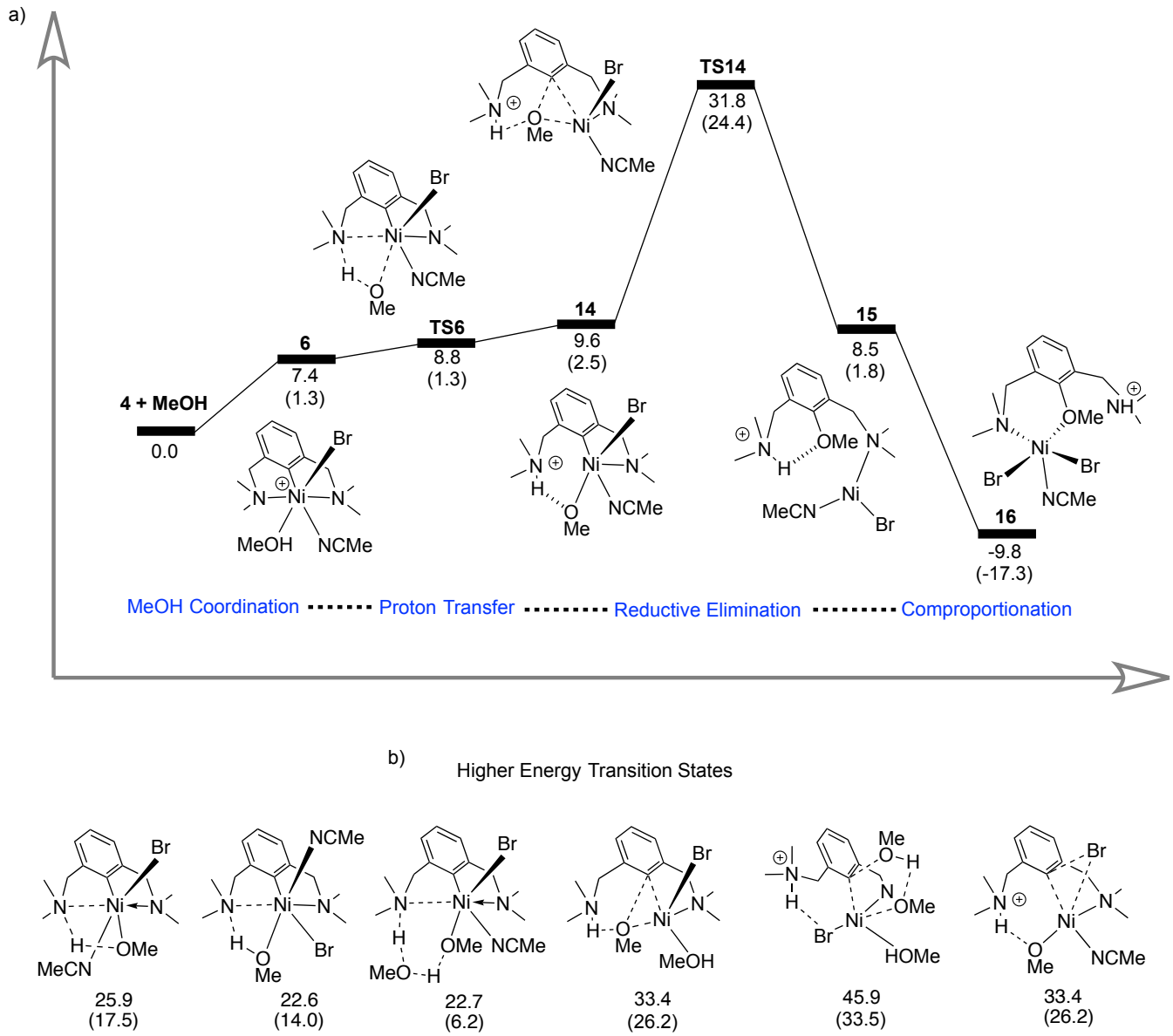

Scheme 4.10. a) Lowest free energy landscape for (and enthalpies) for reaction of 4 with CH_3OH. (b) Representative example of higher energy transitions states examined (kcal/mol).

We also examined the possibility that another CH_3OH might serve as a shuttle for the CH_3OH -to-$NMe_{2(ligand)}$ proton transfer (Scheme 8b, third species from the *left*). This transition state is ~5 kcal/mol) higher in enthalpy than **TS6**; in addition, such CH_3OH proton shuttling is likely also disfavored by the entropy penalty.[15] Interestingly, protonation of the aryl moiety by CH_3OH to generate a de-metalated Ni^{III}

alkoxy complex was found to be thermodynamically unfavourable by 29 kcal/mol (Scheme 4.11). This suggests that the reverse C-H activation should be thermodynamically feasible. Indeed, examples of high-valent nickel promoted C-H activation have been observed by Mirica and Sanford.[16]

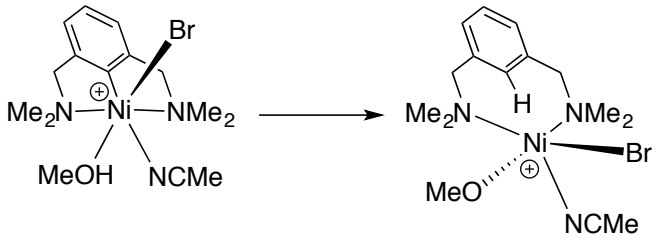

Scheme 4.11. Possible protonation of the aryl moiety by CH_3OH

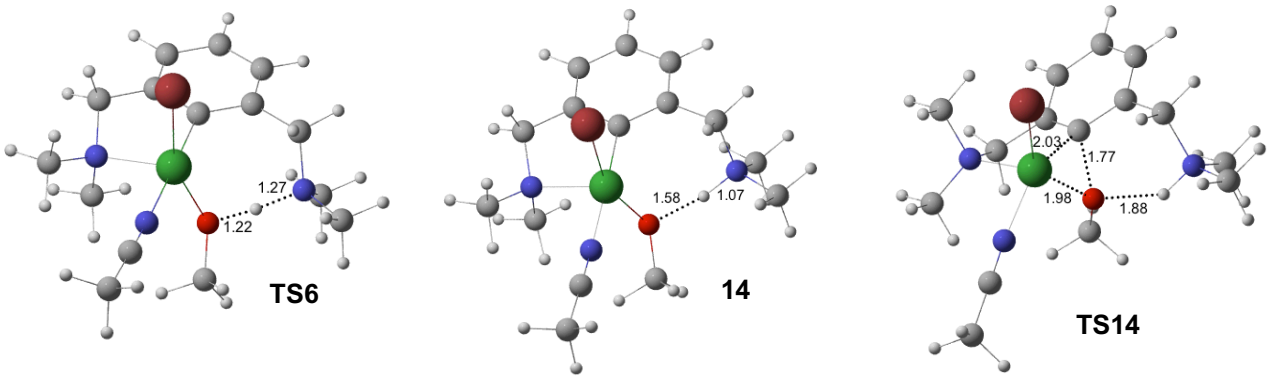

Figure 4.9. 3D representations of proton transfer and reductive elimination transitions states for the reaction of 4 with CH_3OH. Bond and partial bond lengths reported in Å.

Subsequent to the proton transfer, the aryl moiety of the pincer ligand and the methoxide group are *cis* to each other and thus primed for C-O bond forming reductive elimination. Examination of reductive elimination from a variety of ground states allowed us to identify **TS14** as lowest in energy (see SI for alternative transition states). Consistent with a relatively slow reaction, the barrier from **14** to **TS14** is 22.2 kcal/mol, and overall 31.8 kcal/mol relative to **4** and CH_3OH. This large free energy value is most likely due to entropy overestimation, the enthalpy of activation is 24.4 kcal/mol which is more reasonable for a room temperature reaction. The reductive elimination transition states leading to C-Br bond formation were also located, but the barriers for these are 2-5 kcal/mol higher in energy relative to **TS14**, which is just enough to disfavor formation of the C-Br coupling product NC(Br)N.

As an alternative to the proposed inner-sphere, cis-reductive elimination, we also investigated the possibility of direct nucleophilic attack by CH_3OH on the *ipso*-C *atom* (transition states shown in Scheme

8b). This transition state turned out to have a barrier of over 45 kcal/, indicating that it is not competitive with intramolecular reductive elimination. Somewhat unexpectedly, the C-O coupling that generates the Ni^{I} species **15** via **TS14** is endergonic by 8.5 kcal/mol. This finding prompted us to examine the possibility that this species reacts with **4** to generate **16** and **1**. Indeed, this reaction provides an overall exergonic reaction by ~10 kcal/mol. An analogous reaction between the NC(Br)N product of the bromide reductive elimination and **4** does not serve to make the process exergonic.

Given the experimentally measured Ni^{III}/Ni^{IV} oxidation potential of **4** (0.74 V), it seems rather unlikely that Ni^{IV} species might form during the functionalization reactions of this complex in the absence of external oxidants. Nonetheless, it is possible to envisage that some of the more electron-rich intermediates of the reaction (e.g., the Ni^{III}-OCH_3 generated by the deprotonation of the CH_3OH adduct) might be oxidized to a Ni^{IV} species in a disproportionation reaction, as outlined in scheme 4.12. Our calculations showed, however, that the free energy of this reaction is 34.2 kcal/mol with respect to **4** + CH_3OH, which suggests a mechanism far too high in energy to be viable.

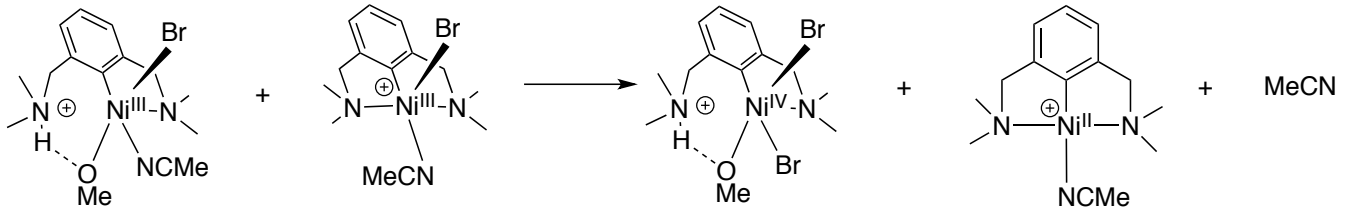

Scheme 4.12. Possible disproportionation reaction between two Ni^{III} complexes

In the case of the coordinatively saturated, 19-electron dicationic species **3**, the reaction needs to go through MeCN dissociation first before CH_3OH can bind to the metal center. Interestingly, dissociation of MeCN is exergonic by ca. 7 kcal/mol, while CH_3OH binding is slightly uphill; overall, the new adduct **18** thus generated is more stable than the starting material **3**. The deprotonation of coordinated CH_3OH appears to be endergonic but all attempts failed to locate a transition state for the direct deprotonation by the NMe_2 moiety. On the other hand, our calculations revealed that reductive elimination from the putative Ni-OCH_3 intermediate (species **19**) is relatively facile with an activation barrier of 17.0 kcal/mol, which is much lower than the corresponding step in the reaction of CH_3OH with the monocationic complex **4** (ca. 31.8 kcal/mol). Moreover, **TS19** connects to product **20** located 5.1 kcal/mol lower than the starting material. The comproportionation reaction with **3** brings the Gibbs energy of the whole process to -27.7 kcal/mol.

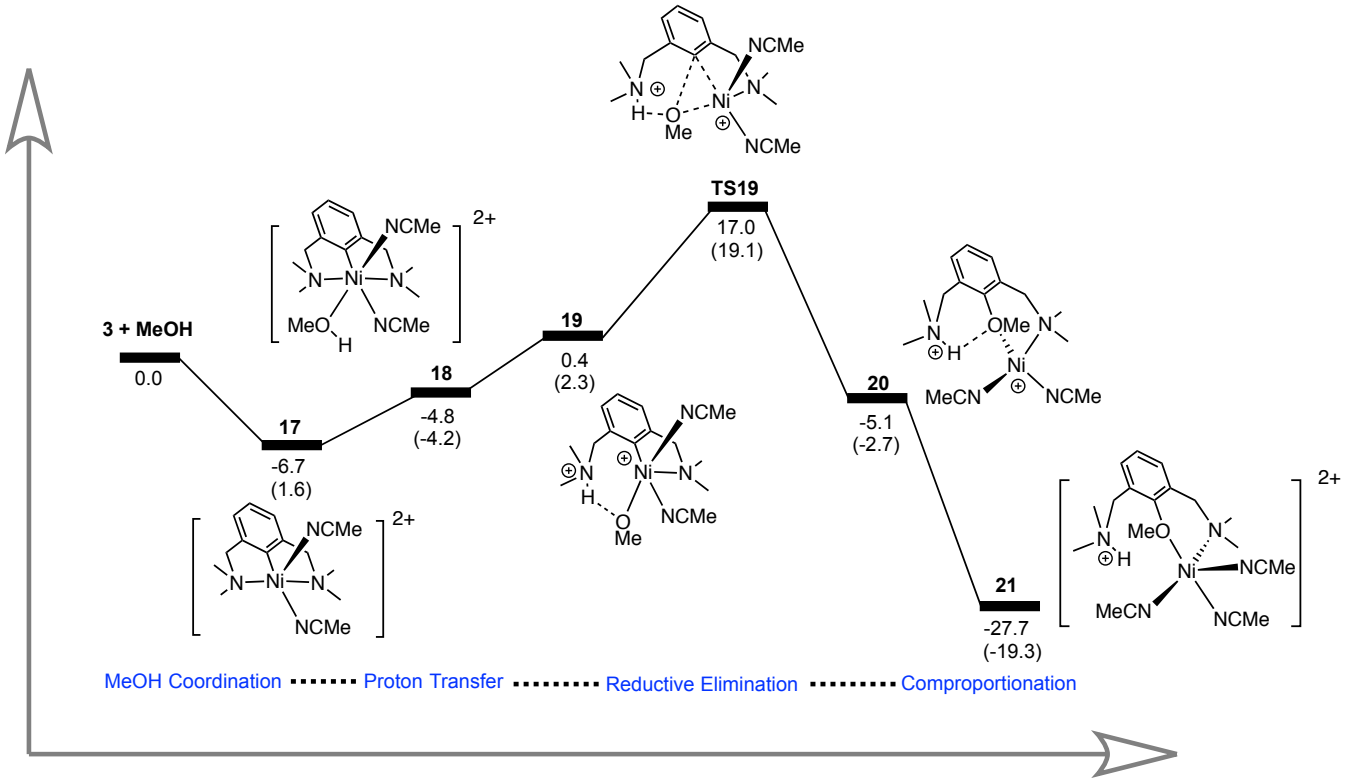

Scheme 4.13. Lowest free energy landscape for (and enthalpies) for reaction of 3 with CH_3OH.

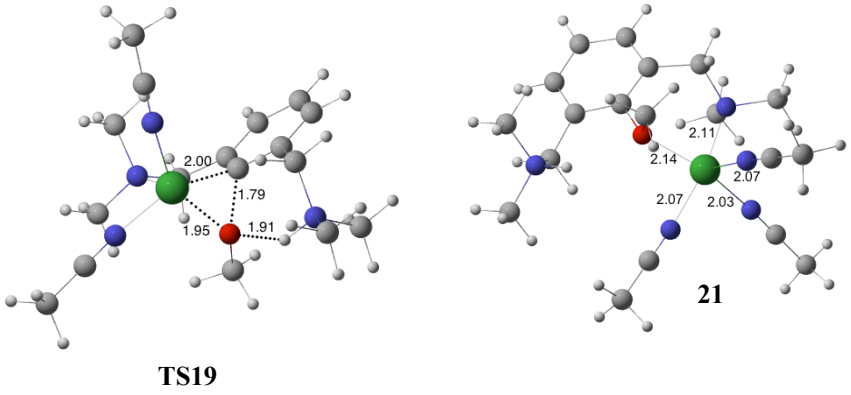

Figure 4.10. 3D representations of reductive elimination transition state and final product for the reaction of 3 with CH_3OH. Bond and partial bond lengths reported in Å.

Kinetic isotope effect calculation. The energy landscape shown in Scheme 4.10 provides an understanding of the observed inverse kinetic isotope value of 0.62 obtained experimentally for the functionalization of **4** with CH_3OH/CD_3OD. The key feature of the energy surface is that the proton

transfer is an endothermic step prior to the rate limiting reductive elimination transition state. This suggested to us that the inverse KIE based on k_{obs} results from an inverse equilibrium isotope effect (EIE). While there are several contributing components to a KIE/EIE, including symmetry factor, mass moment of inertia factor, vibrational excitation, and zero-point energy (ZPE), we have only modeled the ZPE component.

As expected, the proton transfer step (**TS6**) shows normal KIE of about 3.4 (with respect to **6)**, because the O-H bond is breaking. However, since this transition state is prior to the rate-limiting transition state and the intermediate resulting from this transition state is endothermic, the KIE/EIE values of this step does not impact the overall observed KIE value. The steps that will impact the observed KIE are the CH_3OH coordination equilibrium and the rate limiting reductive elimination. Thus, the overall inverse KIE value results from an inverse KIE value for the step **4** → **TS14** and an inverse EIE value for **4** → **6**, since species **4** is the resting state. The predicted KIE value for **4** → **TS14** is 0.57, whereas that the predicted EIE for **4** → **6** is 0.76. This inverse EIE is likely the result of additional vibrational modes formed when CH_3OH coordinates to the Ni metal center. In accordance with this notion, inspection of the stretching vibrational modes for free CH_3OH /CD_3OD shows a difference of ~3500 cm^{-1} which is very similar to the difference in stretching modes for **6** and its isotopologue. However, consideration of lower frequency modes such as bending, wagging, and rocking, as well as new isotope-sensitive modes due to substrate coordination, leads to a preference for the coordination of CD_3OD over CH_3OH, thus leading to an inverse EIE. Parkin, Bender and Goldman made similar arguments in rationalizing the observed inverse EIE's for the coordination and oxidative addition of H_2/D_2 to iridium and tungsten metal centers.[17]

C-N functionalization of the monocationic and dicationic species 4 and 3 with CH_3NH_2. The energy landscape for the reaction of **4** with CH_3NH_2 is shown in Scheme 4.14a. Coordination of CH_3NH_2 to the Ni(III) center in **4** was found to be exothermic by 4.7 kcal/mol and endergonic by 2.8 kcal/mol. Unlike in the case of the CH_3OH reactions discussed above, we did not succeed in locating a transition state for the direct deprotonation of coordinated CH_3NH_2 by the NMe_2 arm of the pincer ligand. Therefore, we elected to consider the alternative scenario of an outer-sphere deprotonation mechanism wherein a second molecule of CH_3NH_2 would act as a deprotonating agent. The transition state for this type of deprotonation was located at 19.5 kcal/mol (**TS22**), and the deprotonated species **23** is 20.2 kcal/mol above **4**. Release of $CH_3NH_3^+$ from **23** leads to the charge-neutral, 19-electron Ni(III) amide complex **24** from which C-N or C-Br bond formation can occur. As was the case in the CH_3OH reaction, our calculations showed that

C-Br reductive elimination is disfavored kinetically, whereas C-N bond formation is much more favorable kinetically (activation energy ~ 30 kcal/mol).

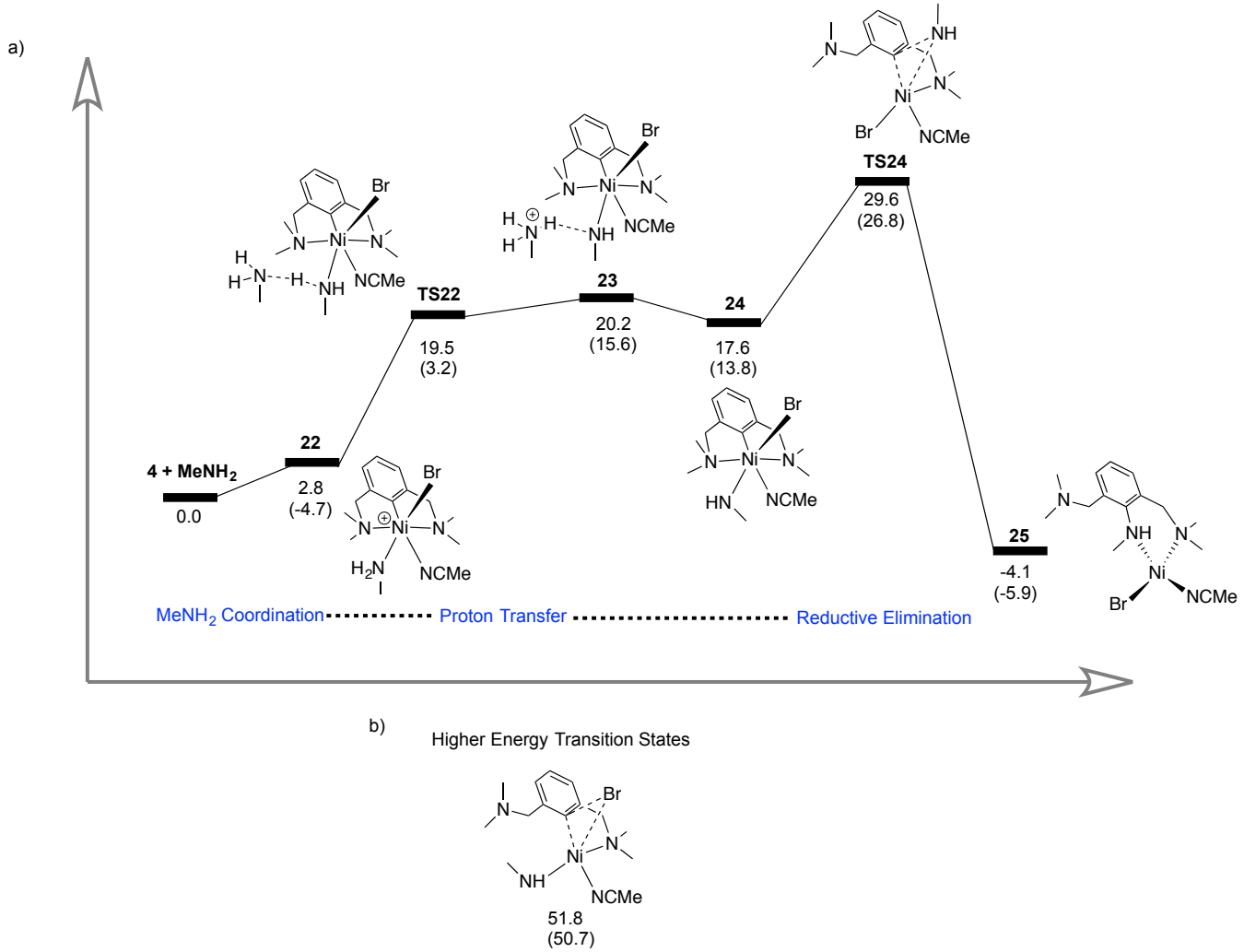

Scheme 4.14. Lowest free energy landscape for (and enthalpies) for reaction of 4 with CH_3NH_2. (b) Representative example of higher energy transitions states examined. (kcal/mol)

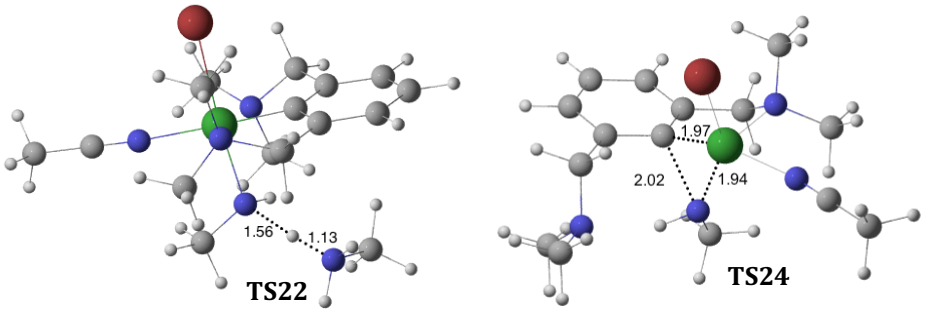

Figure 4.11. 3D representations of proton transfer and reductive elimination transition states for the reaction of 4 with CH_3NH_2. Bond and partial bond lengths reported in Å.

The analogous backbone functionalization starting from the dicationic complex **3** and CH_3NH_2 starts with MeCN dissociation to form the penta-coordinated species **17** (Scheme 4.15), followed by exothermic/exergonic substrate uptake to generate the CH_3NH_2 adduct **26**. It is significant that substitution of MeCN by the substrate is thermodynamically favored (by -10.4 kcal/mol), and that even the deprotonation of coordinated CH_3NH_2 proceeds rather easily via an outer sphere mechanism, *i.e.*, mediated by a second molecule of substrate (< 4 kcal/mol). Thus, C-N reductive elimination is rate determining with a relatively accessible transition state **TS28** at 9.6 kcal/mol. It is worth noting that a slightly greater activation energy (10.5 kcal/mol) was required for an alternative pathway involving the disruption of the chelating form of the pincer ligand. Much like CH_3NH_2 functionalization from **4**, this mechanism does not require comproportionation with starting material to be favourable thermodynamically.

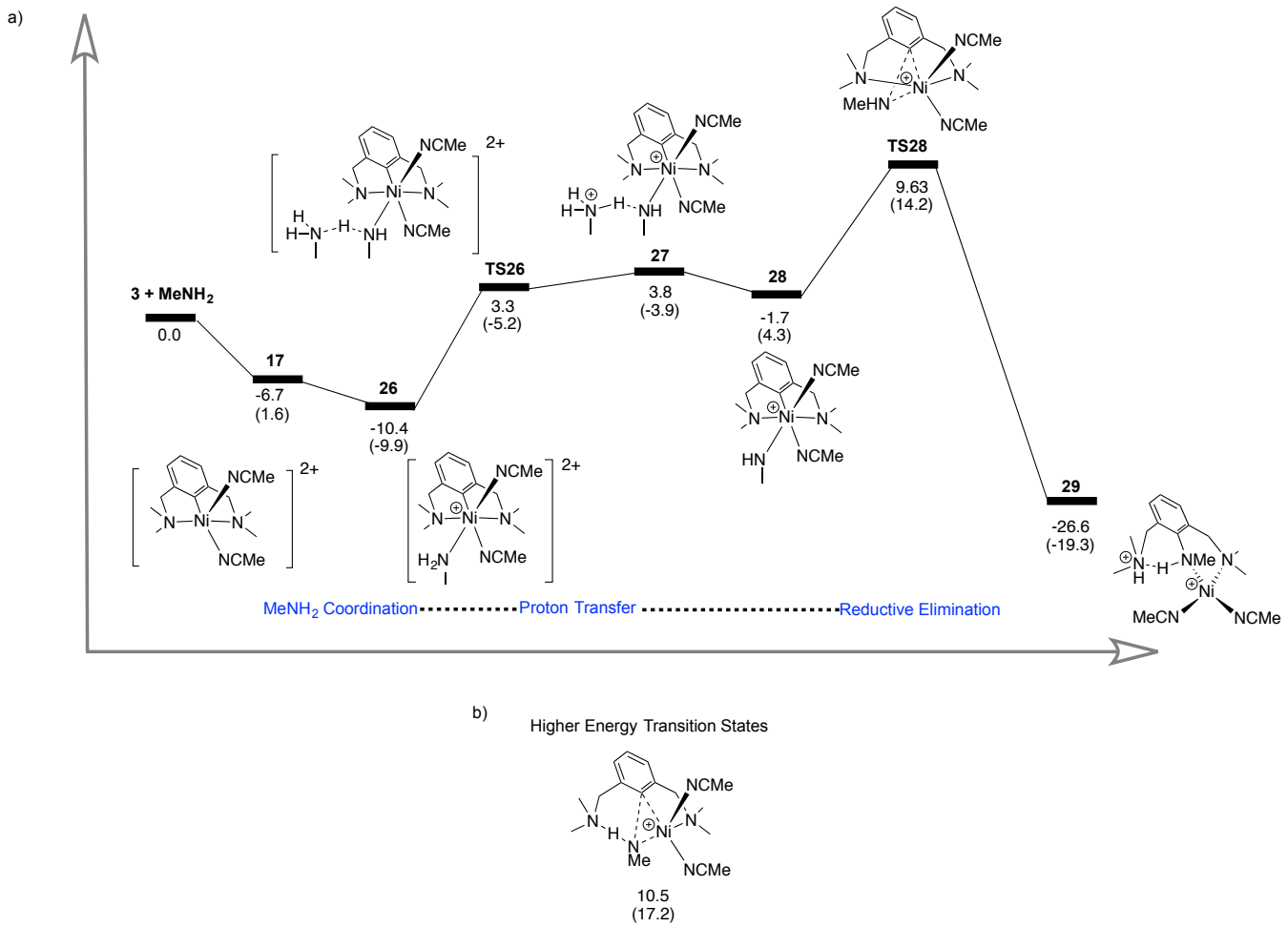

Scheme 4.15. Lowest free energy landscape for (and enthalpies) for reaction of 3 with CH_3NH_2.

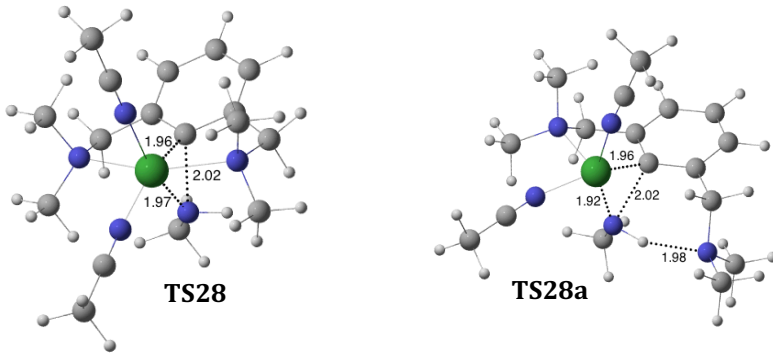

Figure 4.12. 3D representations of reductive elimination transition states for the reaction of 3 and CH_3NH_2. Bond and partial bond lengths reported in Å.

4.4 CONCLUSION

This work has resulted in the synthesis and characterization of the new divalent and trivalent cationic Ni complexes **1**, **3**, and **4**, as well as an examination of their reactivities towards protic substrates. The divalent complex **1** was found to undergo a sluggish functionalization of its Ni^{II}-Ar moiety with CH_3OH; this reactivity requires aerobic conditions, and in this sense is reminiscent of the previously reported C-O and C-N bond formation from pyrazole based NCN-type pincer complexes isolated in our group. These observations hint at the involvement of cationic Ni^{III} intermediates. The successful isolation and characterization of monocationic and dicationic Ni^{III} complexes discussed in this report allowed us to confirm the viability of this hypothesis. Furthermore, we have established that several side reactions diminish the yield of backbone functionalization. For instance, a comproportionation reaction between in-situ generated Ni^{I} species and the Ni^{III} precursors limits to 50% the conversion of the mono- and dicationic trivalent species **3** and **4** into the functionalization product $NC(OCH_3)N$. This undesirable side reaction can, however, be circumvented by performing the reaction under aerobic conditions, because the in-situ generated divalent complex **1** can, in turn, undergo C-O coupling thereby improving the overall coupling yield. It should be noted, however, that aerobic reaction conditions did not lead to substantial increases in C-N coupling yields. Finally, another side reaction is the rapid oxidation of amines by the cationic Ni^{III} complexes; this side reaction also forms the cationic Ni^{II} complex **1**.

DFT calculations revealed a number of valuable observations. Substrate uptake by the nickel center is surprisingly difficult, especially in the case of the monocationic complex **4**; however, once coordination takes place, the requisite deprotonation is fast. Reductive elimination of the methoxy and amide ligand is favoured compared to C-Br bond formation, both kinetically and thermodynamically. This suggests that the reverse reaction, oxidative addition, should be accessible from Ni^{I} and that one could devise a Ni^{I}/Ni^{III} catalytic cycle for the conversion of C-Br bonds into C-O bonds.[18] Moreover, the fact that protonation of the aryl moiety is thermodynamically disfavored suggests that electrophilic type C-H activation of a pincer ligand from a Ni^{III} complex should be possible. Future investigations will explore these two avenues.

4.5 EXPERIMENTAL SECTION

General Procedures. Unless otherwise indicated, all manipulations were carried out using standard Schlenk and glove box techniques under a dry nitrogen atmosphere and using solvents which were dried to water contents of less than 10 ppm by passing through activated aluminum oxide columns (MBraun SPS); moisture contents were determined using a Mettler-Toledo C20 coulometric Karl Fischer titrator. The starting materials were purchased from Aldrich ($AgSBF_6$; 3,5-dimethoxybromophenol; $CuBr_2$; CD_3OD) and used without further purification. Literature procedures were used to synthesize $NiBr_2(NCiPr)$,[19] NC(H)N, [20] and $(NCN)NiBr_2$.[7]

The NMR spectra were recorded on the following spectrometers: Bruker AV400rg (^1H at 400 MHz) and Bruker ARX400 (^1H at 400 MHz and $^{13}C\{^1H\}$ at 100.56 MHz). Chemical shift values are reported in ppm (δ) and referenced internally to the residual solvent signals (^1H and ^{13}C: 7.16 and 128.06 ppm for C_6D_6) or externally. Coupling constants are reported in Hz. The elemental analyses were performed by the Laboratoire d'Analyse Élémentaire, Département de chimie, Université de Montréal.

EPR. The EPR spectra were collected on a Bruker Elexys E500 X-band spectrometer. The samples were prepared by dissolving under an inert atmosphere, the Ni(III) complex **3** or **4** (0.1 mM) with a dry solvent (MeCN for **3**, and MeCN/toluene or CH_2Cl_2/toluene for **4**) in a 4 mm EPR tube. Measurements were then carried out either in a liquid (293 K) or in a frozen solution (120 K).

$[(NCN)Ni^{III}(MeCN)_3][SbF_6]_2$, 3. A dry Schlenk flask was charged with MeCN (15 mL), the charge-neutral dibromo precursor $(NCN)Ni^{III}Br_2$, **2** (0.400 g, 0.976 mmol), and $AgSbF_6$ (0.671 g, 1.95 mmol). The flask was wrapped in aluminium foil and the suspension was stirred for 30 min at r.t. The final reaction mixture was concentrated under vacuum to ~4 mL, followed by addition of Et_2O (15 mL) and filtration to isolate a red precipitate, which was then washed with 3 × 10 mL of Et_2O to give a red powder (0.684 g, 84% yield). Anal Calc for $C_{18}H_{28}F_{12}N_5NiSb_2$ (844.64): C, 25.60; N, 8.12; H, 3.34. Found: C, 25.10; N, 8.27; H, 3.38.

$[(NCN)Ni^{III}(Br)(MeCN)][SbF_6]$, 4. A dry Schlenk flask was charged with MeCN (5 mL), the dicationic complex **3** (0.150 g, 0,178 mmol), and the charge-neutral dibromo precursor $(NCN)Ni^{III}Br_2$, **2** (0.080 g, 0.196 mmol). The reaction mixture was stirred at r.t. for 20 min, followed by concentration of the resulting purple solution to ~1 mL. Addition of Et_2O (10 mL) and canula followed by filtration washing of the

residual solid with 5 × 10 mL of Et_2O gave a purple powder (0.170 g, 83% Yield). Anal Calc for $C_{14}H_{22}N_3F_6BrNiSb$ (606.96): C, 27.72; N, 6.93; H, 3.66. Found: C, 27.59; N, 6.92; H, 3.53.

4.6 SUPPORTING INFORMATION

[(NCN)Ni^{II}(MeCN)][OTf], 1. A dry Schlenk flask was charged with MeCN (10 mL), the charge-neutral bromo precursor (NCN)Ni^{II}Br (0.150 g, 0.455 mmol), and AgOTf (0.128 g, 0.500 mmol). The flask was wrapped in aluminium foil and the suspension was stirred for 10 min at r.t. The stirring was then stopped and the resulting white solid was left to settle for another 10 min before filtration and evaporation of the yellow filtrate under vacuum. Addition of CH_2Cl_2 (5 mL) and hexanes (20 mL) to the yellow residues led to precipitation of a yellow powder. Filtration and washing of the yellow powder with 5 × 8 mL of hexanes yielded a bright yellow powder (0.128 g, 64% yield). ^{1}H NMR C_6D_6, δ 6.89 (1H, t, J_{HH} = *7.5,* H_1), δ 6.29 (2H, d, J_{HH} = *7.5,* H_2), δ 2.76 (4H, s, H_3), δ 2.20 (12H, s, H_4), δ 0.620 (3H, s, H_5). ^{13}C NMR C_6D_6, δ 147.13 (1C, s, C_1), δ 125.72 (2C, s, C_2), δ 118.74 (2C, s C_3), δ 116.10 (1C, s, C_4), δ 71.97 (2C, s, C_5), δ 49.90 (4C, s, C_6), δ 0.16 (1C, s, C_8), C_7 absent. Anal Calc for $C_{15}H_{22}F_3N_3NiO_3S$ (440.11): C, 40.94; N, 9.55; H, 5.04; S, 7.28. Found: C, 40.55; N, 9.22; H, 5.01; S, 7.21.

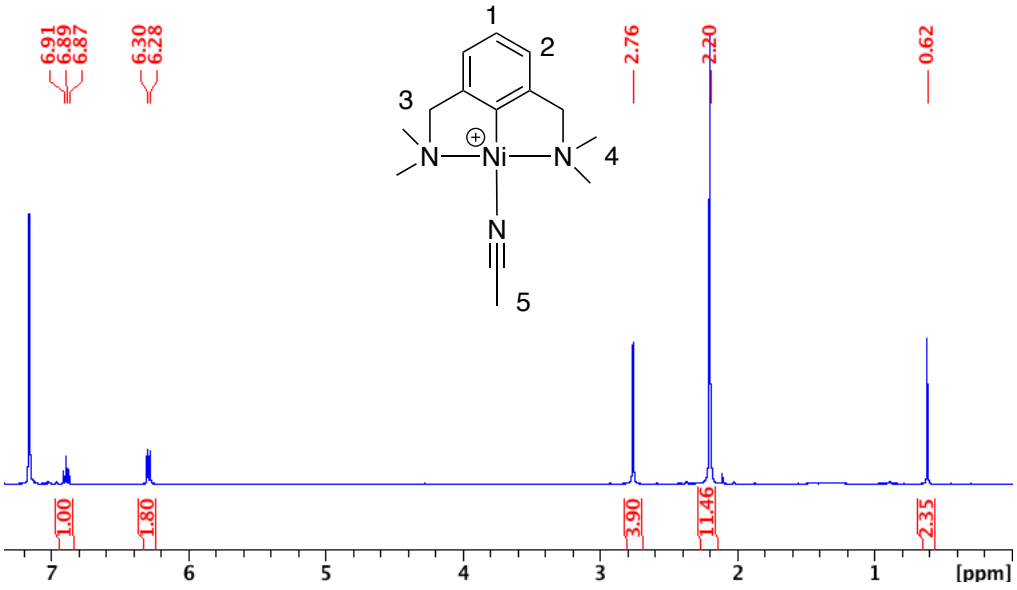

Figure 4.13. ^{1}H NMR spectrum for complex 1 in C_6D_6

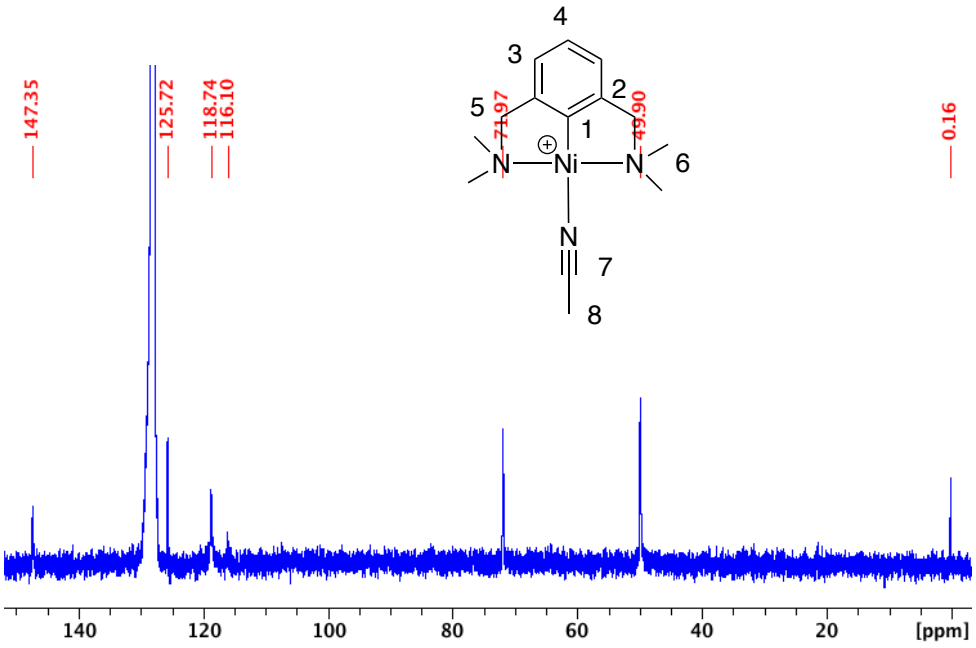

Figure 4.14. ^{13}C NMR spectrum for complex 1 in C_6D_6

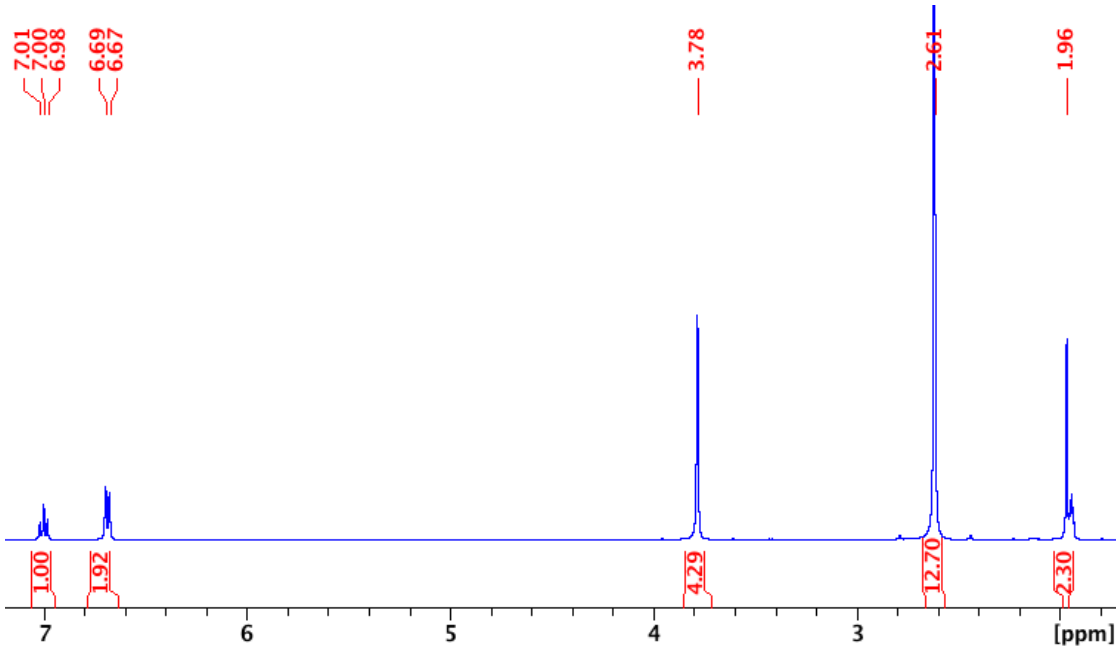

Figure 4.15. ^{1}H NMR spectrum for complex 1 in CD_3CN

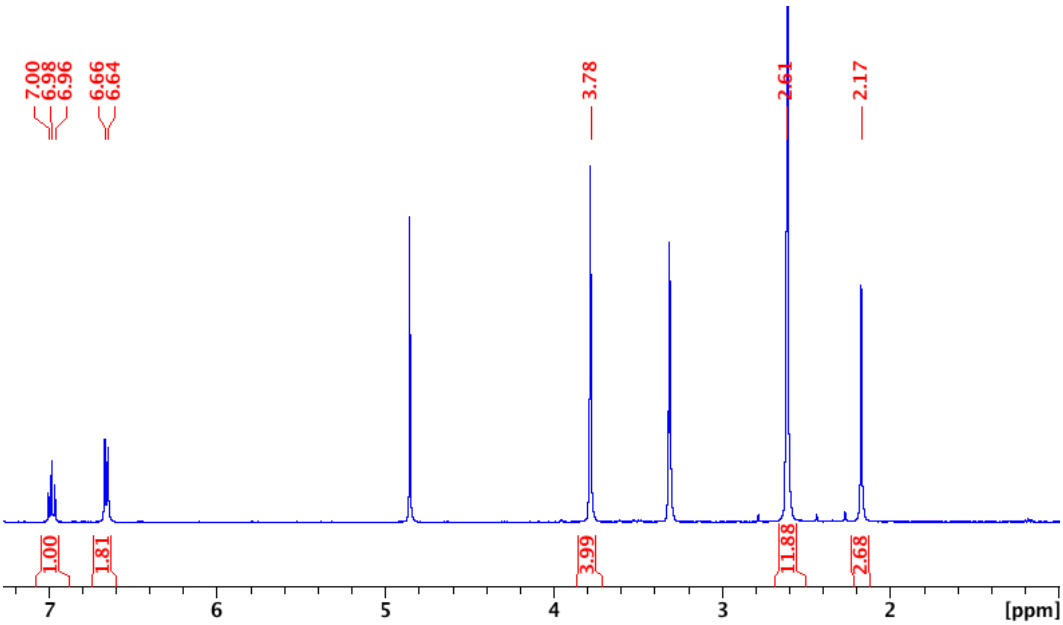

Figure 4.16. ^{1}H NMR spectrum for complex 1 in CD_3OD

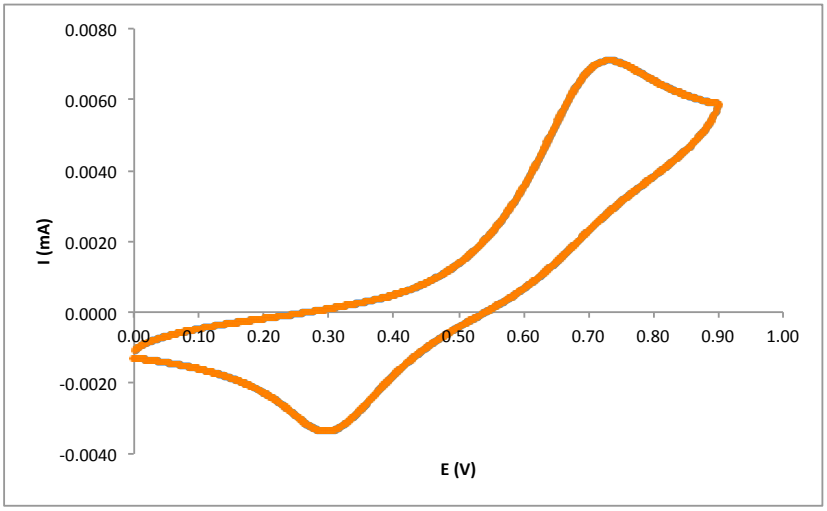

Figure 4.17. Cyclovoltammetry of a 0.1 mM MeCN solution of complex 1 and 100 mM $TBAPF_6$. Scan rate is 100 mv/s

Table 4.2. Crystal Data Collection and Refinement Parameters for Complex 1, 3 and 4

	1	**3**	**4**
chemical formula	$C_{14}H_{22}N_3Ni,CF_3O_3S$	$C_{18}H_{28}N_5Ni,2(F_6Sb)$	$F_6Sb,C_{14}H_{22}BrN_3Ni$
Fw	440.12	844.66	606.71
***T* (K)**	273(2)	105	296(2)
wavelength (Å)	1.34139	1.34139	1.54178
space group	P -1	P 1 2/c 1	Pbca
***a* (Å)**	8.7331(4)	17.8511(16)	17.6753(7)
***b* (Å)**	8.8394(4)	13.1607(12)	8.7815(4)
***c* (Å)**	13.0001(6)	23.922(2)	13.3218(6)
□□(deg)	87.077(2)	90	90
□ (deg)	73.0820(10)	90	90.647(2)
□ (deg)	83.4130(10)	90	90
Z	2	8	4
***V* (Å^3)**	953.61(8)	5620.1(9)	2067.62(16)
ρ_{calcd} (g cm^{-3})	1.533	1.997	1.949
μ (mm^{-1})	6.631	14.520	14.285
θ range (deg)	4.381 − 60.785	3.214 − 60.603	2.500 − 72.318
R1[a] [I > 2σ(I)]	0.0289	0.0625	0.0343
wR2[b] [I > 2σ(I)]	0.0795	0.1735	0.0907
R1 [all data]	0.0291	0.0645	0.0343
wR2 [all data]	0.0797	0.1756	0.0908
GOF	1.055	1.066	1.124

[a] $R_1=\Sigma(||F_o|-|F_c||)/\Sigma|F_o|$

[b] $wR_2=\{\Sigma[w(F_o^2-F_c^2)^2]/\Sigma[w(F_o^2)^2]\}^{½}$

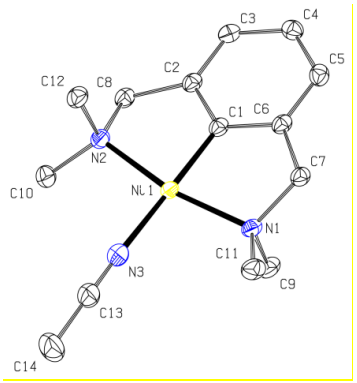

Figure 4.18. Molecular view of 1. Thermal ellipsoids are shown at the 50% level, and the OTf counter anion and all H atoms are omitted for clarity. Selected bond distances (Å) and angles (°): Ni1-N1= 1.9775(12); Ni1-N2= 1.9727(11); Ni1-C1= 1.8245(14); Ni1-N3= 1.9252(14); N1-Ni1-N2= 166.44(5); C1-Ni1-N3= 177.81(5); Ni1-N3-C13= 176.73(14).

NC(OMe)N. A dry Schlenk flask was charged with MeOH (10 mL) and the dicationic complex **3** (0.100 g, 0.118 mmol), and the mixture stirred at r.t. for 1 h. The red solution turned yellow and solvent is evaporated. Evaporation of the yellow mixture gave a yellow solid, which was treated with 10 mL of H_2O and 2 drops of NH_4OH (pH ~10) and extracted with 3 ×10 mL of Et_2O. Evaporation of the combined Et_2O layer gave a colorless oil (13 mg, 50%). ^{1}H NMR C_6D_6, δ 7.47 (2H, d, J_{HH} = *7.6,* H_2), δ 7.05 (1H, t, J_{HH} = *7.6,* H_1), δ 3.70 (3H, s, H_5), δ 3.49 (4H, s, H_3), δ 2.16 (12H, s, H_4).^{13}C NMR C_6D_6, δ 158.28 (1C, s, C_1), δ 132.93 (2C, s, C_3), δ 130.07 (2C, s C_2), δ 124.00 (1C, s, C_4), δ 61.89 (1C, s, C_7), δ 58.35 (2C, s, C_5), δ 45.58 (4C, s, C_6).

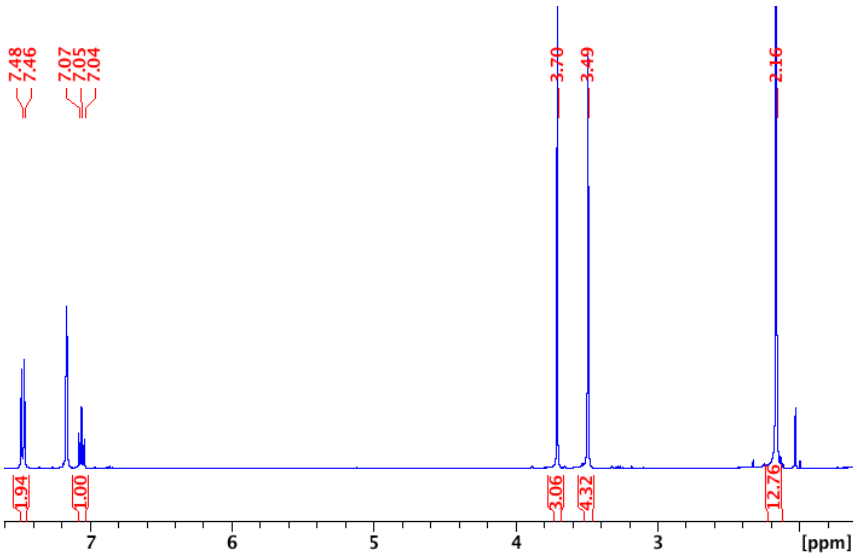

Figure 4.19. ^{1}H NMR spectrum for NC(OMe)N in C_6D_6

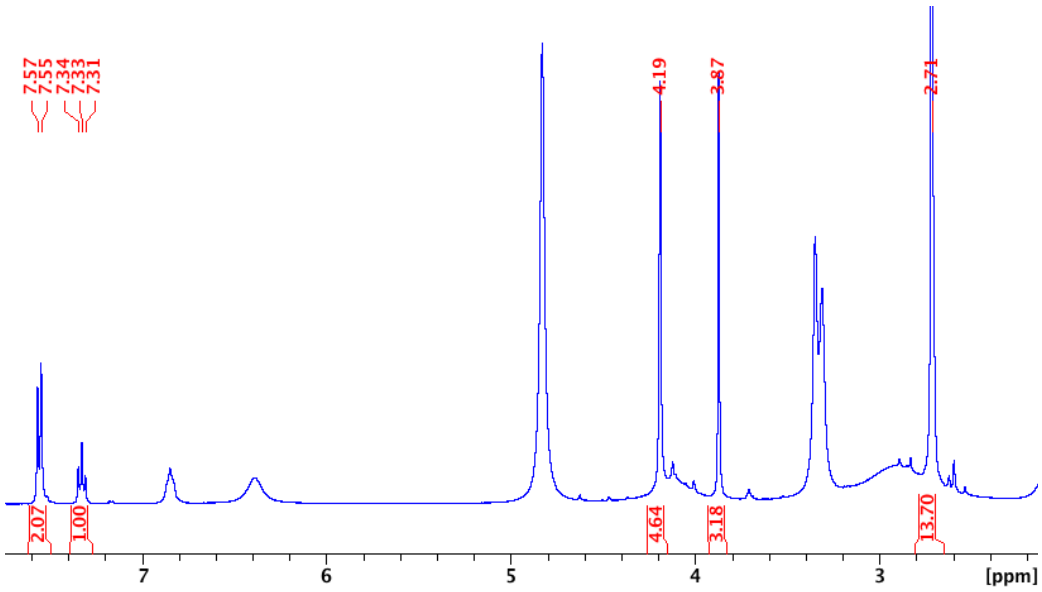

Figure 4.19. ^{1}H NMR spectrum for the crude mixture of the aerobic reaction of 3 with MeOH in CD_3OD. Integrated peaks correspond to NC(OMe)N. The broad peaks correspond to divalent complex 1.

General procedure for the C-O functionalization of divalent complex 1, monocationic complex 4 and dicationic complex 3. These reactions were conducted by charging an NMR tube with complex **1** (8 mg, 0.016 mmol) or a J-Young NMR tube with complex **4** (10 mg, 0.016 mmol) and **3** (14 mg, 0.016

mmol) in CD_3OD (0.750 mL). Yields were determined by ^1H NMR using 1-bromo-3,5-dimethoxybenzene as standard (0.0035 g, 0.016 mmol).

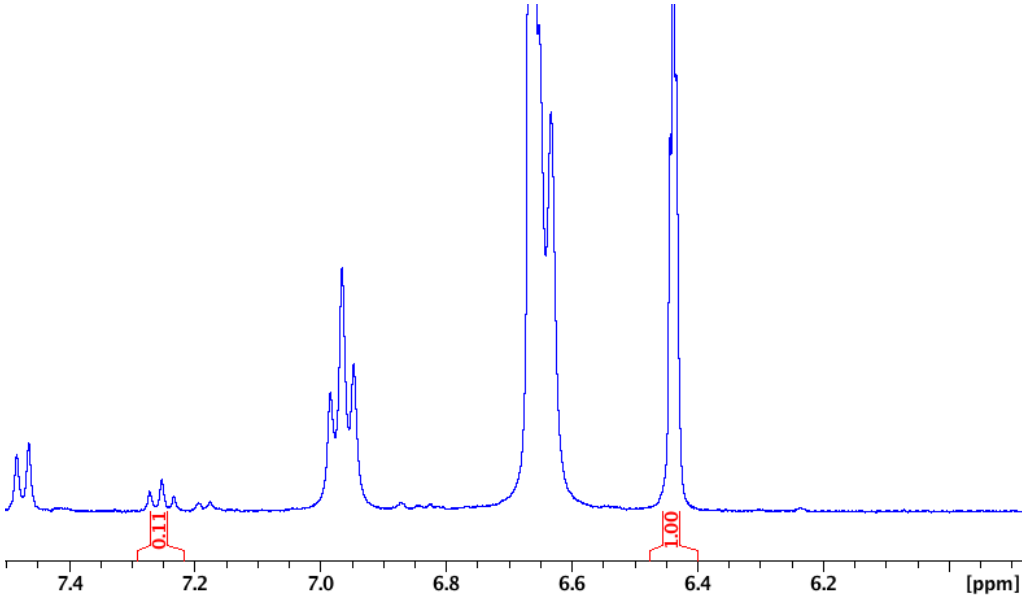

Figure 4.20. ^1H NMR spectrum for the crude mixture of the aerobic reaction of 1 with CD_3OD after 24 h. IS integrated to 1.00

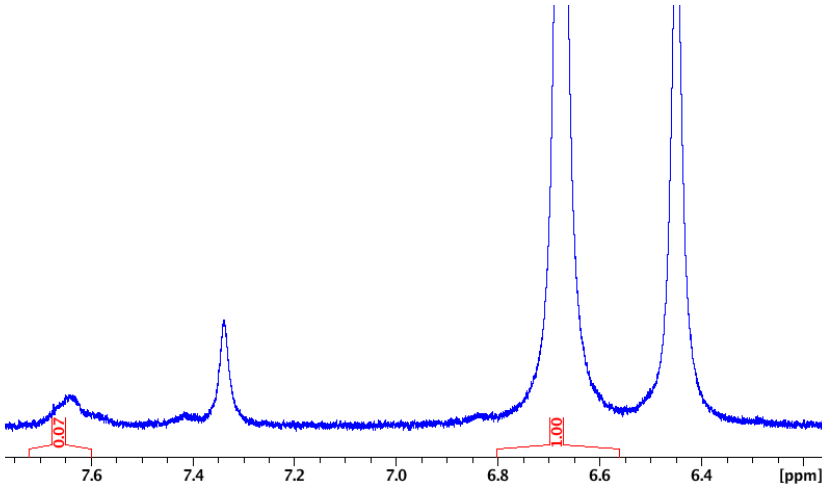

Figure 4.21. ^1H NMR spectrum for the crude mixture of the anaerobic reaction of 4 with CD_3OD after 10 minutes. Integrated peak corresponds to the 2 ortho hydrogens of NC(OMe)N. The peak integrated to one corresponds to the IS (2 hydrogens)

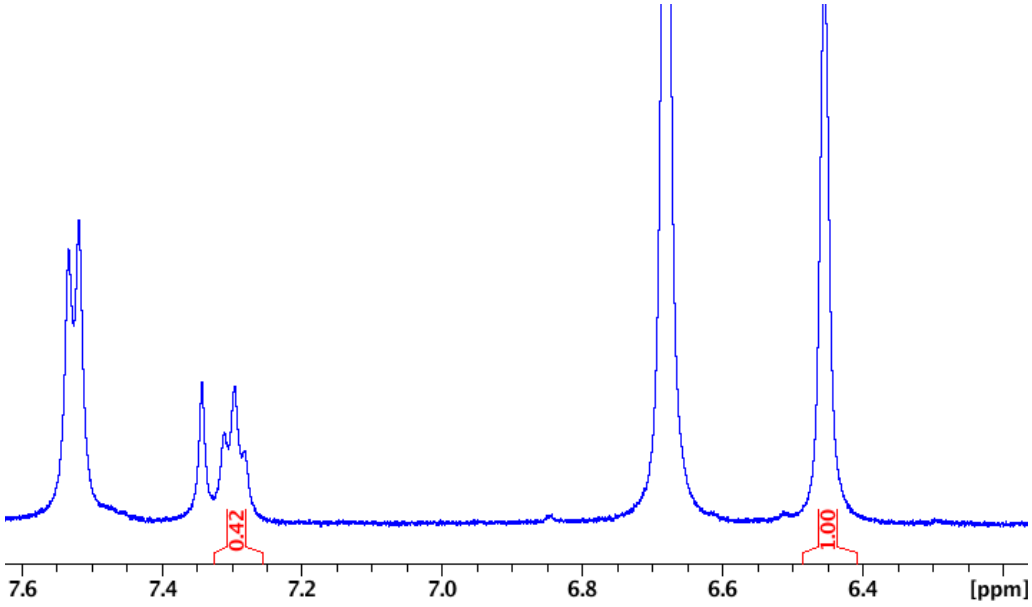

Figure 4.22. ^{1}H NMR spectrum for the crude mixture of the anaerobic reaction of 4 with CD_3OD after 2 h. Integrated peak corresponds to the para-hydrogen of NC(OMe)N. The peak integrated to 1 corresponds to the IS.

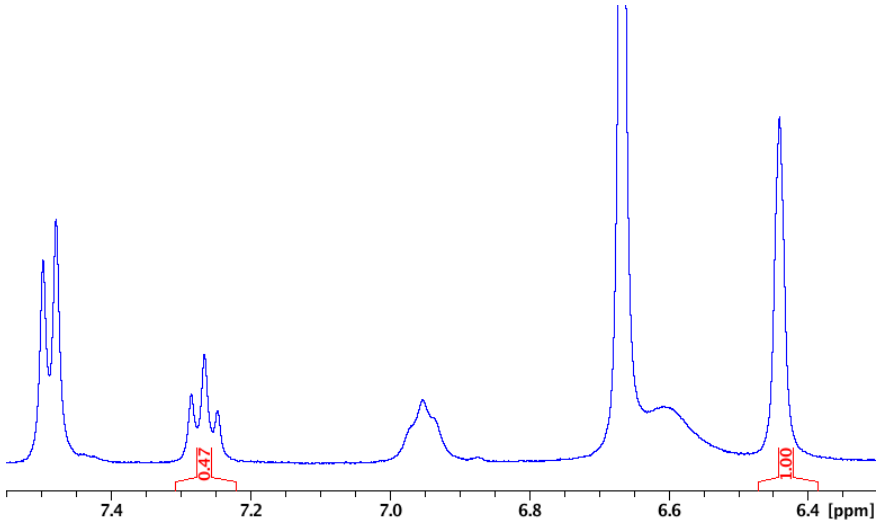

Figure 4.23. ^{1}H NMR spectrum for the crude mixture of the anaerobic reaction of 3 with CD_3OD after 10 minutes. Integrated peak corresponds to the para-hydrogen of NC(OMe)N. The peak integrated to 1.00 corresponds to the IS.

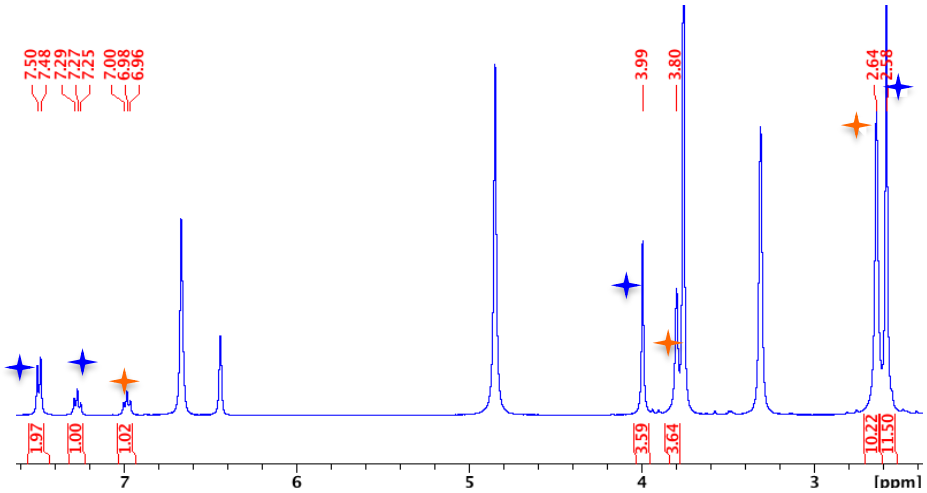

Figure 4.24. ^{1}H NMR spectrum for the anaerobic reaction of 3 with CD_3OD after 2 h. Blue stars correspond to NC(OMe)N, orange stars to divalent complex 1.

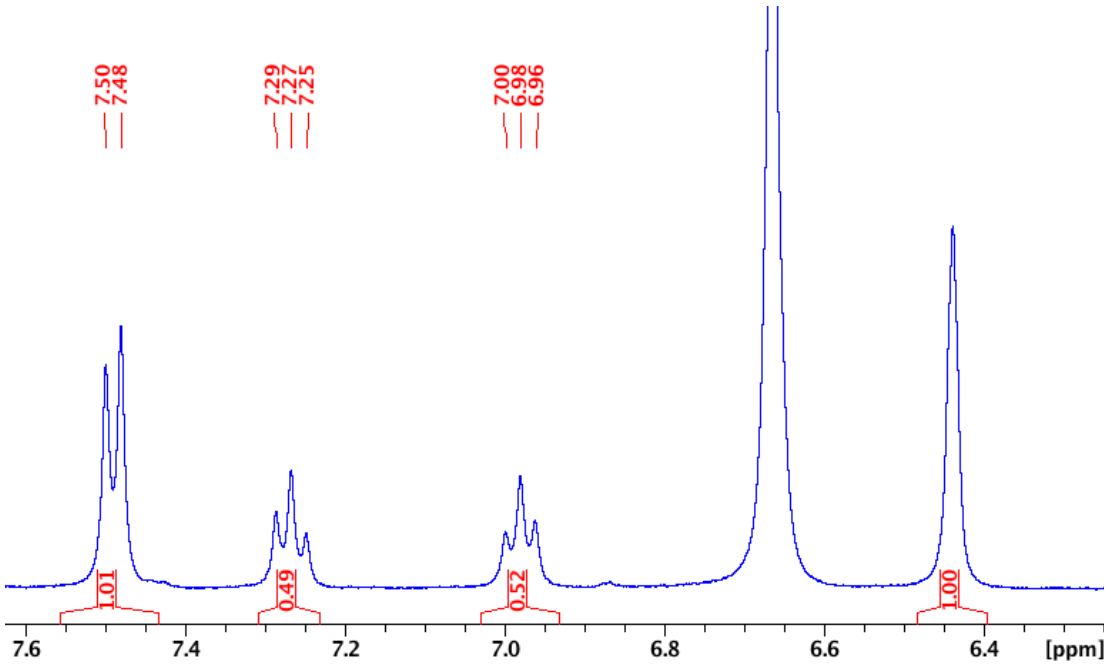

Figure 4.25. ^{1}H NMR spectrum for the crude mixture of the anaerobic reaction of 3 with CD_3OD after 2 h. IS integrated to 1.00

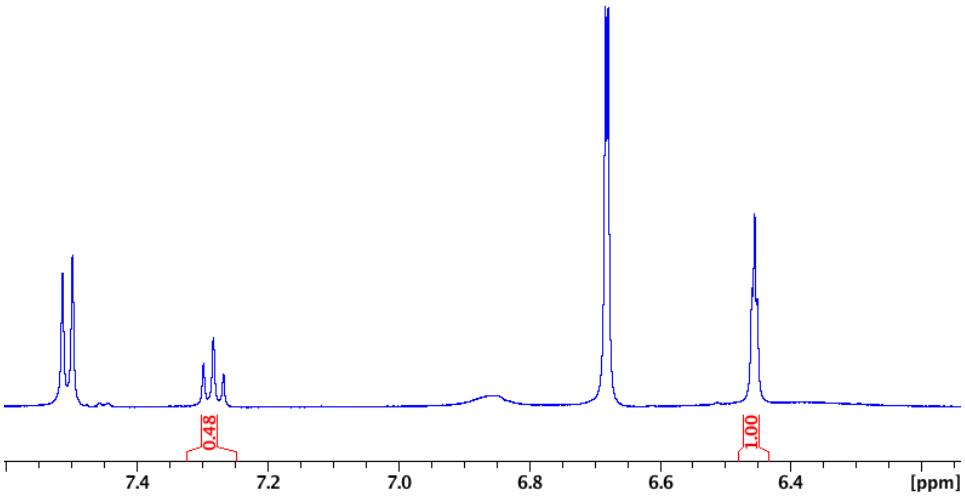

Figure 4.26. ^{1}H NMR spectrum for the crude mixture of the aerobic reaction of 3 with CD_3OD after 2 h. IS integrated to 1.00

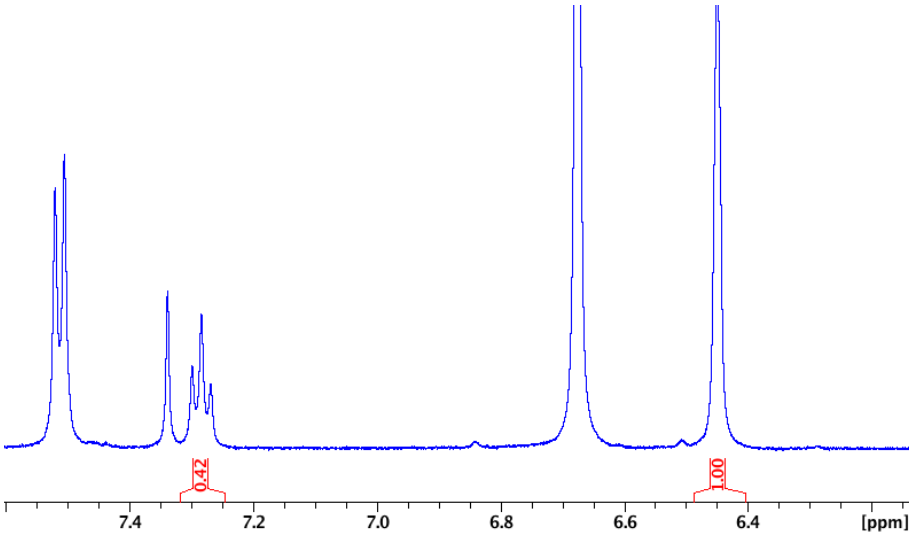

Figure 4.27. ^{1}H NMR spectrum for the crude mixture of the aerobic reaction of 4 with CD_3OD after 2 h. IS integrated to 1.00

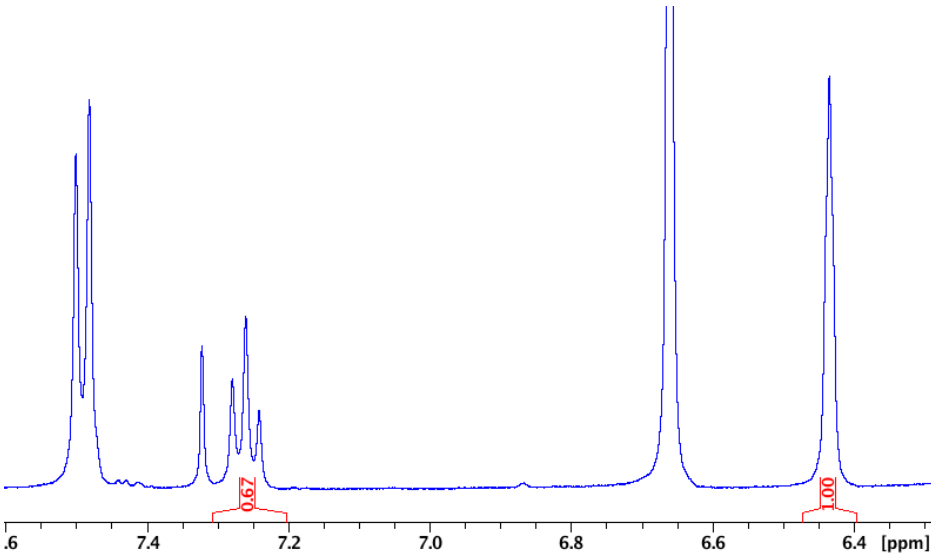

Figure 4.28. ^{1}H NMR spectrum for the crude mixture of the aerobic reaction of 4 with CD_3OD after 24 h. IS integrated to 1.00

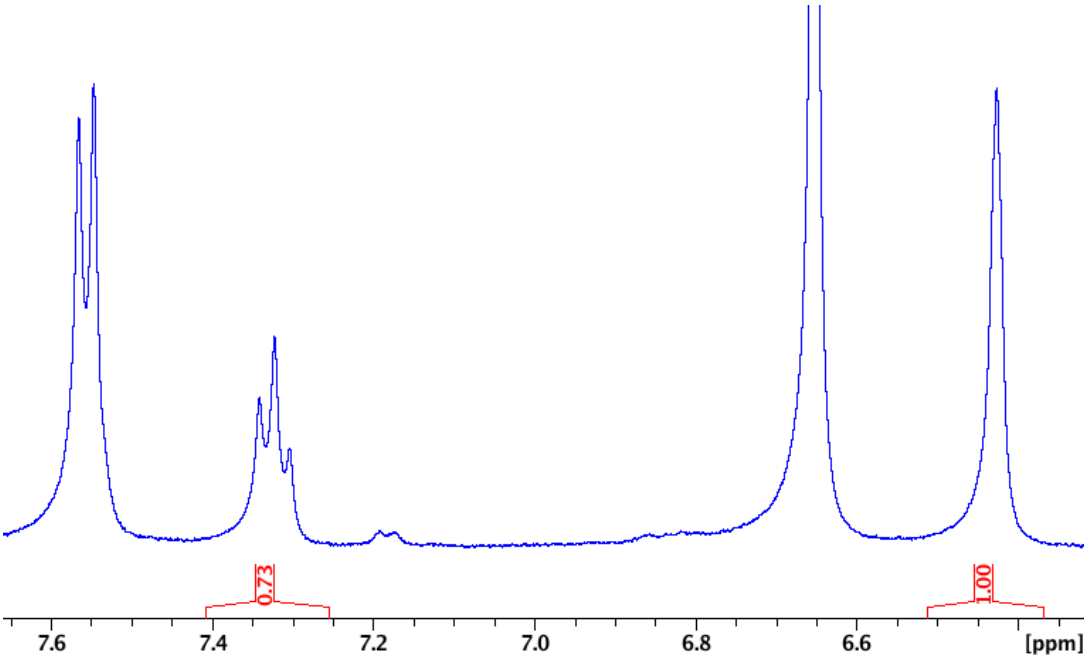

Figure 4.29. ^{1}H NMR spectrum for the crude mixture of the aerobic reaction of 4 with CD_3OD after 96 h. IS integrated to 1.00

General procedure for the functionalization of 3 and 4 with $MeNH_2$ under N_2. These reactions were conducted by stirring for 5 minutes complex **3** (50 mg, 0.059 mmol) or complex **4** (50 mg, 0.082 mmol) under N_2 in a 33% $MeNH_2$ solution in ethanol (5 mL). The reaction mixtures were evaporated and worked

up by base extraction, and the yields were determined by ^{1}H NMR using 1-bromo-3,5-dimethoxybenzene as standard (0.013 g, 0.059 mmol).

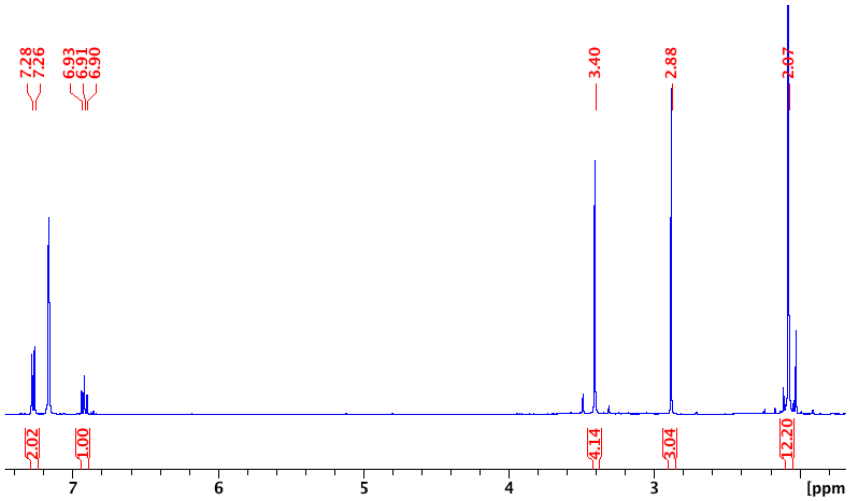

Figure 4.30. ^{1}H NMR spectrum for NC(NHMe)N in C_6D_6

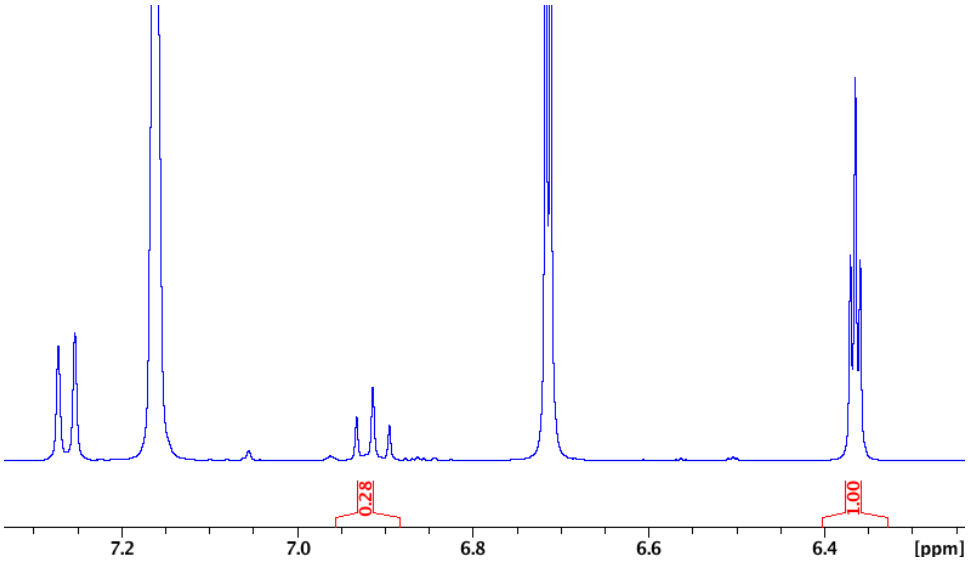

Figure 4.31. ^{1}H NMR spectrum for the reaction of 4 with $MeNH_2$ 33% under nitrogen with internal standard (integrated to 1.00) in C_6D_6.

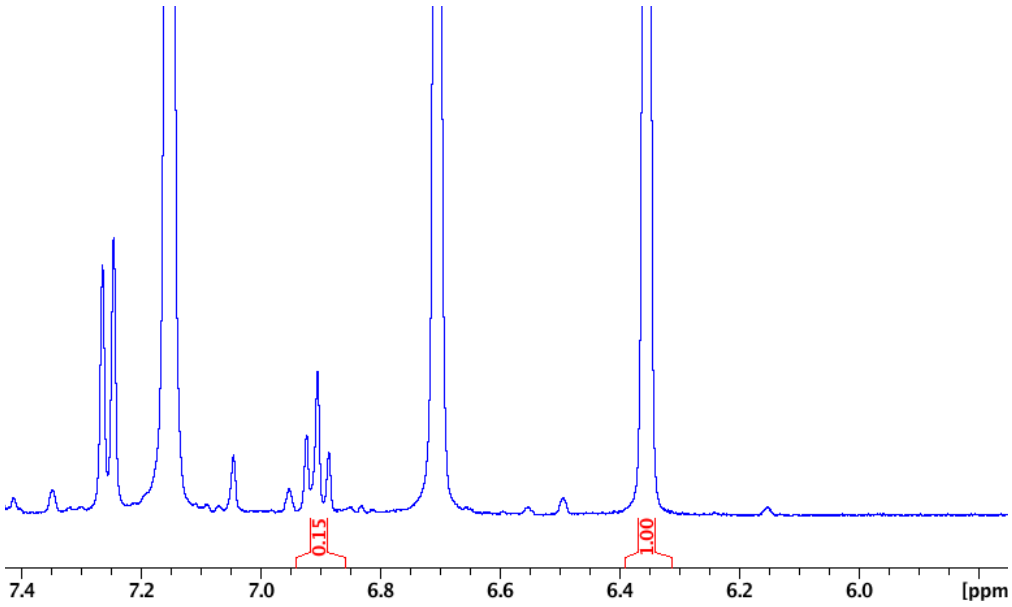

Figure 4.32. ^{1}H NMR spectrum for the reaction of 3 with $MeNH_2$ 33% under nitrogen with internal standard (integrated to 1.00) in C_6D_6.

General procedure for the functionalization of 3 and 4 with $MeNH_2$ in air. These reactions were conducted by stirring for 2 h complex **3** (0.050 mg, 0.059 mmol) or complex **4** (0.050 mg, 0.082 mmol) in a 33% $MeNH_2$ solution in ethanol (5 mL). The reaction mixtures were evaporated and worked up by base extraction, and the yields were determined by ^{1}H NMR using 1-bromo-3,5-dimethoxybenzene as standard (0.013 g, 0.061 mmol).

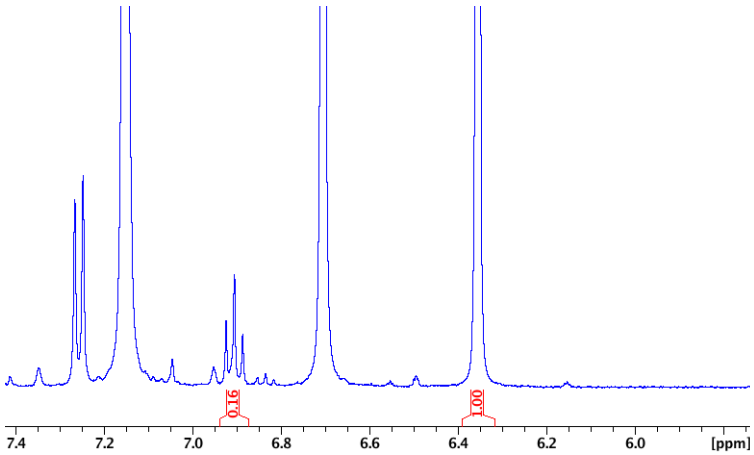

Figure 4.33. ^{1}H NMR spectrum for the reaction of 3 with $MeNH_2$ 33% in air with internal standard (integrated to 1.00) in C_6D_6.

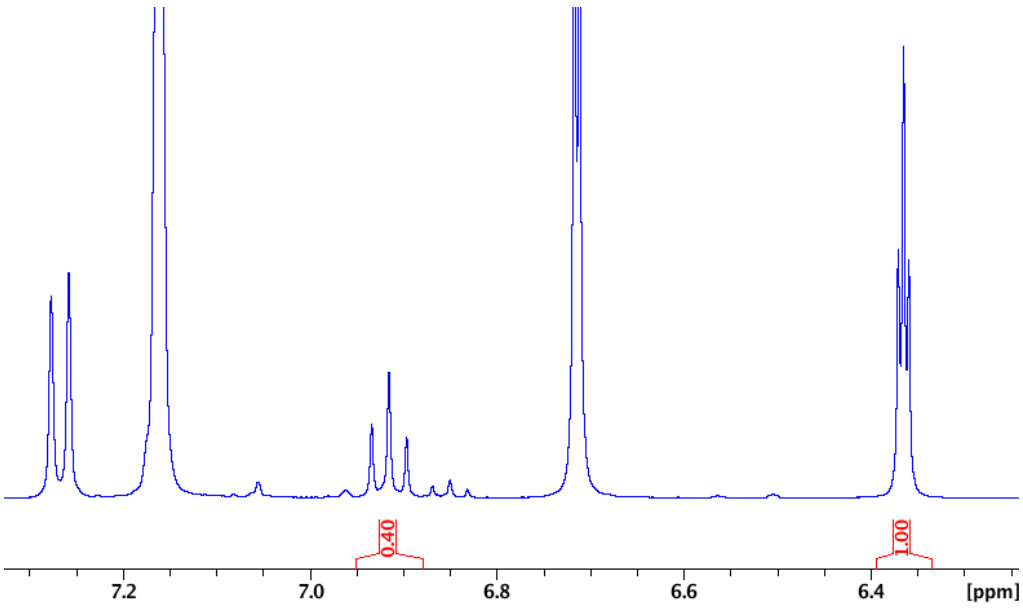

Figure 4.34. ^{1}H NMR spectrum for the reaction of 4 with $MeNH_2$ 33% in air with internal standard (integrated to 1.00) in C_6D_6

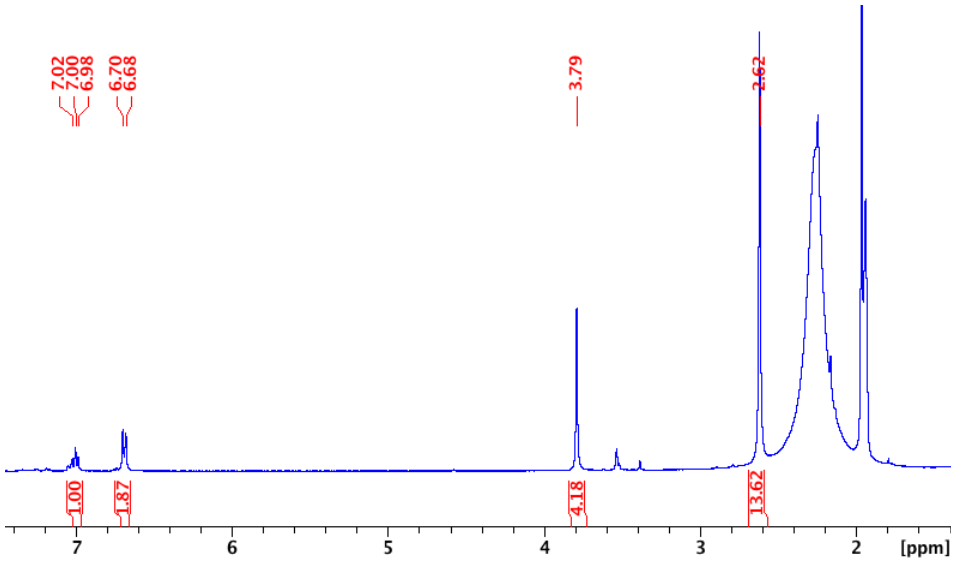

Figure 4.35. ^{1}H NMR of the reaction between 3 and 20 equivalents of $tBuNH_2$ in CD_3CN.

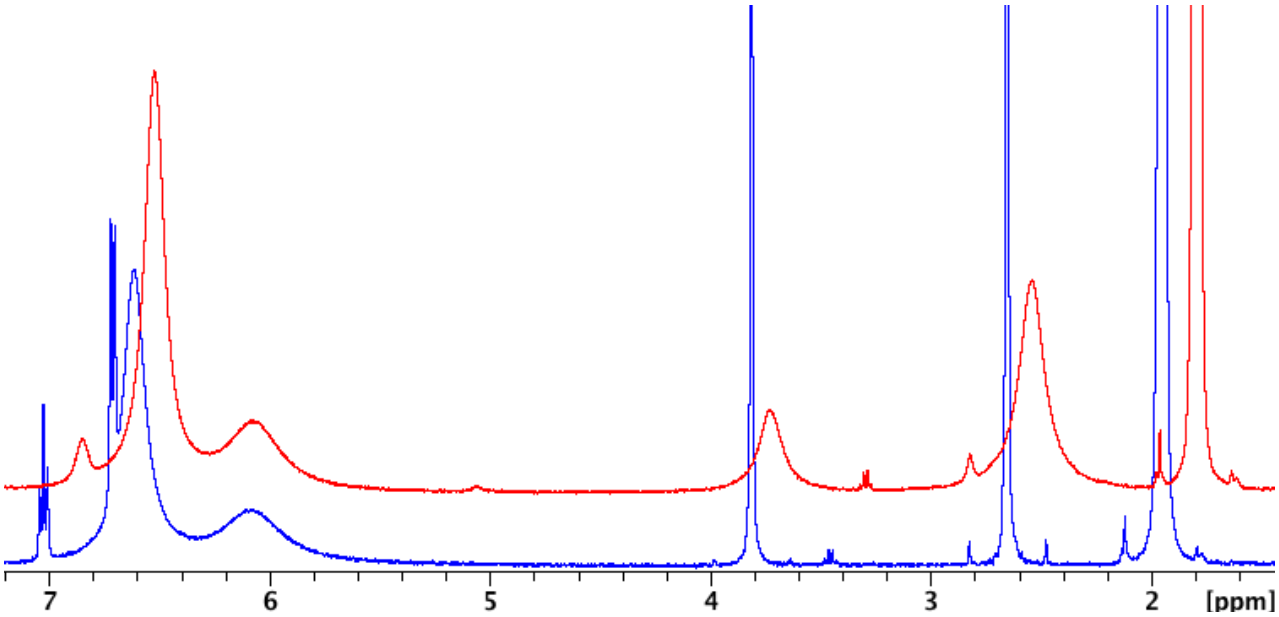

Figure 4.36. ^{1}H NMR of the reaction between 3 and $NiCl(PPh_3)_3$ in CD_3CN. The red spectrum corresponds to 1 h reaction time and the blue one 15 h.

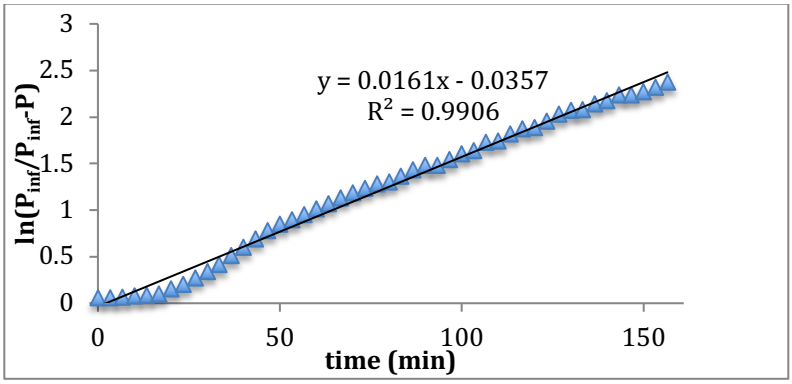

Figure 4.37. Time profile of the reaction of complex 4 with CD_3OD

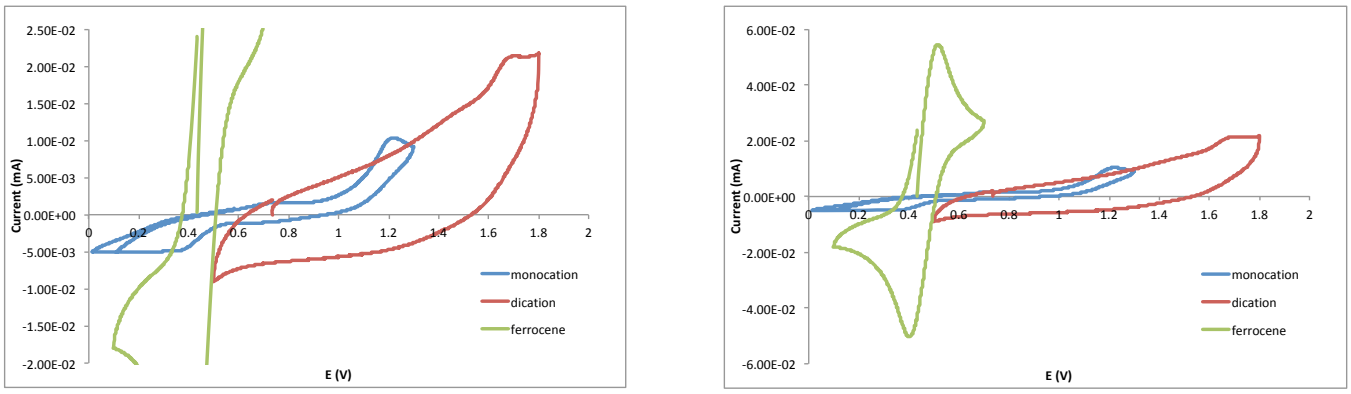

Figure 4.38. Cyclovoltammetry of a 0.1 mM MeCN solution of complex 3 and 4 with 100 mM $TBAPF_6$. Scan rate for 4 50 mv/s, 3 is 100 mv/s. The oxydation potential of ferrocene was measured to be 0.515 V.

Procedure for the optimization and determination of the Gibbs energy

All DFT calculations were performed using Gaussian 09 package.[21] Geometry optimizations were carried out using the mixed basis set 6-31g** for all light atoms (C, H, O, N) and def2TZVP for Ni and Br. The M06-L[22] functional was used in implicit MeCN/MeOH/EtOH solvents using the SMD model. Local minima were located by convergence and the absence of imaginary frequencies in the frequency calculation. Transition states were assessed by the existence of a single imaginary frequency along the expected reaction coordinate and have been linked to intermediates by Intrinsic reaction coordinates calculation. The electronic energy was obtained by single point calculation with def2TZVP for all atoms, from the optimized geometries. The thermal energy was

calculated by the sum of the electronic energy and the thermal correction to Gibbs free energy obtained from the frequency calculations. Zero-point energies were obtained by adding the zero-point correction obtained from the frequency calculation to the electronic energy obtained from the single point calculation. CYLview generated 3D molecular representations.[23]

Calculation of redox potential. The redox potential of complexes **3** and **4** were calculated using the following procedure. First, we calculated the Gibbs free energy of the redox process for each complex. (We neglected the Gibbs free energy of the electron in the calculations)[24]

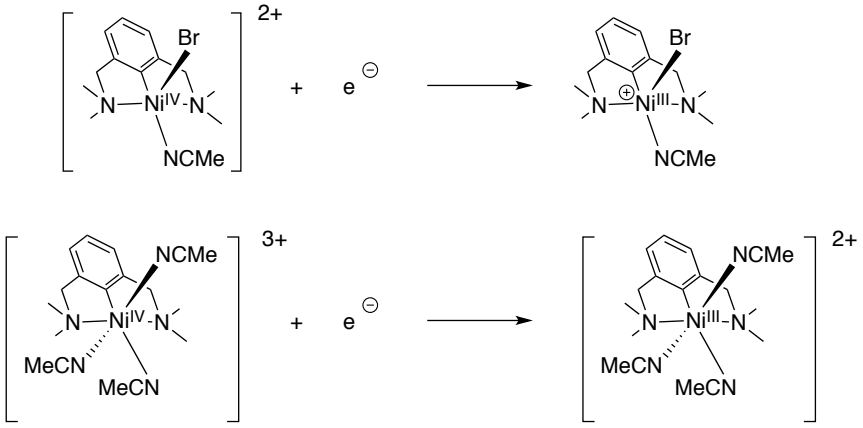

Scheme 4.16. Redox reaction of dicationic complex 3 and monocationic complex 4

Redox potentials were calculated using the Nernst equation where n is the number of electron exchanged and F is the Faraday constant (96 485 C/mol). Redox potential with respect to ferrocene was obtained by substracting the value obtained in (1) with the absolute potential of the Fc^{+}/Fc couple ca. 4.99 V.[25]

$$E° = -\Delta G°/nF \quad (1)$$

The results are indicated in Tables S1-S5.

M06	(NCN)Ni(III)(MeCN)3	(NCN)Ni(IV)(MeCN)3
Electronic energy (hartree)	-2484.1898032	-2483.9513112
Gibbs correction (hartree)	0.3777280	0.3832950
Gibbs (hartree)	-2483.8120752	-2483.5680162
ΔG redox (kJ/mol)		-640.7769045
E^o (V)		6.6412075
E^o vs FC (V)		1.6512075
E^o_{exp} (V)		1.13

Table 4.3. Redox potential of dicationic complex 3 obtained from the M06 functional.

M06L	(NCN)Ni(III)(MeCN)3	(NCN)Ni(IV)(MeCN)3
Electronic energy (hartree)	-2484.8150376	-2484.5922531
Gibbs correction (hartree)	0.3785660	0.3824640
Gibbs (hartree)	-2484.4364716	-2484.2097891
ΔG redox (kJ/mol)		-595.1549037
E^o (V)		6.1683671
E^o vs FC (V)		1.1783671
E^o_{exp} (V)		1.13

Table 4.4. Redox potential of dicationic complex 3 obtained from the M06L functional.

wB97-xD	(NCN)Ni(III)(MeCN)3	(NCN)Ni(IV)(MeCN)3
Electronic energy (hartree)	-2484.6890027	-2484.4434607
Gibbs correction (hartree)	0.3830560	0.3915740
Gibbs (hartree)	-2484.3059467	-2484.0518867
ΔG redox (kJ/mol)		-667.0345300
E^o (V)		6.9133495
E^o vs FC (V)		1.9233495
E^o_{exp} (V)		1.13

Table 4.5. Redox potential dicationic complex 3 obtained from the wB97-xD functional.

B3LYP	(NCN)Ni(III)(MeCN)3	(NCN)Ni(IV)(MeCN)3
Electronic energy (hartree)	-2485.0140395	-2484.7756973
Gibbs correction (hartree)	0.3779730	0.3858620
Gibbs (hartree)	-2484.6360665	-2484.3898353
ΔG redox (kJ/mol)		-646.4800156
E		6.7003163
vs FC		1.7103163
experimental		1.13

Table 4.6. Redox potential of dicationic complex **3** obtained from the B3LYP functional.

M06L	(NCN)Ni(III)(Br)(MeCN)	(NCN)Ni(IV)(Br)(MeCN)
Electronic energy (hartree)	-4793.4611318	-4793.2468091
Gibbs correction (hartree)	0.2932670	0.2947710
Gibbs (hartree)	-4793.1678648	-4792.9520381
ΔG redox (kJ/mol)		-566.6530008
E		5.8729647
vs FC		0.8829647
experimental		0.74

Table 4.7. Redox potential for monocationic complex 4 obtained from the M06L functional

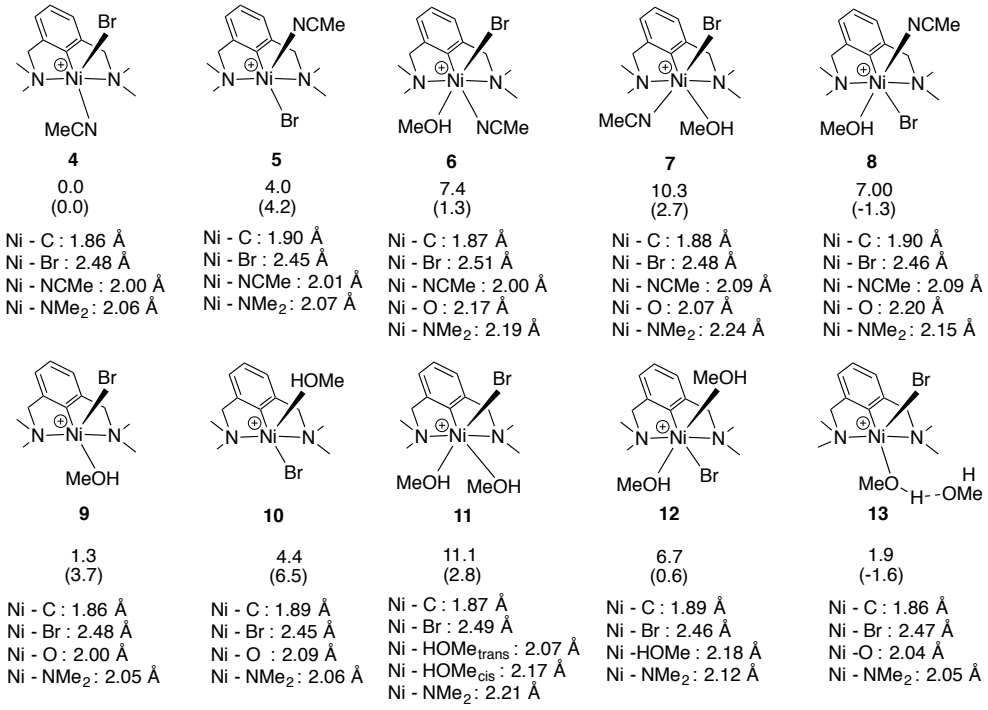

Scheme 4.17. Monocationic complex 4 and different coordination isomers of MeOH and MeCN. Gibbs free energy and enthalpy (in parenthesis) are given with respect to 4

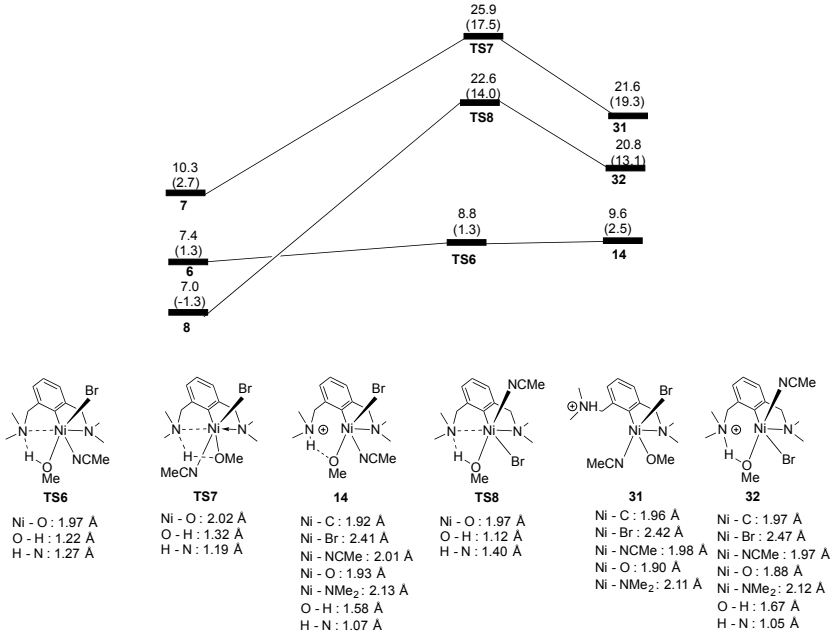

Scheme 4.18. Deprotonation of intermediate 6, 7 and 8. Gibbs free energy and enthalpy (in parenthesis) are given with respect to 4

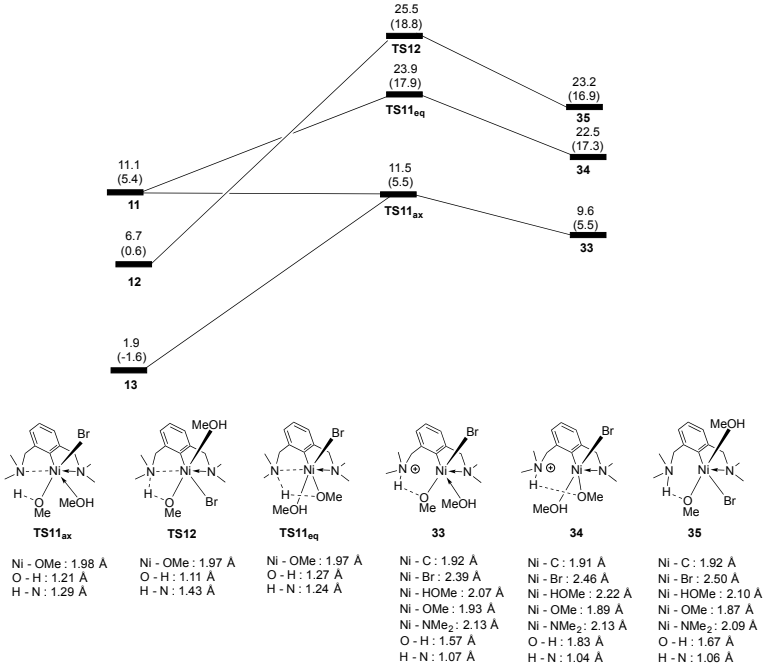

Scheme 4.19. Deprotonation of intermediate 11, 12 and 13. Gibbs free energy and enthalpy (in parenthesis) are given with respect to 4

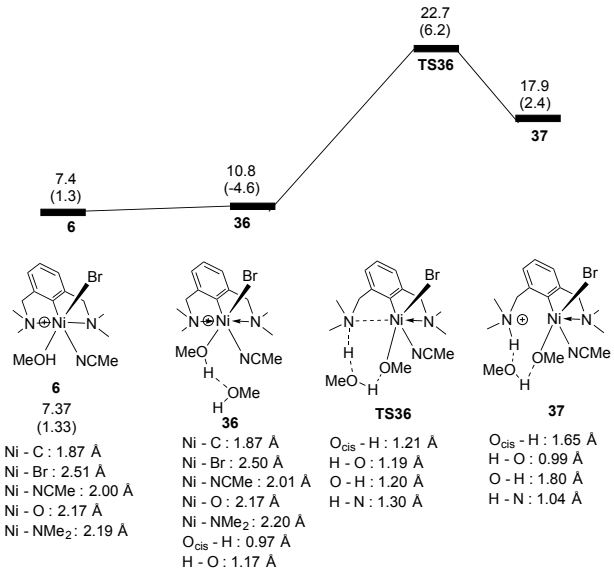

Scheme 4.20. Deprotonation of 17 by a second coordination sphere MeOH. Gibbs free energy and enthalpy (in parenthesis) are given with respect to 4

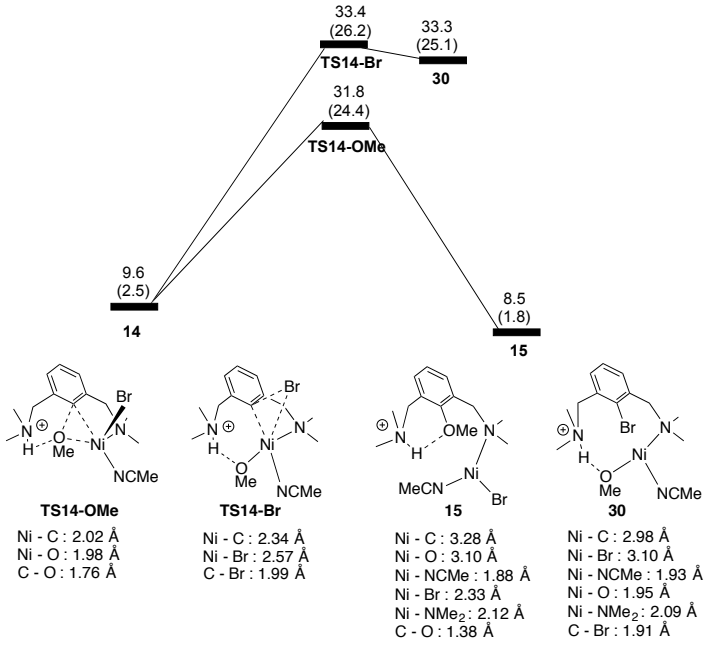

Scheme 4.21. Reductive elimination of OMe and Br moieties from 14. Gibbs free energy and enthalpy (in parenthesis) are given with respect to 4

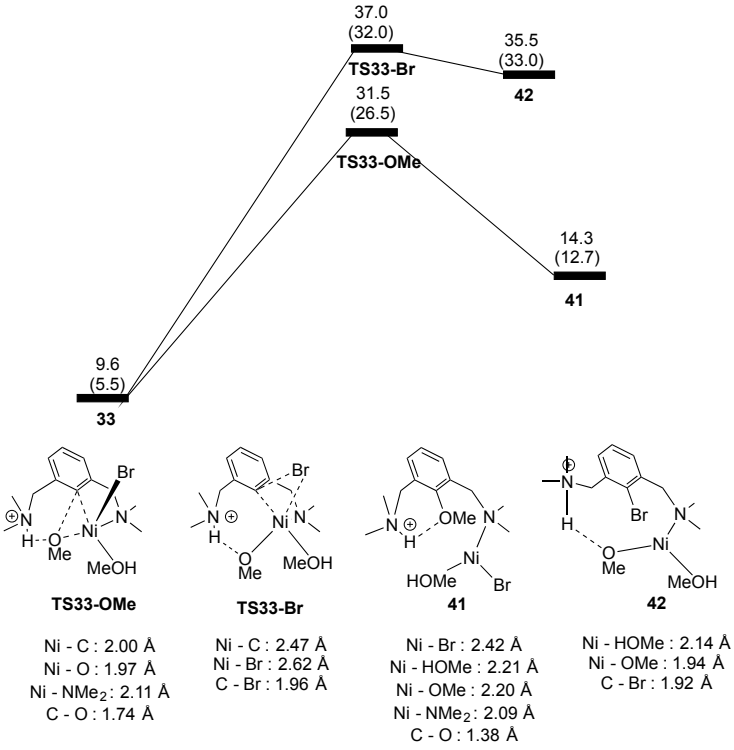

Scheme 4.22. Reductive elimination of OMe and Br moieties from 40. Gibbs free energy and enthalpy (in parenthesis) are given with respect to 4

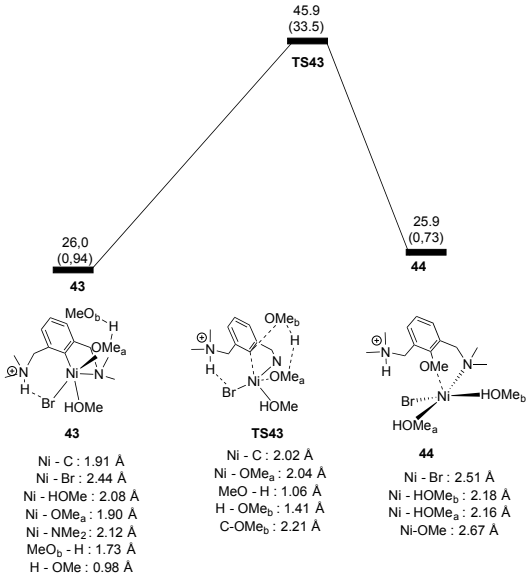

Scheme 4.23. Nucleophilic attack on the *ipso* carbon of the aromatic cycle. Gibbs free energy and enthalpy (in parenthesis) are given with respect to 4

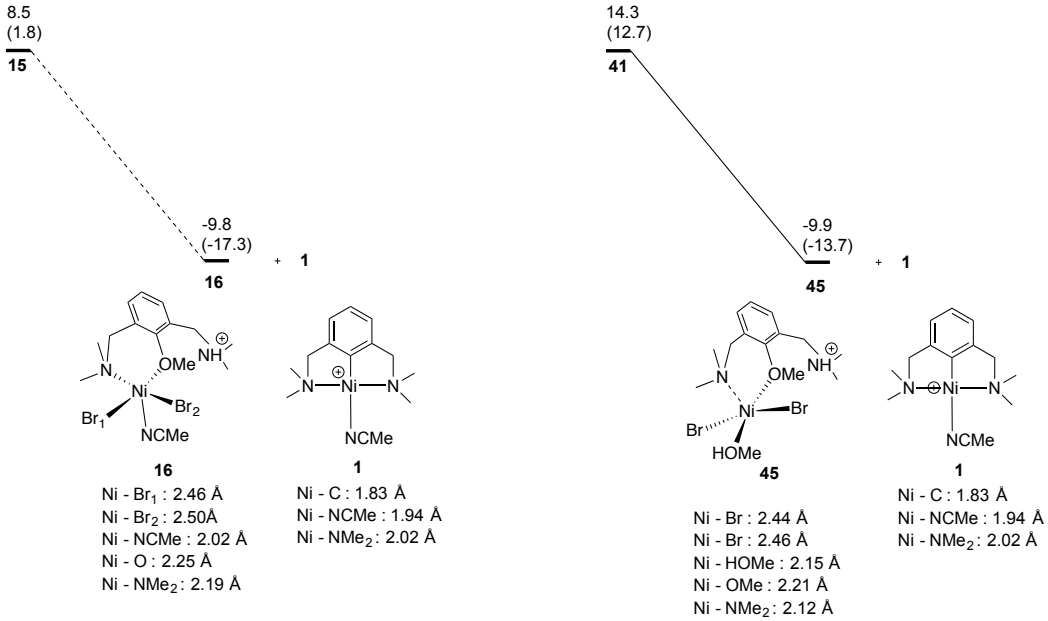

Scheme 4.24. Comproportionation reaction between 15, 41 and 4. Gibbs free energy and enthalpy (in parenthesis) are given with respect to 4

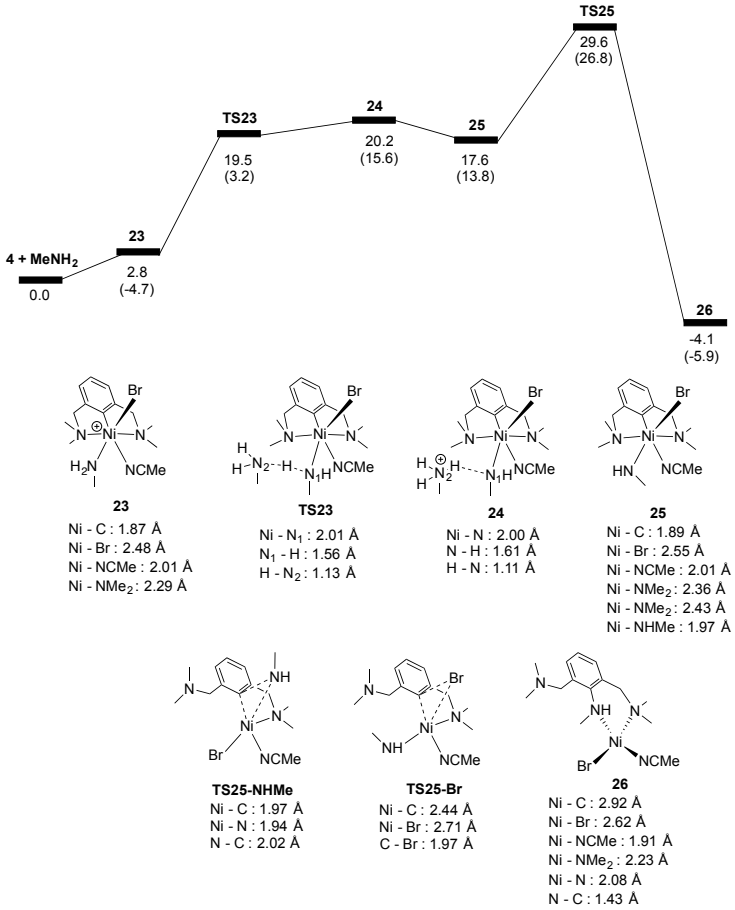

Scheme 4.25. $MeNH_2$ functionalization from 4. Gibbs free energy and enthalpy (in parenthesis)

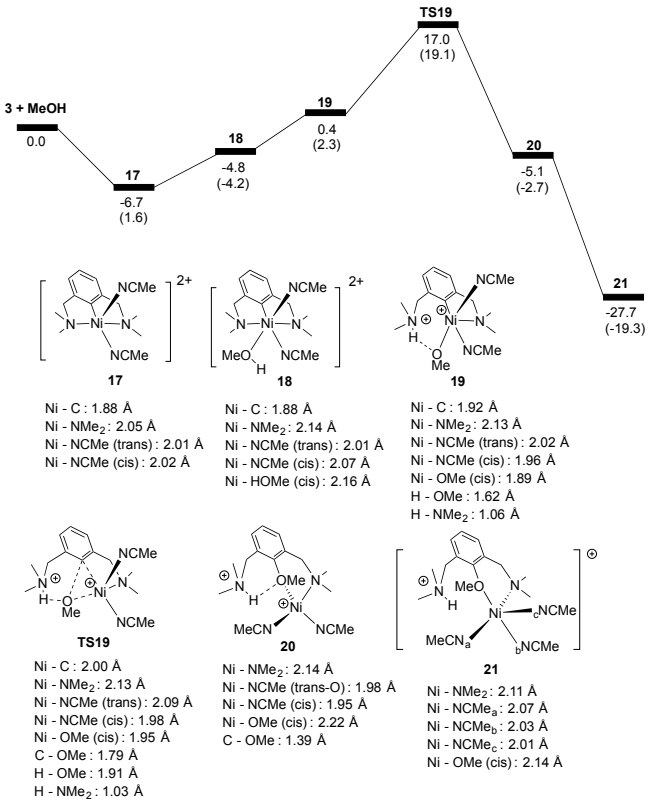

Scheme 4.26. MeOH functionalization from 3. Gibbs free energy and enthalpy (in parenthesis)

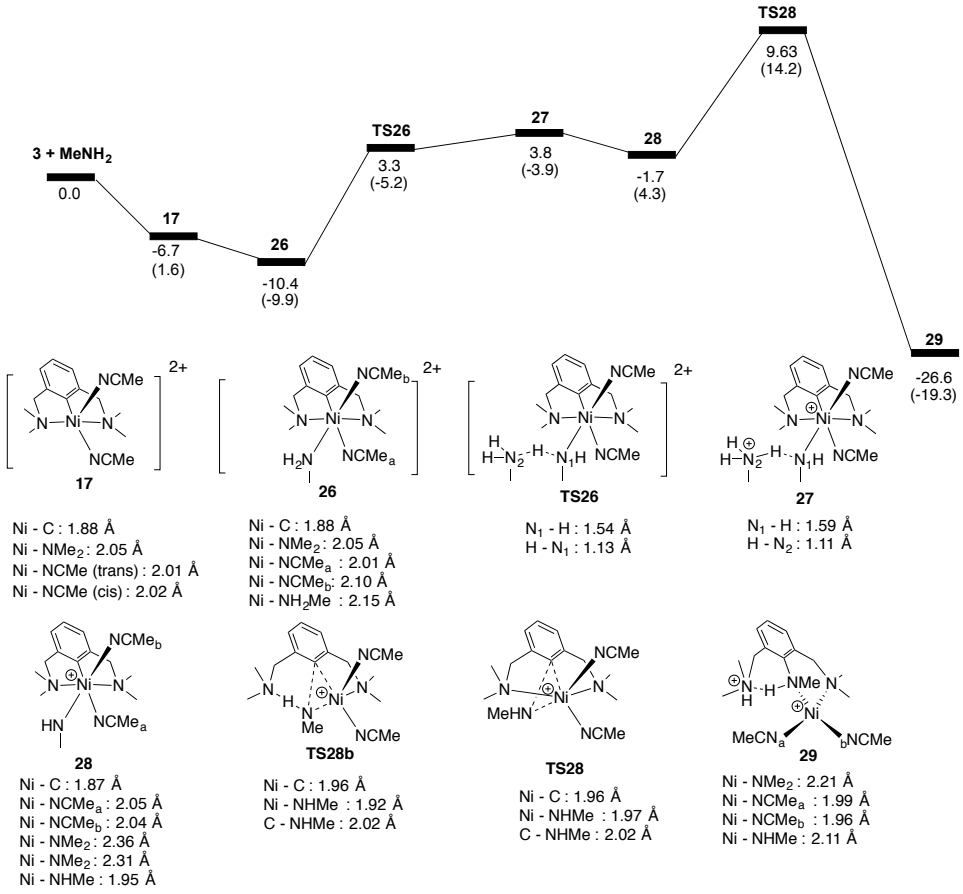

Scheme 4.27. $MeNH_2$ functionalization from 3. Gibbs free energy and enthalpy (in parenthesis)

M06L	$(MeOH)_2$	$(MeOD)_2$	6	6-D
EEsp (hartree)	-115.756198	-115.756198	-4909.2154617	-4909.2154617
zpe (hartree)	0.051574	0.038597	0.398307	0.385068
EEsp + zpe (hartree)	-115.7046240	-115.7176010	-4908.8171547	-4908.8303937
dZPE H/D(kcal/mol)		8.1430675		8.30747
ddZPE(kcal/mol)				0.1644
EIE				0.75767

Table 4.8. EIE for 4 → 6

M06L	6	6-D	TS6	TS6-D
EEsp (hartree)	-4909.2154617	-4909.2154617	-4909.209744	-4909.209744
zpe (hartree)	0.398307	0.385068	0.3937	0.381609
EEsp + zpe (hartree)	-4908.8171547	-4908.8303937	-4908.8160435	-4908.8281345
dZPE H/D(kcal/mol)		8.30747		7.58710
ddZPE(kcal/mol)				-0.72037
EIE				3.37357

Table 4.9. KIE for 6 → TS6

M06L	6	6-D	14	14-D
EEsp (hartree)	-4909.2154617	-4909.2154617	-4909.214522	-4909.214522
zpe (hartree)	0.398307	0.385068	0.399761	0.386374
EEsp + zpe (hartree)	-4908.8171547	-4908.8303937	-4908.8147605	-4908.8281475
dZPE H/D(kcal/mol)		8.30747		8.40034
ddZPE(kcal/mol)				0.0929
EIE				0.85491

Table 4.10. EIE for 6 → 14

M06L	$(MeOH)_2$	$(MeOD)_2$	TS14	TS14-D
EEsp (hartree)	-115.756198	-115.756198	-4909.1788314	-4909.1788314
zpe (hartree)	0.051574	0.038597	0.399239	0.385476
EEsp + zpe (hartree)	-115.7046240	-115.7176010	-4908.7795924	-4908.7933554
dZPE H/D(kcal/mol)		8.1430675		8.6362825
ddZPE(kcal/mol)				0.32881
EIE				0.57406

Table 4.11. KIE for 4 → TS14

MeOH vib (cm^{-1})	description	d4-MeOD vib (cm^{-1})	Δvib (cm^{-1})
3848	OH strech	2801	1047
3167	CH strech asymm	2348	819
3094	CH strech asymm	2295	799
3024	CH strech symm	2171	853
1499	CH bend symm	1173	326
1470	CH3 pyram	1097	373
1459	CH3 rocking	1067	392
1397	HOC bending symm	1051	346
1181	HCO bending/rocking	1011	170
1119	C-O strech	915	204
1071	HCO bend asymm	789	282
308	OH rot	223	85
	ΣΔvib (cm^{-1})		5696
	ΣΔvib stretch (cm^{-1})		3518

Table 4.12. Vibrational modes for MeOH/CD_3OD

6-H vib (cm^{-1})	description	6-D vib (cm^{-1})	Δvib (cm^{-1})
3832	O-H strech	2791	1041
3194	asymmetric CH3 streching	2367	827
3116	asymmetric CH3 streching	2312	804
3035	symmetric CH3 streching	2178	857
1483	CH3 symmetric bending	1058	425
1461	CH3 pyram	1133	328
1460	CH3 pyram	988	472
1455	CH3 bending	1050	405
1388	H-O-C bending	1095	293
1146	CH3 rocking	886	260
1101	HOC asymmetric bending	802	299
326	Ni-O coord	293	33
304	OH bend	254	50
299	Ni-O coord	237	62
	ΣΔvib (cm^{-1})		6156
	Σδvib stretch (cm^{-1})		3529

Table 4.13. Vibrational modes for 6

14-H vib (cm^{-1})	description	14-D vib (cm^{-1})	Δvib (cm^{-1})
3062	asymmetric CH3 streching	2269	793
3046	asymmetric CH3 streching	2258	788
2972	symmetric CH3 streching	2131	841
2661	N-H strech	1981	680
1607	N-H bend	1280	327
1545	N-H bend	1155	390
1478	CH3 bending	1068	410
1461	CH3 bending	1057	404
1305	N-H bend	1018	287
1249	N-H bend	1001	248
1197	CH3 rocking	939	258
1185	CH3 rocking	930	255
1177	CH3 rocking	913	264
1176	CH3 rocking	908	268
465	OCH3 rocking	457	8
320	OCH3 rocking	313	7
451	OCH3 rocking	440	11
	ΣΔvib (cm^{-1})		6239
			3102

Table 4.14. Vibrational modes for 14

TS14-H vib (cm^{-1})	description	TS14-D vib (cm^{-1})	Δvib (cm^{-1})
3361	N-H stretch	2462	899
3130	asymmetric CH3 streching	2322	808
3115	asymmetric CH3 streching	2312	803
3020	symmetric CH3 streching	2163	857
1508	N-H bend	1255	253
1490	CH3 bend	1064	426
1473	CH3+N-H bend	1200	273
1462	CH3 bend	1052	410
1457	CH3 pyr	1121	336
1455	CH3+N-H bend	1104	351
1408	N-H bend	1068	340
1362	N-H bend	965	397
1184	N-H bend	888	296
1166	OCH3 rocking	904	262
1163	OCH3 rocking	910	253
839	C-N-H bend	832	7
456	O-H-N	450	6
	ΣΔvib (cm^{-1})		6977
	ΣΔvib stretch (cm^{-1})		3367

Table 4.15. Vibrational modes for TS14

	ΔΔZPE (kcal/mol)	EIE
4 + MeOH/D → **6**	0.164	0.76
6 → TS6	-0.720	3.4 (KIE)
6 → 14	0.0929	0.85
14 → TS14-OMe	0.236	0.67
4 + MeOH/D → TS14	0.329	0.57

Table 4.16. ΔΔZPE and EIE for MeOH/D coordination and deprotonation equilibria.

$EIE = \exp(-\Delta\Delta ZPE_{H/D}/RT)$

Table 4.17. Electronic energy, Gibbs correction and Enthalpy correction for calculated structures

M06L	$(MeOH)_2$
Enthalpy correction (hartree)	0.114055
Enthalpy (kcal/mol)	-145206.5513
Gibbs correction (hartree)	0.074099
Electronic Energy (hartree)	-231.5189177
Gibbs (kcal/mol)	-145231.624

M06L	MeCN (solvated in MeOH)
Enthalpy correction (hartree)	0.049941
Enthalpy (kcal/mol)	-83298.8535
Gibbs correction (hartree)	0.022534
Electronic Energy (hartree)	-132.7971179
Gibbs (kcal/mol)	-83316.051

M06L	MeCN (solvated in EtOH)
Enthalpy correction (hartree)	0.049921
Enthalpy (kcal/mol)	-83298.93891
Gibbs correction (hartree)	0.022501
Electronic Energy (hartree)	-132.797234
Gibbs (kcal/mol)	-83316.145

M06L	$(MeNH_2)_2$ (solvated in EtOH)
Enthalpy correction (hartree)	0.139801
Enthalpy (kcal/mol)	-120248.0607
Gibbs correction (hartree)	0.09919
Electronic Energy (hartree)	-191.7701766
Gibbs (kcal/mol)	-120273.5441

M06L	$MeNH_3$ (solvated in EtOH)
Enthalpy correction (hartree)	0.084136
Enthalpy (kcal/mol)	-60408.13511
Gibbs correction (hartree)	0.056572
Electronic Energy (hartree)	-96.3520804
Gibbs (kcal/mol)	-60425.43152

M06L	(1) (solvated in MeOH)
Enthalpy correction (hartree)	0.3644570
Enthalpy (kcal/mol)	-1392420.5862505
Gibbs correction (hartree)	0.2958590
Electronic Energy (hartree)	-2219.3614072
Gibbs (kcal/mol)	-1392463.6314955

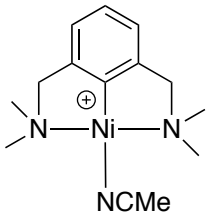

1

M06L	(1) (solvated in EtOH)
Enthalpy correction (hartree)	0.3644660
Enthalpy (kcal/mol)	-1392420.7690413
Gibbs correction (hartree)	0.2957770
Electronic Energy (hartree)	-2219.3617075
Gibbs (kcal/mol)	-1392463.8713888

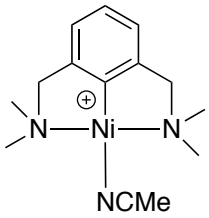

1

M06L	(4) (solvated in MeOH)
Enthalpy correction (hartree)	0.367362
Enthalpy (kcal/mol)	-3007663.839
Gibbs correction (hartree)	0.29337
Electronic Energy (hartree)	-4793.457145
Gibbs (kcal/mol)	-3007710.269

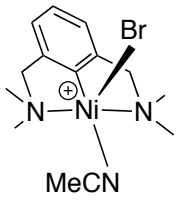

4

0.0
(0.0)

M06L	(4) (sovated in EtOH)
Enthalpy correction (hartree)	0.367429
Enthalpy (kcal/mol)	-3007663.858
Gibbs correction (hartree)	0.293515
Electronic Energy (hartree)	-4793.457243
Gibbs (kcal/mol)	-3007710.239

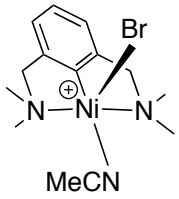

4

0.0
(0.0)

M06L	(3) (solvated in MeOH)
Enthalpy correction (hartree)	0.4696210
Enthalpy (kcal/mol)	-1558922.5068910
Gibbs correction (hartree)	0.3777790
Electronic Energy (hartree)	-2484.8082774
Gibbs (kcal/mol)	-1558980.1377460

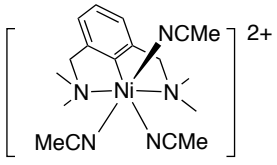

3

M06L	(3) (solvated in EtOH)
Enthalpy correction (hartree)	0.4696260
Enthalpy (kcal/mol)	-1558922.0653193
Gibbs correction (hartree)	0.3771220
Electronic Energy (hartree)	-2484.8075787
Gibbs (kcal/mol)	-1558980.1115793

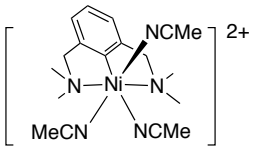

3

M06L	(5)
Enthalpy correction (hartree)	0.366694
Enthalpy (kcal/mol)	-3007659.594
Gibbs correction (hartree)	0.292313
Electronic Energy (hartree)	-4793.449713
Gibbs (kcal/mol)	-3007706.269

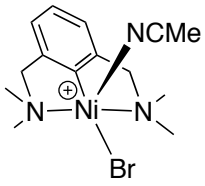

5

4.0
(4.2)

M06L	(6)
Enthalpy correction (hartree)	0.425373
Enthalpy (kcal/mol)	-3080265.781
Gibbs correction (hartree)	0.341018
Electronic Energy (hartree)	-4909.2154617
Gibbs (kcal/mol)	-3080318.713

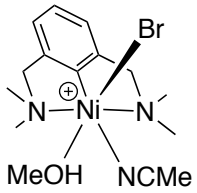

6

7.4
(1.3)

M06L	(TS6)
Enthalpy correction (hartree)	0.420223
Enthalpy (kcal/mol)	-3080265.4241138
Gibbs correction (hartree)	0.337547
Electronic Energy (hartree)	-4909.209744
Gibbs (kcal/mol)	-3080317.3033038

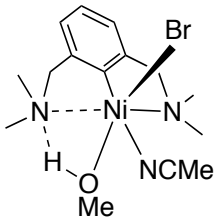

TS6

M06L	(7)
Enthalpy correction (hartree)	0.426062
Enthalpy (kcal/mol)	-3080264.43
Gibbs correction (hartree)	0.344187
Electronic Energy (hartree)	-4909.213998
Gibbs (kcal/mol)	-3080315.807

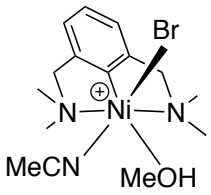

7

10.3
(2.7)

M06L	(TS7)
Enthalpy correction (hartree)	0.4206840
Enthalpy (kcal/mol)	-3080249.5686948
Gibbs correction (hartree)	0.3400030
Electronic Energy (hartree)	-4909.1849369
Gibbs (kcal/mol)	-3080300.1960223

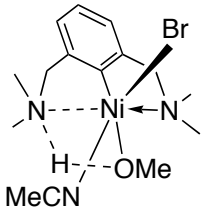

TS7

M06L	(8)
Enthalpy correction (hartree)	0.426027
Enthalpy (kcal/mol)	-3080268.366
Gibbs correction (hartree)	0.34514
Electronic Energy (hartree)	-4909.220237
Gibbs (kcal/mol)	-3080319.123

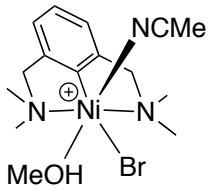

8

7.00
(-1.3)

M06L	(TS8)
Enthalpy correction (hartree)	0.421219
Enthalpy (kcal/mol)	-3080253.0833850
Gibbs correction (hartree)	0.340852
Electronic Energy (hartree)	-4909.191073
Gibbs (kcal/mol)	-3080303.5136775

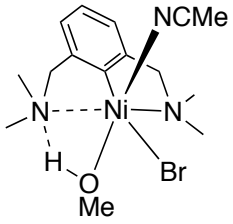

TS8

M06L	(9)
Enthalpy correction (hartree)	0.373709
Enthalpy (kcal/mol)	-2996964.608
Gibbs correction (hartree)	0.303413
Electronic Energy (hartree)	-4776.412925
Gibbs (kcal/mol)	-2997008.719

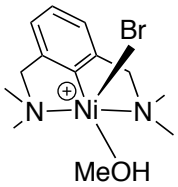

9

1.3
(3.7)

M06L	(10)
Enthalpy correction (hartree)	0.372878
Enthalpy (kcal/mol)	-2996961.744
Gibbs correction (hartree)	0.302914
Electronic Energy (hartree)	-4776.407529
Gibbs (kcal/mol)	-2997005.646

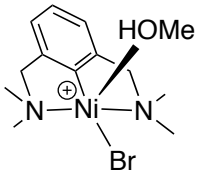

10

4.4
(6.5)

M06L	(11)
Enthalpy correction (hartree)	0.432478
Enthalpy (kcal/mol)	-3069566.107
Gibbs correction (hartree)	0.355655
Electronic Energy (hartree)	-4892.17199
Gibbs (kcal/mol)	-3069614.750

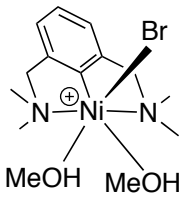

11

11.1
(2.8)

M06L	(TS11ax)
Enthalpy correction (hartree)	0.4274240
Enthalpy (kcal/mol)	-3069566.0082715
Gibbs correction (hartree)	0.3503710
Electronic Energy (hartree)	-4892.1660826
Gibbs (kcal/mol)	-3069614.3590290

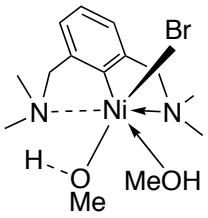

$TS11_{ax}$

M06L	(TS11eq)
Enthalpy correction (hartree)	0.4278080
Enthalpy (kcal/mol)	-3069553.6381758
Gibbs correction (hartree)	0.3508740
Electronic Energy (hartree)	-4892.1467533
Gibbs (kcal/mol)	-3069601.9142608

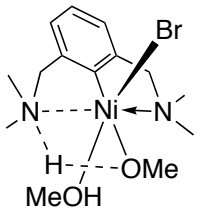

$TS11_{eq}$

M06L	(12)
Enthalpy correction (hartree)	0.432717
Enthalpy (kcal/mol)	-3069570.921
Gibbs correction (hartree)	0.355799
Electronic Energy (hartree)	-4892.179205
Gibbs (kcal/mol)	-3069619.188

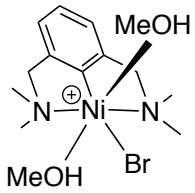

12

6.7
(0.6)

M06L	(TS12)
Enthalpy correction (hartree)	0.428221
Enthalpy (kcal/mol)	-3069552.7593620
Gibbs correction (hartree)	0.352397
Electronic Energy (hartree)	-4892.145766
Gibbs (kcal/mol)	-3069600.3389220

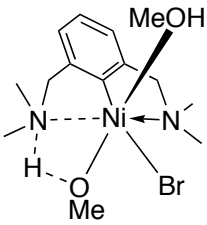

TS12

M06L	(13)
Enthalpy correction (hartree)	0.431695
Enthalpy (kcal/mol)	-3069573.15
Gibbs correction (hartree)	0.350692
Electronic Energy (hartree)	-4892.181736
Gibbs (kcal/mol)	-3069623.980

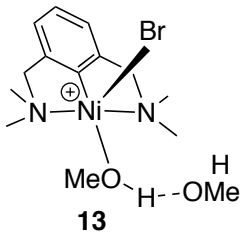

13

1.9
(-1.6)

M06L	(14)
Enthalpy correction (hartree)	0.426309
Enthalpy (kcal/mol)	-3080264.603
Gibbs correction (hartree)	0.34366
Electronic Energy (hartree)	-4909.214522
Gibbs (kcal/mol)	-3080316.466

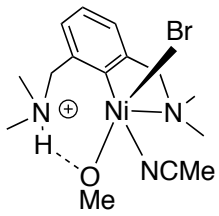

14

M06L	(TS14-OMe)
Enthalpy correction (hartree)	0.4255290
Enthalpy (kcal/mol)	-3080242.6972560
Gibbs correction (hartree)	0.3432450
Electronic Energy (hartree)	-4909.1788314
Gibbs (kcal/mol)	-3080294.3304660

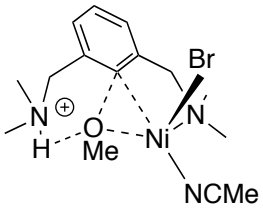

TS14-OMe

M06L	(TS14-Br)
Enthalpy correction (hartree)	0.4226740
Enthalpy (kcal/mol)	-3080240.9337928
Gibbs correction (hartree)	0.3401520
Electronic Energy (hartree)	-4909.1731661
Gibbs (kcal/mol)	-3080292.7163478

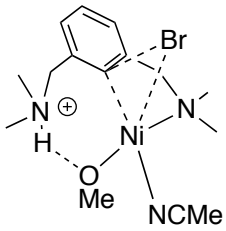

TS14-Br

M06L	(31)
Enthalpy correction (hartree)	0.426581
Enthalpy (kcal/mol)	-3080251.887
Gibbs correction (hartree)	0.342689
Electronic Energy (hartree)	-4909.194529
Gibbs (kcal/mol)	-3080304.529

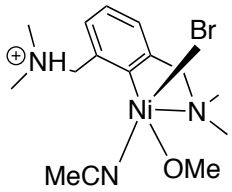

M06L	(32)
Enthalpy correction (hartree)	0.426259
Enthalpy (kcal/mol)	-3080254.0262038
Gibbs correction (hartree)	0.344579
Electronic Energy (hartree)	-4909.197616
Gibbs (kcal/mol)	-3080305.2804038

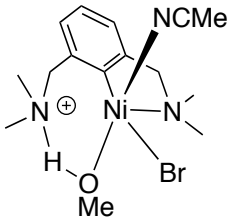

M06L	(36)
Enthalpy correction (hartree)	0.483852
Enthalpy (kcal/mol)	-3152874.97
Gibbs correction (hartree)	0.394452
Electronic Energy (hartree)	-5024.985797
Gibbs (kcal/mol)	-3152931.069

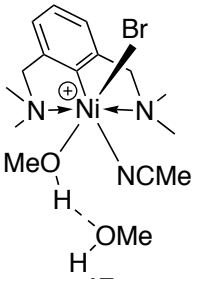

M06L	(TS36)
Enthalpy correction (hartree)	0.476413
Enthalpy (kcal/mol)	-3152864.1987598
Gibbs correction (hartree)	0.388696
Electronic Energy (hartree)	-5024.961192
Gibbs (kcal/mol)	-3152919.2411773

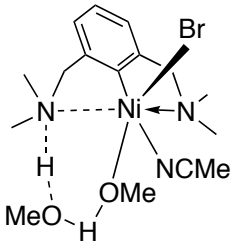

M06L	(37)
Enthalpy correction (hartree)	0.485175
Enthalpy (kcal/mol)	-3152868.024
Gibbs correction (hartree)	0.396053
Electronic Energy (hartree)	-5024.97605
Gibbs (kcal/mol)	-3152923.948

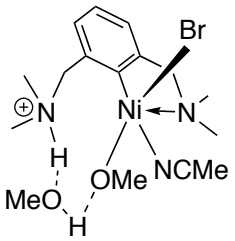

M06L	(33)
Enthalpy correction (hartree)	0.432892
Enthalpy (kcal/mol)	-3069566.014
Gibbs correction (hartree)	0.352775
Electronic Energy (hartree)	-4892.171559
Gibbs (kcal/mol)	-3069616.287

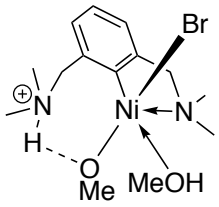

M06L	(TS33-OMe)
Enthalpy correction (hartree)	0.431902
Enthalpy (kcal/mol)	-3069545.0842213
Gibbs correction (hartree)	0.353413
Electronic Energy (hartree)	-4892.137216
Gibbs (kcal/mol)	-3069594.3360688

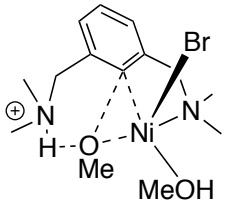

M06L	(TS33-Br)
Enthalpy correction (hartree)	0.4294910
Enthalpy (kcal/mol)	-3069539.5506753
Gibbs correction (hartree)	0.3509250
Electronic Energy (hartree)	-4892.1259861
Gibbs (kcal/mol)	-3069588.8508403

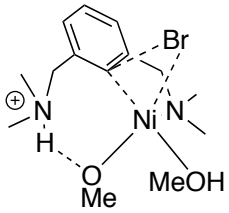

M06L	(34)
Enthalpy correction (hartree)	0.433317
Enthalpy (kcal/mol)	-3069554.244
Gibbs correction (hartree)	0.355101
Electronic Energy (hartree)	-4892.153229
Gibbs (kcal/mol)	-3069603.325

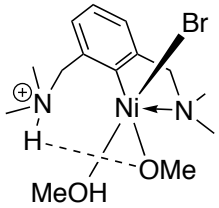

M06L	(35)
Enthalpy correction (hartree)	0.433651
Enthalpy (kcal/mol)	-3069554.624
Gibbs correction (hartree)	0.357091
Electronic Energy (hartree)	-4892.154167
Gibbs (kcal/mol)	-3069602.665

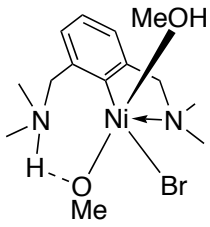

M06L	(15)
Enthalpy correction (hartree)	0.429152
Enthalpy (kcal/mol)	-3080265.324
Gibbs correction (hartree)	0.345838
Electronic Energy (hartree)	-4909.218513
Gibbs (kcal/mol)	-3080317.604

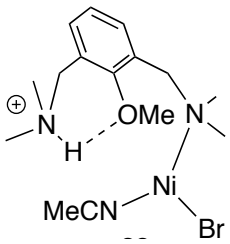

M06L	(30)
Enthalpy correction (hartree)	0.42761
Enthalpy (kcal/mol)	-3080240.119
Gibbs correction (hartree)	0.343696
Electronic Energy (hartree)	-4909.176803
Gibbs (kcal/mol)	-3080292.775

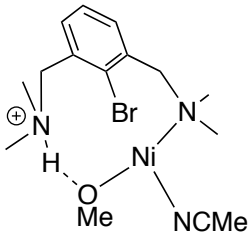

M06L	(41)
Enthalpy correction (hartree)	0.435068
Enthalpy (kcal/mol)	-3069558.85
Gibbs correction (hartree)	0.351133
Electronic Energy (hartree)	-4892.16232
Gibbs (kcal/mol)	-3069611.520

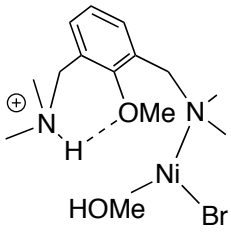

M06L	(42)
Enthalpy correction (hartree)	0.431278
Enthalpy (kcal/mol)	-3069538.544
Gibbs correction (hartree)	0.348735
Electronic Energy (hartree)	-4892.126169
Gibbs (kcal/mol)	-3069590.340

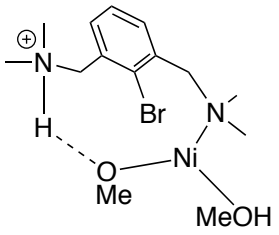

M06L	(16)
Enthalpy correction (hartree)	0.432272
Enthalpy (kcal/mol)	-4695527.674
Gibbs correction (hartree)	0.344831
Electronic Energy (hartree)	-7483.3449
Gibbs (kcal/mol)	-4695582.543

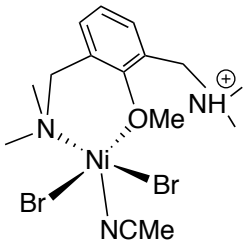

M06L	(45)
Enthalpy correction (hartree)	0.439726
Enthalpy (kcal/mol)	-4684828.471
Gibbs correction (hartree)	0.353787
Electronic Energy (hartree)	-7466.301831
Gibbs (kcal/mol)	-4684882.398

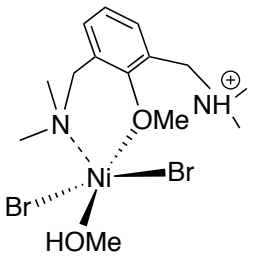

M06L	(22)
Enthalpy correction (hartree)	0.439335
Enthalpy (kcal/mol)	-3067792.563
Gibbs correction (hartree)	0.357106
Electronic Energy (hartree)	-4889.351786
Gibbs (kcal/mol)	-3067844.162

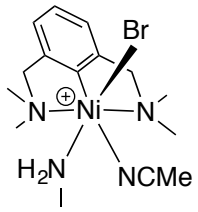

M06L	(TS22)
Enthalpy correction (hartree)	0.506586
Enthalpy (kcal/mol)	-3127908.7305838
Gibbs correction (hartree)	0.418054
Electronic Energy (hartree)	-4985.221695
Gibbs (kcal/mol)	-3127964.2844138

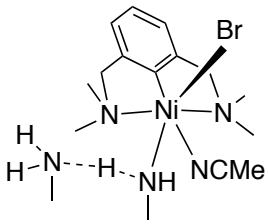

M06L	(23)
Enthalpy correction (hartree)	0.509098
Enthalpy (kcal/mol)	-3127907.275
Gibbs correction (hartree)	0.419398
Electronic Energy (hartree)	-4985.2218867
Gibbs (kcal/mol)	-3127963.562

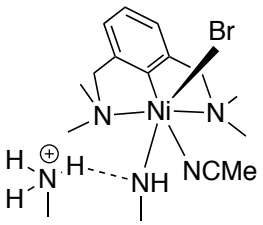

M06L	(24)
Enthalpy correction (hartree)	0.423568
Enthalpy (kcal/mol)	-3067489.961
Gibbs correction (hartree)	0.342623
Electronic Energy (hartree)	-4888.8537849
Gibbs (kcal/mol)	-3067540.754

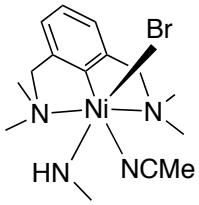

M06L	(TS24-NHMe)
Enthalpy correction (hartree)	0.422838
Enthalpy (kcal/mol)	-3067476.9585518
Gibbs correction (hartree)	0.340239
Electronic Energy (hartree)	-4888.832334
Gibbs (kcal/mol)	-3067528.7894243

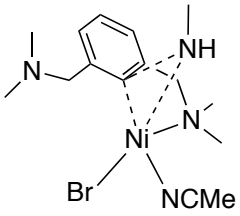

M06L	(TS24-Br)
Enthalpy correction (hartree)	0.421011
Enthalpy (kcal/mol)	-3067453.045
Gibbs correction (hartree)	0.335752
Electronic Energy (hartree)	-4888.7923980
Gibbs (kcal/mol)	-3067506.545

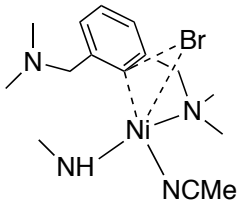

M06L	(25)
Enthalpy correction (hartree)	0.427168
Enthalpy (kcal/mol)	-3067509.629
Gibbs correction (hartree)	0.342999
Electronic Energy (hartree)	-4888.888728
Gibbs (kcal/mol)	-3067562.445

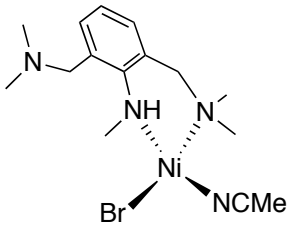

M06L	(46)
Enthalpy correction (hartree)	0.423145
Enthalpy (kcal/mol)	-3067458.915
Gibbs correction (hartree)	0.336641
Electronic Energy (hartree)	-4888.8038867
Gibbs (kcal/mol)	-3067513.197

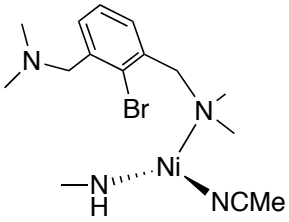

M06L	(17)
Enthalpy correction (hartree)	0.4160450
Enthalpy (kcal/mol)	-1475622.1034613
Gibbs correction (hartree)	0.3384490
Electronic Energy (hartree)	-2352.0050545
Gibbs (kcal/mol)	-1475670.7949513

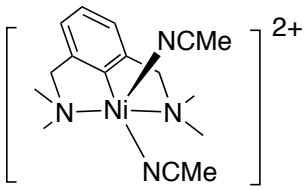

M06L	(18)
Enthalpy correction (hartree)	0.4754460
Enthalpy (kcal/mol)	-1548226.2111670
Gibbs correction (hartree)	0.3877030
Electronic Energy (hartree)	-2467.7682128
Gibbs (kcal/mol)	-1548281.2698995

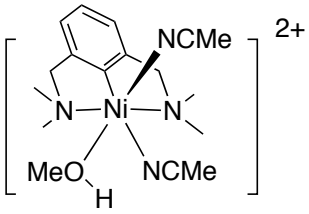

M06L	(19)
Enthalpy correction (hartree)	0.475379
Enthalpy (kcal/mol)	-1548224.604
Gibbs correction (hartree)	0.387894
Electronic Energy (hartree)	-2467.7655838
Gibbs (kcal/mol)	-1548279.5

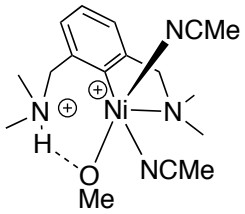

M06L	TS19
Enthalpy correction (hartree)	0.475029
Enthalpy (kcal/mol)	-1548207.859
Gibbs correction (hartree)	0.387289
Electronic Energy (hartree)	-2467.7385494
Gibbs (kcal/mol)	-1548262.916

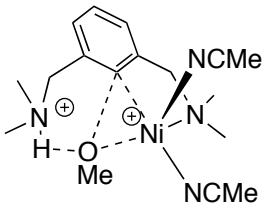

M06L	(20)
Enthalpy correction (hartree)	0.478872
Enthalpy (kcal/mol)	-1548229.653
Gibbs correction (hartree)	0.3907
Electronic Energy (hartree)	-2467.7771242
Gibbs (kcal/mol)	-1548284.981

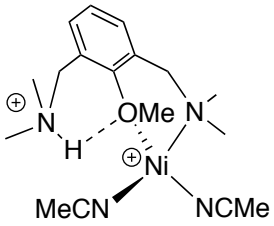

M06L	(21)
Enthalpy correction (hartree)	0.53191
Enthalpy (kcal/mol)	-1631447.294
Gibbs correction (hartree)	0.435072
Electronic Energy (hartree)	-2600.4479170
Gibbs (kcal/mol)	-1631508.06

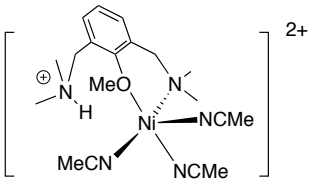

M06L	(26)
Enthalpy correction (hartree)	0.4896030
Enthalpy (kcal/mol)	-1535757.1228368
Gibbs correction (hartree)	0.4033200
Electronic Energy (hartree)	-2447.9113127
Gibbs (kcal/mol)	-1535811.2654193

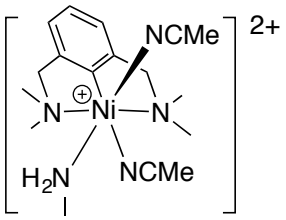

M06L	(TS26)
Enthalpy correction (hartree)	0.556649
Enthalpy (kcal/mol)	-1595876.506
Gibbs correction (hartree)	0.464483
Electronic Energy (hartree)	-2543.7861410
Gibbs (kcal/mol)	-1595934.34

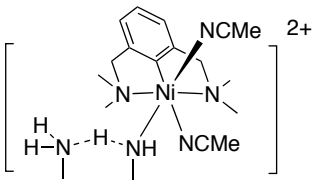

M06L	(27)
Enthalpy correction (hartree)	0.558812
Enthalpy (kcal/mol)	-1595875.216
Gibbs correction (hartree)	0.465425
Electronic Energy (hartree)	-2543.7862471
Gibbs (kcal/mol)	-1595933.816

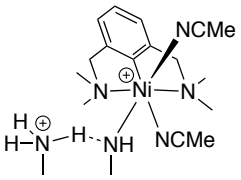

M06L	(28)
Enthalpy correction (hartree)	0.4733430
Enthalpy (kcal/mol)	-1535458.8457318
Gibbs correction (hartree)	0.3856710
Electronic Energy (hartree)	-2447.4197107
Gibbs (kcal/mol)	-1535513.8599118

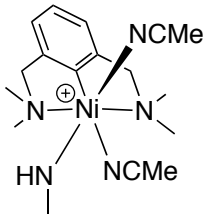

M06L	(TS28)
Enthalpy correction (hartree)	0.473571
Enthalpy (kcal/mol)	-1535448.948
Gibbs correction (hartree)	0.388158
Electronic Energy (hartree)	-2447.4041652
Gibbs (kcal/mol)	-1535502.545

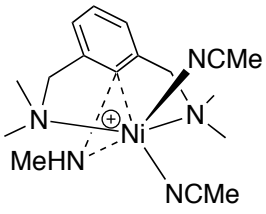

M06L	(TS28a)
Enthalpy correction (hartree)	0.471919
Enthalpy (kcal/mol)	-1535445.923
Gibbs correction (hartree)	0.383036
Electronic Energy (hartree)	-2447.3976933
Gibbs (kcal/mol)	-1535501.697

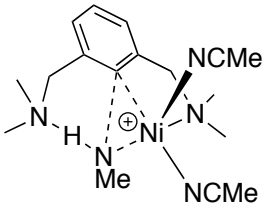

M06L	(29)
Enthalpy correction (hartree)	0.4760190
Enthalpy (kcal/mol)	-1535482.4714205
Gibbs correction (hartree)	0.3862670
Electronic Energy (hartree)	-2447.4600372
Gibbs (kcal/mol)	-1535538.7908005

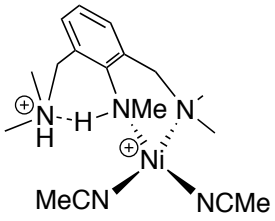

M06L	Ni(IV)
Enthalpy correction (hartree)	0.377833
Enthalpy (kcal/mol)	-4612176.098
Gibbs correction (hartree)	0.303997
Electronic Energy (hartree)	-7350.459264
Gibbs (kcal/mol)	-4612222.430

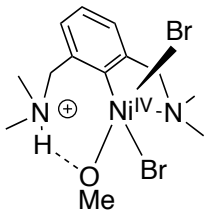

M06L	(43)
Enthalpy correction (hartree)	0.492011
Enthalpy (kcal/mol)	-3142169.946
Gibbs correction (hartree)	0.404334
Electronic Energy (hartree)	-5007.93415610
Gibbs (kcal/mol)	-3142224.963

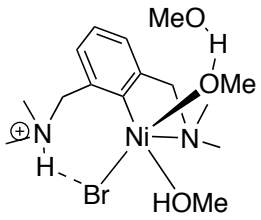

43

M06L	(TS43)
Enthalpy correction (hartree)	0.487406
Enthalpy (kcal/mol)	-3142141.283
Gibbs correction (hartree)	0.400544
Electronic Energy (hartree)	-5007.8838726
Gibbs (kcal/mol)	-3142195.789

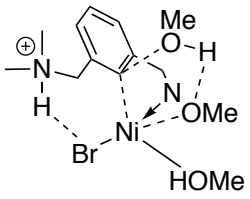

TS43

M06L	(44)
Enthalpy correction (hartree)	0.493215
Enthalpy (kcal/mol)	-3142170.156
Gibbs correction (hartree)	0.405677
Electronic Energy (hartree)	-5007.935695
Gibbs (kcal/mol)	-3142225.086

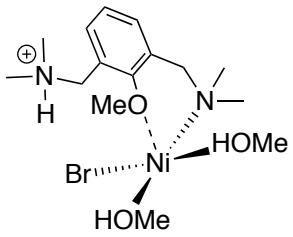

44

M06L	C-H arylated Ni^{III}
Enthalpy correction (hartree)	0.424841
Enthalpy (kcal/mol)	-3080247.729
Gibbs correction (hartree)	0.346521
Electronic Energy (hartree)	-4909.186163
Gibbs (kcal/mol)	-3080296.875

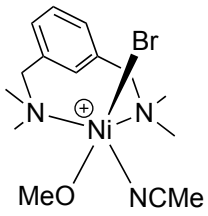

4.7 REFERENCES

[1] (a) Terrett, J. A.; Cuthbertson, J. D.; Shurtleff, V. W.; MacMillan, D. W. Switching on Elusive Organometallic Mechanisms with Photoredox Catalysis. *Nature* **2015**, *524* (7565), 330–334. (b) Lim, C.-H.; Kudisch, M.; Liu, B.; Miyake, G. M. C–N Cross-Coupling via Photoexcitation of Nickel–Amine Complexes. *J. Am. Chem. Soc.* **2018**, *140* (24), 7667–7673. (c) Martinez, G. E.; Nugent, J. W.; Fout, A. R. Simple Nickel Salts for the Amination of (Hetero)Aryl Bromides and Iodides with Lithium Bis(Trimethylsilyl)Amide. *Organometallics* **2018**, 37, 2941-2944. (d) Green, R. A.; Hartwig, J. F. Nickel-Catalyzed Amination of Aryl Chlorides with Ammonia or Ammonium Salts. *Angew. Chem. Int. Ed.* **2015**, *54* (12), 3768–3772. (e) Borzenko, A.; Rotta-Loria, N. L.; MacQueen, P. M.; Lavoie, C. M.; McDonald, R.; Stradiotto, M. Nickel-Catalyzed Monoarylation of Ammonia. *Angew. Chem. Int. Ed.* **2015**, *54* (12), 3773–3777.

[2] (a) Koo, K.; Hillhouse, G. L. Carbon-Nitrogen Bond Formation by Reductive Elimination from Nickel(II) Amido Alkyl Complexes. *Organometallics* **1995**, *14* (9), 4421–4423. (b) Han, R.; Hillhouse, G. L. Carbon−Oxygen Reductive-Elimination from Nickel(II) Oxametallacycles and Factors That Control Formation of Ether, Aldehyde, Alcohol, or Ester Products. *J. Am. Chem. Soc.* **1997**, *119* (34), 8135–8136. (c) Lin, B. L.; Clough, C. R.; Hillhouse, G. L. Interactions of Aziridines with Nickel Complexes:

Oxidative-Addition and Reductive-Elimination Reactions That Break and Make C−N Bonds. *J. Am. Chem. Soc.* **2002**, *124* (12), 2890–2891

[3] (a) Zhou, W.; Schultz, J. W.; Rath, N. P.; Mirica, L. M. Aromatic Methoxylation and Hydroxylation by Organometallic High-Valent Nickel Complexes. *J. Am. Chem. Soc.* **2015**, *137* (24), 7604–7607. (b) Zhou, W.; Rath, N. P.; Mirica, L. M. Oxidatively-Induced Aromatic Cyanation Mediated by Ni(III). *Dalton Trans.* **2016**, *45* (21), 8693–8695. (c) Zhou, W.; Watson, M. B.; Zheng, S.; Rath, N. P.; Mirica, L. M. Ligand Effects on the Properties of Ni(III) Complexes: Aerobically-Induced Aromatic Cyanation at Room Temperature. *Dalton Trans.* **2016**, *45* (40), 15886–15893.

[4] (a) Camasso, N. M.; Sanford, M. S. Design, Synthesis, and Carbon-Heteroatom Coupling Reactions of Organometallic Nickel(IV) Complexes. *Science* **2015**, *347* (6227), 1218–1220. (b) D'Accriscio, F.; Borja, P.; Saffon-Merceron, N.; Fustier-Boutignon, M.; Mezailles, N.; Nebra, N. C-H Bond Trifluoromethylation of Arenes Enabled by a Robust, High-Valent Nickel(IV) Complex. *Angew. Chem. Int. Ed.* **2017**, *56* (42), 12898–12902.

[5]Cloutier, J.-P.; Vabre, B.; Moungang-Soumé, B.; Zargarian, D. Synthesis and Reactivities of New NCN-Type Pincer Complexes of Nickel. *Organometallics* **2015**, *34* (1), 133–145.

[6] Cloutier, J.-P.; Zargarian, D. *Organometallics* **2018**, *37* (9), 1446–1455.

[7] This trivalent complex was introduced over three decades ago by van Koten's group: Grove, D. M.; Van Koten, G.; Zoet, R.; Murrall, N. W.; Welch, A. J. *J. Am. Chem. Soc.* **1983**, *105* (5), 1379–1380.

[8] Grove, D. M.; Van Koten, G.; Ubbels, H. J. C.; Zoet, R.; Spek, A. L. *Organometallics* **1984**, *3* (7), 1003–1009.

[9] (a) Baho, N.; Zargarian, D. *Inorg. Chem.* **2007**, *46*, 7621-7632. (b) Lapointe, S.; Vabre, B.; Zargarian, D. *Organometallics* **2015**, *34* (14), 3520–3531. (c) Lefèvre, X.; Spasyuk, D. M.; Zargarian, D. *J. Organomt. Chem.* **2011**, *696*, 864-870. (d) Wang, R.; Groux, L. F.; Zargarian, D. *Organometallics* **2002,**

21, 5531-5539. (e) Spasyuk, D. M.; Gorelsky, S. I.; van der Est, A.; Zargarian, D. *Inorg. Chem*. **2011**, *50*, 2661–2674. (f) Groux, L. F.; Zargarian, D. *Organometallics*, **2003**, *22* (15), pp 3124–3133.

[10] For example, the Ni-N_{NCMe} distances in **3** are longer by ca. 16 esd in the axial positions than in the equatorial plane; this is attributed to the partial anti-bonding character of the axial interactions involving the singly-occupied d_{z2} orbital.

[11] Grove, D. M.; van Koten, G.; Mul, W. P.; van der Zeijden, A. A. H.; Terheijden, J. *Organometallics* **1986**, *5*, 322.

[12] Stol, M.; Snelders, D. J. M.; Godbole, M. D.; Havenith, R. W. A.; Haddleton, D.; Clarkson, G.; Lutz, M.; Spek, A. L.; van Klink, G. P. M.; van Koten, G. *Organometallics* **2007**, *26* (16), 3985–3994.

[13] Lin, W.; Bodenstein, T.; Mereacre, V.; Fink, K.; Eichhofer, A. *Inorg. Chem.* **2016**, *55* (5), 2091–2100.

[14] Amine oxidation by ferrocenium is reported in the literature see: Torriero, A. A. J.; Shiddiky, M. J. A.; Burgar, I.; Bond, A. M. *Organometallics* **2013**, *32* (20), 5731–5739.

[15] We did not calculate the proton shuttle pathway for **8** for the following reason: the adduct **8**(MeOH) corresponding to complex **8** with another MeOH in the second coordination sphere is located 8.94 kcal/mol above reactants which is already higher than **TS6**.

[16] Chong, E.; Kampf, J. W.; Ariafard, A.; Canty, A. J.; Sanford, M. S. *J. Am. Chem. Soc.* **2017**, *139* (17), 6058–6061. (b) Zhou, W.; Zheng, S.; Schultz, J. W.; Rath, N. P.; Mirica, L. M. *J. Am. Chem. Soc.* **2016**, *138* (18), 5777–5780.

[17] (a) Hascall, T.; Rabinovich, D.; Murphy, V. J.; Beachy, M. D.; Friesner, R. A.; Parkin, G. *J. Am. Chem. Soc.* **1999**, *121* (49), 11402–11417. (b) Abu-Hasanayn, F.; Krogh-Jespersen, K.; Goldman, A. S. *J. Am. Chem. Soc.* **1993**, *115* (18), 8019–8023. (c) Bender, B. R.; Kubas, G. J.; Jones, L. H.; Swanson, B. I.; Eckert, J.; Capps, K. B.; Hoff, C. D. *J. Am. Chem. Soc.* **1997**, *119* (39), 9179–9190.

[18] It is interesting to note that the feasibility of C-N oxidative addition to an in-situ generated monovalent nickel species has been demonstrated in a very recent report: Cao, Z.-C.; Xie, S.-J.; Fang, H.; Shi, Z.-J. Ni-Catalyzed Cross-Coupling of Dimethyl Aryl Amines with Arylboronic Esters under Reductive Conditions. *J. Am. Chem. Soc.* **2018**, *140* (42), 13575–13579.

[19] Vabre, B.; Lambert, M. L.; Petit, A.; Ess, D. H.; Zargarian, D. *Organometallics* **2012**, *31*, 6041–6053.

[20] Yamamoto, Y.; Chen, X.; Kojima, S.; Ohdoi, K.; Kitano, M.; Doi, Y.; Akiba, K. *J. Am. Chem. Soc.* **1995,** *117*, 3922-3932.

[21] Frisch, M. J.; Trucks, G. W.; Schlegel, H. B.; Scuseria, G. E.; Robb, M. A.; Cheeseman, J. R.; Scalmani, G.; Barone, V.; Mennucci, B.; Petersson, G. A.; Nakatsuji, H.; Caricato, M.; Li, X.; Hratchian, H. P.; Izmaylov, A. F.; Bloino, J.; Zheng, G.; Sonnenberg, J. L.; Hada, M.; Ehara, M.; Toyota, K.; Fukuda, R.; Hasegawa, J.; Ishida, M.; Nakajima, T.; Honda, Y.; Kitao, O.; Nakai, H.; Vreven, T.; Montgomery, J. A., Jr.; Peralta, J. E.; Ogliaro, F.; Bearpark, M. J.; Heyd, J.; Brothers, E. N.; Kudin, K. N.; Staroverov, V. N.; Kobayashi, R.; Normand, J.; Raghavachari, K.; Rendell, A. P.; Burant, J. C.; Iyengar, S. S.; Tomasi, J.; Cossi, M.; Rega, N.; Millam, N. J.; Klene, M.; Knox, J. E.; Cross, J. B.; Bakken, V.; Adamo, C.; Jaramillo, J.; Gomperts, R.; Stratmann, R. E.; Yazyev, O.; Austin, A. J.; Cammi, R.; Pomelli, C.; Ochterski, J. W.; Martin, R. L.; Morokuma, K.; Zakrzewski, V. G.; Voth, G. A.; Salvador, P.; Dannenberg, J. J.; Dapprich, S.; Daniels, A. D.; Farkas, Ö.; Foresman, J. B.; Ortiz, J. V.; Cioslowski, J.; Fox, D. J. *Gaussian 09, Revision B.01*; Gaussian, Inc.: Wallingford, CT, USA,

[22] Zhao, Y.; Truhlar, D. G. A new local density functional for main-group thermochemistry, transition metal bonding, thermochemical kinetics, and noncovalent interactions. *J. Chem. Phys* **2006**, *125*, 194101. b) Zhao, Y.; Truhlar, D. G. Density Functionals with Broad Applicability in Chemistry. *Acc. Chem. Res* **2008**, *41*, 157. c) Zhao, Y.; Truhlar, D. The M06 suite of density functionals for main group thermochemistry, thermochemical kinetics, noncovalent interactions, excited states, and transition elements: two new functionals and systematic testing of four M06-class functionals and 12 other functionals. *Theor Chem Acc* **2008**, *120*, 215. For basis sets see: d) Hay, P. J.; Wadt, W. R. Ab initio effective core potentials for molecular calculations. Potentials for the transition metal atoms Sc to Hg. *J. Chem. Phys.* **1985**, *82*, 270. e) Weigend, F.; Ahlrichs, R. Balanced basis sets of split valence, triple zeta valence and quadruple zeta valence quality for H to Rn: Design and assessment of accuracy. *Phys.*

Chem. Chem. Phys. **2005**, *7*, 3297. For the SMD model see: f) Marenich, A. V.; Cramer, C. J.; Truhlar, D. G. Universal solvation model based on solute electron density and on a continuum model of the solvent defined by the bulk dielectric constant and atomic surface tensions. *J. Phys. Chem. B* **2009**, *113*, 6378.

[23] CYLview, 1.0b; Legault, C. Y., Université de Sherbrooke, 2009 (http://www.cylview.org)

[24] Bartmess, J. E. *J. Phys. Chem.* **1994**, *98* (25), 6420–6424.

[25] Namazian, M.; Lin, C. Y.; Coote, M. L. *J. Chem. Theory Comput.* **2010**, *6* (9), 2721–2725.

Chapitre 5: Conclusion et Perspectives

Il est maintenant bien établi que les états d'oxydation +III et +IV du nickel sont non seulement accessibles mais aussi capable de promouvoir la formation de liens carbone-hétéroatomes. La construction d'un ligand possédant de bons donneurs σ comme les ligands anioniques alkyles et aryles ou neutre comme les amines et pyridines semblent favoriser la formation de nickels haut-valent. Ainsi le ligand NCN contenant deux bras pyrazoles était un excellent candidat, susceptible de permettre d'isoler et caractériser de nouveaux complexes de Ni^{III} et Ni^{IV}. Malheureusement, deux caractéristiques de cette plateforme compliquent les choses. D'abord la planarité du ligand rend le complexe issu de la nickellation peu soluble et son oxydation problématique. Les poudres obtenues après avoir traité le complexe de Ni^{II} avec $CuBr_2$, Br_2 et N-bromosuccinimide sont complètement insolubles dans la plupart des solvants organiques et donc difficiles à caractériser. Ensuite, l'introduction de groupements électrodonneurs comme méthoxylate sur le cycle aromatique ou de groupements alkyles sur les pyrazoles fait dramatiquement chuter les rendements de nickellation.

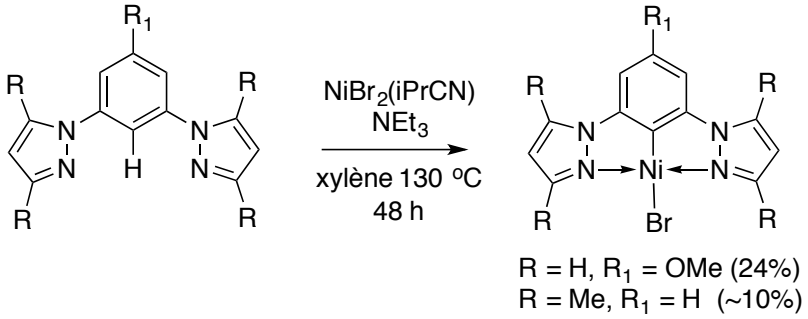

Schéma 5.1 Synthèse de complexes pinceurs NCN substitués

L'utilisation de pyrazole substitué avec des groupements électroattracteurs CF_3 permettrait d'accroitre la solubilité du complexe et possiblement le rendement de nickellation. Le schéma 5.2 décrit la voie synthétique.[1] Le complexe obtenu peut être ensuite oxydé avec le réactif approprié et sa réactivité peut être étudiée.

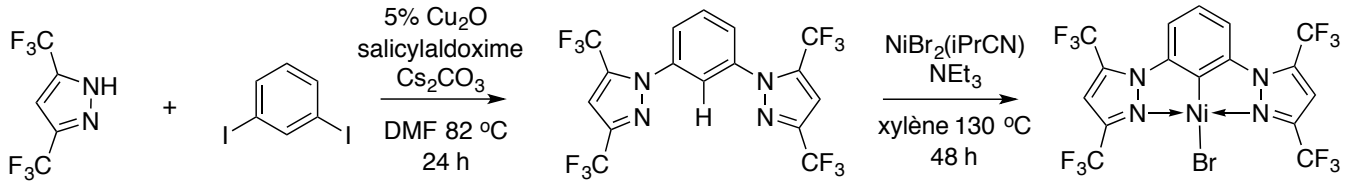

Schéma 5.2 Synthèse de complexes pinceurs NCN substitués

Malgré qu'il n'ait pas été possible d'isoler un complexe de nickel trivalent, sa réactivité face aux alcools et amines en condition aérobique laisse croire à la participation d'un Ni^{III} cationique. Les rendements pour la formation de liens C-O avec les alcools sont relativement bons (65-77%) sauf pour le trifluorométhanol qui ne donne que 15% de produit fonctionnalisé et majoritairement du ligand.

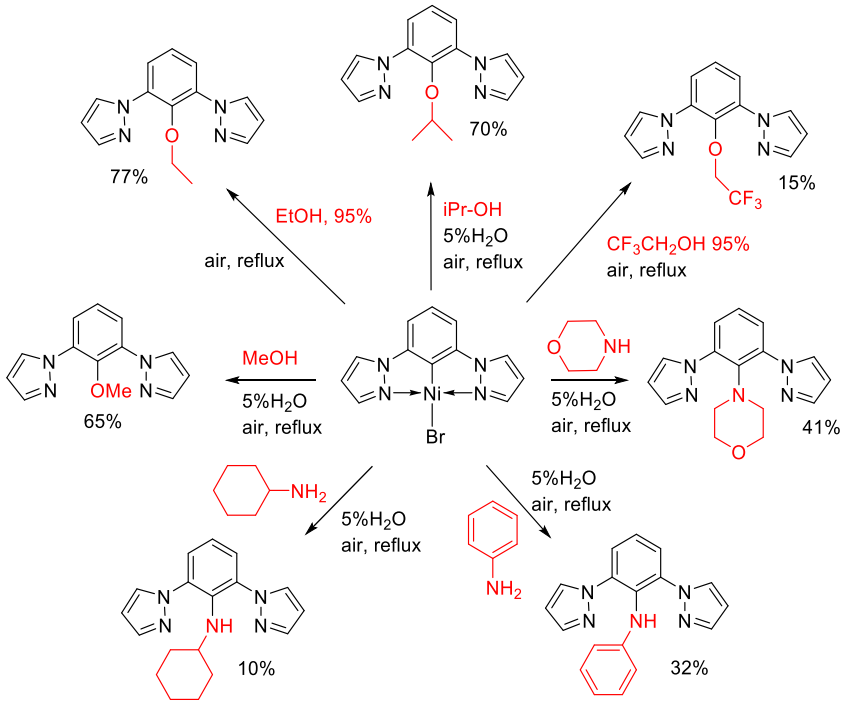

Schéma 5.3. Formation de lien C-O et C-N à partir du complexe NCN pyrazole

Le mécanisme de la réaction de couplage à partir du Ni^{II} reste nébuleux et il serait intéressant d'en connaitre les principales étapes. Des expériences préliminaires montrent que le système $(NCN_{NMe2})Ni^{II}Br$ possède une réactivité semblable. La comparaison des vitesses de fonctionnalisation de ces deux systèmes peut fournir de précieux indices sur le mécanisme. De façon parallèle, l'ajout de groupements éléctoattracteurs/donneurs sur le cycle aromatique du ligand permettrait d'influencer les vitesses de formation des liens C-O et C-N. Par exemple, si l'oxydation en Ni^{III} cationique a bel et bien lieu, un groupement ED devrait stabiliser la charge qui se développe sur le centre métallique. Cette stabilisation doit accélérer la vitesse de réaction en diminuant l'énergie d'activation de cette étape. Une variation de vitesse indiquerait donc que cette étape constitue l'étape limitante où qu'elle a lieu avant l'étape limitante.

Il a aussi été possible d'isoler un complexe Ni^{II} de type alcoolate. L'oxydation de ce dernier à l'aide de Br_2 et H_2O_2 n'a pu mener à des complexes de Ni^{III} alcoolates bien définis. L'encombrement stérique engendrée par le ligand BHT pourrait cependant empêcher l'élimination réductrice de ce dernier et ainsi permettre d'isoler un complexe cationique trivalent du nickel. La cyclovoltampérométrie montre que le ferrocénium serait suffisant pour lui enlever un électron (-73 mV par rapport au couple ferrocène/ferrocénium).

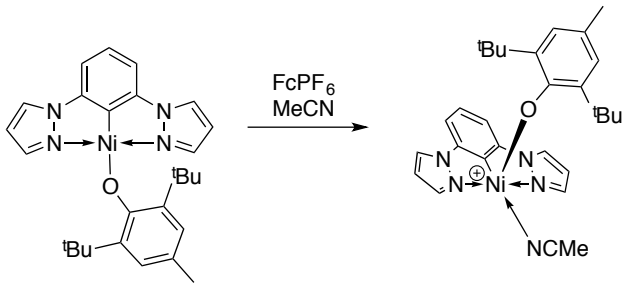

Schéma 5.4. Synthèse d'un complexe de Ni^{III} alcoolate cationique

La fonctionnalisation C-O, C-N et C-halogène du lien C-Ni^{III} lorsque le complexe $(NCN_{NMe2})Ni^{III}Br_2$ est traité sous azote, avec des alcools aliphatiques, des amines primaires et des acides forts supporte l'hypothèse qu'un intermédiaire de nickel trivalent est impliqué dans la fonctionnalisation à partir du Ni^{II}. La formation de NC(OH)N à partir H_2O et $NC(NH_2)N$ partir d'une solution aqueuse de NH_3 sont particulièrement intéressantes puisque l'activation de ces deux molécules est souvent difficile. Les observations suivantes ont permis la proposition d'un mécanisme de fonctionnalisation. Le potentiel d'oxydation élevé (0.69 mV par rapport au Fc/Fc^+) du complexe Ni^{III} étudié rend la participation d'un intermédiaire de Ni^{IV} peu probable spécialement en l'absence d'oxydant externe. Une réaction de comproportionation entre un Ni^{III} et un intermédiaire Ni^{III} plus facile à oxyder est possible. Cependant un suivi cinétique montre que l'ordre réactionnel du Ni^{III} est 1, il est donc possible de mettre cette hypothèse de côté. La participation du ligand dans la déprotonation du substrat est appuyée par deux observations. D'abord la formation du lien C-O ne nécessite pas de base externe. Ensuite la valeur de l'effet cinétique isotopique $k_{obs}(H) / k_{obs}(D)$ de 0.47 indique que la déprotonation est le résultat d'un ou plusieurs pré-équilibres ayant lieu avant l'étape limitante. Deux options ont été envisagées pour la formation de lien C-X étudiée au chapitre 3, soit l'attaque directe sur le carbone du lien C-Ni, soit la coordination du substrat suivi de l'élimination réductrice. La réaction (éq. 1) illustrée au schéma suivant indique que la formation du lien C-Br est probablement dû à une élimination réductrice. Le temps de réaction avec HBF_4 est très similaire à celui avec HBr (30 minutes) alors que le mélange réactionnel ne contient que 2 équivalents

d'ions bromure. Une attaque de l'extérieure verrait sa vitesse dépendre de la concentration en Br^-. Aucune formation de lien C-Br n'est observée en milieu aprotique indiquant l'importance de la protonation du bras azoté (2).

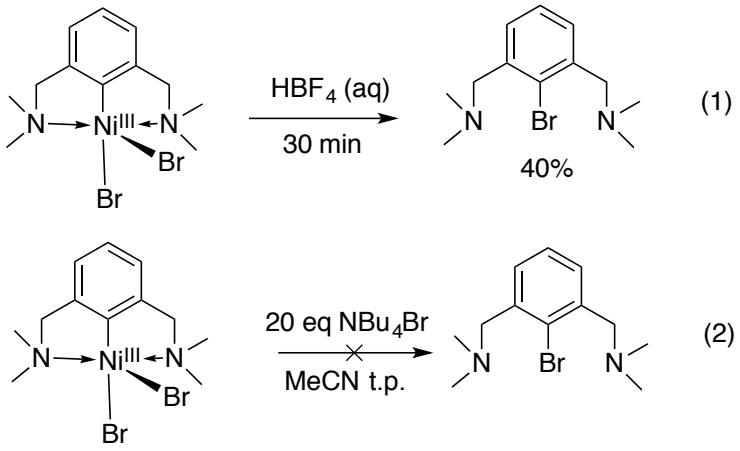

Schéma 5.5. (1) Réaction de $(NCN_{NMe2})Ni^{III}Br_2$ avec HBF_4 (2) avec un large excès de Br^-

Les observations ci-dessus ont permis la proposition de mécanismes pour la formation de lien C-O et C-N illustré au schéma 5.6. D'abord la coordination du substrat au centre métallique a lieu rendant ce dernier plus acide. Les alcools sont déprotonnés par le bras du ligand alors que les amines le sont par une seconde molécule de substrat. La formation du lien C-O et C-N par élimination réductrice génère ensuite un nickel monovalent. Le Ni^I ainsi généré est suceptible de réagir avec un Ni^{III} pour former un complexe de Ni^{II}, cette hypothèse est appuyée par le fait que le rendement ne dépasse pas les 50% et que la réaction de $(NCN_{NMe2})Ni^{III}Br_2$ avec MeOH sous azote génère environ 50% de $(NCN_{NMe2})Ni^{II}Br$.

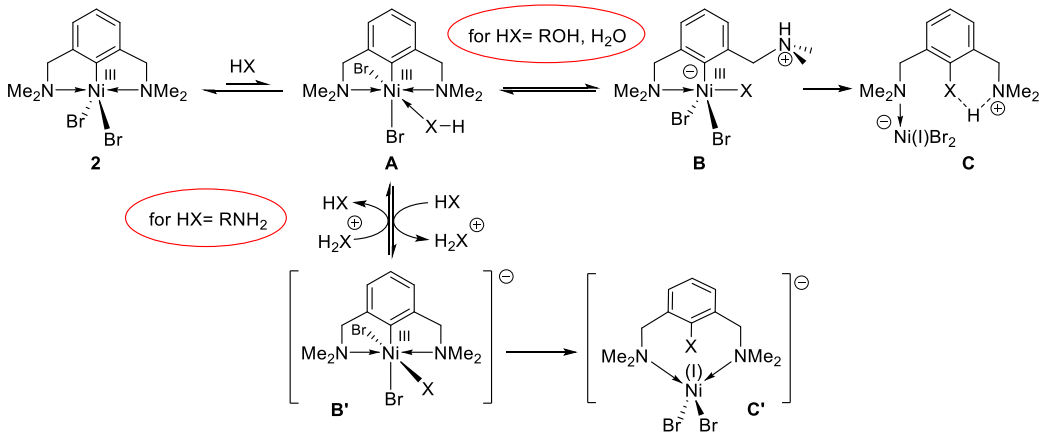

Schéma 5.6. Mécanismes de réaction pour la formation de lien C-O et C-N

À l'image de McMillan, nous avons proposé l'intervention d'un Ni^{III} cationique comme espèce active dans la formation de lien C-O à partir de Ni^{II}. Il se trouve qu'un complexe cationique de Ni^{II} traité avec du MeOH en présence d'O_2 (air) forme aussi le produit NC(OMe)N (Schéma 5.7).

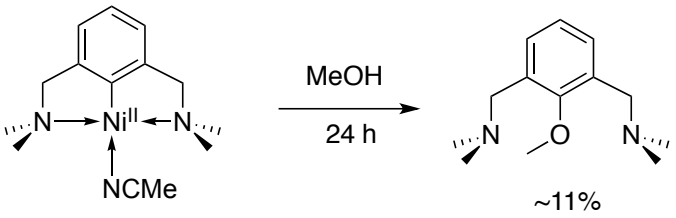

Schéma 5.7. Formation d'un lien C-O à partir d'un Ni^{II} cationique

Cette observation implique la formation d'un Ni^{III} dicationique comme intermédiaire réactionnel. Le chapitre 4 a montré comment il est possible, à partir du complexe neutre $(NCN_{NMe2})Ni^{III}Br_2$, d'isoler un complexe cationique et un complexe dicationique de Ni^{III}. En traitant le complexe neutre trivalent avec 2 équivalents de sels d'argent on obtient le complexe Ni^{III} dicationique. Ce complexe possède la géométrie octaédrique avec la configuration électronique d^7. La RPE confirme la présence d'un seul électron célibataire localisé principalement dans une orbitale appartenant majoritairement au centre métallique. Le complexe cationique a été obtenu en faisant réagir 1 équivalent du complexe dicationique avec 1 équivalent du complexe neutre. Le complexe obtenu est de géométrie pyramide à base carrée, l'électron célibataire est localisé dans une orbitale partagée entre le centre métallique et le ligand bromure.

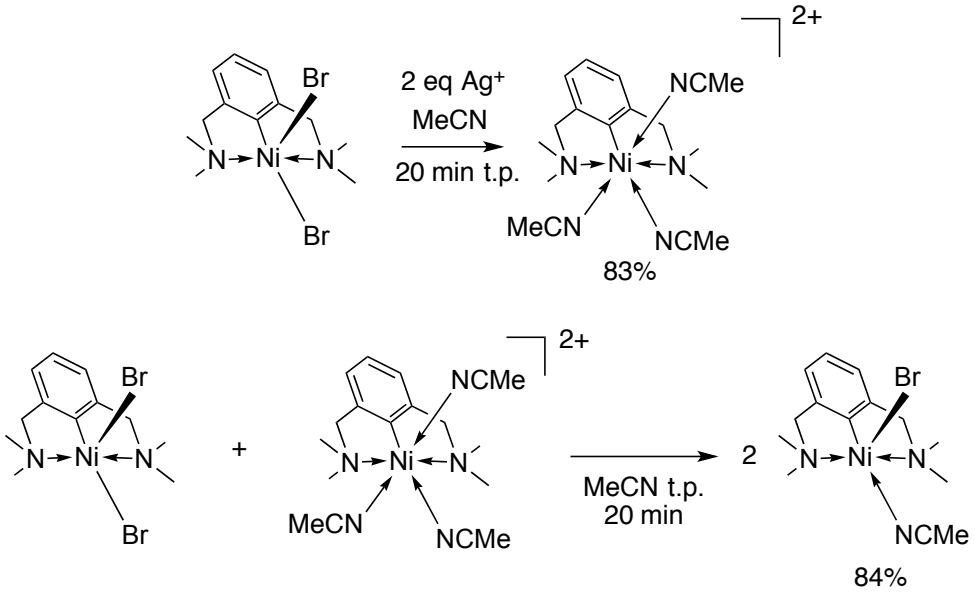

Schéma 5.8. Synthèse de complexes de Ni^{III} cationique et dicationique

Les complexes obtenus réagissent comme prévu face au alcools et amines. Un suivi RMN ^{1}H montre que le rendement maximal de la réaction sous azote avec CD_3OD est 50%. Le suivi montre aussi la formation de $[(NCN)Ni^{II}(MeCN)]^{+}$ appuyant l'hypothèse d'une réaction de comproportionation entre le Ni^{I} issu de l'élimination réductrice et le complexe cationique/dicationique de départ. Un suivi cinétique montre un $k_{obs}(H) / k_{obs}(D)$ de 0.62. La cinétique et la thermodynamique des étapes proposées au chapitre 3 ont été calculées par DFT.

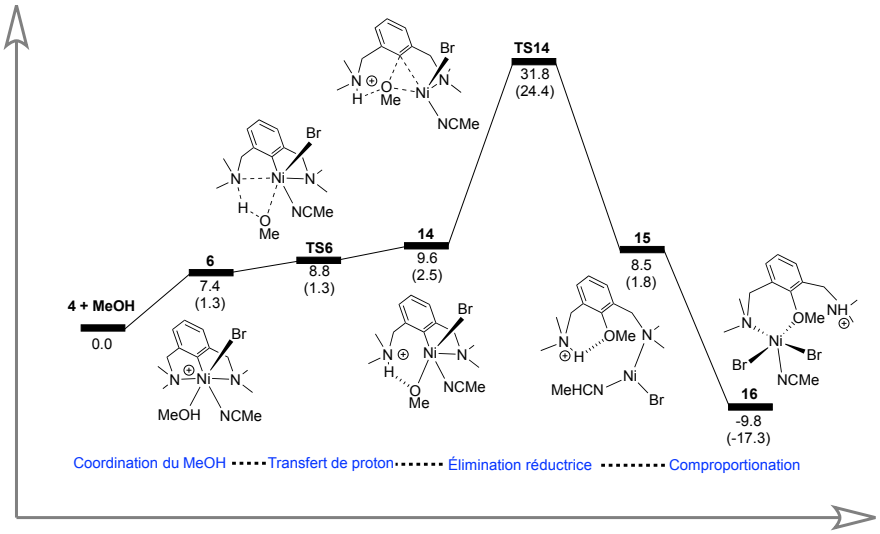

Schéma 5.8. Surface d'énergie potentielle (Gibbs) pour la réaction du complexe monocationique avec MeOH

La DFT montre que la coordination du MeOH au centre métallique est difficile thermodynamiquement. La déprotonation par le bras azoté est facile avec une barrière énergétique de 9 kcal/mol. L'élimination réductrice de l'alcoolate est l'étape limitante avec une barrière de 32 kcal/mol. Le processus redox entre le nickel monovalent généré par la formation du lien C-O et le complexe de départ rend le procédé viable thermodynamiquement. La DFT a aussi permis de rationaliser l'effet isotopique inverse en montrant que l'apparition de nouveaux modes de vibration de basse énergie (cisaillement, bascule et torsion) due à la coordination du MeOH/CD_3OD favorise la coordination du CD_3OD. Ceci fait accroitre la concentration des intermédiaires deutérés **6** et **14** sur le schéma et donc la vitesse de réaction. La DFT montre aussi que la réaction est plus rapide à partir du dication tel qu'observé de façon expérimentale.

Un des grands inconvénients des réactions de fonctionnalisation présentées dans la présente thèse souffrent généralement de mauvais rendements. Le rendement des réactions des Ni^{III} neutres, cationiques et dicationiques est affaiblie par la réaction de comproportionation Ni^{I}/Ni^{III}. Une façon de pallier cette tare

serait d'ajouter un oxydant capable d'oxyder le Ni^{I} en Ni^{II} afin d'empêcher le processus rédox secondaire. Les expériences de fonctionnalisation en conditions aérobiques semblent montrer que l'oxygène n'est pas suffisant pour éliminer le Ni^{I} et que les meilleurs rendements sont simplement dûs à la capacité du $[(NCN)Ni^{II}(MeCN)]^{+}$ à effectuer le couplage C-O. Des expériences préliminaires montrent que l'ajout de ferrocénium n'a pas l'effet escompté et les rendements ne sont pas meilleurs en sa présence. Une autre réaction parasite vient limiter les rendements des réactions avec les amines. En effet, les Ni^{III} cationiques et monocationiques étudiés sont capables d'oxyder les amines. Il pourrait donc être possible d'utiliser les complexes trivalents afin de générer des aldéhydes à partir d'amines en milieu aqueux.[2]

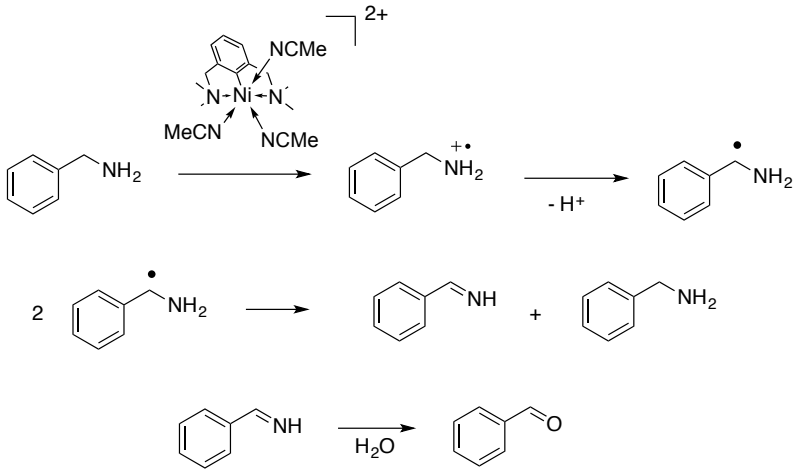

Schéma 5.9. Synthèse de benzaldéhyde à partir de l'oxydation de benzylamine en milieu aqueux

Un autre problème inhérent au système est l'impossibilité d'effectuer une réaction catalytique à partir des complexes de Ni^{II}/Ni^{III} puisque la réaction consomme le produit de départ. L'inspection du mécanisme issu des calculs DFT offre cependant 2 observations susceptibles de contourner cet inconvénient.

5.2 Activation C-Br à partir de Ni^{III}

La DFT montre que l'élimination réductrice du ligand bromure est défavorisée cinétiquement et thermodynamiquement. La barrière d'activation calculée est de 33.4 kcal/mol et la réaction est endergonique par 33.3 kcal/mol par rapport au complexe de départ. Ceci indique que l'addition oxydante d'un Ni^{I} sur un lien C-Br possède une barrière cinétique basse et que la réaction est thermodynamiquement

favorisée (Schéma 5.10). Il serait donc possible d'envisager un cycle catalytique de fonctionnalisation des liens C-Br basée sur le schéma 5.11.

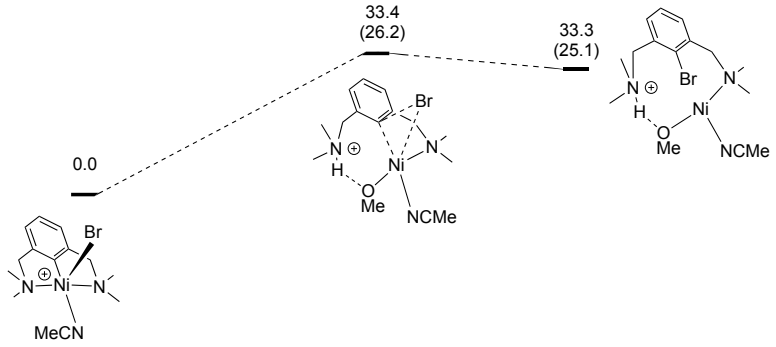

Schéma 5.10. Paramètre cinétique et thermodynamique de la formation d'un lien C-Br par élimination réductrice

Dans cette proposition il est assumé que le pré-catalyseur et le catalyseur de Ni^{I} sont stables. D'abord le pré-catalyseur réagit avec l'alcoolate de sodium pour former le catalyseur. Celui-ci effectue l'addition oxydante du lien C-Br pour former un complexe de Ni^{III} qui subit une élimination réductrice pour former le lien C-O. Le catalyseur est regénéré lorsque le $Ni^{I}Br$ réagit avec le NaOMe. Ceci est une preuve de concept et un mécanisme similaire menant au même produit peut être imaginé.

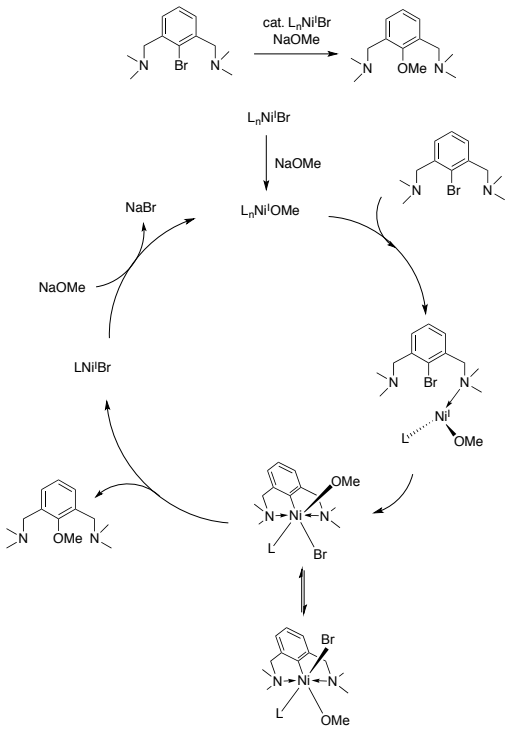

Schéma 5.11. Cycle catalytique Ni^{I}/Ni^{III} pour la formation de lien C-O

5.3 Activation C-H à partir de Ni^{III}

La formation de complexes pinces par nickellation du C-H est fréquemment utilisée pour les ligands pinceurs à base de phosphites et de phosphine. Cette réaction est très rapide pour les ligands de type POCOP, elle peut être effectuée à température pièce dans un temps de 5 minutes. Cependant le ligand POCN doit quant à lui être chauffé à 80 °C afin d'effectuer la nickellation du lien C-H et le ligand NCN présenté dans cette thèse ne peut être formé de cette façon. Il a été établi que le mécanisme de cette réaction est un mécanisme de type substitution aromatique électrophile passant par un intermédiaire dans lequel le carbone *ispo* interagit avec le Ni^{II} avant l'étape de nickellation.[3]

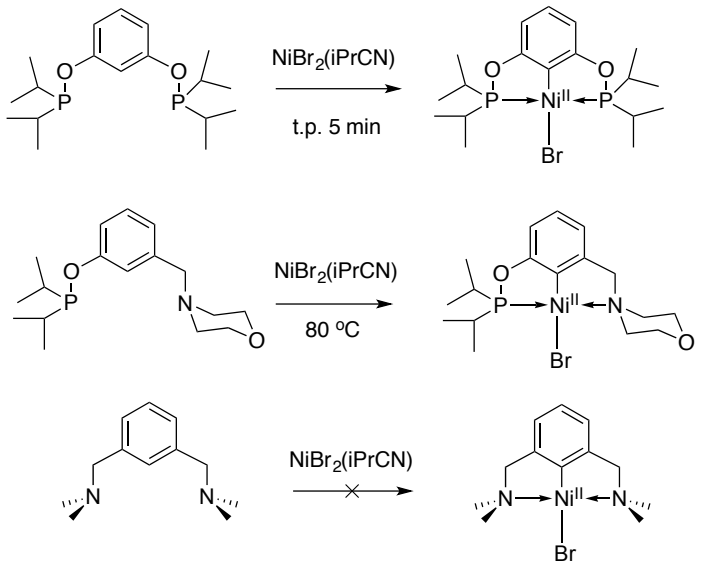

Schéma 5.12. Synthèse de complexe POCOP, POCN et NCN par activation C-H

L'étude DFT a démontré que la protonation du lien C-Ni^{III} par le ligand MeOH dans le complexe cationique est endergonique par environ 30 kcal/mol. C'est-à-dire que l'activation du lien C-H par un Ni^{III} cationique devrait être favorisée thermodynamiquement puisque c'est la réaction inverse. L'espèce produite par cette protonation est similaire à l'intermédiaire formé avant la nickellation du système POCOP. Le schéma 5.13 montre l'intermédiaire pré-nickellation du ligand POCOP et l'intermédiaire généré par la protonation du lien C-Ni^{III}. Il serait donc envisageable d'effectuer des réactions de fonctionnalisation de lien C-H à l'aide de nickel Ni^{III}, d'ailleurs des réactions similaires ont été effectuées par Mirica et Sanford.[4]

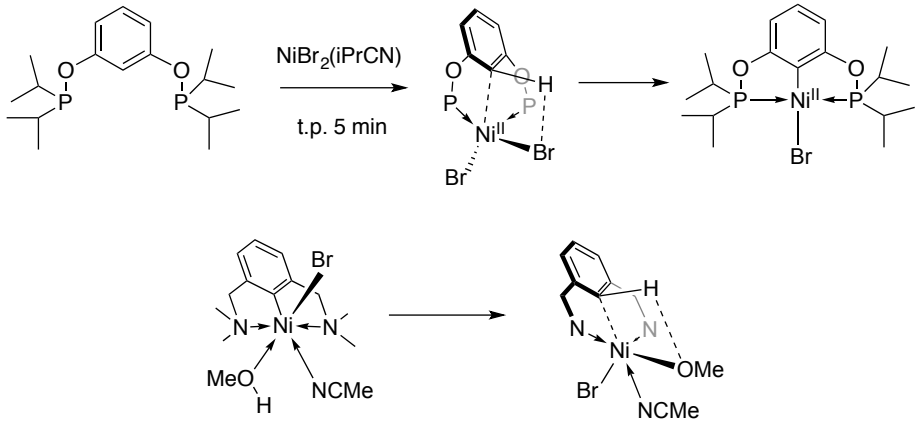

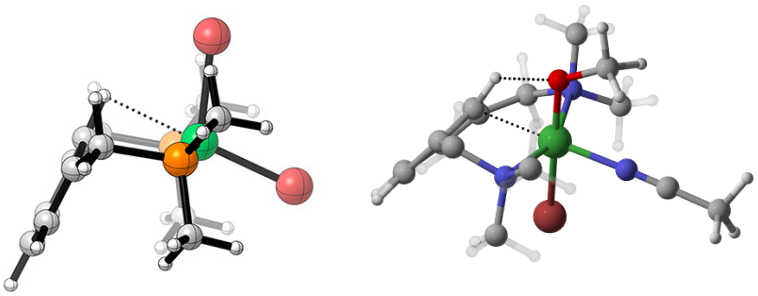

Schéma 5.13. (Haut) Activation C-H du ligand POCOP par un Ni^{III} (milieu) protonation d'un lien C-Ni, (bas) représentation 3D des deux intermédiaires impliqués

5.4 Insertion

L'implication des nickels haut-valent dans les mécanismes de couplage C-C, C-O, C-N et C-halogène est maintenant démontrée mais il reste encore beaucoup de réactivité à explorer. Par exemple, les réactions d'insertion comme l'insertion de CO dans un lien Métal-Carbone peuvent être favorisée par l'oxydation du centre métallique.[5] Il serait intéressant de tenter l'insertion de monoxyde de carbone sur des groupements plus difficile comme CF_3. Le schéma 5.17 montre l'insertion du CO dans un lien Ni-CF_3 par l'entremise d'un Ni^{IV}.

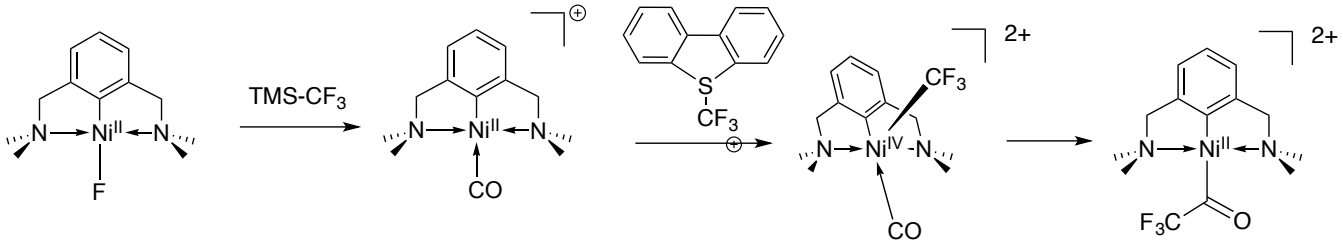

Schéma 5.14. Insertion de CO dans un lien Ni-CF_3 induite par oxydation

5.4 Références

[1] Cristau, H.-J.; Cellier, P. P.; Spindler, J.-F.; Taillefer, M. *Eur. J. Org. Chem.* **2004**, *2004* (4), 695–709.

[2] Torriero, A. A. J.; Shiddiky, M. J. A.; Burgar, I.; Bond, A. M. *Organometallics* **2013**, *32* (20), 5731–5739.

[3] Vabre, B.; Lambert, M. L.; Petit, A.; Ess, D. H.; Zargarian, D. *Organometallics* **2012**, *31* (17), 6041–6053.

[4] (a) Zhou, W.; Zheng, S.; Schultz, J. W.; Rath, N. P.; Mirica, L. M. *J. Am. Chem. Soc.* **2016**, *138* (18), 5777–5780.
(b) Chong, E.; Kampf, J. W.; Ariafard, A.; Canty, A. J.; Sanford, M. S. *J. Am. Chem. Soc.* **2017**, *139* (17), 6058–6061.

[5] Magnuson, R. H.; Meirowitz, R.; Zulu, S.; Giering, W. P. Oxidatively *J. Am. Chem. Soc.* **1982**, *104* (21), 5790–5791.